AUGMENTED REALITY AND 3D TECHNOLOGY IN CLINICAL PRACTICE

WITH SPECIAL EMPHASIS ON CRANIOSYNOSTOSIS

Jene Meulstee

Augmented Reality and 3D Technology in Clinical Practice

with special emphasis on Craniosynostosis

Jene Willem Meulstee

COLOFON

Augmented reality and 3D technology in clinical practice - with special emphasis on craniosynostosis

Academic thesis, Radboud Institute for Health Sciences, The Netherlands

Support for publication and distribution of this thesis was kindly provided by:

Cover design idea:	Jene Meulstee
Cover design lay-out:	Marilou Maes, Persoonlijk Proefschrift
Design and lay-out:	Ferdinand van Nispen, *my*-thesis.nl
Printing:	Proefschriftenprinten.nl, Ede, The Netherlands
ISBN:	978-90-832727-1-9

Augmented Reality and 3D Technology in Clinical Practice

with special emphasis on Craniosynostosis

Proefschrift ter verkrijging van de graad van doctor

aan de Radboud Universiteit Nijmegen

op gezag van de rector magnificus prof. dr. J.H.J.M. van Krieken,

volgens besluit van het college voor promoties

in het openbaar te verdedigen op

donderdag 6 oktober 2022

om 10.30 uur precies

door

Jene Willem Meulstee
geboren op 28 maart 1986
te Arnhem

PROMOTOREN:
Prof. dr. T.J.J. Maal
Prof. dr. S.J. Bergé

COPROMOTOREN:
Dr. W.A. Borstlap
Dr. H.H.K. Delye

MANUSCRIPTCOMMISSIE:
Prof. dr. R.H.M.A. Bartels
Prof. dr. H. van Goor
Prof. dr. E. Wolvius (Erasmus MC)

CONTENTS

CHAPTER 1

General Introduction

INTRODUCTION

The impact of technology on today's society and our daily lives is unmistakable. Since the beginning of the Third Industrial Revolution in the mid-1980s,[1] smartphones have improved and changed our way of communicating, computers have enhanced the efficiency of almost every work process, and the Internet has become a source of essential (and less essential) information.

Similarly, technology has left a major footprint on healthcare. Many medical procedures have been improved, and efficiency has enabled doctors to provide more and better treatment to their patients. Revolutionary technical developments such as image-guided surgery and robotics have enabled physicians to execute more advanced and complex surgeries. Some technologies have even disrupted clinical procedures. For example, the introduction of X-ray and ultrasound have changed the way some diseases are diagnosed. Primarily, this is the result of new developments themselves and of the increased acceptance of technology. Furthermore, new professionals such as clinical technologists and new departments such as a 3D Lab support new technology to nest into healthcare.

The term 'innovation' is generally used to describe new technology. The WHO describes innovation as a method that improves the efficiency, effectiveness, quality, sustainability, safety, and/or affordability of healthcare.[2,3] This concise and fitting description of innovation can help us evaluate its impact. The aim of this project is to improve clinical care through the implementation of innovations. The WHO's definition and measures will be used throughout this thesis, wherever possible, to evaluate the impact. Yet, the most important outcome parameter that will be used is the actual clinical implementation.

This thesis focuses mainly, but not exclusively, on the care and treatment of craniosynostosis patients.

CRANIOSYNOSTOSIS

Craniosynostosis is a congenital defect caused by the premature fusion of one or more sutures of the cranium. As a result, the normal growth and development of

the skull is obstructed. This can result in an abnormal skull shape or a cranium with too little volume for the underlying brain to develop properly. This in turn can cause increased intracranial pressure and can lead to behavioural or developmental disorders.[4] Craniosynostosis occurs in about one in 2200 births, which means that there are about 100 newborn patients a year in the Netherlands.[5,6] Craniosynostosis can be a part of a syndrome or be present in an isolated form. Depending on which suture is prematurely fused, different types of craniosynostosis can be classified (Figure 1).

Scaphocephaly is the most common form of craniosynostosis, occurring in 55 to 60% of all the cases. It is the result of a partial or complete premature fusion of the sagittal suture. As a result, growth perpendicular to the sagittal suture is inhibited, resulting in a reduced lateral diameter of the head. Additionally, compensatory growth in the antero-posterior direction results in an elongated skull. Scaphocephaly has a male to female ratio of almost 4:1.[7–10]

Trigonocephaly refers to the typical triangular shape of the forehead due to the premature fusion of the metopic suture in the front of the head. As a result, a steeply curved frontal head is formed. Trigonocephaly is seen in 15% of the isolated craniosynostosis cases and is most common in males.[7]

Plagiocephaly is caused by the unilateral premature fusion of the left or right coronal suture.[7,11] Unilateral coronal synostosis results in an asymmetric head shape as well as in facial asymmetry. In pronounced cases, harlequin eye deformity, which occurs because the orbit on the affected side is elevated, is present. In addition, obliquity of the facial midline may be observed. Besides (unilateral) plagiocephaly, both the coronal sutures could be fused. This results in brachycephaly, a condition that displays no asymmetry of the face but results in a skull shape in which the anterior part of the skull is tall and flat, and is therefore sometimes called the 'flat head syndrome'.[7]

In case more sutures are affected, the dysmorphology of the skull is more severe. Oxycephaly (or turricephaly), for example, is the result of the synostosis of both coronal and lambdoidal sutures and forces the skull to grow in the upward direction.

In the Radboudumc, two surgical options are provided to patients suffering from craniosynostosis: endoscopic-assisted craniosynostosis surgery in combination with helmet therapy and open reconstructive surgery.

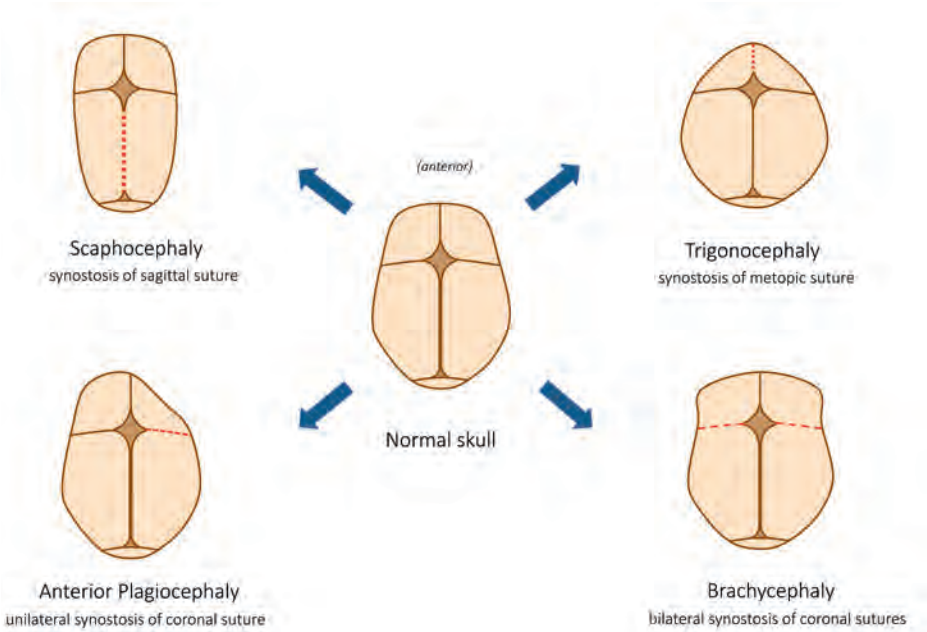

Figure 1: Top view of a normal skull (middle), including sutures and fontanelles (brown). Depending on which suture is affected (red dotted-lines), craniosynostosis can lead to various cranial malformations.

ENDOSCOPIC-ASSISTED CRANIOSYNOSTOSIS SURGERY

Endoscopic-Assisted Craniosynostosis Surgery (EACS) in combination with post-operative helmet therapy is the preferred treatment option in the Radboudumc.[12] During this surgical procedure, a small opening is created in the skin and the cranium; this opening is large enough to insert and manoeuvre an endoscope inside the cranium (Figure 2). Under endoscopic vision, a strip of bone from beside the fused suture is carefully removed from under the skin through the small incision(s). In all cases, a post-operative helmet therapy is complementary, and it is initiated almost directly after the surgery. The remolding helmet directs the cranial growth in the desired direction to obtain normalization of the head.[13] The small amount of intraoperative blood loss (around 40 ml) and a mean surgery time of about 60 minutes[12] are very important advantages of EACS.[14] Since only small incisions are required, the scars are moderately small and post-operative swelling

is kept to a minimum. The majority of patients are discharged the morning after the surgery without intensive care unit stay. Parental concerns and family anxiety are significantly lower in comparison to other procedures.[15,16]

EACS and helmet therapy is generally used for young children below the age of 6 months. This is because the normal and fast expansion of the brain, which is important during remolding helmet therapy, gradually reduces at later age.[17] In addition, the thickness of the bone that surrounds the fused suture increases, making it harder to cut and swiftly remove the bone piece through the small incisions. Therefore, open reconstructive surgery is a better fitting treatment option for older patients.

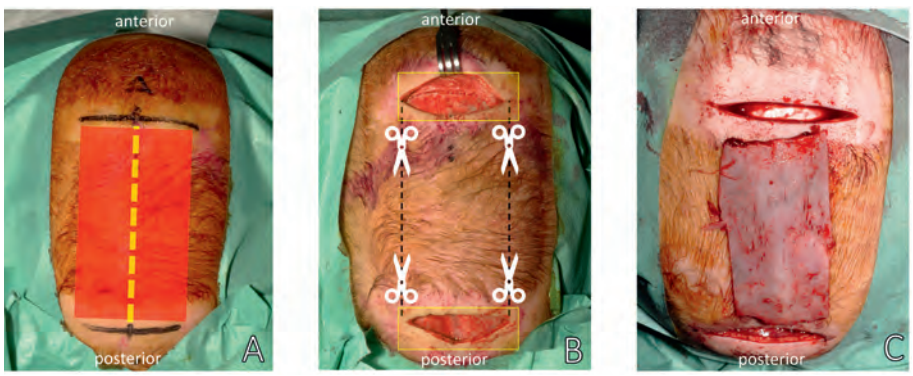

Figure 2: Top view of endoscopic assisted craniectomy. A.) The red area indicates the bone strip that surrounds the fused sagittal suture (yellow dotted line) under the skin of a scaphocephaly patient. The coronal and lambdoid sutures are marked (black). B.) Two small incisions are made in the skin and skull (yellow boxes). Under endoscopic guidance, the bone strip is cut from both sides. C.) Removal of the bone strip.

OPEN RECONSTRUCTIVE SURGERY

Open cranial vault reconstruction is ideally performed around the age of 10 months or later. During this procedure, a bicoronal (ear-to-ear) incision is made and skin and periost are stripped from the cranium. Next, the parts of the cranium that are affected by the craniosynostosis are dissected and temporally removed from the patient. These parts are reconstructed into a new shape. The aim is to create a larger cranium with an aesthetically improved shape. With resorbable fixation material, the dissected and reconstructed bone pieces are placed back into the patient. An illustration of an open cranial vault reconstruction is shown

in Figure 3. Compared to EACS, open reconstructive surgery is a major surgical procedure with important morbidity. Since there are many options available to dissect and reconstruct a cranial shape, a fitting surgical strategy is fundamental to achieve the best surgical outcome.

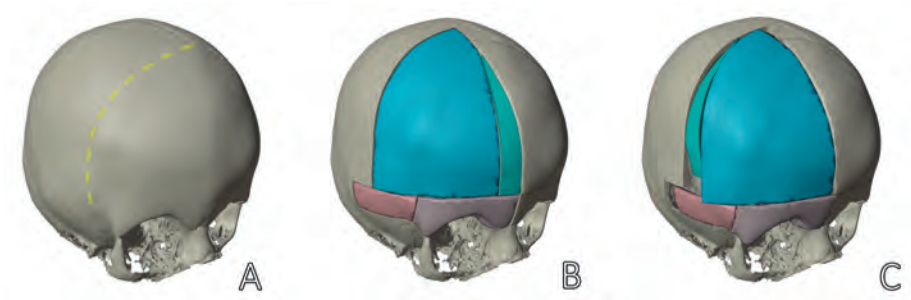

Figure 3: Open cranial vault reconstruction in an anterior plagiocephaly patient. A.) The prematurely fused right coronal suture (yellow dotted line) results in an abnormal skull shape and retraction of the right orbit. B.) Cranial osteotomies divide the deformed area into different bone segments. C.) The bone segments and right orbit are repositioned to create a larger and esthetical improved cranial shape and restore (facial) symmetry.

THE CRANIOFACIAL TEAM

The surgery, as well as the diagnosis, treatment planning and follow-up of craniosynostosis patients are performed by members of the craniofacial (CFA) team. In our University Hospital, the team consists of oral and maxillofacial surgeons, neurosurgeons, orthodontists and technical physicians (Figure 4). Furthermore, clinical assistants, clinical geneticists, (pediatric) anesthetists, critical care specialists and researchers fulfill an essential role and allow the team to offer every patient the best possible care. For patients, the goal is to grow into an adult who can function adequately in society with an aesthetically acceptable face. Since 2012, the Radboudumc is one of the two nationally appointed expert centers for the treatment of craniosynostosis in the Netherlands, Rotterdam being the other one, and is a member of the European Reference Network (ERN) for craniosynostosis.

The CFA team continuously evaluates the current treatment processes and investigates the use of new technologies in order to further improve the treatment of craniosynostosis together with the Radboudumc 3D Lab. The results of this collaboration have proven to be effective and have led to the successful

implementation of various 3D technologies throughout various phases of treatment (Figure 5).

Figure 4: Different team members and specialities form the craniofacial team in the Radboudumc.

THE 3D LAB

By providing 3D services, research, teaching and training, the 3D Lab aims to improve clinical practice and patient care by implementing new technologies. Since the start of the 3D Lab in 2006, it has evolved into an indispensable entity that has a significant impact on healthcare. The team includes technical physicians, medical engineers, game developers and industrial engineers. Originally, the 3D Lab was established as a division of the oral & maxillofacial surgery department, but meanwhile it is involved in over 15 medical departments at our University Hospital, and represented in more than 10 medical centers in the Netherlands.

3D technologies such as the virtual planning of surgeries, 3D printing of anatomical models, artificial intelligence to automatically segment anatomical structures, robotics to demarcate and transfer a cutting pattern and many other techniques are investigated and applied by the 3D Lab in the last decennium. The lab is fully

integrated into the clinic, allowing the lab engineers, doctors and patients to work closely together. This cooperation enables professionals to make 3D technologies quickly and easily accessible for both the doctor and the patient.

This thesis will evaluate the effect of various new technologies for the treatment of craniosynostosis and their other clinical applications. The most used 3D techniques that will be used in this project are discussed below.

Figure 5: 3D technology can be used at different moments of the treatment. In this figure, four different phases of the treatment are represented as gears that together describe the treatment process.

3D STEREOPHOTOGRAMMETRY

To diagnose cranial abnormalities or monitor the development of the cranial shape over time, the use of 3D photos is very helpful. 3D stereophotogrammetry is an imaging technique to create a 3D surface photo of the patient in a fraction of a second. The Radboudumc is a worldwide pioneer in implementing 3D photography for various clinical purposes. The 3DMDcranial System (3dMD Limited, London, United Kingdom) uses five pods that are positioned around and above the patient. Each pod consists of a colour camera and two greyscale cameras. The system projects onto the patient an infrared light pattern that can be captured by the greyscale cameras. The deformation of this pattern is used

to reconstruct a 3D image. Next, the texture information captured by the colour camera can be mapped onto the reconstruction and a fully detailed 3D image of the patient is acquired.[18]

The most important advantages of 3D stereophotogrammetry are the fast acquisition time (~ 2 milliseconds) and the fact that there is no exposure to ionizing radiation.[19] Therefore, it is an appropriate imaging modality to study the crania of newborn patients and healthy controls. The implementation of 3D photos for diagnosis will be investigated in part 1, while part 4 of this thesis explores the use of 3D photos for evaluation of surgical procedures.

VIRTUAL SURGICAL PLANNING

Virtual surgical planning (VSP) makes it possible to explore a surgical outcome before an operation itself is performed. Based on imaging, such as magnetic resonance imaging (MRI) or computed tomography (CT) scans, generally created for diagnostic purposes, the patient's anatomy can be reconstructed and visualized in a 3D environment. As the next step, various surgical procedures can be simulated based on this reconstruction. For example, by virtually manipulating the position of a patient's maxilla, the surgeon can see the effect of this displacement on dental occlusion and facial profile. In this way, various surgical strategies can be evaluated in advance and the best solution for individual patients can be determined.[20]

During open cranial vault reconstruction, surgeons aim to reconstruct an aesthetically appealing cranial shape with sufficient volume. Since there are many options for dissection and reconstruction, a fitting surgical strategy is fundamental to achieve the best surgical outcome. Virtual surgical planning can help the surgeons to find this optimal surgical strategy. In part 2 of this thesis, the use of virtual surgical planning for craniosynostosis patients will be evaluated and discussed.

3D PRINTING

Along with pre-operative virtual surgical planning, an accurate and precise transfer in to the operation room as well as a meticulous execution of this surgical plan is important to achieve an optimal treatment result. 3D printing is a technique that can be used to help the surgeon transferring the VSP directly to the patient since patient-specific cutting guides can be fabricated.[21] The benefits of 3D

printed surgical guides have been proven for applications in and outside oral and maxillofacial surgery, such as reconstructive trauma surgery, knee surgery and spinal surgery.[22–24]

During open reconstructive craniosynostosis surgery, 3D printed surgical guides can aid the surgeon in performing the reconstruction according to the planning and facilitate a precise and rapid reconstruction.[25] An optimal functional and aesthetic result can be achieved because the subjectivity of intraoperative bone fragment placement is minimized.[21,26,27] In part 3 and 4 of this thesis, the use of 3D printed surgical guides will be evaluated and compared to other transfer methods.

AUGMENTED REALITY

Augmented reality (AR) is a visualization technique to display virtual elements into the 'real world'. Augmented reality is a collective term for many applications and methods. For instance, AR can be used to place virtual content onto a photo or a video. This added virtual layer could show navigation directions on a smartphone or enhance your face with puppy ears on a Snapchat photo. However, there are many other options to achieve AR. When a semi-transparent display is used to create AR, it becomes possible to show virtual content directly into the real environment. This method is used, for example, in cockpits of fighter planes and helicopters to highlight enemy targets. An even more sophisticated AR technique uses a head-mounted display (HMD) with two semi-transparent displays. The latter has the advantage of always being consistent with the user's sight, and the virtual content can be viewed in real 3D by using stereoscopic view. This technology really enables the fusion of 3D virtual objects with the real environment.

Although AR is considered a modern technology, the first AR headset was designed as early as 1968. Ivan Sutherland, from Harvard University, developed an AR headset and attached it to the ceiling of his laboratory[28] (Figure 6). With a flexible mechanical structure, he was able to measure the user's head position. It was, therefore, also named the 'The Sword of Damocles'.[29] With a special and expensive NASA computer, Sutherland precisely calculated how the user looked at virtual 3D objects. From this, he could display wire-frame images of 3D objects at 30 frames per second (which is only half the speed of today's modern AR devices).

In 1990, Tom Caudell was looking for solutions to improve the complex process of aircraft manufacturing at Boing. Caudell developed a HMD to virtually display

complex wiring instructions for airplanes. Because virtual wiring instructions could be modified or adjusted more easily than physical templates, his technique speed up the process.[30] Tom Caudell was also the first who used the term 'Augmented Reality'.

In 1992, Louis Rosenburg created an AR system that enabled physical objects to interact with virtual objects.[31] By wearing an exoskeleton, Rosenburg manipulated two robot hands as if they were his own. This system was used to train the United States Air Force pilots. Later, AR was also used in fighter planes and helicopters to display relevant information in a heads-up display of pilots.[32]

In the 90s, various implementations of AR in the fields of arts, movie clips and sports were introduced. The company SportVision used a real-time camera recording of an American Football game and projected, in real-time, a virtual yellow yard line over the field.[33] With smart visualization techniques, the line was never projected over the players. It was always perfectly aligned with the field, which ensured that the virtual yard marker blended perfectly into 'reality'. Sportvision even won an Emmy Award for this technique.

All the examples above have a very specific purpose or rely on sophisticated set-ups and complex hardware. Yet, this changed when Google launched a HMD for general consumers in 2013 and the expectations of this Google Glass were very high. The Google Glass could, for example, display an anatomical image or health record information on its virtual display in the top right corner of the user's view. In the Radboudumc, the Google Glass was used to broadcast a surgical procedure from the surgeon's perspective to train residents (Figure 6). Eventually, because of the small and low-quality display, and the short battery life, the actual added value of the Google Glass turned out to be limited. Nevertheless, its introduction raised significant awareness and stimulated the formation of ideas and concepts about the possibilities of AR for medical practice.

In 2014, a Silicon Valley-based start-up company presented the first HMD with a stereoscopic view: the Meta Glasses. This device could visualize 3D objects, track objects and follow the users' hands. Because these features made it possible to really interact with the virtual models, the Meta Glasses created an authentic mixed reality experience and therefore expanded the possibilities of AR (Figure 6).

The Meta Glasses was also the starting point for the 3D Lab to explore new clinical use cases of AR. Yet, the low resolution, the small field of view and all the cables that needed to be connected to a high-performance computer made this device somewhat impractical. Regrettably, the Meta company has gone bankrupt in 2018.

The Microsoft HoloLens, introduced in August 2016, was one of the first HMD devices with a high-quality display and a proper field of view. The wireless design of the HoloLens stimulates the user to inspect 3D objects or 'holograms' from different positions and view angles, and, therefore, the benefits of 3D could be fully utilised. Although the HoloLens was officially launched as a developer device, the quality of the visualization and it's practicability make the HoloLens an exciting device to be used in a medical setting. For example, with AR, a virtual 3D planning or a patient scan can be observed directly in a surgeon's view at the corresponding position on a patient.

Ever since, several other AR-HMD have been released, including the Meta Glasses 2 (2016), the HoloLens 2 (2019) and the Magic Leap (2018). Furthermore, future glasses and updates have been announced by various companies, including Apple, Meta and Google. It is challenging to predict how future developments and technological innovations will affect the current status of AR and which processes could be disrupted by AR. According to Swab, AR is one of the techniques that preludes the Fourth Industrial Revolution, where our physical, biological and digital worlds blend together.[1] Besides this, several market analysis reports are also optimistic, and expect that the AR market will reach a total value of 100 billion in the next 5-10 years.[34–36] The healthcare, gaming and defence industries are mentioned as the main growth drivers. Yet, (medical) AR is still immature at this moment and research into new applications and the added value of AR is now needed.

In part 3 of this thesis, the potential of various AR applications will be investigated, including a solution to improve the surgery of craniosynostosis patients.

Figure 6: Examples of head mounted AR displays that allow users to visualize virtual content in a real environment. Left: the set-up of Ivan Sutherland developed in 1968, where the display was attached to the ceiling (https://lookingglassxr.com/augmented-reality). Top right: Google Glass used in 2013 during orthognathic surgery in the Radboudumc. Lower right: the Meta Glasses allowed users to interact with virtual chess pieces in a real world setting (https://www.cnet.com/science/meta).

OBJECTIVES AND THESIS OUTLINE

The main objective of this thesis is to determine whether the treatment of craniosynostosis can be improved by the development and implementation of 3D techniques. The complete treatment of craniosynostosis can be divided into four phases: diagnosis, planning, surgery and evaluation (Figure 5). Likewise, this thesis is divided into four parts, each representing a phase of the treatment cycle. The research questions for each of the four parts are stated below. Together, these parts reveal how 3D technology affects the care and cure of craniosynostosis patients. A second objective of this thesis is to evaluate whether 3D technologies, initially applied for craniosynostosis, can be implemented in other clinical procedures and in other hospitals.

PART 1 – DIAGNOSIS

The diagnosis of craniosynostosis is very important since the clinical outcome can benefit from an early and adequate detection. Although CT scanning is the current gold standard for diagnosis, 3D stereophotogrammetry in combination with software algorithms could be implemented to diagnose and classify patients with various types of craniosynostosis. The research question that will be answered in this part is as follows: *Can the diagnosis and follow-up of craniosynostosis be improved by the implementation of 3D stereophotogrammetry?*

PART 2 – PLANNING

Planning of surgical procedures is done to create a patient-specific treatment plan. The potential of virtual surgical planning and preparation will be discussed. The research question that will be answered in this part is as follows: *What are the (dis)advantages of 3D planning during the preparation of craniosynostosis surgery?*

PART 3 – SURGERY

Surgery of craniosynostosis could be improved using a proper transfer technique. When an optimal treatment plan is created, this should be accurately transferred to the patient during surgery. The research question that will be answered in this part is as follows: *Which 3D methods could be used to transfer a virtual planning in to the operation room?*

PART 4 – EVALUATION

Evaluation of patients after surgery and during treatment is important for monitoring the patient's well-being. Objective evaluation of surgical outcomes could be used to further improve the entire process of diagnosis, planning, surgery and evaluation, wherever possible. The research questions that will be answered in this part is as follows: *How could 3D techniques be used to evaluate surgery and treatment outcomes? How could this be implemented and does this benefit the treatment of (new) patients?*

The chapters and parts of the thesis are presented on the next page.

Part 1 Diagnosis

Chapter 2 The normal evolution of the cranium in 3D

Chapter 3 A new method for 3D evaluation of the cranial shape and the automatic identification of craniosynostosis using 3D stereophotogrammetry

Part 2 Planning

Chapter 4 Virtual surgical planning of open cranial vault reconstructions

Chapter 5 Comparison of 3D and augmented reality kidney models with conventional imaging data in the preoperative assessment of children with Wilms tumors

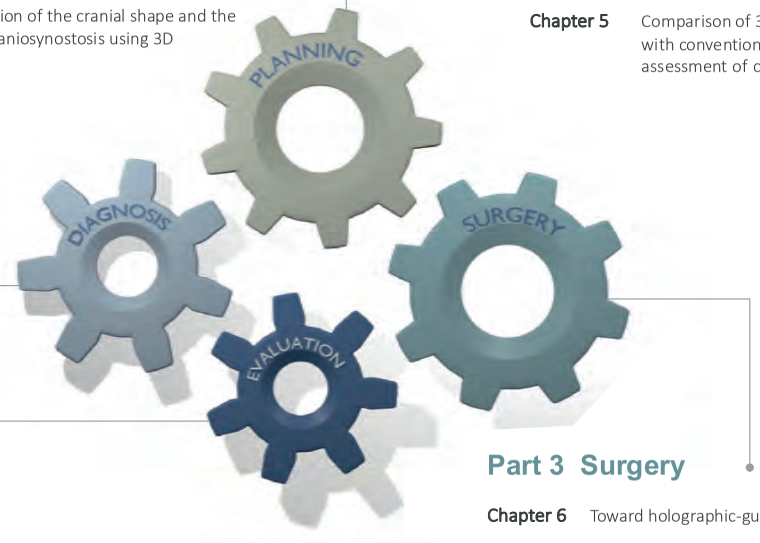

Part 4 Evaluation

Chapter 10 Longitudinal 3D follow-up and secondary treatment aspects after endoscopic and open scaphocephaly surgery

Chapter 11 Evaluation of open cranial vault surgery

Part 3 Surgery

Chapter 6 Toward holographic-guided surgery

Chapter 7 Surgical guides versus augmented reality to transfer a virtual surgical planning for open cranial vault reconstruction: a pilot study

Chapter 8 Holographic augmented reality for a DIEP flap harvest

Chapter 9 Augmented reality guided condylectomy

REFERENCES

1. Schwab K. The fourth industrial revolution. *Inf Technol Libr*. 2017;40(1):192. doi:10.6017/ITAL.V40I1.13193
2. Kimble L, Rashad M. What do we mean by innovation in healthcare? *Eur Med J*. 2017;1(1):89-91. doi:EMJ Innov. 2017;1[1]:89-91
3. WHO | Innovation. Accessed August 2, 2020. https://www.who.int/topics/innovation/en/
4. Kabbani H, Raghuveer TS. Craniosynostosis. *Am Fam Physician*. 2004;69(12):2863-2870.
5. Thijssen J, Mathijssen I. Richtlijn Behandeling en Zorg voor Craniosynostose. Published online 2012:1-26. http://www.erasmusmc.nl/47469/51016/3210630/3210939/1.3.3_Definitieve_richtlijn_craniofaciale_chirurgie_(lekenversie).pdf
6. Cornelissen M, Ottelander B den, Rizopoulos D, et al. Increase of prevalence of craniosynostosis. *J Cranio-Maxillofacial Surg*. Published online 2016. doi:10.1016/j.jcms.2016.07.007
7. Aleck K. Craniosynostosis syndromes in the genomic era. *Semin Pediatr Neurol*. 2004;11(4):256-261. doi:10.1016/j.spen.2004.10.005
8. Heuzé Y, Boyadjiev SA, Marsh JL, et al. New insights into the relationship between suture closure and craniofacial dysmorphology in sagittal nonsyndromic craniosynostosis. *J Anat*. 2010;217(2):85-96. doi:10.1111/j.1469-7580.2010.01258.x
9. Lajeunie E, Le Merrer M, Bonaïti-Pellie C, Marchac D, Renier D. Genetic study of scaphocephaly. *Am J Med Genet*. 1996;62(3):282-285. doi:10.1002/(SICI)1096-8628(19960329)62:3<282::AID-AJMG15>3.0.CO;2-G
10. Kapp-Simon K a, Speltz ML, Cunningham ML, Patel PK, Tomita T. Neurodevelopment of children with single suture craniosynostosis: a review. *Childs Nerv Syst*. 2007;23(3):269-281. doi:10.1007/s00381-006-0251-z
11. Colosima C, Tartaro A, Cama A, Tortori-Donati P. The Craniosynostoses. In: *Pediatric Neuroradiologie: Brain Head and Neck Spine*. ; 2005:1289-1314.
12. Delye HHK, Arts S, Borstlap WA, et al. Endoscopically assisted craniosynostosis surgery (EACS): The craniofacial team Nijmegen experience. *J Cranio-Maxillofacial Surg*. 2016;44(8):1029-1036. doi:10.1016/j.jcms.2016.05.014
13. Ridgway EB, Berry-Candelario J, Grondin RT, Rogers GF, Proctor MR. The management of sagittal synostosis using endoscopic suturectomy and postoperative helmet therapy. *J Neurosurg Pediatr*. 2011;7(6):620-626. doi:10.3171/2011.3.PEDS10418
14. Shah MN, Kane AA, Petersen JD, Woo AS, Naidoo SD, Smyth MD. Endoscopically assisted versus open repair of sagittal craniosynostosis: The St. Louis Children's Hospital experience - Clinical article. *J Neurosurg Pediatr*. Published online 2011. doi:10.3171/2011.5.PEDS1128
15. Braun TL, Eisemann BS, Olorunnipa O, Buchanan EP, Monson LA. Safety outcomes in endoscopic versus open repair of metopic craniosynostosis. *J Craniofac Surg*. 2018;29(4):856-860. doi:10.1097/SCS.0000000000004299
16. Birgfeld CB, Dufton L, Naumann H, et al. Safety of Open Cranial Vault Surgery for Single-Suture Craniosynostosis: A Case for the Multidisciplinary Team. *J Craniofac Surg*. 2015;26(7):2052-2058. doi:10.1097/SCS.0000000000001940
17. Meulstee JW, de Jong GA, Borstlap WA, Koerts G, Maal TJJ, Delye H. The normal evolution of the cranium in three dimensions. *Int J Oral Maxillofac Surg*. 2020;49(6):739-749. doi:10.1016/j.ijom.2019.10.012
18. Maal TJJ, Van Loon B, Plooij JM, et al. Registration of 3-dimensional facial photographs for clinical use. *J Oral Maxillofac Surg*. 2010;68(10):2391-2401. doi:10.1016/j.joms.2009.10.017
19. Littlefield TR, Kelly KM, Cherney JC, Beals SP, Pomatto JK. Development of a new three-dimensional cranial imaging system. *J Craniofac Surg*. 2004;15(1):175-181. http://www.ncbi.nlm.nih.gov/pubmed/14704586
20. Hua J, Aziz S, Shum JW. Virtual Surgical Planning in Oral and Maxillofacial Surgery. *Oral Maxillofac Surg Clin North Am*. 2019;31(4):519-530. doi:10.1016/j.coms.2019.07.011
21. Coppen C, Weijs W, Bergé SJ, Maal TJJ. Oromandibular reconstruction using 3D planned triple template method. *J Oral Maxillofac Surg*. Published online 2013. doi:10.1016/j.joms.2013.03.004
22. Brouwers L, Gunne AFP Ter, De Jongh MAC, et al. The Value of 3D Printed Models in Understanding Acetabular Fractures. *3D Print Addit Manuf*. 2018;5(1):37-45. doi:10.1089/3dp.2017.0043

23. Sheha ED, Gandhi SD, Colman MW. 3D printing in spine surgery. *Ann Transl Med*. 2019;7(S5):S164-S164. doi:10.21037/atm.2019.08.88
24. Kumar P, Vatsya P, Rajnish RK, Hooda A, Dhillon MS. Application of 3D Printing in Hip and Knee Arthroplasty: A Narrative Review. *Indian J Orthop*. 2021;55(S1):14-26. doi:10.1007/s43465-020-00263-8
25. Macmillan A, Lopez J, Mundinger GS, Major M, Medina MA, Dorafshar AH. Virtual surgical planning for correction of delayed presentation scaphocephaly using a modified melbourne technique. In: *Journal of Craniofacial Surgery*. Vol 29. ; 2018:914-919. doi:10.1097/SCS.0000000000004290
26. Chim H, Wetjen N, Mardini S. Virtual surgical planning in craniofacial surgery. *Semin Plast Surg*. 2014;28(3):150-158. doi:10.1055/s-0034-1384811
27. Mardini S, Alsubaie S, Cayci C, Chim H, Wetjen N. Three-dimensional preoperative virtual planning and template use for surgical correction of craniosynostosis. *J Plast Reconstr Aesthetic Surg*. 2014;67(3):336-343. doi:10.1016/j.bjps.2013.11.004
28. Sutherland IE. A head-mounted three dimensional display. In: *Proceedings of the December 9-11, 1968, Fall Joint Computer Conference, Part I on - AFIPS '68 (Fall, Part I)*. Vol 33. ACM Press; 1968:757. doi:10.1145/1476589.1476686
29. Van Krevelen DWF, Poelman R. A Survey of Augmented Reality Technologies, Applications and Limitations. *Int J Virtual Real*. 2010;9(2):1-20. doi:10.20870/ijvr.2010.9.2.2767
30. Caudell TP, Mizell DW. Augmented reality: an application of heads-up display technology to manual manufacturing processes. In: Institute of Electrical and Electronics Engineers (IEEE); 2003:659-669 vol.2. doi:10.1109/hicss.1992.183317
31. Rosenberg LB. The Use of Virtual Fixtures as Perceptual Overlays to Enhance Operator Performance in Remote Environments. In: ; 1992.
32. Rolland J. Display Systems: Head-Mounted. In: *Encyclopedia of Optical and Photonic Engineering, Second Edition*. CRC Press; 2015:1-13. doi:10.1081/E-EOE2-120009801
33. Poetker B. A Brief History of Augmented Reality (+Future Trends & Impact). g2. Published 2019. Accessed July 13, 2022. https://www.g2.com/articles/history-of-augmented-reality
34. Mordor Intelligence I. *Augmented Reality Market - Growth, Trends, Covid-19 Impactact, and Forecasts (2022 - 2027)*.; 2022.
35. Grand View Research. *Augmented Reality Market Size, Share & Trends Analysis Report By Component (Hardware, Software), By Display (Head-Mounted Display & Smart Glass, Head-Up Display, Handheld Devices), By Application, By Region, And Segment Forecasts, 2022 - 2030*.; 2020.
36. Fortune Business Insights I. *Augmented Reality (AR) Market Size, Share & COVID-19 Impact Analysis, By Component (Hardware, and Software), By Device Type (Head Mounted Display, Heads Up Display, Handheld Devices, Stationary AR Systems, Smart Glasses, Others), By Industry (Gaming, Medi*.; 2021. doi:FBI102553

PART 1

DIAGNOSIS

CHAPTER 2

The normal evolution of the cranium in three dimensions

Jene Meulstee
Guido de Jong
Wilfred Borstlap
Guus Koerts
Thomas Maal
Hans Delye

Jene Meulstee and Guido de Jong contributed equally to this work

International Journal of Oral & Maxillofacial Surgery
Published: November 2019
DOI: 10.1016/j.ijom.2019.10.012

ABSTRACT

Insight into the growth and development of the normal newborn cranial shape is essential to monitor cranial development, to detect and diagnose abnormal skull shapes, and for the long-term follow-up of craniosynostosis surgery. The aim of this study was to analyse the growth pattern of the cranial shape of infants during the first years of life using 3D stereophotogrammetry and 3D computed tomography (CT) with advanced 3D evaluation techniques.

A large set of 3D photographs (n = 199) and CT scans (n = 183), taken between ages 0 and 54 months, was collected. Cranial shapes with artefacts and asymmetries were removed.

Total volumes and intracranial volumes were obtained, as well as 3D and 2D measurements, including the cranial width, cranial length, cranial index, and suture lengths. Growth maps were created for all modalities to indicate 3D growth over time. For the final analysis, a total of 130 3D photographs, 94 hard tissue CT scans, and 76 soft tissue CT scans were used. 3D and 2D measures, volumes, growth maps, and growth animations were obtained. A non-uniform growth was revealed by the 3D growth maps.

This study addresses the need for normative cranial evolution data to monitor healthy cranial development and for detection, follow-up, and treatment planning in craniosynostosis.

INTRODUCTION

During the first years of life, the infant cranium grows very rapidly.[1] Insight into the growth and development of the normal cranial shape is essential to monitor cranial development, detect abnormalities, and evaluate the long-term results of craniosynostosis surgery.[2] Many studies have described the development of the cranial shape by reporting databases with craniometrics for different ages and populations. Craniometric data can be measured directly on the subject's head using two-dimensional (2D) measurement tools or can be derived from plain X-rays.[3–6] Since the introduction of three-dimensional (3D) imaging, new accurate measurement methods for the evaluation of the cranium have become available, including 3D computed tomography (CT) and radiation-free 3D stereophotogrammetry.[1,7–9] Most studies, however, have merely used 3D imaging techniques to create a database of 2D measurements. Yet, these 2D measurements and ratios fail to give an adequate, complete, and detailed description of the cranial shape and its 3D evolution. The literature describing a complete 3D evaluation of the skull during the first months of life is limited.[2] The aim of this study was to analyse the growth pattern of the cranial shape of infants during the first years of life using 3D stereophotogrammetry and 3D-CT with advanced 3D evaluation techniques. This insight could be used to describe normal cranial development, detect and diagnose cranial abnormalities, and evaluate the treatment of craniosynostosis.

PATIENTS AND METHODS

ACQUISITION AND SUBJECTS

A database of 3D craniometrics was established using 3D photographs and CT scans of healthy infants. A 3D stereophotogrammetry set-up (3dMDCranial; 3dMD, Atlanta, GA, USA) with a five-pod configuration was used prospectively for the acquisition of 199 3D photographs of healthy infants. Ethical approval from the regional institutional review board was obtained for this study.

3D PHOTOGRAPHS

The 3D photographs of healthy infants were taken at fixed time intervals (3, 6, 9, 12, 15, 18, and 24 months). Photographs with severe quality inconsistencies were excluded, resulting in a set of 146 3D photographs. Furthermore, 3D photographs

showing a mild, moderate, or severe asymmetry were excluded. To objectively determine asymmetry, the plagiocephalometry method described by Van Vlimmeren et al. was used,[6] with calculation of the oblique diameter difference index (ODDI) and cranial proportion index (CPI) for every 3D photograph. An ODDI of <104.5 and a CPI of <90 was defined as normal. A total of 130 3D photographs of 49 infants were finally included in this study (Figure. 1). In this group, 49% (n = 64) of the photographs were of male subjects.

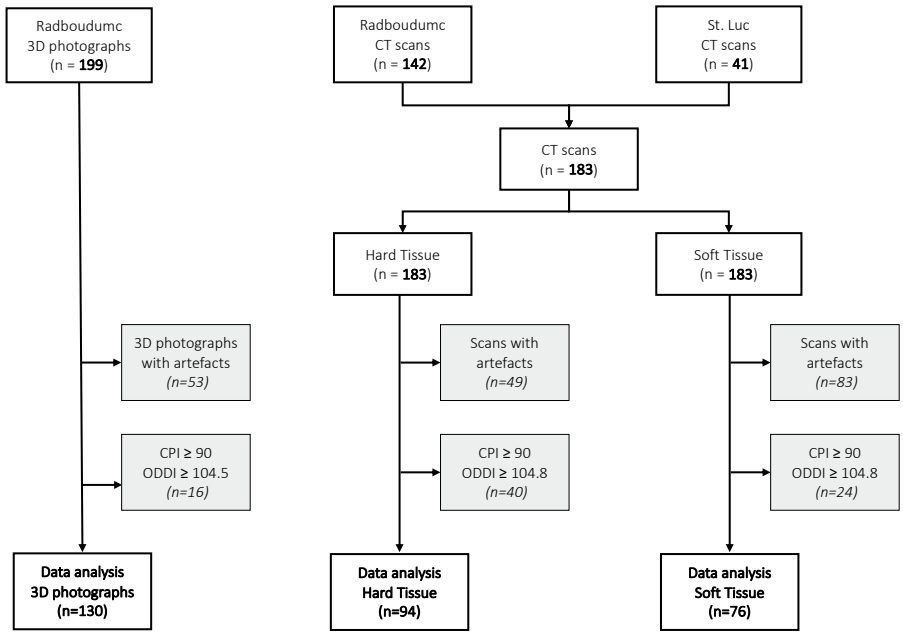

Figure 1: Flowchart of the study and the included 3D photographs and 3D-CT scans.

COMPUTED TOMOGRAPHY

This study retrospectively used anonymized CT scans of infants who had a CT scan performed in Radboudumc, Nijmegen or St-Luc University Medical Hospital, Brussels. The CT scans were performed on clinical indication (e.g. suspicion of head trauma). The CT scans of infants between 0 and 54 months of age were screened and only included if no pathology or morphological changes were present. A part of the Radboudumc set has been described previously.[10] CT scans not capturing the complete cranium or scanned with a slice thickness of >2 mm were excluded, resulting in a total of 183 CT scans. The CT scans were reconstructed into a 3D

shape of the hard tissue (CT-HT) and soft tissue (CT-ST) using Maxilim software (Medicim NV, Mechelen, Belgium). Three-dimensional shapes with clear artefacts were removed from the CT-HT and CT-ST groups. Since the plagiocephalometry method to exclude asymmetric cranial shapes was designed for soft tissue only, a correlation and offset factor was calculated to make the plagiocephalometry method also applicable to hard tissue. Details of the plagiocephalometry method and offset calculation are given in the Appendix. Finally, a total of 94 CT-HT shapes and 76 CT-ST shapes were used in this study (Figure. 1). The CT-HT group was 52% (n = 49) male and the CT-ST group was 50% (n = 38) male. Details of the sex distribution are given in Table 1.

DATA PROCESSING

The quality of all 3D photographs was assessed and minor artefacts were repaired using MeshMixer 3D software (Autodesk Inc., San Francisco, CA, USA). Similar to methods presented previously, nine land-marks were manually marked on the textured 3D photographs (Table 2; Figure. 2) and used to automatically pre-align the 3D photographs in a reference frame (tragus–nasion orientation).[11] The computed cranial focal point (CCFP) was used to automatically position the 3D photographs in identical reference frames (sella turcica–nasion orientation) using MatLab v2017a (The Mathworks Inc., Natick, MA, USA).[12] The 3D photographs were checked for rotational and positional variances and adjusted if necessary. For further analysis, all 3D photographs were normalized to create mesh data with the same number of vertices (data points).[10,11] An annotation tool was created in Unity v5.6.0 (Unity Technologies, San Francisco, CA, USA) to manually position 21 landmarks on the CT-HT (Table 2). Landmarks and the CCFP method were used to automatically position the 3D shapes in the sella turcica–nasion orientation. In the same way as for the 3D photographs, rotational and positional differences were eliminated and the 3D-CT shapes were normalized for further analysis.

MEASUREMENTS

The 3D photographs were grouped into seven predefined age categories and the mean cranial shape was calculated for every group.[10,11] The mean growth was calculated as the difference between a mean cranial shape and the consecutive mean cranial shape and visualized with a growth map. The CT-HT shapes were grouped similar to the 3D photographs, with two additional age groups of 36 and 48 months. The cranial length was given by the most anterior and posterior point

Table 1 Male (M) and Female (F) distribution with mean age and standard deviation per age group for 3D photographs (3DP), CT hard tissue (CT-HT) and CT soft tissue (CT-ST).

	3DP				CT-HT				CT-ST			
	Number		Age (months), mean (SD)		Number		Age (months), mean (SD)		n		Age (months), mean (SD)	
Group (months)	M	F	M	F	M	F	M	F	M	F	M	F
3	14	12	3.1 (0.4)	3.0 (0.2)	3	7	2.3 (1.2)	2.0 (1.6)	3	8	2.3(1.2)	2.0 (1.3)
6	10	12	6.4 (0.7)	5.9 (0.3)	2	1	5.5 (0.7)	6.0 (.)	1	0	6.0 (.)	
9	13	14	9.0 (0.4)	9.0 (0.2)	5	1	9.4 (0.9)	9.0 (.)	3	1	9.7 (0.6)	9.0 (.)
12	10	9	12.0 (0.4)	12.0 (0.2)	3	6	11.7 (1.2)	12.5 (0.5)	3	6	11.7 (1.2)	12.2 (0.8)
15	4	7	15.2 (0.3)	15.1 (0.5)	5	5	15.4 (0.9)	14.8 (0.8)	4	4	15.3 (1.0)	15.3 (0.5)
18	10	8	18.5 (0.8)	18.2 (0.1)	2	5	19.5 (2.1)	19.2 (1.5)	4	4	19.8 (1.5)	19.3 (1.7)
24	3	4	24.3 (0.3)	24.2 (0.1)	7	6	27.1 (2.8)	24.8 (2.2)	7	5	26.6 (2.5)	24.4 (2.3)
36					17	12	36.2 (3.0)	36.0 (2.8)	10	8	37.1 (2.6)	36.5 (3.1)
48					5	2	45.6 (4.8)	44.5 (0.7)	3	2	47.7 (5.5)	44.5 (0.7)

Table 2. Landmarks on 3D photographs and 3D-CT.

3D photographs	**3D CT**
Pretragion (left and right)	Nasion
Lateral canthus (left and right)	Sella turcica
Medial canthus (left and right)	Frontozygomatic suture
Nasal bridge	External acoustic meatus
Nose tip	Frontal intersection of the pterion
Subnasal landmark at the transition of the nose and upper lip	Asterion
	External occipital protuberance
	Anterior fontanelle
	Posterior fontanelle
	Additional landmarks over coronal sutures, *n = 8*

of the cranium. These two points were used to indicate a horizontal measurement plane on the cranial shapes (Figure 2). The maximum cranial width was determined by a line perpendicular to the cephalic length. Cranial width divided by the cranial length and multiplied by 100 resulted in the cranial index (CI). The circumference was calculated using a plane crossing the points that define the cephalic length and cephalic width (Figure 2). For all modalities, the volume measurements were performed above the sella turcica–nasion plane. Total volume (TV) was measured on 3D photographs, CT-HT, and CT-ST. Intracranial volume (ICV) was measured in the CT-HT group. The anterior and posterior components of the TV were computed separately and divided at the position of the sella turcica. On the CT-HT scans, the metopic and sagittal suture lengths were measured over the surface in the

midsagittal axis of the reference frame. The coronal suture length was determined using 11 landmarks, from the left pterion to the right pterion. The lateral orbital distance (LOD) was defined as the distance between the left and right lateral orbital walls. IBM SPSS Statistics version 25.0 (IBM Corp., Armonk, NY, USA) was used for descriptive statistics. The mean, standard deviation, and 95% confidence intervals were calculated for these results. The Student t-test was used to compare plagiocephalometry measurements on CT-HT and the CT-ST, as well as any sex differences between the age groups.

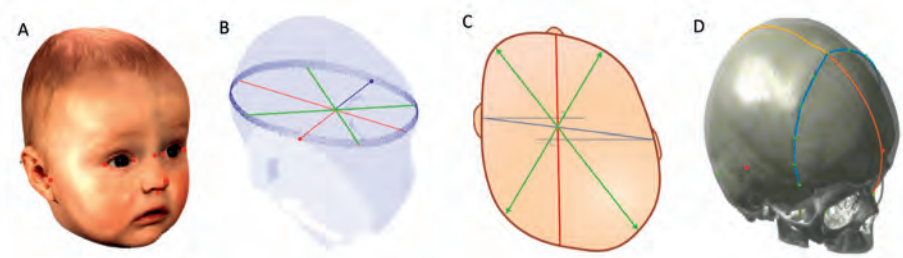

Figure 2: (A) Example of a 3D photograph with manually positioned landmarks (red). (B) The measurement plane was used to define the oblique diameters (green), cranial length, cranial width, and circumference (blue). (C) Illustration of the measurement method to determine the cranial asymmetry score and classification. (D) Lengths of the sutures measured over the CT-HT surface.

RESULTS

CRANIAL INDEX, WIDTH, LENGTH, AND CIRCUMFERENCE

The CI, width, length, and circumference measurements over time for the 3D photographs, CT-HT, and CT-ST are given in Table 3 and Figure 3. During the first 24 months of age, the CI fluctuated between 75 and 78 for all modalities. After this age, the CI increased in both CT-HT and CT-ST. Both the cranial width and cranial length increased over time for all modalities. CT-HT showed lower values compared to the other modalities. All modalities showed a sudden increase in both cranial width and length at around 18 months. The circumference, cranial width, and cranial height all followed the same pattern of growth. Differences between males and females were calculated for all measurements (Table 3, Figures 3–5).

Table 3. The number of subjects per age group, per sex, and per modality and the mean with standard deviation values for the cranial index, cranial width, cranial length, and circumference.

		n		Cranial width (mm)				Cranial length (mm)				Cranial index				Circumference (mm)			
				Male		Female		Male		Female		Male		Female		Male		Female	
Group (months)		Male	Female	Mean	SD	Mean	SD	Mean	SD	Mean	SD	Mean	SD	Mean	SD	Mean	SD	Mean	SD
3DP	3	14	12	114.4	3.6	111.4	6.0	146.0	5.3	143.6	4.5	78	4	78	5	*415.4	9.8	*405.3	9.9
	6	10	12	*124.8	5.3	*118.8	5.4	*159.9	4.1	*152.7	3.9	78	4	78	4	*451.1	8.1	*432.9	10.7
	9	13	14	*127.9	3.4	*122.6	4.2	*164.5	4.6	*159.6	4.8	78	2	77	3	*465.5	11.5	*450.1	11.4
	12	10	9	*129.3	3.2	*125.2	3.3	*171.0	4.4	*163.3	5.5	76	3	77	3	*477.5	8.8	*457.9	9.0
	15	4	7	131.1	4.1	129.4	4.1	168.3	3.4	168.3	5.6	78	4	77	4	474.5	4.0	474.0	11.9
	18	10	8	135.7	3.8	133.5	5.6	174.7	6.2	173.1	5.8	78	4	77	4	490.9	11.2	485.1	13.8
	24	3	4	139.7	6.8	134.9	5.8	182.4	4.6	178.7	5.1	77	6	76	4	510.7	3.2	498.0	11.2
CT-HT	3	3	7	95.9	12.0	100.4	11.1	128.1	11.6	129.8	17.8	74	5	78	4	360.8	37.4	366.5	46.2
	6	2	1	114.0	8.3	113.8	.	145.0	0.8	144.8	.	78	4	79	.	415.0	13.3	411.3	.
	9	5	1	119.6	4.7	114.1	.	151.5	6.3	160.4	.	78	6	71	.	435.3	8.9	443.6	.
	12	3	6	124.2	2.1	120.2	5.5	151.9	8.7	158.3	5.7	82	3	76	5	438.6	18.3	445.1	12.6
	15	5	5	125.3	4.2	120.6	6.5	161.9	6.6	161.3	6.1	78	4	75	4	458.8	13.4	452.0	15.4
	18	2	5	132.1	8.0	127.0	5.1	174.3	0.5	167.4	7.2	76	4	76	6	493.1	11.1	470.6	10.7
	24	7	6	128.1	6.5	124.0	3.8	168.8	3.5	167.1	7.2	76	4	74	2	472.4	10.2	464.5	16.2
	36	17	12	131.5	5.3	127.7	4.4	170.9	6.0	166.1	7.3	77	3	77	3	*480.7	15.3	*467.3	16.8
	48	5	2	134.9	3.9	135.9	3.0	174.9	3.9	177.1	4.1	78	3	78	2	491.6	6.2	491.9	13.2
CT-ST	3	3	8	99.9	12.8	102.3	9.7	135.2	9.7	131.3	11.6	73	6	78	6	377.2	32.5	372.7	32.3
	6	1	0	113.6	.	.	.	150.9	.	.	.	75	.	.	.	422.9	.	.	.
	9	3	1	125.4	7.6	119.0	.	161.3	4.6	166.4	.	77	8	72	.	459.2	3.5	459.9	.
	12	3	6	129.5	1.8	123.7	5.4	160.1	7.7	164.9	6.5	*81	3	*75	2	459.6	16.3	462.4	17.8
	15	4	4	132.5	2.0	124.7	7.6	168.0	7.5	171.2	6.3	*79	2	*73	2	478.1	16.4	474.8	18.6
	18	4	4	136.5	5.9	133.5	6.2	170.1	12.6	175.9	7.3	80	6	76	7	490.1	25.4	495.0	7.3
	24	7	5	134.8	5.7	131.5	4.1	176.3	3.7	175.6	7.3	77	3	75	2	493.6	9.8	488.2	16.3
	36	10	8	*137.9	5.5	*132.4	4.5	176.6	7.1	170.4	6.1	78	3	78	2	498.4	16.9	482.3	15.0
	48	3	2	144.2	2.7	141.9	1.5	182.7	6.1	183.2	1.2	80	3	79	2	516.4	9.6	511.3	7.1

* = statistical significant difference between means of male and female of given age group and modality ($p<0.05$).

VOLUMES

The ICV and the TV for all modalities are shown in Table 4 and Figure 6. The ICV of the CT-HT and TV of all modalities showed a near identical growth pattern compared to the corresponding circumference, cranial width, and cranial length over time. The posterior volume showed a similar curve and had a near constant ratio towards the TV within 2.7%.

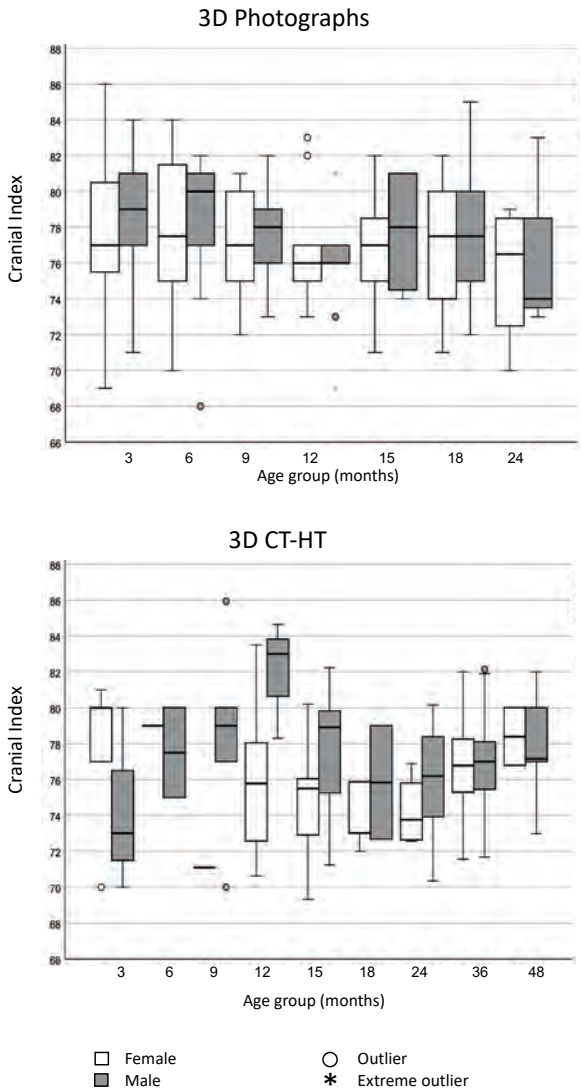

Figure 3: Cranial index (CI) boxplots, illustrating the range of CI values and the male to female ratio for the 3D photographs, and CT-HT.

SUTURE LENGTHS AND LATERAL ORBITAL DISTANCE

The 3D suture length measures for CT-HT over time are given in Table 5 and Figure 7. The strongest increases for all sutures and LOD occurred within the first 9 months of age. At 12 months, the length of all of the sutures and the LOD were equal or even smaller than those at 9 months. After a final increase in length at 15 months, no more growth was present in the dataset for all sutures and the LOD, and the lengths remained the same.

GROWTH MAPS

The growth maps showed the evolution of the cranial shape. Most growth (in millimetres) was seen between 3 and 6 months of age in the frontal and parietal regions, for both 3D photographs and CT-HT. Between 6 and 12 months of age, growth was more prominent in the anterior part of the skull, resulting in an elongation of the head. The posterior part of the skull developed more rapidly between 12 and 18 months. After 12 months, the overall growth reduced compared to the first 12 months. Therefore, a longer time interval of 12 to 24 months was used to create a growth map, which revealed that most growth was present in the frontal and occipital regions (Figures 8 and 9). *Two supplementary video files demonstrate the evolution of the cranium in 3D for the 3D photographs and CT-HT (available online).*

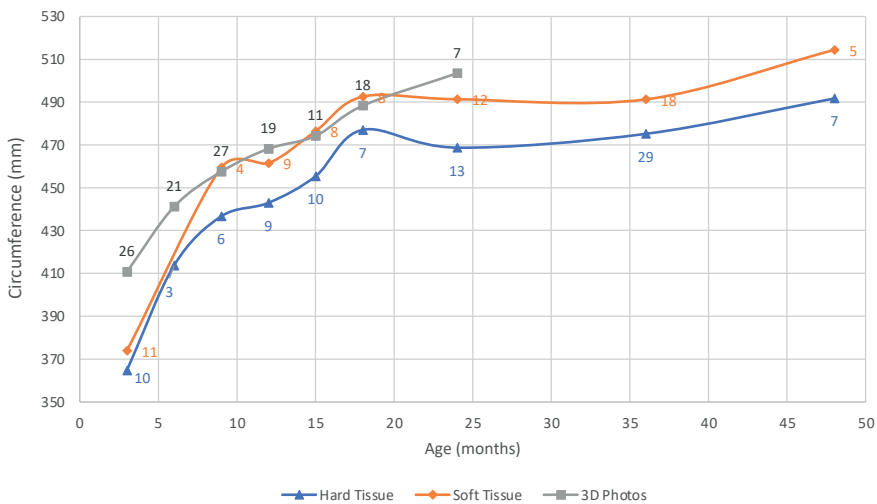

Figure 4: Circumference for all modalities. Coloured numbers indicate the number of subjects

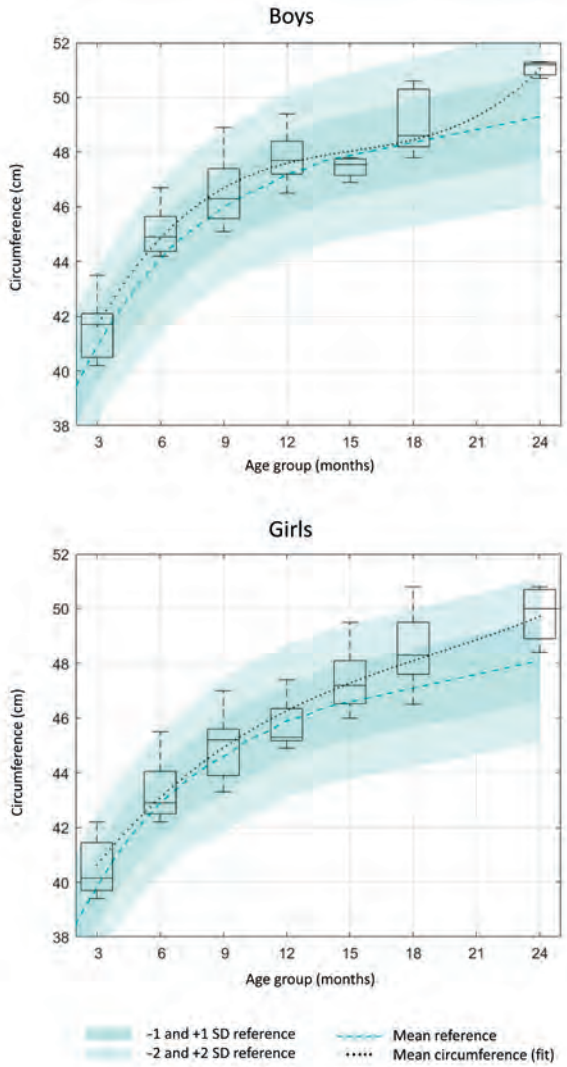

Figure 5: Boxplots of circumference measured on 3D photographs for boys and girls. Circumference reference values based on the Dutch cross-sectional growth study are plotted in the background.[22]

Table 4: The number of subjects per age group, per sex, and per modality and the mean and standard deviation values of the intracranial volume, the intracranial volume above the S–N plane, the total volume above the S–N plane, and the posterior total volume above the S–N plane.

		Number		Intracranial Volume (ml)				Intracranial Volume S-N (ml)				Total Volume S-N (ml)				Total Volume S-N Posterior (ml)			
	Group (months)	M	F	M		F		M		F		M		F		M		F	
				Mean	SD	Mean	SD	Mean	SD	Mean	SD	Mean	SD	Mean	SD	Mean	SD	Mean	SD
3D	3	14	12									*1002	54	*940	64	*630	29	*592	38
	6	10	12									*1281	74	*1140	67	*793	40	*713	40
	9	13	14									1394	92	1272	73	*856	52	*785	43
	12	10	9									1477	87	1334	62	*903	49	*824	40
	15	4	7									1474	54	1456	69	910	34	903	38
	18	10	8									1611	90	1563	126	992	49	962	72
	24	3	4									1770	44	1657	78	1097	30	1023	49
CT-HT	3	3	7	608	196	633	230	576	179	597	220	641	202	687	255	380	100	450	167
	6	2	1	882	153	862	.	833	163	820	.	928	166	932	.	580	81	599	.
	9	5	1	1025	34	1022	.	957	50	959	.	1103	47	1114	.	680	25	719	.
	12	3	6	1020	114	1089	77	959	108	1030	70	1111	135	1187	86	681	83	752	45
	15	5	5	1179	55	1114	124	*1114	56	*1014	60	*1305	71	*1193	59	820	78	779	99
	18	2	5	1395	88	1233	23	*1319	52	*1146	25	*1570	52	*1349	57	*957	64	*852	34
	24	7	6	1259	115	1204	92	1173	105	1134	72	1378	124	1322	86	894	53	838	103
	36	17	12	1302	112	1219	153	1215	100	1153	141	1451	106	1372	147	903	85	874	102
	48	5	2	1345	58	1423	111	1245	43	1300	67	1515	48	1556	81	970	27	1013	63
CT-ST	3	3	8									740	200	724	164	457	121	464	110
	6	1	0									925	.	.	.	591	.	.	.
	9	3	1									1290	49	1238	.	779	9	791	.
	12	3	6									1278	125	1328	141	778	78	835	88
	15	4	4									1483	100	1363	79	923	87	897	99
	18	4	4									1574	199	1531	62	975	95	968	28
	24	7	5									1565	134	1537	84	1007	64	968	91
	36	10	8									1654	130	1527	169	1010	96	953	101
	48	3	2									1755	71	1764	27	1110	53	1132	31

* = statistical significant difference between means of male and female of given age group and modality ($p<0.05$).

Table 5. The number of subjects per age group, per sex, and per modality and the mean and standard deviation values of the 2D and 3D distances measured on the CT-HT.

Group (months)	Number		Lateral Orbital Distance (mm)				3D Distance Metopica Suture (mm)				3D Distance Coronal Sutures (mm)			
			M		F		M		F		M		F	
	M	F	Mean	SD	Mean	SD	Mean	SD	Mean	SD	Mean	SD	Mean	SD
3	3	7	65.5	7.6	64.6	6.8	86.8	10.2	86.8	11.3	181.5	25.4	180.5	19.8
6	2	1	72.3	4.8	74.1	.	98.9	5.2	99.5	.	205.1	15.1	207.3	.
9	5	1	77.3	1.3	78.4	.	106.9	4.5	108.1	.	216.8	7.9	213.9	.
12	3	6	75.7	3.9	76.7	3.1	103.1	9.8	109.1	5.8	215.2	12.7	212.8	7.0
15	5	5	*83.1	2.0	*78.5	2.2	114.3	4.9	114.6	5.4	229.0	7.2	221.0	6.9
18	2	5	85.2	3.0	80.5	2.5	*121.0	1.7	*115.1	2.7	*255.6	14.1	*221.8	5.6
24	7	6	82.1	1.8	80.3	2.5	116.2	8.4	115.8	6.3	227.6	11.4	220.9	9.1
36	17	12	81.5	3.6	80.6	3.3	121.9	7.4	118.7	6.8	230.1	12.6	222.7	12.6
48	5	2	83.8	4.3	84.4	4.9	122.9	3.0	127.3	5.2	237.5	5.4	227.9	13.3

Group (months)	n		3D Distance Sagittal suture (mm)				3D Distance Posterior Fontanelle - Occiput (mm)				3D Distance Nasion - Occiput (mm)			
			Male		Female		Male		Female		Male		Female	
	Male	Female	Mean	SD	Mean	SD	Mean	SD	Mean	SD	Mean	SD	Mean	SD
3	3	7	101.7	6.0	100.0	10.9	46.9	11.4	48.0	16.2	235.4	25.2	234.7	35.2
6	2	1	109.9	1.0	106.4	.	52.0	10.3	55.4	.	260.7	14.4	261.4	.
9	5	1	116.3	6.1	109.1	.	60.1	6.8	72.0	.	283.2	7.6	289.2	.
12	3	6	114.8	7.4	113.8	5.6	58.8	2.0	65.9	13.9	276.5	10.8	288.9	13.8
15	5	5	117.8	12.6	120.9	9.4	63.8	11.1	59.9	6.8	295.8	8.4	295.3	16.5
18	2	5	127.2	0.4	126.7	8.4	65.5	3.0	62.1	6.1	313.8	1.6	304.0	9.2
24	7	6	122.6	11.5	124.9	6.2	64.2	10.5	55.9	9.0	303.0	13.2	296.6	14.3
36	17	12	121.5	8.5	121.7	7.7	64.8	15.7	60.8	9.4	308.2	11.3	301.2	19.4
48	5	2	123.1	6.9	129.5	0.6	70.0	11.5	66.9	7.2	316.0	7.8	323.7	11.8

* = statistical significant difference between means of male and female of given age group and modality ($p<0.05$)

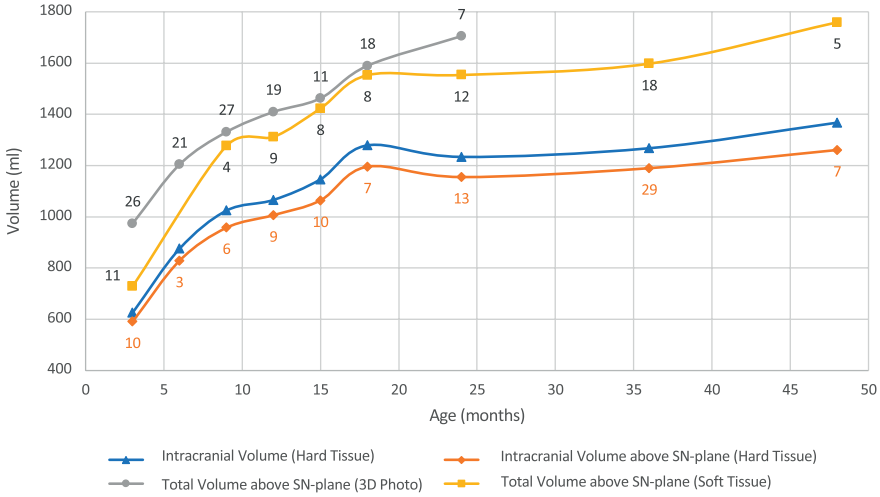

Figure 6: Volume measured on CT-HT, CT-ST, and 3D photographs. Coloured numbers indicate the numbers of subjects used for each age group.

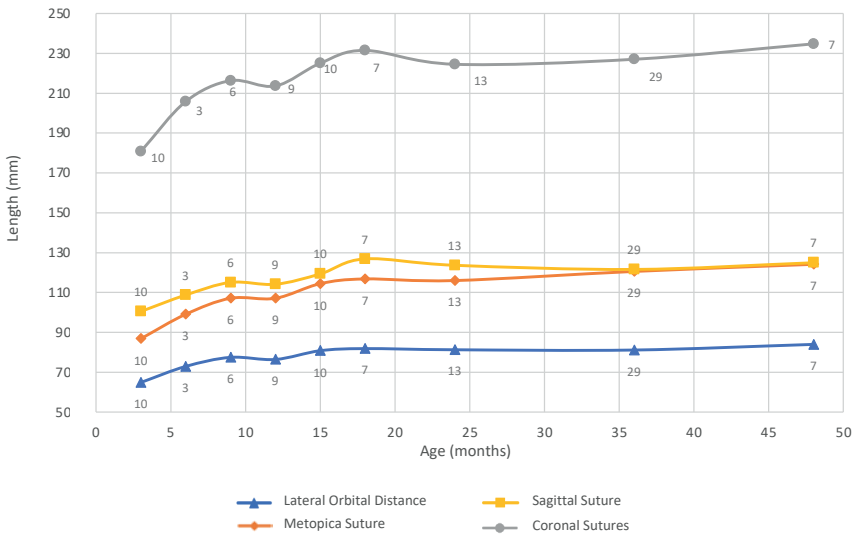

Figure 7: Suture length measured on CT-HT. Coloured numbers indicate the numbers of subjects used for each age group.

DISCUSSION

In this study, the normal growth of the cranium during the first years of life was evaluated extensively using 3D stereophotogrammetry and 3D-CT. Early detection is key in endoscopically assisted craniosynostosis surgery, and normative reference data could be used for adequate and early detection of abnormalities. [2,11] In addition, these reference data could be used by clinical experts to make follow-up assessment during remodelling helmet therapy more objective.[2,13] Also, the data provide a reference for preoperative planning of open reconstructive craniosynostosis surgery in which a virtual reconstruction of the new cranial shape and volume is made.[14] Therefore, this study addresses the need for normative cranial evolution data for detection, follow-up, and planning in craniosynostosis.

Consistent with the literature, the growth maps of the 3D photographs and CT-HT revealed rapid expansion of the cranium in the younger age groups.[1,9,15] Between 3 and 6 months, a strong focus of growth was found to be located in the frontal region and in the central parietal regions, indicating the growth kernels. The locations of the sagittal and coronal sutures were clearly indicated by the colours of the growth maps, emphasizing the importance of sutures for growth of the cranium.[16,17] The focus of growth in the 12–24 months growth map was located in the occipital head region, close to the site of the cerebellum. The timing of the cerebellum volume increase corresponds with the timing of infants starting to walk and develop their balance and muscle coordination functions. Although the relationship between brain functionality and volume is not clear, brain volume might influence brain development and this might be an explanation for the volume increase in this region.[18] Using magnetic resonance imaging (MRI) data, a disproportionate enlargement of the cerebellum during the first 2 years was described by Knickmeyer et al., although this enlargement was even more prominent in the first year.[19]

In the 12–24 months interval, the 3D photographs demonstrated 3–4 mm more frontal growth compared to the CT-HT group. Population and age differences, as well as more and longer hair might have resulted in a greater volume at the back of the head. This larger posterior volume could result in a more posteriorly located CCFP. Consequently, this would lead to a more anterior alignment of the cranial shapes and thus erroneously demonstrate more frontal growth.

The mean cranial shapes created in this study could additionally be used for the evaluation of individual cases. The average cranial shape of a specific age group could be compared directly to 3D photographs or 3D-CT scans of patients and allow a direct evaluation of the cranial shape in 3D. In addition to the graphs and tables, the supplementary videos (Online Complementary Material) provide an optimal insight and understanding of the normal evolution over time. An enormous increase in the cranial size can be noted, while the colours highlight the difference in growth focus during the first 24 months of life. This study is novel in using a large number of time intervals to evaluate cranial growth in 3D.

All CI measurements within the first 24 months of age were in the range of 75 to 78. In line with the literature, the 3D photographs, CT-HT, and CT-ST all demonstrated lower values at 24 months.[9,20] After this period, CT-HT and CT-ST respectively showed an increase in CI up until the age of 48 months towards 78 and 80, which is in line with the findings of Farkas et al.[21] and Dekaban.[4] The CI results are lower than those reported by Meyer-Marcotty et al., who established an average CI of 84 at 6 months of age and 82 at 12 months of age, as measured on 3D photographs of healthy infants.[8] Likus et al. also presented a larger CI of 83 on average, measured on CT scans[1]. Delye et al. measured a mean CI of 84, on CT scans of healthy infants of 6 and 12 months.[2] This indicates that the subjects used in this study have slightly more elongated head shapes. We therefore believe it is important to establish reference measurements obtained from a population that is a good representation of the population of patients treated in a local centre.

Head circumference measured on 3D photographs showed almost identical trends when compared to the nationwide growth study in the Netherlands, which included 14,500 boys and girls of Dutch origin (Figure 5).[22] In the present study, only the data for the 24 months age group of both sexes showed a +1 standard deviation higher circumference, which could also be a consequence of hair in the subjects at this age. Since sexual dimorphism is present at an early stage of life, a distinction between males and females was made in this study. [23,24] Meyer-Marcotty et al. have already described significantly larger values for length, circumference, and volume increase between 6 and 12 months of life in males.[8,9] Joffe et al. measured slightly larger cranial circumferences at birth, 6 months, and 12 months in males.[25] Although these studies used fewer time intervals, the sexual dimorphism with males presenting larger values is in line with the findings

in this study for the 3D photographs during the first 12 months of life (Table 3 and Figure 5). After this period, the results did not reveal a significant difference between males and females. This is in contrast with studies that have stated that sexual dimorphism becomes more pronounced at an older age.[23] This discrepancy might be explained by the smaller sample size of the 18 months and 24 months age groups in the present study or by the fact that 3D photographs are more prone to artefacts at an older age because of the hair volume. Nevertheless, in contrast to expectations, no significant difference was found in the CT-HT and CT-ST groups (Table3). A possible explanation may be the smaller sample sizes of these groups compared to the 3D photographs group.

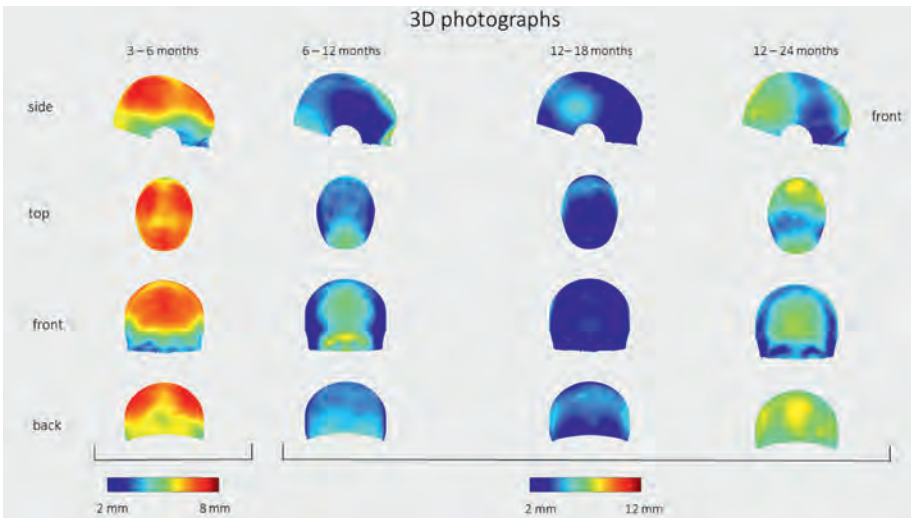

Figure 8: Growth maps of 3D photographs, illustrating the focus of growth between the different time intervals.

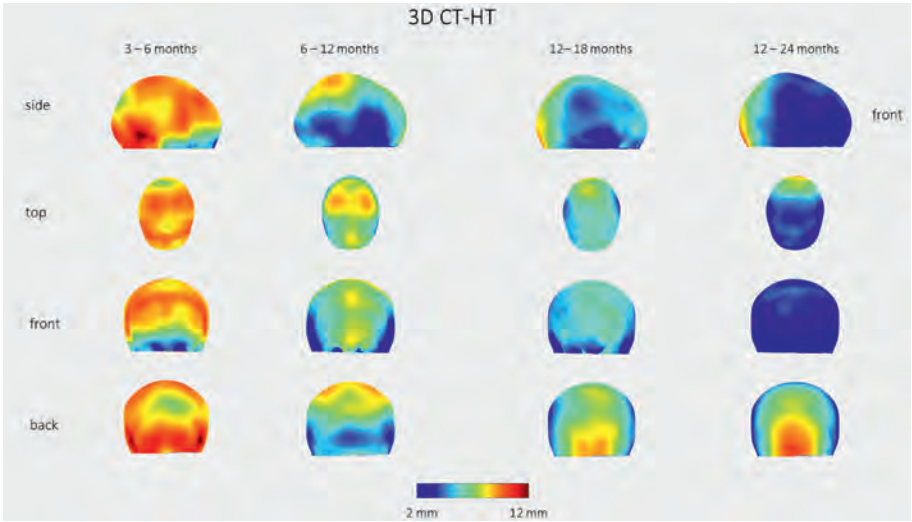

Figure 9: Growth maps of 3D-CT, illustrating the focus of growth between the different time intervals.

Volume measurements based on head circumference have frequently been described.[26,27] A strong correlation between head circumference and the ICV was found in this study and could be calculated using Equation 1. The high correlation of r = 0.987(P < 0.001) means that this method is also feasible for bedside measures. The total volume graph (Figure 6) demonstrates a clear correlation between the increase in TV in the 3D photographs and the increase in CT-HT and CT-ST. Due to the soft tissue, the CT-ST and 3D photographs displayed a larger volume. The latter even showed slightly higher volumes, which can be explained by artefacts such as hair.

Equation 1: $$V_{intracranial} = 6 * 10^{-5} l^{2.7272}_{circumference}$$

The total ICV and the ICV above the sella turcica–nasion plane showed a strong and significant correlation (r = 0.993, P < 0.001). The TV above the sella turcica–nasion plane and the ICV above the sella turcica–nasion plane also had a strong significant correlation (r = 0.987, P < 0.001), making these volumes good estimates of each other. Comparing the ICV, other studies have presented identical growth curves for the first 12 months,[28,29] although Kamdar et al. measured smaller volumes of around 200 ml for all ages on CT scans.[15,28,29] The present study data suggest more rapid growth in the first 18 months of life, with a peak at 18 months. However,

the 18 months age group only included seven scans and thus the data might be less accurate compared to the 15 months and 24 months age group data. In addition, a similar peak for the 18 months group was seen for suture lengths and the circumference measurements based on the CT datasets. This suggests that relatively large heads were included in this group.

Cranial volume is an important factor for the evaluation of cranial surgery. However, different populations, methods, and results are presented in the literature.[28,30,31] Therefore, it is important to interpret the volume data according to the methodology of image acquisition and analysis used. This study used different image modalities, yet the same analysis methods were used. This makes evaluation and follow-up more adequate and emphasizes the importance of this study.

In this study, a total of 382 3D photographs and CT scans were selected for initial inclusion. Due to the strict exclusion criteria, only 300 images were used for final analysis, which resulted in certain age groups with smaller numbers. The 6-month CTST group contained only one scan and was therefore excluded from further analysis. In addition, distinction between males and females resulted in even more samples of a size that was too small to analyse. Yet, the benefit of using stringent exclusion criteria is a clean and pure dataset describing only normal cranial shapes, which is therefore appropriate for surgical evaluation and follow-up.

CONCLUSION

In conclusion, this study analysed the growth pattern of the cranial shape of infants during the first years of life using 3D stereophotogrammetry and 3D-CT. Advanced 3D evaluation demonstrated a focus of growth in the anterior region of the head in the first year of life and more posterior growth after the age of 1 year. Normative data are presented which are of multidisciplinary interest and could be used by paediatricians and maternity consultation clinics to evaluate the growth and shape of infant heads.

ADDITIONAL INFORMATION

No specific funding support was used for this project. The authors have no conflicts of interest relevant to this article to disclose. The study was reviewed by the Ethics Committee on the basis of the Dutch Code of Conduct for Health Research, the Dutch Code of Conduct for Responsible Use, the Dutch Personal Data Protection Act, and the Medical Treatment Agreement Act (File number: CMO:2018-4935). This study did not fall within the remit of the Medical Research Involving Human Subjects Act (WMO). The Ethics Committee passed a positive judgement on the study. Written patient consent was obtained.

APPENDIX

The oblique diameter difference index (ODDI) and cranial proportion index (CPI) described in the plagiocephalometry method by van Vlimmeren et al. was used in this study to exclude asymmetrical cranial shapes.[1] The general exclusion criteria presented in that study were applicable for soft tissue only. However, since the soft tissue (CT-ST) shapes in this study were more prone for artefacts, the hard tissue (CT-HT) shapes were instead used to determine exclusion. Because it was expected that the effect of ODDI and CPI can be structurally different when measured on CT-HT, a correlation and offset factor between the artefact-free CT-ST and CT-HT was calculated for the ODDI and CPI measurements. In total, 97 CT-scans were used to determine the ODDI and CPI on both the CT-HT and the CT-ST shapes and a possible correlation and offset was investigated.

The mean ODDI was 103.1 (SD=2.3) for the CT-HT scans and 102.8 (SD=2.2) for the corresponding CT-ST scans. The paired correlation showed a statistically significant ($p<0.001$) and strong positive correlation for both the ODDI ($r=0.968$) and CPI ($r=0.984$). There was a statistically significant average difference for the ODDI ($t96=4.456$, $p< 0.001$) but no statistical significant average difference for the CPI ($t96=1.961$, $p=0.053$). Therefore, only an offset for the ODDI was applied which was based on the difference of the mean (+0.3). This resulted in a new ODDI of 104.8 and a CPI of 90 to be used as a cut-off for the CT-HT scans.

Supplementary material related to this article can be found, in the online version, at doi: https://doi.org/10.1016/j.ijom.2019. 10.012.

REFERENCES

1. Likus W, Bajor G, Baron J, Markowski J, Milka D, Lepich T. Cephalic index in the first three years of life: study of children with normal brain development based on computed tomography. Sci World J 2014;2014:1–6. http://dx.doi.org/10.1155/2014/502836.
2. Delye H, Clijmans T, Mommaerts MY, Sloten JV, Goffin J. Creating a normative database of age-specific 3D geometrical data, bone density, and bone thickness of the developing skull: a pilot study. J Neurosurg Pediatr 2015;16:687–702. http://dx.doi.org/ 10.3171/2015.4.PEDS1493.
3. McGarry A, Dixon MT, Greig RJ, Hamilton DRL, Sexton S, Smart H. Head shape measurement standards and cranial orthoses in the treatment of infants with deformational plagiocephaly. Dev Med Child Neurol 2008;50:568–76. http://dx.doi.org/10.1111/ j.1469-8749.2008.03017.x.
4. Dekaban AS. Tables of cranial and orbital measurements, cranial volume, and derived indexes in males and females from 7 days to 20 years of age. Ann Neurol 1977;2:485–91. http://dx.doi.org/10.1002/ana.410020607.
5. Bastir M, Rosas A, O'Higgins P. Craniofacial levels and the morphological maturation of the human skull. J Anat 2006;209:637–54.
6. Van Vlimmeren LA, Takken T, Van Adrichem LNA, Van Der Graaf Y, Helders PJM, Engelbert RHH. Plagiocephalometry: a non-invasive method to quantify asymmetry of the skull; a reliability study. Eur J Pediatr 2006;165:149–57. http://dx.doi.org/ 10.1007/s00431-005-0011-1.
7. van Lindert EJ, Siepel FJ, Delye H, Ettema AM, Berge´ SJ, Maal TJJ, Borstlap WA. Validation of cephalic index measurements in scaphocephaly. Childs Nerv Syst 2013;29:1007–14. http://dx.doi.org/10.1007/s00381-013-2059-y.
8. Meyer-Marcotty P, Bo¨hm H, Linz C, Kochel J, Stellzig-Eisenhauer A, Schweitzer T. Three-dimensional analysis of cranial growth from 6 to 12 months of age. Eur J Orthod 2014;36:489–96. http://dx.doi.org/10.1093/ejo/cjt010.
9. Meyer-Marcotty P, Kunz F, Schweitzer T, Wachter B, Bo¨hm H, Waßmuth N, Linz C. Cranial growth in infants—a longitudinal three-dimensional analysis of the first months of life. J Craniomaxillofac Surg 2018;46:987–93. http://dx.doi.org/10.1016/ j.jcms.2018.04.009.
10. de Jong G, Tolhuisen M, Meulstee J, Meulstee JW, van der Heijden F, van Lindert E, Borstlap WA, Maal TJJ, Delye H. Radiation-free 3D head shape and volume evaluation after endoscopically assisted strip craniectomy followed by helmet therapy for trigonocephaly. J Craniomaxillofac Surg 2017;45:661–71. http:// dx.doi.org/10.1016/j.jcms.2017.02.007.
11. Meulstee JW, Verhamme LM, Borstlap WA, VanderHeijdenF, De JongGA, XiT,Berge´ SJ, Delye H, Maal TJJ. A new method for three- dimensional evaluation of the cranial shape and the automatic identification of craniosynostosis using 3D stereophotogrammetry. Int J Oral Maxillofac Surg 2017;46:819–26. http://dx.doi.org/10.1016/j.ijom.2017.03.017.
12. De Jong GA, Maal TJJ, Delye H. The computed cranial focal point. J Craniomaxillofac Surg 2015;43:1737–42. http://dx.doi.org/ 10.1016/j.jcms.2015.08.023.
13. Delye HHK, Arts S, Borstlap WA, Blok LM, Driessen JJ, Meulstee JW, Maal TJJ, van Lindert EJ. Endoscopically assisted craniosynostosis surgery (EACS): The Craniofacial Team Nijmegen experience. J Craniomaxillofac Surg 2016;44:1029–36. http://dx.doi. org/10.1016/j.jcms.2016.05.014.
14. Chim H, Wetjen N, Mardini S. Virtual surgical planning in craniofacial surgery. Semin Plast Surg 2014;28:150–8. http://dx.doi.org/ 10.1055/s-0034-1384811.
15. Kamdar MR, Gomez RA, Ascherman JA. Intracranial volumes in a large series of healthy children. Plast Reconstr Surg 2009;124:2072–5. http://dx.doi.org/10.1097/ PRS.0b013e3181bcefc4.
16. Opperman LA. Cranial sutures as intramembranous bone growth sites. Dev Dyn 2000;219:472–85. http://dx.doi.org/10.1002/1097-0177(2000)9999:9999<:: AID-DVDY1073>3.0.CO;2-F.
17. Jin SW, Sim KB, Kim SD. Development and growth of the normal cranial vault : an embryologic review. J Korean Neurosurg Soc 2016;59:192–6. http://dx.doi.org/ 10.3340/jkns.2016.59.3.192.
18. Leingartner A, Thuret S, Kroll TT, Chou SJ, Leasure JL, Gage FH, O'Leary DD. Cortical area size dictates performance at modality- specific behaviors. Proc Natl Acad Sci U S A 2007;104:4153–8. http://dx.doi.org/ 10.1073/pnas.0611723104.

19. Knickmeyer RC, Gouttard S, Kang C, Evans D, Wilber K, Smith JK, Hamer RM, Lin W, Gerig G, Gilmore JH. A structural MRI study of humanbrain development from birth to 2 years. J Neurosci 2008;28:12176–82. http://dx.doi. org/10.1523/JNEUROSCI.3479-08.2008.

20. Wilbrand JF, Kaps K, Tabak D, Bierther U, Wilbrand M, Neubauer BA, Pons-Kuehne- mann J, Howaldt HP, Hahn A. Normal head shape parameters in the first 2 years of life and effect of helmet therapy. Neuropedia- trics 2017;48:432–41. http://dx.doi.org/10.1055/s-0037-1604482.

21. Farkas LG, Posnick JC, Hreczko TM. Anthropometric growth study of the head. Cleft Palate Craniofac J 1992;29:303–8. http:// dx.doi.org/10.1597/1545-1569(1992) 029<0303:AGSOTH>2.3.CO;2.

22. Fredriks AM, van Buuren S, Burgmeijer RJ, Meulmeester JF, Beuker RJ, Brugman E, Roede MJ, Verloove-Vanhorick SP, Wit JM. Continuing positive secular growth change in The Netherlands 1955–1997. Pediatr Res 2000;47:316–23. http://dx.doi. org/10.1203/00006450-200003000-00006.

23. BulyginaE,MitteroeckerP, AielloL.Ontogeny of facial dimorphism and patterns of individual developmentwithin onehuman population. Am J Phys Anthropol 2006;131:432–43. http://dx. doi. org/10.1002/ajpa.20317.

24. Matthews H, Penington T, Saey I, Halliday J, Muggli E, Claes P. Spatially dense morphometrics of craniofacial sexual dimorphism in 1-year-olds. J Anat 2016;229:549–59. http:// dx.doi.org/10.1111/ joa.12507.

25. Joffe TH, Tarantal AF, Rice K, Leland M, Oerke AK, Rodeck C, Geary M, Hindmarsh P, Wells JC, Aiello LC. Fetal and infant head circumference sexual dimorphism in primates. Am J Phys Anthropol 2005;126:97–110. http://dx.doi.org/10.1002/ajpa.20035.

26. Martini M, Klausing A, Lu¨chters G, Heim N, Messing-Ju¨nger M. Head circumference—a useful single parameter for skull volume development in cranial growth analysis? Head Face Med 2018;14:3. http:// dx.doi. org/10.1186/s13005-017-0159-8.

27. Lindley AA, Benson JE, Grimes C, Cole TM, Herman AA. The relationship in neonates between clinically measured head circumference and brain volume estimated from head CT-scans. Early Hum Dev 1999;56:17–29. http://dx.doi.org/10.1016/ s0378-3782(99)00033-x.

28. Abbott AH, Netherway DJ, Niemann DB, Clark B, Yamamoto M, Cole J, Hanieh A, Moore MH, David DJ. CT-determined intra- cranial volume for a normal population. J Craniofac Surg 2000;11:211–23.

29. van Veelen MLC, Jippes M, Carolina JCA, de Rooi J, Dirven CMF, van Adrichem LNA, Mathijssen IM. Volume measurements on three-dimensional photogrammetry after extended strip versus total cranial remodeling for sagittal synostosis: a comparative cohort study. J Craniomaxillofac Surg 2016;44:1713–8. http://dx.doi.org/10.1016/ J.JCMS.2016.07.029.

30. Freudlsperger C, Steinmacher S, Ba¨chli H, Somlo E, Hoffmann J, Engel M. Metopic synostosis: measuring intracranial volume change following fronto-orbital advancement using three-dimensional photogrammetry. J Craniomaxillofac Surg 2015;43:593–8.http://dx.doi.org/10.1016/j.jcms.2015.02.017.

31. Seeberger R, Hoffmann J, Freudlsperger C, Berger M, Bodem J, Horn D, Engel M. Intracranial volume (ICV) in isolated sagittal craniosynostosis measured by 3D photocephalometry: a new perspective on a controversial issue. J Craniomaxillofac Surg 2016;44:626–31. http://dx.doi.org/10.1016/j.jcms.2016.01.02

CHAPTER 3

A new method for 3D evaluation of the cranial shape and the automatic identification of craniosynostosis using 3D stereophotogrammetry

Jene Meulstee
Luc Verhamme
Wilfred Borstlap
Ferdi van der Heijden
Guido de Jong
Tong Xi
Stefaan Bergé
Hans Delye
Thomas Maal

International Journal of Oral & Maxillofacial Surgery
Published: April 2017
DOI: 10.1016/j.ijom.2017.03.017

ABSTRACT

Craniosynostosis is a congenital defect which can result in abnormal cranial morphology. Three dimensional (3D) stereophotogrammetry is potentially an ideal technique for the evaluation of cranial morphology and diagnosis of craniosynostosis because it is fast and harmless. This study presents a new method for objective characterization of the morphological abnormalities of scaphocephaly and trigonocephaly patients using 3D photographs of patients and healthy controls.

Sixty 3D photographs of healthy controls in the age range of 3–6 months were superimposed and scaled. Principal component analysis (PCA) was applied to find the mean cranial shape and the cranial shape variation in this normal population. 3D photographs of 20 scaphocephaly and 20 trigonocephaly patients were analysed by this PCA model to test whether cranial deformities of scaphocephaly and trigonocephaly patients could be objectively identified.

PCA was used to find the mean cranial shape and the cranial shape variation in the normal population. The PCA model was able to significantly distinguish scaphocephaly and trigonocephaly patients from the normal population.

3D stereophotogrammetry in combination with the presented method can be used to objectively identify and classify the cranial shape of healthy newborns, scaphocephaly and trigonocephaly patients.

INTRODUCTION

Craniosynostosis is a congenital defect that causes one or more sutures of the newborn's skull to ossify prematurely. As a result, normal skull growth is impeded in the direction perpendicular to the affected sutures, resulting in abnormal cranial morphology. In addition to abnormal skull growth, craniosynostosis can result in complications such as intracranial hypertension, visual impairment, and limitation of brain growth.[1–3] To prevent or resolve these complications, surgical treatment is required. Today, a variety of surgical treatment options are available. The most commonly used types of surgery for patients with a single-suture craniosynostosis include cranial vault remodelling, spring-mediated cranioplasty and endoscopically assisted strip craniectomy followed by remolding helmet therapy.[4,5] Because there is still a lack of a proper validated method to evaluate the cranial vault of craniosynostosis patients and to establish an objective quantification of the severity of the abnormality, there is no consensus on which of the treatment options provides the best longterm functional and aesthetic outcome. Therefore, the follow-up of craniosynostosis treatment and finally the determination of the optimal surgical procedure remains a rather subjective matter.[6–8] Three-dimensional (3D) stereophotogrammetry is a fast and patient-friendly method to evaluate the complete 3D morphology of the cranial shape. Because no potentially harmful ionizing radiation is required, 3D stereophotogrammetry is an ideal technique to acquire a 3D image of the cranial shape for diagnosis and during follow-up. The aim of this study was to present a new method for the objective evaluation of the 3D morphology of the cranial shape. 3D photographs of a healthy control group were used to establish the normal cranial shape and its variations. Scaphocephaly and trigonocephaly patients were compared with the controls and principal component analysis (PCA) was used to test if there was a significant difference between the groups.

PATIENTS AND METHODS

SUBJECTS

A total of 100 3D stereophotographs were included in this prospective study. This dataset included 20 3D photographs of patients with scaphocephaly and 20 3D photographs of patients with trigonocephaly. The included scaphocephaly and

trigonocephaly patients suffering from isolated, non-syndromic premature closure of respectively the sagittal or the metopic suture. Diagnosis was confirmed using a computed tomography (CT) scan. The pre-operative 3D photographs of the scaphocephaly patients were taken at an average age of 4.1 months (range 2.9–5.1 months) and the 3D photographs of the trigonocephaly patients at an average age of 4.0 months (range 3.0–5.1 months). A total of 60 3D photographs of healthy controls were included in the age range of 3–6 months. All control subjects were without known associated anomalies. The study protocol was approved by the medical ethical commission of the institution in which the study was carried out: 17934 file number NL17934.091.07

Table 1: Landmark positions

Landmark positions
Pretragion (left and right)
External cantion (left and right)
Internal cantion (left and right)
Nasal bridge
Subnasal landmark at the transition of the nose and upper lip

DATA ACQUISITION

Three-dimensional stereophotogrammetry (3dMDCranial 3DMD, Atlanta, USA) with a five-pod configuration was used for image acquisition. The 3D photographs of all subjects were acquired by a trained photographer. In case the reflection of hair caused artefacts on the 3D photograph, the subjects were photographed with a tight nylon skull cap. All 3D photographs of the patients were acquired one day prior to surgery. Severe quality inconsistency in the acquired 3D photographs was an exclusion criterion.

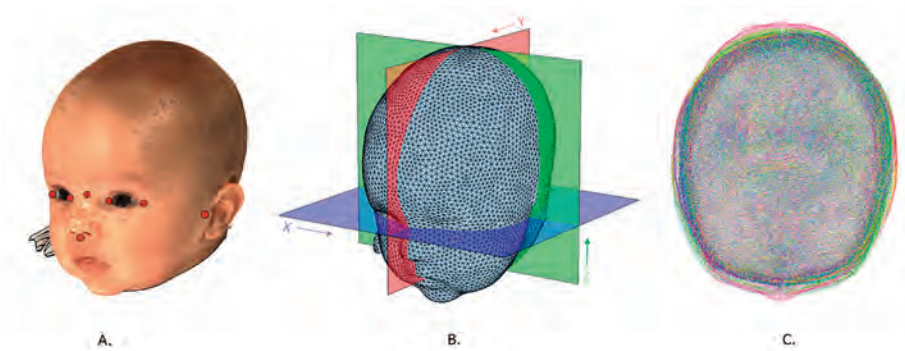

Figure 11: Overview of the three-dimensional (3D) superimposition method. (A) 3D photograph with texture. The red points indicate the landmark positions according to Table 1. (B) Landmarks and computed cranial focal point method used for superposition of the cranial shapes. Reference planes were used for alignment. (C) Top view of the final registration and scaling of the cranial shapes.

SUPERIMPOSITION OF 3D PHOTOGRAPHS

For adequate analysis, every 3D photograph needed to be positioned in the same coordinate system and therefore rotations and translations needed to be eliminated. To achieve this, all 3D photographs were imported into the 3DMDPatient software (3dMD, Atlanta, GA, USA). Eight anatomical landmarks were manually identified on the 3D photographs (Table 1). The 3D photographs and landmarks were subsequently exported to the technical computing software Matlab (MATLAB v2012b, The Mathworks Inc., Natick, MA, USA). In Matlab, a horizontal plane defined by the exocanthion, endocantion, and pretragion points and a vertical plane, perpendicular to the horizontal plane and positioned through the subnasal point were generated. Based on the method described by Brons et al., the planes were used to eliminate the rotations[9] (Figure 1). All 3D photographs were translated to the origin of the reference frame using the computed cranial focal point (CCFP) presented by de Jong et al.[10] This resulted in a dataset of 3D stereophotographs in the same coordinate system without rotational and translational differences.

RESAMPLING AND SCALING

All the aligned and correctly positioned 3D photographs consisted of a different number of vertices (3D points). For further analysis of the 3D photographs it was required to create mesh data with the same number of vertices and therefore a resampling was applied. Resampling was done using a reference shape, consisting of a hemi-icosphere in the form of a cranial shape and a raycasting algorithm.[11] A total of 4,501 rays, cast from the origin of the reference shape, were used and therefore every cranial shape consisted of 4,501 vertices after resampling. The volume of every cranial shape was calculated using the horizontal plane as a lower boundary. Finally, every cranial shape was scaled towards the same volume to eliminate differences in cranial size. A scaling, identical in every direction was used which adjusted only the size and preserved the shape of the modified 3D photographs.

PRINCIPAL COMPONENT ANALYSIS

PCA is a statistical method which can describe a large number of high dimensional data with a smaller number of relevant parameters.[12–14] 3D photographs of a population can be analysed by PCA to find and isolate the different variations of the 3D shapes in this population. PCA can be used to extract only the relevant and most prominent variations, such as the length of the skull and disregard minor

variations, such as artefacts in the 3D photographs caused by hair. The directions of the isolated variations are called principal components (PCs). The most prominent variation in the population is described by principal component 1 (PC1), followed by principal component 2 (PC2) etc. The value of a PC describes the deviation from the mean shape in standard deviations (SD). The effect of a PC can be visualized by simulating a value of -2 and 2 standard deviations. In this study, PCA was applied to the modified 3D photographs of the control population. This resulted in a set of PCs labelling the directions of variation in the control population. The cranial shape of every individual can be reconstructed by these PCs and the found values (describing the magnitude of every PC). The morphological effect of the first two PCs is shown in Figure 2. The PCs, calculated from the control population, were then applied to the scaphocephaly patients and the trigonocephaly patients. This was done to determine if, and in which direction, the patients were different from the controls. A mathematical description is given in the Appendix. A significant difference in values of the PCs was used to distinguish a scaphocephaly or trigonocephaly shape from a normal cranial shape. Four PCs that exposed the most prominent differences between the controls and scaphocephaly patients were selected. Likewise, four PCs that revealed a difference between the controls and trigonocephaly patients were selected[14].

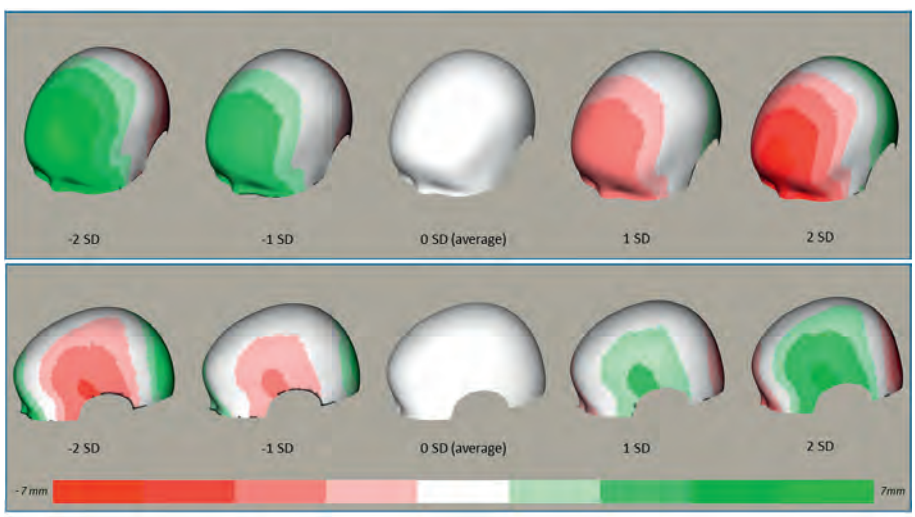

Figure 2: Overview of the effect of principal component 1 (upper) and principal component 2 (lower) of the control population. A +2 and -2 SD was applied to illustrate the effect. Green indicates volume increase and red a volume decrease.

STATISTICAL ANALYSIS

IBM SPSS software (version 22.0.0.1, IBM corp., Armonk, NY, USA) was used to perform the statistical data analysis. Descriptive statistics were used to explore the variation of the values in the PC's for the three different groups. The absolute values (in SD) of the four selected PCs were summed for every control and for every patient. A Student paired t test was applied to test for significant differences between the control population and the patient population based on the four selected PCs. The level of significance was set at 5% ($p \leq 0.05$).

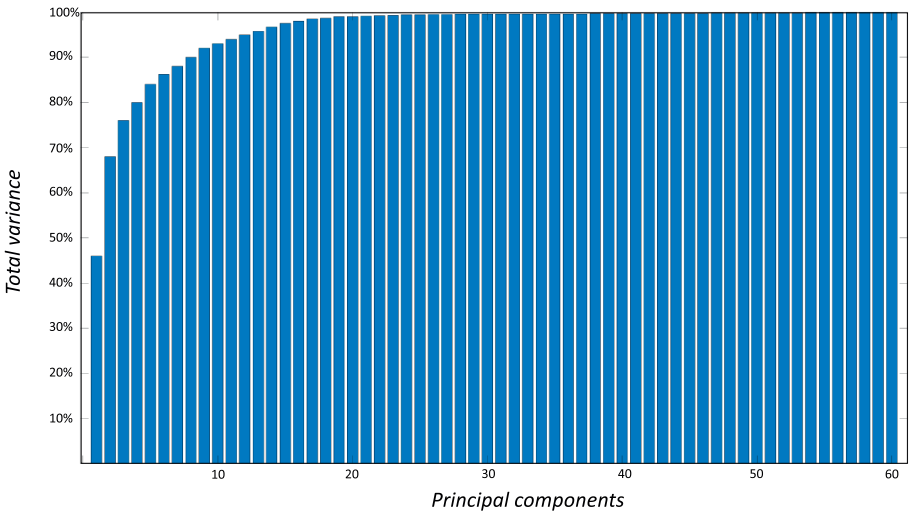

Figure 3: The cumulative effect for every principal component was calculated and expressed as a ratio of the total variance in the control population. Most of the variance of the control population is described by the first principal components.

RESULTS

VARIATIONS IN THE NORMAL POPULATION

PCA of the control group resulted in a mean cranial shape of the control population and a set of PCs describing the variations in the control population. The effect of PC1 is displayed in Figure 2. This morphological effect is an increase of the complete frontal region to the anterior direction, including an anterior displacement of the orbital region. In total, the cranial shape became more elongated without a reduction of the lateral diameter of the cranium. PC1 accounted for 46% of the

total variation in the control population. The effect of PC2 is displayed in Figure 2. PC2 primarily affected the lateral diameter of the cranial shape. In addition, an increment of the posterior part of the cranial shape was seen. PC2 accounted for 23% of the total variation. For every PC the effect of the total variation was calculated and demonstrated in a cumulative bar graph in Figure 3.

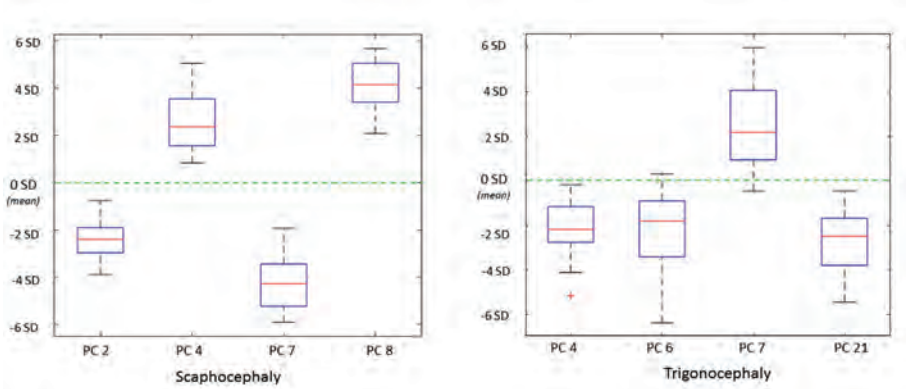

Figure 4: Boxplot of the four selected principal components (PCs) to distinguish scaphocephaly patients from the controls (left) and to distinguish trigonocephaly patients from the controls (right). The y-axis displays the variation of the control population, expressed as standard deviations. Green dotted line indicates the mean cranial shape of the control population. All the PCs in the figure confirmed a significant difference ($p < 0.001$) between patients and controls.

SCAPHOCEPHALY

The values for the scaphocephaly patients were calculated using the PCA model of the normal population. Four PCs deviated significantly from the normal population indicated by the boxplot in Figure 4. These PCs corresponded with an elongation in the anteroposterior direction because of an increment of the posterior part, a decreased lateral diameter, increased frontal bossing, posterior narrowing, and an increased frontal region in the upward direction. The absolute values of the four selected PCs for scaphocephaly were summed. This resulted in a mean of 3.2 (SD 1.3) for the controls and a mean of 13.4 (SD 2.7) for the scaphocephaly patients. A Student t test confirmed a significant difference between the control population and the scaphocephaly patients ($p < 0.001$; 95% confidence interval 8.7– 11.6). For the scaphocephaly patients, the mean values of these four PCs were used to simulate the effect in 3D. This is demonstrated in Figure 5. The colour map indicates the effect of the four PCs compared with the mean cranial shape of the control population.

TRIGONOCEPHALY

The four PCs that exposed the largest difference for trigonocephaly patient and controls were selected. These PCs corresponded with a smaller forehead, temporal narrowing, reduced frontal bossing, and a decreased orbital width. The values of the four PCs are displayed by the boxplots in Figure 4. The summed absolute values of these four PCs resulted in a mean of 3.1 (SD 1.2) for the controls and a mean of 9.7 (SD 2.7) for the trigonocephaly patients. This difference between the control population and the trigonocephaly patients was statistically significant ($p < 0.001$; 95% confidence interval 5.1–8.0). The mean values of the 4 PCs for trigonocephaly were used to simulate the morphological effect. The colour map in Figure 6 demonstrates the effect of these four PCs in 3D.

DISCUSSION

The combination of 3D stereophotogrammetry and the evaluation with the use of PCA provides a new method for an objective and automatic characterization of the cranial morphology. PCA was applied on a dataset of 3D photographs to find and isolate cranial shape variations in a normal population. Using these variations, the cranial shape of scaphocephaly and trigonocephaly patients could be distinguished from a normal cranial shape. This method provides an objective tool for the physician to detect whether a cranial shape is normal or can be classified as scaphocephaly or trigonocephaly using a 3D photograph.

Since Virchow described the abnormal shape of the head in 1851, there has been a wide variety in methods to evaluate the cranial shape.[15] A standard method for documentation of the cranial shape has not been adopted. The most common methods include clinical observations and (calliper) anthropometrics directly on the patient's head.[16,17] Wilbrand et al. argued that calliper measurements provide highly precise information as long as a strictly standardized protocol is followed; the patient should be in a standard position, the examiner should be trained, and the patient should be cooperative.[18] Because of these conditions, exact measurements and documentation are challenging.[16,19] In addition, these measurements are two–dimensional, and therefore do not provide an adequate description of the 3D cranial shape.

Today, different imaging modalities are able to acquire the 3D shape of the newborn's cranium. The 3dMDCranial System is able to capture a 360-degree full head image and is specifically designed for surface imaging of the cranial shape. The clinical reproducibility of the 3DMD acquisition system was investigated by Maal et al. and was found to be 0.4 mm.[20] The system error of the 3DMD system was described by Boehnen and Flynn[21] and was found to be ±0.1 mm. The most important advantages of 3D stereophotogrammetry are the fast and short acquisition time (less than 2 ms) and the fact that there is no exposure to ionizing radiation.[9,22] Therefore, 3D stereophotogrammetry is a good imaging modality to study the cranial shape of the patient and to monitor its development over time. Although different studies claim that they use the advantages of 3D stereophotogrammetry, most studies do not use the full potential of 3D stereophotogrammetry and tend to reproduce simple 2D anthropometrics.[23–27] Several studies presented excellent 3D evaluation methods for the skull, yet these studies used 3D CT.[28–31] To the best of our knowledge, no other studies have used 3D stereophotogrammetry in combination with a complete 3D evaluation of the cranial shape for diagnosis and detection of cranial abnormalities compared to normal cranial shape variations.

By using PCA on a database of 3D photographs of controls, the average 3D cranial shape and the variations of the control population were determined. Using this method, we can compare a 3D photograph not only to the average cranial shape but also to the range of normal variations in the control population. This is a subtle and elegant way to determine how much a patient's cranial shape deviates from a shape that is assumed to be 'normal'.

Scaphocephaly patients are characterized by an elongated cranial shape in the anteroposterior direction and a reduced lateral diameter of the cranial shape mediotemporally. To a lesser extent, this morphological variation is also present in a normal population since there are newborns with more rounder or narrower head shapes.[32] Therefore, it was expected that we could use a multiplication of these normal variations to detect the scaphocephaly shape. Indeed, manipulating the four selected PC's for scaphocephaly patients to the mean cranial shape clearly confirmed this hypothesis by revealing an elongated cranial shape with a reduced lateral diameter (Figure 5). This proves we created an accurate method for the identification of scaphocephaly.

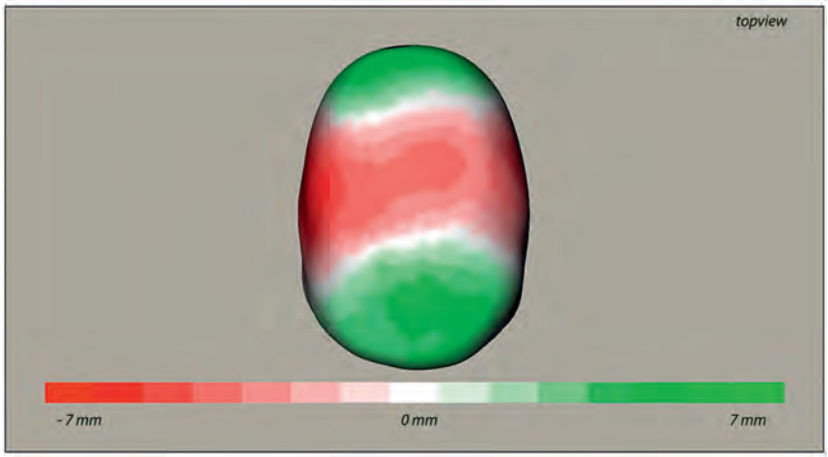

Figure 5: The four principal components which were selected to identify the scaphocephaly patients were used to manipulate the mean cranial shape. This resulted in an elongated cranial shape with a reduced lateral diameter. Colours indicate a volume increase (green) or a volume decrease (red).

Somewhat surprising, we were able to find a significant difference between controls and trigonocephaly patient using a combination of four PCs. This means that although a typical wedge-shaped forehead is not present in the dataset of controls, a combination of four PCs can generate a form of trigonocephaly (Figure. 6). Also this model can be used to significantly identify trigonocephaly patients.

The PCA model used in this present study included 3D photographs in the age range of 3–6 months. A limitations is that the PCA model can only recognize and analyse the cranial vault variations in this specific age interval. To compensate for this and to increase the clinical use, more age variation should be included.[9]

One limitation of 3D photogrammetry is that only the outer surface of the head can be captured and no hard tissue structures can be used for accurate alignment of the patients. Superimposition based on the combination of manually placed landmarks on the outer surface and the semi-automatic CCFP calculation may be a source of minor variability. More research is needed to automate the superimposition of 3D photographs and overcome inaccuracies in registration. Automatic superimposition would also reduce the processing time and improve reproducibility.

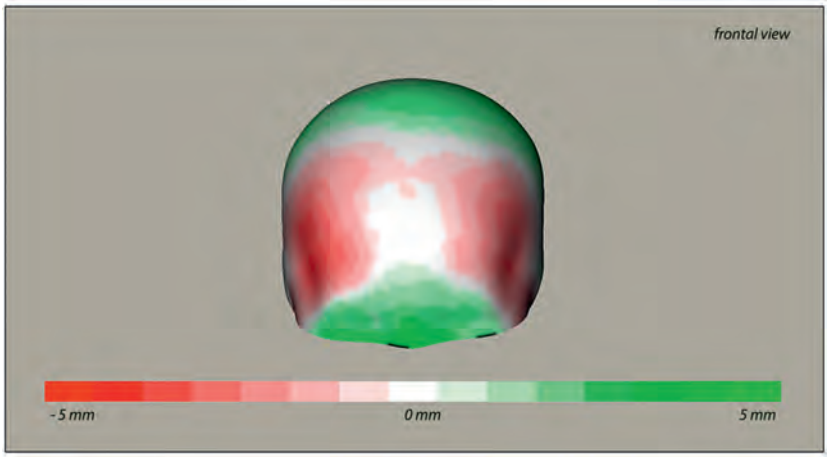

Figure 6: The four PC's which were selected to identify the trigonocephaly patients were used to manipulate the mean cranial shape. The resulted cranial shape demonstrates temporal narrowing and a reduced orbital width. Colours indicate a volume increase (green) or a volume decrease (red).

In the present study, all the cranial shapes were scaled to the same size to correct for growth. A limitation of scaling in this study is the assumption that the normal cranial shape will grow uniformly in the first 3 and 6 months. In addition, it was assumed that there were no morphological shape differences between males and females. In order to make comparison of patients even more accurate, a future study which investigates the 3D modification of the cranial shape as a result of growth and sex would be a valuable contribution.[8]

The PCA model used in this study, created from normal cranial shapes, was able to successfully identify all 40 patients. However, introducing more variation in the model, by including also abnormal cranial shapes may improve the model's robustness, even in severe cranial deformities.

The presented method is a clinical tool for the evaluation of the cranial shape. Using only a 3D photo, this method can be used to detect if a cranial shape is normal or abnormal in an objective manner. In contrast to 2D measurements, such as calliper measurements and other 2D measurements, this model regards the complete 3D morphology of the cranial shape and yet it produces only a few simple outcome measurements. Therefore, this method is an addition and a major improvement to the currently used clinical diagnostic methods for cranial abnormalities.

The determination of diagnostic cut-offs which can quantify the rate of abnormality would be a logical next step. Quantification of the rate of severity can also be used for objective evaluation of cranial development and follow-up of craniosynostosis patients during and after treatment. The results of different surgical treatments can be compared without the use of harmful radiation.

CONCLUSION

In conclusion, this study presented a new method to evaluate cranial shape abnormalities of scaphocephaly patients and trigonocephaly patients. Three-dimensional stereophotogrammetry in combination with PCA was able to calculate the mean cranial shape and to describe the normal variation of the cranial shape in a control population. This PCA model was able to significantly differentiate craniosynostosis patients from controls. This is a promising method for the objective evaluation and identification of craniosynostosis using solely 3D stereophotogrammetry.

APPENDIX

Principal Component Analysis (PCA) was applied to the superimposed, resampled and scaled 3D photographs of the control population. Every cranial shape in the dataset was represented as an **3*m***x1 element vector: $x = (x_1, y_1, z_1, \dots, x_m, y_m, z_m)^T$ with ***mm*** = 4501 (number of vertex points, calculated using the ray casting algorithm). The mean cranial shape of the control population, containing N=60 cranial shapes, was calculated using:

$$\bar{X}_{control} = \frac{1}{N}\sum_{i=1}^{N} x_i$$

For each cranial shape its deviation from the mean was calculated:

$$dx_i = x_i - \bar{X}_{control}$$

Using the Singular Value Decomposition (SVD), the eigenvectors: $\Phi_{control}$ and the corresponding eigenvalues: $\lambda_{control}$ of the control population were calculated. Cranial shapes of the control population can be reconstructed by:

$$x \approx \bar{X}_{control} + \Phi_{control}\, b$$

The vector $\boldsymbol{b}$ defines a set of parameters describing the cranial shape of a patient. Cranial morphology can be changed by varying the elements of $\boldsymbol{b}$. The PCA model of the control population was used to determine the parameters for the scaphocephaly and trigonocephaly patients. For every patient, the parameters $\boldsymbol{b}$ were calculated using:

$$b = \boldsymbol{\Phi}_{control}{}^{T} (X_{patient} - \bar{X}_{control})$$

$\boldsymbol{X}_{patient}$ was a modified 3D photograph of a patient (scaphocephaly or trigonocephaly). The variance of the every parameter, $\boldsymbol{b}_i$ across the control dataset was given by $\boldsymbol{\lambda}_{control,i}$. The parameters of the controls and the patients were expressed as standard deviations (SD) from the mean cranial shape by:

$$b_{SD} = \frac{b_i}{\sqrt{\lambda_{control,i}}}$$

The parameters, expressed in SD's, of the controls were compared to the scaphocephaly and trigonocephaly patients.

REFERENCES

1. Kabbani H, Raghuveer T. Craniosynostosis. Am Fam Physician 2004;69(12):2863–70.
2. Delashaw JB, Persing JA, Broaddus WC, Jane JA. Cranial vault growth in craniosynostosis. J Neurosurg 1989;70:159–65. http:// dx.doi.org/10.3171/jns.1989.70.2.0159.
3. Bristol RE, Lekovic GP, Rekate HL. The effects of craniosynostosis on the brain with respect to intracranial pressure. Semin Pediatr Neurol 2004;11:262–7. http://dx. doi.org/10.1016/j.spen.2004.11.001.
4. Kirmi O, Lo SJ, Johnson D, Anslow P. Craniosynostosis: a radiological and surgical perspective. Semin Ultrasound CT MRI 2009;30:492–512. http://dx.doi.org/ 10.1053/j.sult.2009.08.002.
5. Taylor JA, Maugans TA. Comparison of spring-mediated cranioplasty to minimally invasive strip craniectomy and barrel staving for early treatment of sagittal craniosynostosis. J Craniofac Surg 2011;22:1225–9. http://dx.doi.org/10.1097/ scs.0b013e31821c0f10.
6. van Lindert EJ, Siepel FJ, Delye H, Ettema AM, Berge´ SJ, Maal TJ, Borstlap WA, et al. Validation of cephalic index measurements in scaphocephaly. Childs Nerv Syst 2013;29:1007–14. http://dx.doi.org/ 10.1007/ s00381-013-2059-y.
7. Marcus JR, Stokes TH, Mukundan S, Forrest CR. Quantitative and qualitative assessment of morphology in sagittal synostosis: mid-sagittal vector analysis. J Craniofac Surg 2006;68:680–6.
8. Delye H, Clijmans T, Mommaerts MY, Sloten JV, Goffin J. Creating a normative database of age-specific 3D geometrical data, bone density, and bone thickness of the developing skull: a pilot study. J Neurosurg Pediatr 2015;16:687–702. http://dx.doi.org/ 10.3171/2015.4.PEDS1493.
9. Brons S, Van Beusichem ME, Maal TJJ, et al. Development and reproducibility of a 3D stereophotogrammetric reference frame for facial soft tissue growth of babies and young children with and without orofacial clefts. Int J Oral Maxillofac Surg 2013;42:2– 8. http://dx.doi.org/10.1016/j.ijom.2012.07.006.
10. de Jong GA, Maal TJJ, Delye H. The computed cranial focal point. J Craniomaxillofac Surg 2015;43:1737–42. http://dx.doi.org/ 10.1016/j.jcms.2015.08.023.
11. Moller T, Trumbore B. Fast, minimum storage ray/triangle intersection. ACM SIGGRAPH 2005 Courses on – SIGGRAPH '05, 7. New York, NY, USA: ACM Press; 2005 . http://dx.doi.org/10.1145/ 1198555.1198746.
12. Shlens J. A Tutorial on principal component analysis. Int J Remote Sens 2014;51. https:// www.researchgate.net/publication/ 261404279_A_Tutorial_on_Principal_ Component_Analysis. Accessed April 21, 2016.
13. Mitteroecker P, Gunz P. Advances in geometric morphometrics. Evol Biol 2009;36:235–47. http://dx.doi.org/10.1007/ s11692-009-9055-x.
14. Cootes TF, Taylor CJ, Cooper DH, Graham J. Active shape models-their training and application. Comput Vis Image Underst 1995;61:38–59. http://dx.doi.org/10.1006/ cviu.1995.1004.
15. Virchow R. Ueber den Cretinismus, namentlich in Franken, und ueber pathologische Schaedelformen. Verh Phys Med Gesamte Wurzbg 1851;2:231–71. papers3:// publication/uuid/B866E753-7A12-4119-BA0A-9CEDD0012953.
16. Farkas LG. Accuracy of anthropometric measurements: past, present, and future. Cleft Palate-Craniofacial J 1996;33:10–22. http://dx.doi.org/10.1597/1545-1569(1996) 033<0010:AOAMPP>2.3.CO:2.
17. Mcgarry A, Dixon MT, Greig RJ, Hamilton DRL, Sexton S, Smart H. Head shape measurement standards and cranial orthoses in the treatment of infants with deformational plagiocephaly. Dev Med Child Neurol 2008;50:568–76. http://dx.doi.org/10.1111/ j.1469-8749.2008.03017.x.
18. Wilbrand JF, Wilbrand M, Pons-Kuehne- mann J, Blecher JC, Christophis P, Howaldt HP, Schaaf H, et al. Value and reliability of anthropometric measurements of cranial deformity in early childhood. J Craniomaxillofac Surg 2011;39:24–9. http://dx.doi.org/ 10.1016/j.jcms.2010.03.010.
19. Mortenson PA, Steinbok P. Quantifying positional plagiocephaly: reliability and valid- ity of anthropometric measurements. J Craniofac Surg 2006;17:413–9. http://dx. doi.org/10.1097/00001665-200605000- 00005.
20. Maal TJ, van Loon B, Plooij JM, Rangel F, Ettema AM, Borstlap WA, Berge´ SJ. Registration of 3-dimensional facial photographs for clinical use. J Oral Maxillofac Surg 2010;68:2391–401. http://dx.doi.org/ 10.1016/j.joms.2009.10.017.

21. Boehnen C, Flynn P. Accuracy of 3D scan-ning technologies in a face scanning scenario. Proceedings of International Conference on 3-D Digital Imaging and Modeling, 3DIM. 2005:310–7. http://dx.doi.org/10.1109/3DIM.2005.13.
22. Littlefield TR, Kelly KM, Cherney JC, Beals SP, Pomatto JK. Development of a new three-dimensional cranial imaging system. J Craniofac Surg 2004;15:175–81. http:// www.ncbi.nlm.nih.gov/pubmed/14704586.
23. Wilbrand JF, Szczukowski A, Blecher JC, Pons-Kuehnemann J, Christophis P, Howaldt HP, Schaaf H. Objectification of cranial vault correction for craniosynostosis by three-dimensional photography. J Cranio-Maxillo-facial Surg 2012;40:726–30. http://dx.doi. org/10.1016/j.jcms.2012.01.007.
24. Mendonca DA, Naidoo SD, Skolnick G, Skladman R, Woo AS. Comparative study of cranial anthropometric measurement by traditional calipers to computed tomography and three-dimensional photogrammetry. J Craniofac Surg 2013;24:1106–10. http:// dx.doi.org/10.1097/scs.0b013e31828dcdcb.
25. Schaaf H, Malik CY, Streckbein P, Pons- Kuehnemann J, Howaldt H-P, Wilbrand J-F. Three-dimensional photographic analysis of outcome after helmet treatment of a non-synostotic cranial deformity. J Craniofac Surg 2010;21:1677–82. http://dx.doi.org/ 10.1097/SCS.0b013e3181f3c630.
26. Schaaf H, Pons-Kuehnemann J, Malik CY, Streckbein P, Preuss M, Howaldt HP, Wilbrand JF. Accuracy of three-dimensional photogrammetric images in non-synostotic cranial deformities. Neuropediatrics 2010;41:24–9. http://dx.doi.org/10.1055/s- 0030-1255060.
27. Berry-Candelario J, Ridgway EB, Grondin RT, Rogers GF, Proctor MR. Endoscope-assisted strip craniectomy and postoperative helmet therapy for treatment of craniosynostosis. Neurosurg Focus 2011;31:E5. http:// dx.doi.org/10.3171/2011.6.FOCUS1198.
28. Heuze Y, Boyadjiev SA, Marsh JL, Kane AA, Cherkez E, Boggan JE, Richtsmeier JT. New insights into the relationship between suture closure and craniofacial dysmorphology in sagittal nonsyndromic craniosynostosis. J Anat 2010;217:85–96. http://dx.doi. org/10.1111/j.1469-7580.2010.01258.x.
29. Heuze Y, Martınez-Abadıas N, Stella JM, Senders CW, Boyadjiev SA, Lo LJ, Richts-meier JT. Unilateral and bilateral expression of a quantitative trait: asymmetry and symmetry in coronal craniosynostosis. J Exp Zool B Mol Dev Evol 2012;318(318):109– 22. http://dx.doi.org/10.1002/jezb.21449.
30. Saber NR, Phillips J, Looi T, Usmani Z, Burge J, Drake J, Kim PC. Generation of normative pediatric skull models for use in cranial vault remodelling procedures. Child's Nerv Syst 2012;28:405–10. http://dx.doi.org/10.1007/s00381-011-1630-7.
31. Mendoza CS, Safdar N, Okada K, Myers E, Rogers GF, Linguraru MG. Personalized assessment of craniosynostosis via statistical shape modeling. Med Image Anal 2014;18:635–46. http://dx.doi.org/10.1016/ j.media.2014.02.008.
32. Likus W, Bajor G, Baron J, Markowski J, Milka D, Lepich T. cephalic index in the first three years of life: study of children with normal brain development based on computed tomography. Sci World J 2014;2014:1–6. http://dx.doi.org/10.1155/2014/5028

PART 2

PLANNING

CHAPTER 4

Virtual surgical planning of open cranial vault reconstructions

Jene Meulstee

INTRODUCTION

During open cranial vault reconstruction (OCVR), the cranial vault of a craniosynostosis patient is dissected and reconstructed more optimally. The goal of this procedure is to increase the cranial volume and create an aesthetically improved cranial shape. Since there are many options to dissect and reconstruct a cranial shape, a fitting surgical strategy is fundamental to achieve the best surgical outcome. With virtual surgical planning (VSP), it becomes possible to contemplate the surgical strategy before the operation is performed. Based on a computed tomography (CT) scan, the bony structures of a patient's skull can be visualized in three dimensions (3D). Next, osteotomies can be simulated and the resulting bone segments can, in turn, virtually be positioned on a new position. This chapter presents seven reasons why VSP makes an essential contribution to the treatment of OCVR.

1 - SIMULATING DIFFERENT TREATMENT STRATEGIES

Multiple surgical strategies can be explored to determine the best fitting solution for every patient. For every type of craniosynostosis (e.g. scaphocephaly, trigonocephaly, or plagiocephaly), standardized or commonly used reconstruction approaches are known and the decision which strategy is used is mostly based on the subjective preference of the surgeon.[1,2] However, apparently small differences in cranial morphology among patients might result in a different outcome even if the same surgical strategy is used.[3,4] This can be illustrated by the VSP of three different trigonocephaly patients (Figure 1). The frontal bones of patient A are consistently curved in the lateral direction, as well as in the upward direction. A commonly used method of swapping and rotating the frontal segments will result in a flat and wide forehead with an elegant fit on the (advanced) orbital bar. Yet, using the same strategy in patient B will result in the small and pointy forehead, since the curvature of the frontal segments is less constant in patient B. Likewise, the prominent metopic ridge of patient C requires another approach to create a flat and wide forehead.

Similarly, the outcome of a surgical approach can vary significantly for patients with unilateral plagiocephaly. A bilateral advancement and reconstruction of the orbitae and the forehead can be used to achieve symmetry. However, in many cases, an unilateral reconstruction of the orbital bar suffices to create an admirable

result. These different strategies, and their effects, can be simulated using a VSP. In addition, the 3D visualization allows the user to inspect the cranial shape and the VSP from multiple vantage points which are not possible intraoperatively.[5] Also, varying the point of deflection of the orbital bar can have a tremendous effect on the final reconstruction. Varying the distance of the osteotomy from the midline can improve symmetry as is visualized in Figure 2. The VSP is used to find this optimal deflection point by simulating its effect.

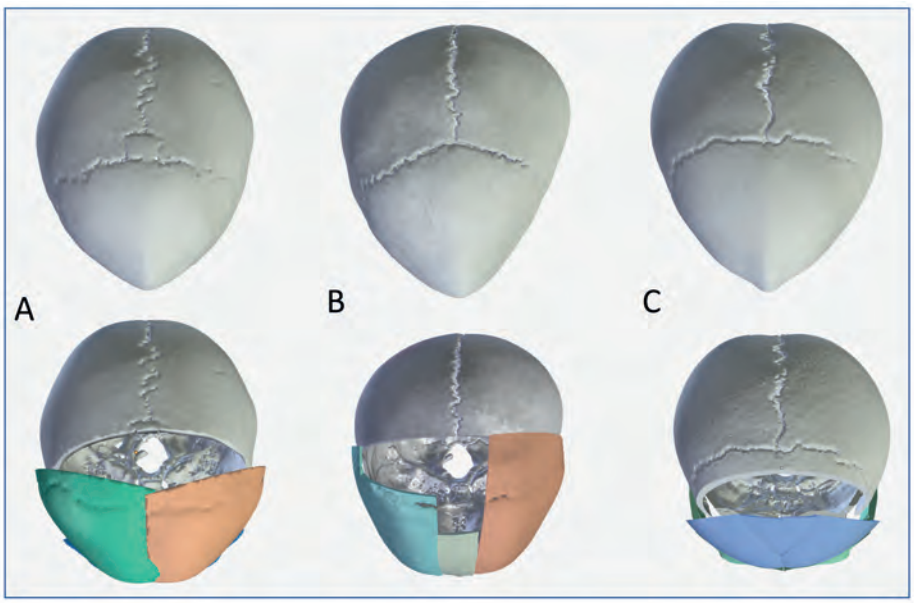

Figure 1: Variations in cranial morphology of trigonocephaly patients require a different surgical strategy. In patient A, the frontal parts are symmetrically rotated. In patient B, asymmetrical rotations and osteotomies were applied. In patient C, the metopic ridge was removed first, followed by an symmetrical rotation of the frontal parts.

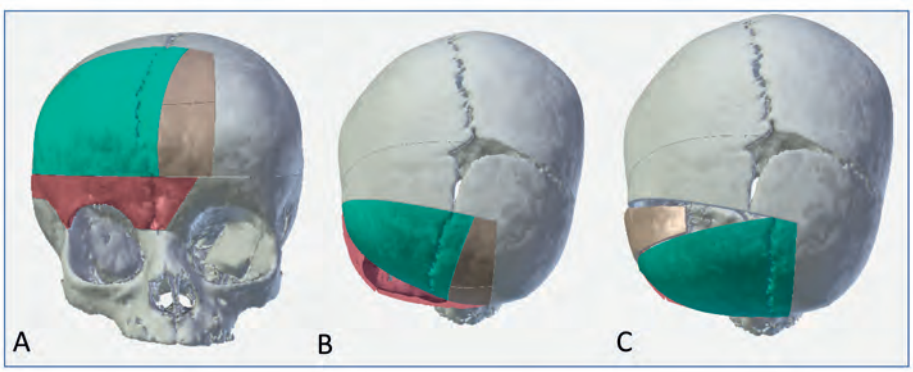

Figure 2: Planning of a plagiocephaly patient, where the fused right coronal suture resulted in a retracted orbit and a flattened forehead. Multiple surgical approaches were

simulated during the virtual planning. With a deflection point, a little left from the midline of the nasion, the symmetry of the orbital region could be restored. The forehead was reconstructed on the newly created orbital bar. By simulating the final reconstruction, the osteotomies could be optimized and gaps between the cranial segments minimized. A.) frontal view of the planned osteotomies. B.) top view showing the right orbital advancement (red). C.) top view with a simulation of the forehead reconstruction.

These examples show that, due to individual differences, patient-specific solutions are desired and that a conventional or standard approach is not always the best match for a patient. Nevertheless, the planning process often begins with the elaboration of common and/or standard reconstruction strategies. By simulating different scenarios, it can be ruled out that there is still a solution that could work better. From our experience, the first scenario that is virtually explored rarely turned out to be the best fitting strategy, which underlies the importance of testing different strategies.

2 - PLANNING WITH REFERENCE VALUES

Detailed information concerning the normal shape and development of the cranium is available from the literature and research.[6] Volumes, ratios, 2D- and 3D measurements can be useful during the planning of open reconstructions. These measurements provide a detailed insight into where the abnormality is most prominent and which part of the skull will benefit most from a correction. For example, reference measurements, such as the interorbital distance and the angle between orbitae and nasion, serve as guidelines when the orbital advancement is virtually reconstructed (Figure 3).[6,7]

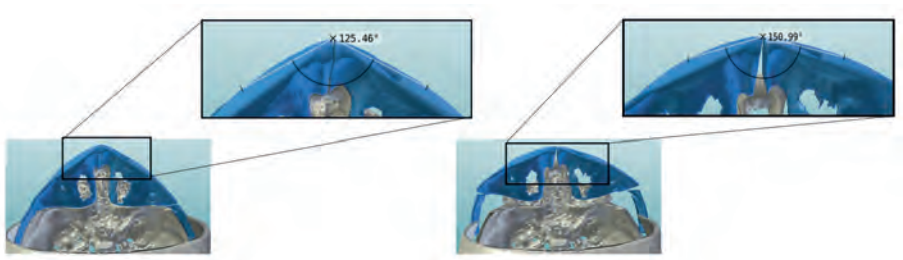

Figure 3: During the virtual planning of a trigonocephaly patient, measurements can be performed and reference values can be consulted.

The main purpose of OCVR is to increase the intracranial volume. The intracranial volume of a virtual reconstruction can be calculated and compared with the current situation and with reference measurements from the literature. In addition, the shape of a patient can be compared to an average skull composed of a set of CT scans of age-correlated children with no skull abnormality. This makes it possible to create a transparent 3D overlay during the planning, which serves as a starting point.

The morphology of the patient's cranium itself can also be used as a reference during planning. In Figure 4, the unaffected side of a plagiocephaly patient helps to determine the new position of the affected side by mirroring and using this projection on the right side as a virtual template. This template directs how the right orbital bar needs to be manipulated and advanced to restore symmetry.

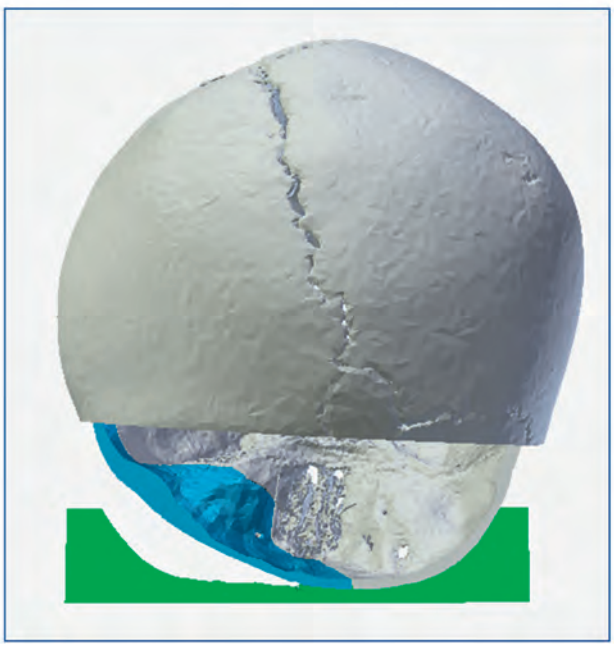

Figure 4: Top view of a plagiocephaly patient. The right retracted orbit (blue) can be compared to the unaffected left side. The left side is mirrored and used as a virtual template for the right side (green) to restore symmetry.

3 - SELECTING THE OPTIMAL OSTEOTOMY LINES

After the craniofacial team has decided about the optimal treatment plan, based on the virtual simulation (step 1), and the comparison with reference values (step 2), the virtual osteotomy lines can be determined. Dissecting the cranium into many bone segments makes it feasible to sculpt a cranium in any desirable shape. This would, however, result in a less solid reconstruction and require more fixation material. In addition, using multiple bone segments might create undesirable visible or palpable steps between the bone segments. Therefore, one should aim to use larger bone segments and the use of multiple and smaller bone segments should be avoided, especially in the facial region, such as the forehead. Ideally, bone segments from another location are moved to a new position in a way that the curvature and shape are optimally utilized.

During the actual surgery, once the osteotomies have determined the borders of a segment, the freedom of the reconstruction is limited. This makes it nearly impossible to find the optimum between the osteotomies and the ideal position of the bone segments. Since osteotomies are irreversible and making segments larger is not possible, adjusting the bone segments will result in even smaller or multiple segments as a consequence.

In a virtual environment, bone segments can be translocated and manipulated in a way that their curvature matches the newly formed shape. Thereafter, virtual osteotomies can be created. This paradoxical backward planning makes it possible to find the optimal position of bone segments first, and determine the corresponding osteotomies later.

4 - BACKWARD PLANNING

Another advantage of backward planning is that the optimal bone-to-bone contact can be pursued. Because the osteotomies are defined after a final position of the bone segment is determined, an optimal cutting pattern can be strategically designed. For example, creating a bone segment using a skewed osteotomy line can result in a segment with maximal occlusion at its final position. The benefit is that this will lead to solid construction, less fixation material is needed, and the risk

of steps between the segments is lower.[4] Figure 5 demonstrates how a skewed osteotomy can provide maximal occlusion during the reconstruction.

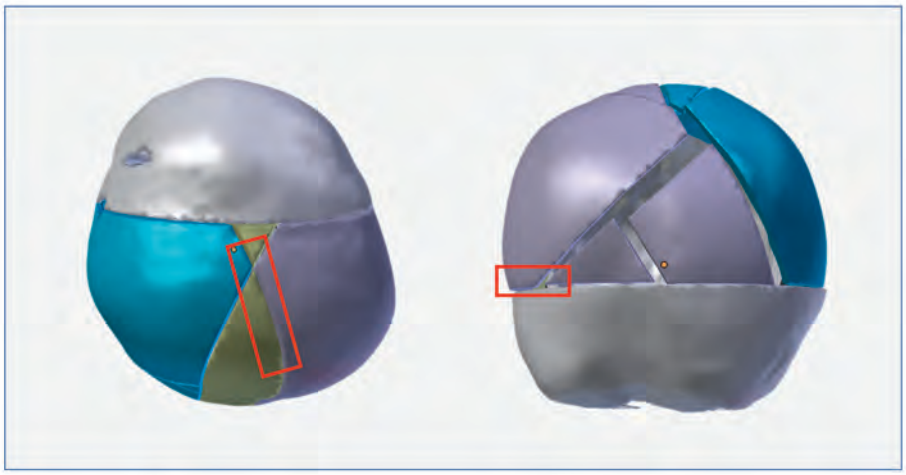

Figure 5: With backward planning, the ideal position of osteotomy lines can be decided. In this example, a curved osteotomy over the midline ensures an optimal fit to the skull-base when this segment is transformed into its new position.

5 - MORE PREDICTABLE SURGERY

Next to the planning of the cranial contour and volume, the VSP makes the surgical procedure itself more transparent. For example, the exact height of a transverse osteotomy above the orbitae might depend on the bone thickness at this level. Inspecting bone thickness and bone thickness irregularities preoperatively, will help the surgeons extrapolate the craniotomies and can help determine which craniotomy instrument is optimal for performing the osteotomy. Also, the course and location of the sinus sagittalis superior or the sinus transversus under the skull can be inspected and considered when planning the osteotomies.

Occasionally, the planning suggests that the best option is to make an osteotomy in, or through a suture. By discussing the planning in advance, the pros and cons can be weighted or alternatives can be devised. In addition, surgeons' preferences can be integrated in the planning.

6 - REDUCE SURGERY TIME

From our experience, elaborating and discussing the surgical plan in advance improves the collaboration between the different specialists who perform surgery together. Having a proper reconstruction plan, which is in accordance with the surgical team, can make the surgery itself more fluent and faster.[3,5] Discussions about osteotomies or how the bone segments should be manipulated can be held outside the surgery room. This also makes collaboration between surgeons more efficient and will possibly reduce surgery time.

Figure 6: Discussing several surgical approaches with the team before the actual surgery.

7 - IMPROVE PATIENT INFORMATION

A VSP can be used to inform the patient's family and discuss the procedure. OCVR has a great impact on the patient and the patient's family. Explaining the VSP to the patient's family step by step helps parents/relatives understand and inform them about the procedure. In addition, after the surgery and during follow-up, questions and concerns can be discussed using the VSP, which leads to a well-informed patient's family.

REFERENCES

1. Greensmith AL, Holmes AD, Lo P, Maxiner W, Heggie AA, Meara JG. Complete Correction of Severe Scaphocephaly: The Melbourne Method of Total Vault Remodeling. *Plast Reconstr Surg*. 2008;121(4):1300-1310. doi:10.1097/01.prs.0000304592.56498.d6
2. Lee BS, Hwang LS, Doumit GD, et al. Management options of non-syndromic sagittal craniosynostosis. *J Clin Neurosci*. 2017;39:28-34. doi:10.1016/j.jocn.2017.02.042
3. Burge J, Saber NR, Looi T, et al. Application of CAD/CAM Prefabricated Age-Matched Templates in Cranio-Orbital Remodeling in Craniosynostosis. *J Craniofac Surg*. 2011;22(5):1810-1813. doi:10.1097/SCS.0b013e31822e8045
4. Macmillan A, Lopez J, Mundinger GS, Major M, Medina MA, Dorafshar AH. Virtual surgical planning for correction of delayed presentation scaphocephaly using a modified melbourne technique. In: *Journal of Craniofacial Surgery*. Vol 29. ; 2018:914-919. doi:10.1097/SCS.0000000000004290
5. Shah A, Patel A, Steinbacher DM. Simulated frontoorbital advancement and intraoperative templates enhance reproducibility in craniosynostosis. *Plast Reconstr Surg*. 2012;129(6):1011e-1012e. doi:10.1097/PRS.0b013e31824effa7
6. Delye H, Clijmans T, Mommaerts MY, Sloten JV, Goffin J. Creating a normative database of age-specific 3D geometrical data, bone density, and bone thickness of the developing skull: a pilot study. *J Neurosurg Pediatr*. 2015;16(6):687-702. doi:10.3171/2015.4.PEDS1493
7. Freudlsperger C, Steinmacher S, Bächli H, Somlo E, Hoffmann J, Engel M. Metopic synostosis: Measuring intracranial volume change following fronto-orbital advancement using three-dimensional photogrammetry. *J Cranio-Maxillofacial Surg*. 2015;43(5):593-598. doi:10.1016/j.jcms.2015.02.017

CHAPTER 5

Comparison of 3D and augmented reality kidney models with conventional imaging data in the preoperative assessment of children with Wilms tumors

Lianne Wellens
Jene Meulstee
Cornelis van de Ven
Terwisscha van Scheltinga
Annemieke Littooij
Marry van den Heuvel-Eibrink
Marta Fiocco
Anne Rios
Thomas Maal
Marc Wijnen

JAMA Network Open
Published: April 2019
DOI: 10.1001/jamanetworkopen.2019.2633

ABSTRACT

Nephron-sparing surgery can be considered in well-defined cases of unilateral and bilateral Wilms tumors, but the surgical procedure can be very challenging for the pediatric surgeon to perform. The objective of this study was to assess the added value of personalized three-dimensional (3D) kidney models derived from conventional imaging data to enhance preoperative surgical planning.

In a survey study, the conventional imaging data of 10 Dutch children with Wilms tumors were converted to 3D prints and augmented reality (AR) holograms and a panel of pediatric oncology surgeons (n = 7) assessed the quality of the different imaging methods during preoperative evaluation. Differences in the assessment of 4 anatomical structures (tumor, arteries, veins, and urinary collecting structures) were evaluated using questionnaires. A Likert scale measured differences between the imaging methods.

Compared with conventional imaging, the 3D print and the AR hologram models were evaluated by the surgeons to be superior for all anatomical structures. There were no differences in anatomical assessment between the two 3D techniques (the 3D print and AR hologram). In this study, the 3D kidney models were associated with improved anatomical understanding among the surgeons and can be helpful in future preoperative planning of nephron-sparing surgery for Wilms tumors. These models may be considered as a supplementary visualization in clinical care.

INTRODUCTION

Wilms tumors (WTs) are the most frequently occurring pediatric cancers of the kidney. The survival rate of children with WT is around 90%,[1-3] yet approximately 5% of the cases present with bilateral disease, which reveals an overall survival rate of approximately 80%.[4]

In the presentation of bilateral disease, nephron-sparing surgery is the preferred or recommended treatment of choice. Compared with unilateral tumors, bilateral disease carries a higher risk for end-stage renal disease (12%) and secondary morbidity.[4,5] The benefit of nephron-sparing surgery in unilateral WT is debatable. The excellent survival of patients with unilateral WT has motivated investigation into reducing treatment morbidity while preserving survival by considering nephron-sparing surgery.[6,7] To reduce the probability of long-term kidney function loss, to reduce the occurrence of perioperative complications, and to facilitate complete tumor resection, a personalized planning and surgical strategy is essential.

Magnetic resonance imaging (MRI) and computed tomography (CT) are used for diagnosis and to differentiate between tumor and healthy renal tissue. Pediatric surgeons plan the surgery of WT based on the two-dimensional (2D) interpretation of these conventional imaging techniques. The use of three-dimensional (3D) visualizations is hoped to further improve the understanding of the exact tumor location and the assessment of relevant anatomical structures, such as arteries, veins, and urinary collection structures. Data from MRI and CT can be used, possibly fused, and reconstructed into 3D visualizations.[8]

The technique of 3D visualization is gradually gaining potential in many surgical disciplines and can be used to define the optimal surgical strategy.[9-12] These new techniques can even further improve the assessment of the relevant anatomy and enhance preoperative surgical planning. The 3D printing of organs and structures has proved valuable for multiple disciplines within the engineering field and clinical practice, such as urology, neurosurgery, cardiac surgery, plastic surgery, and maxillofacial surgery.[12-14] However, 3D printing is not the current standard of care. In addition, augmented reality (AR) is a technology that can visualize virtual 3D objects in the real world. The implementation of AR is promising as a

supplementary operating tool; its value currently is being assessed in different medical specialties.[15]

In this study, we compared the use of two 3D visualization techniques: 3D printing and AR, for optimizing the surgical planning of nephron-sparing surgery for WT. To our knowledge, the added value of different 3D visualization methods in addition to conventional imaging in children with cancer has never before been investigated. A panel of pediatric oncology surgeons in the Netherlands was asked to evaluate the 3D visualization techniques and report about the potential added value of their use before surgery.

METHODS

POPULATION

Imaging data from 10 patients diagnosed with a WT in the Princess Máxima Center for Pediatric Oncology, Utrecht, the Netherlands, between January 1, 2016, and May 1, 2017, were included in our study. Patients with metastases at diagnosis were excluded, and 3 patients presenting with bilateral WTs were selectively included. Seven other patients were selected based on best-quality conventional imaging available. Data from conventional imaging (MRI and/or CT scans) were derived from these 10 selected patients. In most patients, MRI was the preferred imaging technique for diagnosis and optimal tumor assessment. Computed tomography was performed to clarify vascular anatomy when nephron-sparing surgery was likely to be performed. The Medical Research Involving Human Subjects Act did not apply to this study, and we received official approval from the medical research ethics committees of the University Medical Center Utrecht, Utrecht, the Netherlands. All data were deidentified; therefore, it was not necessary, according to Dutch Law, to ask for informed consent. This study followed the Standards for Quality Improvement Reporting Excellence (SQUIRE) reporting guideline for quality improvement.[16]

IMAGING METHODS

Contrast-enhanced MRI of the abdomen was performed on a 1.5-T MRI system (Achieva; Philips Medical Systems). Coronal 3D, T2-weighted imaging along with fat-suppressed T1-weighted imaging before and after the administration of

gadolinium-based contrast medium was acquired.[17] Computed tomography was performed with the 16-row multiple detector CT (Brilliance 16P; Philips Medical Systems). All patients received 1.5 mL/kg of contrast medium, with a maximum of 120mL scanned in the arterial phase (injection rate of 2 mL/s, with saline solution pushed through the injection line immediately after the injection of the contrast bolus [injection rate of 2 mL/s and a volume of 8-10 mL depending on the age of the patient]) in accordance with standard protocol. Exposure settings were adjusted to patient size (range, 104-150 mA and 80-90 kV[p]). Thin section images were reconstructed with 0.90-mm thickness and stored in a 512 × 512 data matrix.

3D SEGMENTATION

The MRI or CT scans from each patient were loaded as digital imaging and communications in medicine (DICOM) files and segmented by an information technology expert from Materialise of Leuven, Belgium. After consulting the pediatric radiologist (A.S.L.) and a pediatric surgeon (C.P.v.d.V.), the correct anatomical segmentations were generated based on the conventional imaging by using Mimics Innovation Suite 3D segmentation software, version 20 (Materialise). Each anatomical structure (kidney parenchyma, tumor, arteries, veins, and kidney urinary collecting structures) was segmented separately and given a different color. After the full segmentation was completed, small windows were cut out of the kidney parenchyma, allowing a full view of the tumor and its border separated from the healthy tissue, intrarenal vasculature, and urinary collecting structures. Segmentations were saved as a stereolithography file (.STL) that was suitable for 3D printing and AR.

3D PRINTING

The 3D models were printed using 3D printing technology (Z Corporation) at Materialise. The printer deposits a liquid binder onto thin layers of powder via the ink-jet printheads, which reacts with an agent in the powder to create a solid, multicolor 3D model.

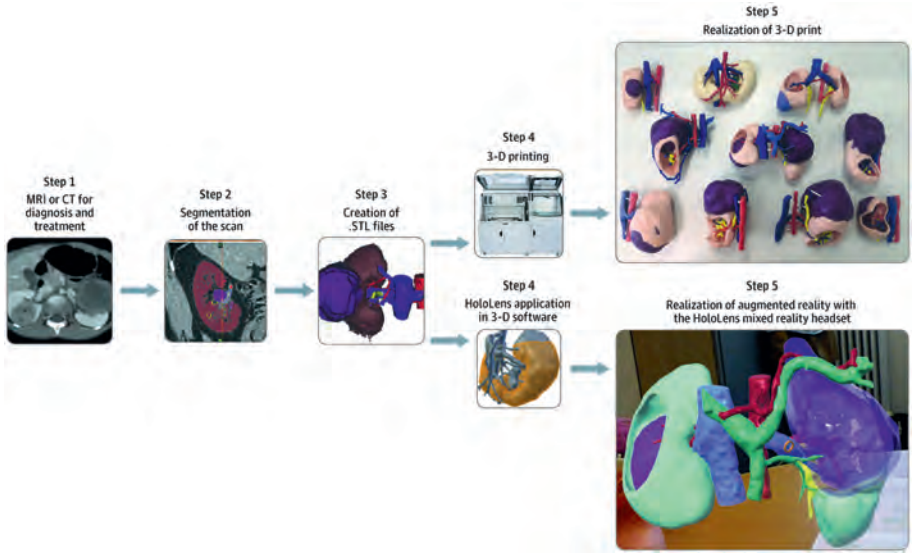

Figure 1: Workflow diagram depicting the construction process of 3D visualizations. From the patient-derived magnetic resonance image (MRI), computed tomographic (CT) image, or both, a corresponding 3D print and augmented reality hologram was made. In step 3, segmentations were saved as stereolithography (.STL) files.

AUGMENTED REALITY

A mixed reality headset (HoloLens; Microsoft Corp) was used for AR visualization. The headset uses a head-mounted display with a stereo see-through display and a wireless design. This composition provides a realistic 3D image and stimulates the user to inspect holograms from different positions and view angles. The spatial impression enables physicians to analyze complex anatomical structures in an interactive way and enhances their perspective of the surgical site.[18] First, from the exported 3D models, minor artifacts were repaired in proprietary 3D software (MeshMixer; AutoDesk Inc). The mesh density of every 3D model was optimized and consisted of 2000 to 15 000 triangles depending on the size of the models. This process guaranteed a clear visualization on the headset without losing quality. Second, the Unity 3D software framework, version 5.6.5 (Unity Technologies) was used to create an application for the headset to visualize the kidney, tumors, and relevant anatomy in 3D. Voice instructions were implemented to rotate, adjust, or manipulate the anatomical 3D objects. Visualization options were created to make structures transparent, look inside the kidney, separate the tumor from the kidney, and zoom in on specific structures. Although each 3D model was different and unique to each patient's tumor and organ anatomy, the architecture and

user interface of the application were similar across the sample group. Finally, the application was imported to the headset. *An example of a patient's WT is provided in the Video (see online version).*

Table 1: Patient Characteristics

Patient Number / sex / age (years)	Type of Wilms Tumor	Preoperative Conventional Imaging available
1 / M / 2	Unilateral	MRI
2 / M / 2	Bilateral	MRI / CT
3 / M / 3	Bilateral	MRI / CT
4 / F / 2	Unilateral	MRI
5 / M / 4	Bilateral	MRI / CT
6 / F / 3	Unilateral	MRI
7 / F / 5	Unilateral	MRI
8 / F / 5	Unilateral	MRI
9 / F / 7	Unilateral	MRI
10 / F / 4	Unilateral	MRI

DATA ACQUISITION

A panel of 7 experts, consisting of 6 pediatric oncology surgeons and 1 pediatric urologist with oncology experience, were asked to individually evaluate the MRI and/or CT images before surgery for every patient. Expertise of the 7 surgeons varied from less than 1 year to 30 years. Two-dimensional images were shown using a DICOM viewer, version 2.4.1 (The Horos Project). Afterward, the surgeons completed a questionnaire regarding the quality of this conventional imaging on the visualization of the anatomical structures in the kidney. Surgeons were asked to score the visibility of the 4 anatomical structures: tumor, arteries, veins, and urinary collecting structures from 1 to 5 (1 indicates completely disagree; 2, disagree; 3, neutral; 4, agree; and 5, completely agree). Scores were requested for the conventional imaging (MRI and/or CT) and for the 3D visualizations (3D print and AR), as well as to assess the decision making of the surgeons to perform nephron-sparing surgery or a nephrectomy and their preoperative preparation. *The questionnaires are provided in the eAppendix (online version)*. Next, the 3D print of the corresponding patient was provided to the members of the panel. They were asked to complete a second questionnaire with the same questions used for the conventional imaging techniques but with supplementary questions about the added value of the 3D print in assessing the tumor, artery and venous structures, and urinary collecting structures. The mixed reality headset was then

introduced to visualize the AR hologram of the corresponding patient, and the same questions used to assess the 3D print were given in the third questionnaire. The above events took place in 1 session per expert for a maximum of 3 hours used to score all 3 modalities for the 10 patients. The cycle of questionnaires for conventional imaging, 3D print, and AR was repeated for every patient, resulting in the opinions of the 7 experts about all 10 patients.

STATISTICAL ANALYSIS

Statistical analyses were performed using GraphPad prism, version 7 (GraphPad Software). To compare scores on the MRI and/or CT, 3D print, and AR hologram, the nonparametric-grouped, Wilcoxon matched-pair signed rank test was used. The Mann-Whitney test was used to compare the difference between questions about the 4 anatomical structures for the individual patients. A 2-sided $P < .025$ (adjusted for multiple testing) was used to test for a significant difference between the conventional imaging and the 3D visualizations.

RESULTS

PATIENT CHARACTERISTICS AND 3D VISUALIZATIONS

Of the 10 patients, 7 were girls, and the mean (SD) age was 3.7 (1.7) years. The kidney, WT, arteries, veins, and urinary collecting structures were reconstructed as shown in Figure 1. For patient 2, the urinary collecting structures were not reconstructed because of insufficient conventional imaging. The characteristics of the 10 patients are summarized in Table 1. For all 4 anatomical structures, the 3D print and the AR hologram received higher scores compared with the conventional imaging (Figure 2). When scores for the 4 anatomical structures were compared between the 3D print and the AR hologram, no difference was found (Figure 2).

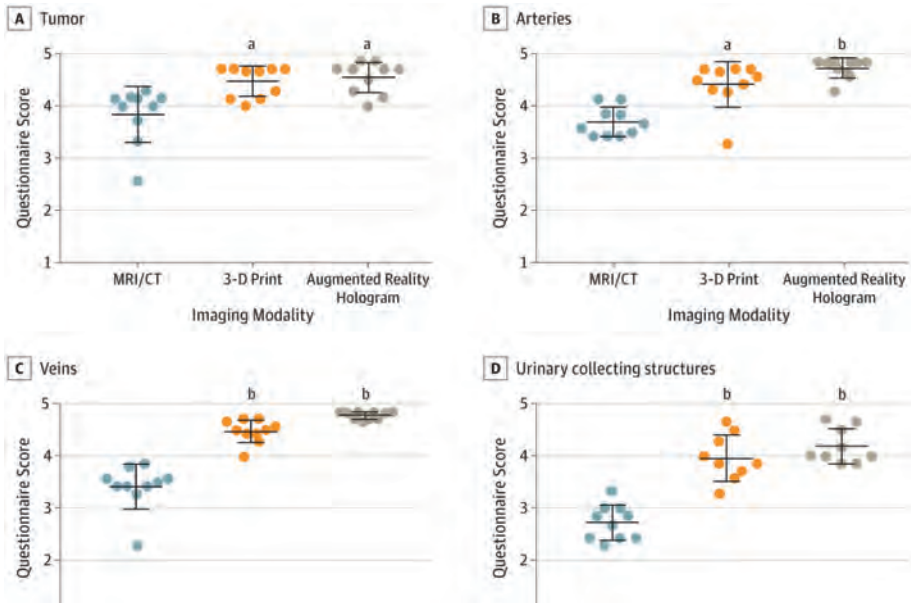

Figure 2: Questionnaire results about conventional imaging, 3D Prints, and AR Holograms. Surgeons scored the visibility of the 4 anatomical structures from 1 to 5 (1 indicates completely disagree; 2, disagree; 3, neutral; 4, agree; and 5, completely agree) for conventional imaging (MRI and/or CT) and for the 3D visualizations (3D print and AR holograms), with results showing the comparison of means of 10 patients. Center lines indicate the medians; error bars, the interquartile ranges. [a]: P < .01 compared with MRI/CT. [b]: P < .001 compared with MRI/CT.

ASSESSMENT OF ALL 4 ANATOMICAL STRUCTURES

Both 3D print and AR holograms led to better assessment of the tumor, arteries, veins, and urinary collection structures compared with conventional imaging (Figure 2 and Table 2) (tumor: median scores for conventional imaging, 4.07; interquartile range [IQR], 3.62-4.15 vs 3D print, 4.67; IQR, 4.14-4.71; P = .008 and AR hologram, 4.71; IQR, 4.26-4.75; P = .002; arteries: conventional imaging, 3.62; IQR, 3.43-3.93 vs 3D print, 4.54; IQR, 4.32-4.71; P = .002 and AR hologram, 4.83; IQR, 4.64-4.86; P < .001; veins: conventional imaging, 3.46; IQR, 3.39-3.62 vs 3D print, 4.50; IQR, 4.39-4.68; P < .001 and AR hologram, 4.83; IQR, 4.71-4.86; P < .001; and urinary collecting structures: conventional imaging, 2.76; IQR, 2.43-3.00 vs 3D print, 3.86; IQR, 3.64-4.39; P < .001 and AR hologram, 4.00; IQR, 3.93-4.58; P < .001). There was no significant difference between conventional imaging and 3D printing or AR in individual cases. *Data from all individual cases and the corresponding assessment of the pediatric surgeons is shown in the eFigure in the Supplement.*

Table 2: Results of the survey among 7 pediatric surgeons

	Score, Median (IQR)		
Anatomical structure	MRI / CT	3D Print	AR Hologram
Tumor	4.07 (3.62 – 4.15)	4.67 (4.14 – 4.71)	4.71 (4.26 – 4.75)
Arteries	3.62 (3.43 – 3.93)	4.54 (4.32 – 4.71)	4.83 (4.64 – 4.86)
Veins	3.46 (3.39 – 3.62)	4.50 (4.39 – 4.68)	4.83 (4.71 – 4.86)
Urinary collecting structures	2.76 (2.42 – 3.00)	3.86 (3.64 – 4.39)	4.00 (3.93 – 4.58)

3D KIDNEY MODEL FOR NEPHRON-SPARING SURGERY

In 9 of 10 patients, the 3D print and the AR model were created for research purposes and evaluated after the treatment had been administered. For patient 2, the 3D model was printed 1 week before surgery because there was a bilateral tumor in a horseshoe kidney. The pediatric surgeons used the model as an assisting tool because of the abnormal anatomical vasculature. A surgical assistant held the 3D printed model for real-time guidance during surgery (Figure 3).

DISCUSSION

Preoperative imaging is paramount in achieving good results during oncologic surgery. In nephronsparing surgery for WT, the risk of positive resection margins is high[6,19]; therefore, it is necessary to improve the present procedure. As opposed to bilateral WT, nephron-sparing surgery in unilateral WT is still debatable, but surgeons recently showed a higher interest in its use for unilateral WT to preserve long-term renal function.[6,7] However, the use of nephron-sparing surgery is reported to lead to incomplete tumor resection in 30% of unilateral cases, which results in reoperation and additional radiotherapy.[6] The novel 3D visualization techniques presented here may be a useful added tool when planning nephron-sparing surgery in unilateral and bilateral WT. In this study, we constructed personalized, high-quality physical and AR 3D models of pediatric unilateral and bilateral WT to create practice objects for preoperative planning.

To our knowledge, we were the first to reconstruct MRIs and/or CT images of kidneys of 10 patients with WTs in both 3D prints and AR holograms. We found a reported added value of both of our 3D models in association with the preoperative assessment by surgeons of the 4 anatomical structures (tumor, arteries, veins, and urinary collecting structure). These data are consistent with previous studies that used 3D prints in adults with renal cell carcinoma.[20,21]

Detailed understanding of the surgical anatomy of WTs and the surrounding anatomical renal structures in children can be a challenge based on standard 2D conventional imaging visualizations alone. The lack of ionizing radiation exposure and the improved soft-tissue contrast makes the MRI an attractive imaging method in children.[22] However, when only MRI is performed, the challenge lies in the accurate detection of the vasculature in these small children. This challenge is particularly true with complex renal anatomy, which often is the case in children with WTs. This study indicated that new, preoperative 3D imaging processing strategies helped increase the surgeons' knowledge about the kidney anatomy, thus assisting in improving the planning of tumor resection and optimizing the procedure of choice: nephron-sparing surgery or nephrectomy. This method could improve radicality of tumor resection and spare healthy kidney tissue, thereby preserving long-term renal function.

Converting the existing conventional imaging data to 3D visualization contributes to overall anatomical understanding.[23] In this study, no differences were found between the type of 3D visualization; therefore, the choice between 3D printing and AR reconstruction may be based on personal preference. Of the multiple 3D printing techniques, we used the Z-Corp technology, which is able to print accurate models while using different colors. A solid printed model may occlude relevant anatomy, such as blood vessels in the kidney or tumor. To overcome this obstacle, an opening window or transparent material may be used to provide a view inside the model.[24] Before the start of this study, we printed examples of kidneys with different techniques. We found that the opening window in the solid Z-Corp model best clarified the anatomy. The cost for these multicolored, 3D printed models was typically $500 (US dollars) and had a manufacturing time of 4 to 5 days. In comparison, the production of an AR reconstruction takes 1 to 2 hours and is, apart from the labor time, costless after initial hardware costs of $3000 to $5000 (US dollars) for the mixed reality headset. The relatively short lead time between chemotherapy and surgery can be an important advantage of the headset. This advantage might make AR reconstruction more feasible and preferable in certain cases. In addition, the AR hologram represented an adaptive and interactive technology compared with the 3D print in which every structure can easily be opened, switched to transparent, or moved away by giving a voice command.

The wireless design of the mixed reality headset and the use of voice commands for interaction creates the additional possibility of using the headset during surgery.[25] The AR visualization can be consulted in the operation theater to visualize the anatomy, diseased portion, and 3D vascularization. In the future, the AR holograms can be fused with the real anatomy of the patient to create a mixed reality setting, as previously described in neurosurgery.[26] However, more research is needed on how to fuse the virtual holograms with the real nonrigid and deformable anatomy of young patients.

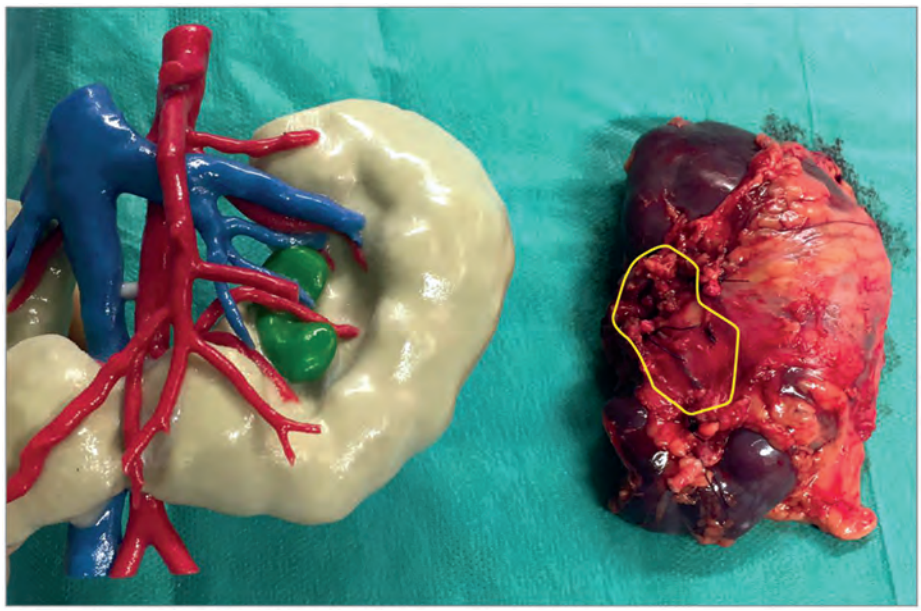

Figure 3: Wilms tumor 3D Print and corresponding kidney. The yellow outline of the kidney specimen indicates the tumor location.

Challenges still exist for the clinical application of the proposed novel 3D visualization techniques. Conventional medical imaging techniques produce a large amount of information, but good interpretation of these data requires years of expertise. Diffusion-weighted imaging in MRI already shows the increasing potential to discriminate tumor from healthy tissue.[17] To further objectify these data with scientific accuracy to convert them into 3D prints or AR holograms, more research about standardized algorithms is needed. In addition, high-quality conventional imaging (MRI or CT) is key for obtaining useful preoperative 3D imaging. We had to exclude several cases based on insufficient imaging quality.

There is a need for more research into standardizing the optimal imaging method (MRI, CT, or CT angiogram), section thickness, and timing for contrast enhancement, specifically in children of different ages. In the present study, the segmentation was performed manually in close collaboration between an information technology expert, a pediatric radiologist, and a pediatric oncology surgeon. Standardizing this process may save valuable time for medical experts.

CONCLUSION

This study suggests that 3D visualization may have an added value for surgeons in the preoperative assessment of children with WT. Additional understanding of the anatomy by using 3D technology was found for all 4 anatomical structures (the tumor, arteries, veins, and urinary collecting structures). Future research should be aimed at improving the speed, accuracy, and automation of the segmentation process for the 3D visualization and expanding its clinical use in pediatric oncologic surgery.

REFERENCES

1. Nakamura L, RitcheyM. Current management of Wilms' tumor. Curr Urol Rep. 2010;11(1):58-65. doi:10.1007/s11934-009-0082-z
2. Dome JS, Graf N, Geller JI, et al. Advances in Wilms tumor treatment and biology: progress through international collaboration. J Clin Oncol. 2015;33(27):2999-3007. doi:10.1200/JCO.2015.62.1888
3. Pritchard-Jones K, Moroz V, Vujanic G, et al; Children's Cancer and Leukaemia Group (CCLG) Renal Tumours Group. Treatment and outcome of Wilms' tumour patients: an analysis of all cases registered in the UKW3 trial. Ann Oncol. 2012;23(9):2457-2463. doi:10.1093/annonc/mds025
4. Davidoff AM, Interiano RB,Wynn L, et al. Overall survival and renal function of patients with synchronous bilateral Wilms tumor undergoing surgery at a single institution. Ann Surg. 2015;262(4):570-576. doi:10.1097/SLA.0000000000001451
5. Davidoff AM, Giel DW, Jones DP, et al. The feasibility and outcome of nephron-sparing surgery for children with bilateral Wilms tumor: the St Jude Children's Research Hospital experience: 1999-2006. Cancer. 2008;112(9):2060-2070. doi:10.1002/cncr.23406
6. Wilde JC, Aronson DC, Sznajder B, et al. Nephron sparing surgery (NSS) for unilateral Wilms tumor (UWT): the SIOP 2001 experience. Pediatr Blood Cancer. 2014;61(12):2175-2179. doi:10.1002/pbc.25185
7. Interiano RB, Delos Santos N, Huang S, et al. Renal function in survivors of nonsyndromic Wilms tumor treated with unilateral radical nephrectomy. Cancer. 2015;121(14):2449-2456. doi:10.1002/cncr.29373
8. Sato M, Tateishi K, Murata H, et al. Three-dimensional multimodality fusion imaging as an educational and planning tool for deep-seated meningiomas. Br J Neurosurg. 2018;32(5):509-515. doi:10.1080/02688697.2018.1485877
9. VannierMW, Marsh JL. Three-dimensional imaging, surgical planning, and image-guided therapy. Radiol Clin North Am. 1996;34(3):545-563.
10. Crossingham JL, Jenkinson J,Woolridge N, Gallinger S, Tait GA, Moulton CA. Interpreting three-dimensional structures from two-dimensional images: a web-based interactive 3D teaching model of surgical liver anatomy. HPB (Oxford). 2009;11(6):523-528. doi:10.1111/j.1477-2574.2009.00097.x
11. Cimerman M, Kristan A. Preoperative planning in pelvic and acetabular surgery: the value of advanced computerised planning modules. Injury. 2007;38(4):442-449. doi:10.1016/j.injury.2007.01.033
12. Shin J, Truong QA. Manufacturing better outcomes in cardiovascular intervention: 3D printing in clinical practice today. Curr Treat Options Cardiovasc Med. 2018;20(12):95. doi:10.1007/s11936-018-0692-1
13. Diment LE, Thompson MS, Bergmann JHM. Clinical efficacy and effectiveness of 3D printing: a systematic review. BMJ Open. 2017;7(12):e016891. doi:10.1136/bmjopen-2017-016891
14. Yang T, Lin S, Xie Q, et al. Impact of 3D printing technology on the comprehension of surgical liver anatomy. Surg Endosc. 2019;33(2):411-417. doi:10.1007/s00464-018-6308-8
15. van Oosterom MN, van der Poel HG, Navab N, van de Velde CJH, van Leeuwen FWB. Computer-assisted surgery: virtual- and augmented-reality displays for navigation during urological interventions. Curr Opin Urol. 2018;28(2):205-213. doi:10.1097/MOU.0000000000000478
16. Ogrinc G, Davies L, Goodman D, Batalden P, Davidoff F, Stevens D. SQUIRE 2.0 (Standards for Quality Improvement Reporting Excellence): revised publication guidelines from a detailed consensus process. BMJ Qual Saf. 2016;25(12):986-992. doi:10.1136/bmjqs-2015-004411
17. Littooij AS, Nikkels PG, Hulsbergen-van de Kaa CA, van de Ven CP, van den Heuvel-Eibrink MM, Olsen OE. Apparent diffusion coefficient as it relates to histopathology findings in post-chemotherapy nephroblastoma: a feasibility study. Pediatr Radiol. 2017;47(12):1608-1614. doi:10.1007/s00247-017-3931-9
18. Nam KW, Park J, Kim IY, Kim KG. Application of stereo-imaging technology to medical field. Healthc Inform Res. 2012;18(3):158-163. doi:10.4258/hir.2012.18.3.158
19. Kieran K, Williams MA,McGregor LM, Dome JS, Krasin MJ, Davidoff AM. Repeat nephron-sparing surgery for children with bilateral Wilms tumor. J Pediatr Surg. 2014;49(1):149-153. doi:10.1016/j.jpedsurg.2013.09.048
20. Wake N, Bjurlin MA, Rostami P, Chandarana H, HuangWC. Three-dimensional printing and augmented reality: enhanced precision for robotic assisted partial nephrectomy. Urology. 2018;116:227-228. doi:10.1016/j.urology.2017.12.038

21. Maddox MM, Feibus A, Liu J,Wang J, Thomas R, Silberstein JL. 3D-printed soft-tissue physical models of renal malignancies for individualized surgical simulation: a feasibility study. J Robot Surg. 2018;12(1):27-33. doi:10.1007/s11701-017-0680-6
22. Mathews JD, Forsythe AV, Brady Z, et al. Cancer risk in 680,000 people exposed to computed tomography scans in childhood or adolescence: data linkage study of 11 million Australians. BMJ. 2013;346:f2360. doi:10.1136/bmj.f2360
23. Knoedler M, Feibus AH, Lange A, et al. Individualized physical 3Dimensional kidney tumor models constructed from 3Dimensional printers result in improved trainee anatomic understanding. Urology. 2015;85(6):1257-1261.doi:10.1016/j.urology.2015.02.053
24. Fan G, Li J, Li M, et al. Three-dimensional physical model-assisted planning and navigation for laparoscopic partial nephrectomy in patients with endophytic renal tumors. Sci Rep. 2018;8(1):582. doi:10.1038/s41598-017-19056-5
25. Incekara F, Smits M, Dirven C, Vincent A. Clinical feasibility of a wearable mixed-reality device in neurosurgery. World Neurosurg. 2018;118:e422-e427. doi:10.1016/j.wneu.2018.06.208
26. Meulstee JW, Nijsink J, Schreurs R, et al. Toward holographic-guided surgery. Surg Innov. 2019;26(1):86-94.doi:10.1177/1553350618799

PART 3

SURGERY

CHAPTER 6

Toward holographic-guided surgery

Jene Meulstee
Johan Nijsink
Ruud Schreurs
Luc Verhamme
Tong Xi
Hans Delye
Wilfred Borstlap
Thomas Maal

Surgical Innovation
Published: September 2018
DOI: 10.1177/1553350618799552

ABSTRACT

The implementation of augmented reality (AR) in image-guided surgery (IGS) can improve surgical interventions by presenting the image data directly on the patient at the correct position and in the actual orientation. This approach can resolve the switching focus problem, which occurs in conventional IGS systems when the surgeon has to look away from the operation field to consult the image data on a 2-dimensional screen.

The Microsoft HoloLens, a head- mounted AR display, was combined with an optical navigation system to create an AR-based IGS system. Experiments were performed on a phantom model to determine the accuracy of the complete system and to evaluate the effect of adding AR.

The results demonstrated a mean Euclidean distance of 2.3 mm with a maximum error of 3.5 mm for the complete system. Adding AR visualization to a conventional system increased the mean error by 1.6 mm.

The introduction of AR in IGS was promising. The presented system provided a solution for the switching focus problem and created a more intuitive guidance system. With a further reduction in the error and more research to optimize the visualization, many surgical applications could benefit from the advantages of AR guidance.

INTRODUCTION

The use of 3-dimensional (3D) imaging for diagnosis, presurgical preparations, postoperative assessment, and follow-up is standard care in many surgical disciplines.[1] In image-guided surgery (IGS), medical images are consulted during surgery for guidance.[2] Critical or hidden structures such as nerves, blood vessels, and tumors can be indicated during surgery by tracking the position of surgical instruments in relation to the position of the patient.[3] In addition, IGS can be used during surgery to follow a preoperatively defined surgical plan.[4] IGS is widely used in different surgical specialties. For example, in plastic surgery, IGS is used to indicate the location of perforating vessels during free flap surgery.[5] In colorectal surgery, IGS and 3D imaging can be used for planning and navigation of colon resections and for visualization of the vascular anatomy.[6] IGS can provide real-time and accurate feedback and is frequently used during trauma and reconstructive surgery and accurate implant placement in craniomaxillofacial surgery.[7,8] Because of its high accuracy, IGS is widely implemented in neurosurgery for cranial, spinal, or skull base procedures.[9-11] For pelvic and acetabular surgery, IGS and 3D planning are used to determine the best surgical approach and to indicate potential surgical difficulties.[12] Wang et al. also described the potential of IGS for a better understanding and mastery of complex craniofacial surgery.[13] In conclusion, the widely used IGS contributes to faster, safer, and more effective surgical procedures and has a positive effect on surgical outcome.[14-16]

In general, IGS systems display their virtual planning data and the positions of tracked surgical instruments on a 2-dimensional (2D) monitor in the operation theatre. This setup creates a situation in which the surgeon is forced to focus both on the surgical field and the virtual planning simultaneously: the switching focus problem.[17,18] Another disadvantage is that the virtual planning presented on the monitors is often not aligned with the viewpoint of the surgeon. The surgeon must relate these positions mentally, which may hamper his or her intuitive interpretation.[19] In addition, the virtual 3D planning or the image data are presented in 2D, which makes it difficult to conceptualize complex 3D anatomy.[7]

Augmented reality (AR) is the technology of blending virtual objects into the real world. AR makes it possible to create a virtual overlay within the surgeon's view.[20] Image data of a patient can be observed directly at the corresponding position

on a patient in the operation theatre. Therefore, AR may be used to overcome the limitations of conventional IGS and can resolve the switching focus problem.[22] Only a few AR devices are commercially available today. Recently, Microsoft introduced the HoloLens (Microsoft Corporation, Redmond, WA, USA), a head-mounted display (HMD) that is able to visualize AR and thus has the potential to be used in combination with IGS.[21] Currently, implementation of the HoloLens in the medical and surgical field is limited to training and education purposes, where virtual data are visualized separately from the patient.[24-28] No studies describing the combination of the HoloLens and IGS systems have been performed.

In this study, an AR IGS system is presented by integration of the HoloLens in the IGS workflow. The technical background is described, and an accuracy study on a 3D-printed phantom model to test the accuracy of the AR IGS system and compare this to the accuracy of a conventional IGS system is performed.

MATERIAL AND METHODS

Integration of the HoloLens in the IGS workflow requires visualization of planned objects (holograms) at the position and orientation corresponding to the IGS planning. The visualization in AR must be continuously updated with tracking information from the IGS system to ensure adequate visualization. The first goal of this study was to develop a method for linking the IGS information with AR visualization, and the technical background of this method is described. The accuracy of the system is affected by errors originating from the navigation system (navigation error), errors introduced by the user (user error), and errors through the use of AR visualization (AR visualization error). The second goal was to evaluate the effect of adding AR to the IGS system, which was achieved in an accuracy study.

Figure 1: Microsoft HoloLens with frame. Using the reflective markers on the frame, the position of the HoloLens was tracked by the optical tracker.

TECHNICAL BACKGROUND

Optical Tracking System. For object tracking, the PST Base system (PS-Tech, Amsterdam, The Netherlands) was used. The PST Base system is an infrared-based optical dual camera tracker that tracks the position and orientation of objects in relation to a fixed reference with the use of reflective marker spheres with a diameter of 13 mm. The positions of these markers were correlated with markers on the virtual objects. The PST tracking system had a root mean square error <0.5 mm and <1°. The field of view of the PST tracker was cone-shaped and has a range from 20 to 300 cm.[29] Using the PST client software, the recognition of different objects was trained by creating a unique configuration of 4 or more reflective spheres. The position and orientation of these objects were tracked with a frequency of 120 Hz and a latency of 15 to 25 ms. The tracking information was imported in Unity software (v5.6.0, Unity Technologies, San Francisco, CA, USA). Three-dimensional models of the virtual planning were imported in Unity using the stereolithography format and linked to the tracked position and orientation of the physical objects. The coordinates of the tracked position were expressed in the IGS reference frame.

Augmented Reality Visualization. The Microsoft HoloLens was used for the visualization of virtual 3D objects (holograms). The HoloLens uses a HMD with video see-through displays. The virtual content is rendered 3-dimensionally in a stereoscopic way.[22,30] The content on a HMD is always consistent with the user's

view because the display is head-mounted.[31] The HoloLens has an untethered and wireless design, displays holograms with a frame rate of 60 Hz, and weighs 580 g.[32] The Holographic Remoting Player application in Unity was used to stream virtual objects to the HoloLens. The position and orientation of holograms were expressed in a different reference system: the HoloLens reference frame.

Linking the HoloLens to the tracking system. The IGS system and the HoloLens both used their own reference frame. In order to visualize a planned position of a tracked object as a hologram, the planning needed to be expressed in the reference frame of the HoloLens. A transformation between the IGS reference frame and the HoloLens reference frame (${}^{HoloLens}T_{IGS}$) was necessary. The position and orientation of the HoloLens needed to be tracked by the IGS system (in the IGS reference frame). A mount with reflective markers was 3D printed and attached with a unique fit to the side of the HoloLens (Figure 1). The position and orientation of this mount were tracked by the IGS system (${}^{Mount}T_{IGS}$). Since the tracker was attached to the side of the HoloLens, a second transformation was required to correct the offset between position of the mount and the HoloLens reference frame (${}^{HoloLens}T_{Mount}$). This static transformation was determined during a calibration process. The complete transformation, (${}^{HoloLens}T_{IGS}$) was calculated using the following formula:

$$ {}^{HoloLens}T_{IGS} = {}^{HoloLens}T_{Mount}\ {}^{Mount}T_{IGS} $$

This transformation made it possible to visualize objects from the virtual planning as holograms in 3D space on the HoloLens.

ACCURACY STUDY

Two experiments were designed to evaluate the accuracy of the AR IGS system: a tight-fit experiment to evaluate the navigation error and a loose-fit experiment to evaluate the total error of the AR IGS system (navigation error + user error + AR visualization error). The AR visualization error could not be measured directly, since it was impossible to perform physical measurements on virtual holograms. This error was deducted from the results of the experiments. The experiments are described in detail below.

Tight-Fit Experiment. The navigation error is a hardware error, which originates from measuring the position of the reflective markers and the calculation of

the object's position from the markers' positions. The tight-fit experiment was conducted to determine the navigation error. A custom-made measuring board and V-shaped cube were designed in SolidWorks (v2016, Dassault Systems, Waltham, MA, USA) and 3D printed at Oceanz (Oceanz, Ede, The Netherlands) using the selective laser sintering printing technique. Reflective spheres were attached to the corners of the measuring board and could, therefore, be tracked by the IGS system, and they served as the IGS reference frame for planning. In this measuring board, 16 recesses were made in which the 3D-printed cube was tightly fitted (Figure 2). Reflective spheres were attached to track the cube. The cube was placed in all recesses, and the tracked position of the cube in the recess was compared with the planned position on the measuring board.

With the introduction of AR, an additional object was tracked by the tracking system: the HoloLens. Tracking an extra object might increase the navigation error. To determine this potential increase, the tight-fit experiment was performed twice: once in the conventional IGS setup (tight-fit IGS) and once when the (tracked) HoloLens was added to the system (tight-fit AR).

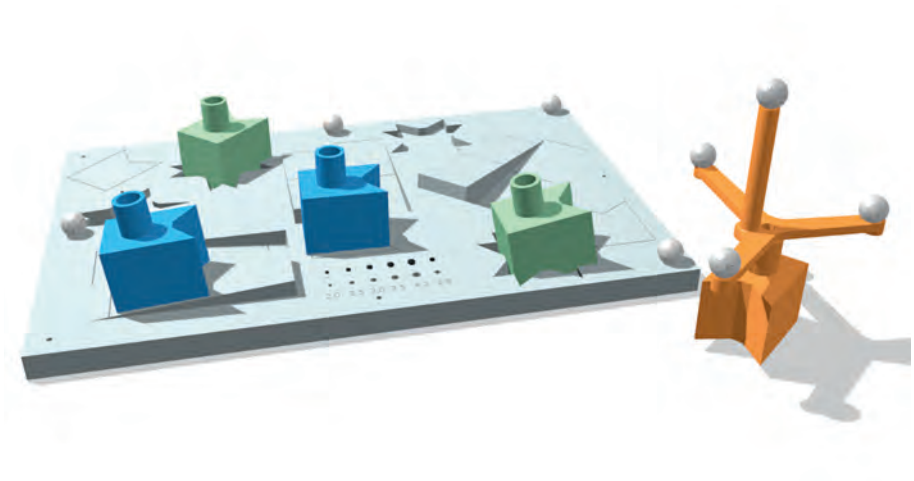

Figure 2: The virtual design of the measuring board and V-shaped tracked cube (orange). The cube was virtually aligned with specific locations on the measuring board. In this figure, the cubes are shown at tight-fitting positions (green) and loose-fitting positions (blue).

Loose-Fit Experiment. In the loose-fit experiment, the planned positions of the cube were not restricted by the design of the measuring board. The cube was positioned at 21 different planned positions on the measuring board. The loose-fit

experiment was performed with and without AR (loose-fit IGS and loose-fit AR). In the loose-fit IGS, the observer positioned the tracked cube on the planned position by visual feedback from a 2D screen. In the loose-fit AR, the observer positioned the tracked cube on the planned position under AR guidance by the HoloLens (Figure 3). The spatial difference between the tracked position of the cube and the virtual planned position was calculated to determine the accuracy of object positioning. In the loose-fit IGS, the combined navigation and user errors were measured. In the loose-fit AR, the combined navigation, user, and AR visualization errors were measured. The size of the AR visualization error could be determined by comparing the results of loose-fit IGS and loose-fit AR. The experiments were performed by 4 observers to investigate interobserver variability.

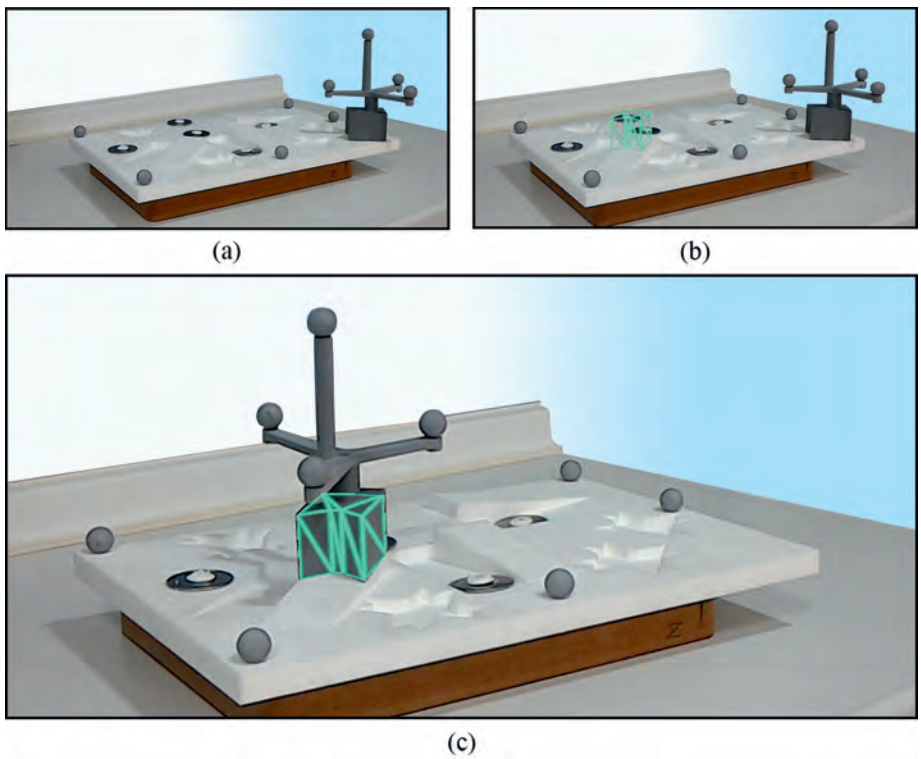

Figure 3: (a) 3D-printed measuring board and the tracked V-shaped cube. (b) Hologram presenting the outline of the planned position of the cube displayed on the measuring board (green outline). (c) The cube is placed at the planned position, indicated by the hologram.

STATISTICAL ANALYSIS

Descriptive statistics were used to represent the size of the navigation error and the overall error found in the tight-fit and loose-fit experiments for translations (Euclidean distance). A Kolmogorov-Smirnov test was used to test for normality. Analysis of variance and post hoc tests with Bonferroni correction were used to determine whether the results of the loose-fit IGS and loose-fit AR differed significantly and to test for differences between the observers. A significance level of .05 was used.

Table 1: Absolute differences in position and orientation between the tracked cube and planned cube in the Tight-fit IGS experiment and Tight-fit AR experiment.

	Tight-fit IGS		Tight-fit AR	
	Mean error ± SD (mm)	Maximum error (mm)	Mean error ± SD (mm)	Maximum error (mm)
X-direction	0.3 ± 0.2	0.8	0.3 ± 0.2	1.0
Y-direction	0.4 ± 0.2	0.8	0.5 ± 0.3	1.2
Z-direction	0.2 ± 0.1	0.6	0.3 ± 0.2	0.8
Euclidean Distance	0.6 ± 0.2	1.0	0.7 ± 0.2	1.4
	Mean error ± SD (°)	Maximum error (°)	Mean error ± SD (°)	Maximum error (°)
X-angle	0.6 ± 0.4	1.8	0.5 ± 0.4	1.8
Y-angle	0.4 ± 0.3	1.2	0.6 ± 0.6	2.5
Z-angle	0.6 ± 0.2	0.9	0.6 ± 0.3	1.5

Table 2: Absolute difference in position and orientation between the tracked cube and planned cube in the Loose-fit experiments without AR and with AR.

	Loose-fit IGS		Loose-fit AR	
	Mean error ± sd (mm)	Maximum error (mm)	Mean error ± sd (mm)	Maximum error (mm)
X-direction	0.3 ± 0.4	1.9	1.0 ± 0.6	2.6
Y-direction	0.4 ± 0.3	1.2	1.6 ± 0.6	3.3
Z-direction	0.3 ± 0.3	1.7	0.9 ± 0.6	2.5
Euclidean Distance	0.7 ± 0.4	2.0	2.3 ± 0.5	3.6
	Mean error ± sd (°)	Maximum error (°)	Mean error ± sd (°)	Maximum error (°)
X-angle	0.4 ± 0.3	1.8	0.7 ± 0.6	2.0
Y-angle	0.5 ± 0.4	2.3	0.9 ± 0.8	2.8
Z-angle	0.4 ± 0.3	1.1	1.2 ± 0.8	2.8

RESULTS

Linking the HoloLens with the IGS system made it possible to display the IGS planning directly in the working field of the user. An additional screen to display the planning data was therefore not required, which eliminated the switching focus problem. The accuracy of the presented method was evaluated with 4 experiments.

TIGHT-FIT EXPERIMENTS

The results of the tight-fit experiment are shown in Table 1. The Kolmogorov-Smirnov test demonstrated that all Euclidean distances were normally distributed ($P > .05$). For the tight-fit IGS experiment, the mean Euclidean distance was 0.6 mm (SD = 0.2), with a maximum error of 1.0 mm. For the tight-fit AR experiment, a mean Euclidean distance of 0.7 mm (SD = 0.2), with a maximum error of 1.4 mm, was reported. This difference was not statistically significant ($P = .99$).

LOOSE-FIT EXPERIMENTS

The results of the placement of the tracked cube in the loose-fitting experiments are summarized in Table 2. The mean Euclidean distances of the loose-fit AR experiment were normally distributed and showed an increase compared with those of the loose-fit IGS experiment, ranging from 0.7 mm (SD = 0.4) to 2.3 mm (SD = 0.5). This difference was statistically significant ($P < .001$). Comparing the Euclidian distance of the 4 observers in the loose-fit AR experiment, the Kolmogorov-Smirnov test proved that the Euclidean distances were normally distributed ($P > .05$). A 1-way analysis of variance test showed no significant difference between the Euclidean distances of the 4 observers ($P = .13$).

DISCUSSION

Recent advances in medical imaging and image processing technologies can be used to establish a detailed virtual operation plan.[33,34] Intuitive transfer of this virtual operation plan to the intraoperative setting to perform surgery according to planning is desirable. IGS systems can be used within the operation theatre to correlate the planning to the position of the patient. The added value of these IGS systems has been proven for many surgical procedures.[14,15] Improvements in

intuitive visualization of the tracking data intraoperatively, tailored to the surgical intervention, are wanted.[8] In this study, a combination of IGS and AR visualization is presented. The implementation of AR in IGS makes it possible to project the virtual planning directly on the patient. The most important advantage is that this solves the switching focus problem, allowing the surgeon to look continuously at the surgical site instead of switching to a monitor when consulting the virtual planning. If a HMD with a stereoscopic view is used to accomplish AR, complex structures and virtual planning can be visualized in 3D at their anatomical position, resulting in more intuitive visualization.

The proposed system can be used for a wide variety of interventions in which the positions of critical (anatomical) structures (bone pieces, blood vessels, nerves, foreign bodies, tumors, etc.) to be visualized during surgery are crucial. An AR-based IGS system could also be used in keyhole surgery and minimally invasive procedures, providing the surgeon with a virtual view of the patient's anatomy and a virtual view of the position of the instruments directly on the patient. AR can compensate for the loss of direct vision and this could improve hand-eye coordination, which may increase focus and efficiency.[31,35,36] AR can serve as a visual guide during delicate surgical procedures when dissecting and exploring the patient's anatomy.[10] Pratt et al. used AR during reconstructive surgery and a manual alignment to visualize relevant anatomy and the localization of perforating vessels directly on the patient in the view of the surgeon.[5] By resolving the switching focus problem and with real 3D visualization, AR might reduce the cognitive load of the surgeon. This setup allows the use of more advanced and complex virtual planning during surgery.

HARDWARE SELECTION

A wide variety of optical tracking systems are available for clinical applications. In this study, the PST Base tracker was used because of its high accuracy, the possibility to develop unique trackable objects, and because the communication protocol can connect the tracker to other software platforms. The HoloLens was used for the AR visualization. Although multiple AR glasses are available today, commercially and noncommercially, many do not provide real 3D visualization by stereo see-through displays. The Meta Glasses 1 and Meta Glasses 2 (Meta Company, San Mateo, CA, USA) provide 3D visualization with a large field of view, but a cable connected to a computer is used. In our experience, the wireless design

of the HoloLens stimulates the user to inspect holograms from different positions and view angles, and the benefits of 3D are therefore fully utilized. Nevertheless, the technology of AR is developing rapidly, and it can be expected that, in the near future updates, other devices or even other techniques will certainly improve the current state of AR. These innovations could make the impact and application of AR in the medical field even more significant.

ACCURACY

An accuracy study of the AR-based IGS system was performed, since the most important question for the functionality of an IGS system is if the accuracy is sufficient for the intended application.[37] The required accuracy completely depends on the type of intervention, yet for most IGS procedures in oral and craniomaxillofacial surgery, neurosurgery, and trauma surgery, an accuracy of 1 to 2 mm is considered acceptable.[11,14,38-40] The accuracy is affected by errors of the system, user, and visualization. The navigation error was determined using tight-fit AR experiments. The results of these experiments showed that the mean error of the complete setup, including the registration error, printing error, and errors introduced by the optical tracking system, was 0.6 mm in a laboratory setup. By implementing a new trackable object, the HoloLens, a small increase of 0.1 mm in error was seen (0.6 to 0.7 mm). Although this difference was not significant, the 0.1-mm increase of the navigation error was included in the error evaluation described below.

The user error in this study can be estimated when the results of the loose-fit IGS experiment are compared with the results of the tight-fit IGS experiment, since the only difference between these experiments was that the user was not restricted when positioning the cube on the measuring board. The tight-fit IGS experiment showed a mean Euclidean distance of 0.6 mm, and the loose-fit IGS experiment showed a mean Euclidean distance of 0.7 mm. From these results, the user error was estimated to be 0.1 mm in the loose-fit IGS experiment. Wearing the HoloLens in the loose-fit AR experiment might have an effect on the user error, and this effect is included in the AR visualization error. Since it was not possible to perform direct measurements on virtual objects, we were not able to separate this effect from the AR visualization error. To reduce the effect of the user error to a minimum, we made the experiments simple to perform for the observers. This was proved by the resulting user error of 0.1 mm in the loose-fit IGS experiment. Therefore,

the assumption that the user error in the loose-fit AR experiment has very limited influence and was equal to the user error in the loose-fit IGS experiment was made. It must be noted that this user error is likely to be higher during real surgical interventions with more complex positioning and limited manoeuvrability of objects.

The loose-fit AR experiment presented the error of the complete setup including the AR visualization error. The results of this experiment showed a mean Euclidean distance of 2.3 mm, with deviations up to 3.6 mm between the actual and planned positions (Table 2). This error was significantly higher than the error in the loose-fit IGS experiment. This difference was expected since this error was the result of the navigation error, user error, and the AR visualization error. The AR visualization error could be extracted by comparing the loose-fit AR experiment (navigation error + user error + AR visualization error) with the tight-fit experiments (navigation error) and loose-fit IGS experiment (navigation error + user error). The navigation error was found to be 0.7 mm, and the user error in our setup was 0.1 mm. Insight of the navigation and user errors in the presented setup made it possible to deduct the misalignment error of the Hologram on the measuring board: the AR-visualization error. The AR visualization error was estimated to be in the range of 1.5 mm (2.3 mm to 0.7 mm to 0.1 mm). This range means that, by the implementation of an AR-based IGS system, the accuracy will be reduced by ~1.6 mm (additional navigation error + AR visualization error). This additional error of 1.6 mm must be taken into account when AR is implemented in a conventional navigation system. Although this is a relatively small error, further reduction of this error and more research is required before the AR-based IGS system can be implemented in surgical procedures that demand a high accuracy. Nevertheless, this study presented a method for linking the HoloLens to an IGS system, resolved the switching focus problem, and created a more intuitive guidance system. Many surgical applications can benefit from the advantages of AR guidance in IGS and make interventions more intuitive. This approach could reduce the user error and may improve the surgical result.

The mean error of 2.3 mm found for the placement of objects under AR guidance was similar to errors found in the literature wherein other AR visualization methods were used. Errors as a result of the augmented data were reported to range from 0.8 to 5 mm.[41-44] In these studies, different methods were developed to realize AR

visualization, which makes it difficult to compare accuracy results. A benefit of the HoloLens is that it was commercially available. The only requirement to combine the HoloLens with an optical tracking system was the use of a 3D-printed frame. These factors give the HoloLens an advantage over other HMDs described in other applications.[17,23,30,45,46]

FUTURE DEVELOPMENTS

In the proposed method, a manual calibration to find the offset between the HoloLens center and the center of the frame was performed once. The resulting transformation, $({}^{HoloLens}T_{Mount})$, was used in all experiments. Inaccuracies introduced during this manual calibration can have a negative effect on the AR visualization error. More dedicated calibration techniques could be implemented to find $({}^{HoloLens}T_{Mount})$ such as the single-point active alignment method or a stereo camera calibration at the start of a session.[47,48] These methods possibly could improve the accuracy of the calibration and thus reduce the AR visualization error.

In this study, jitter, a high-frequency shaking of the holograms, was seen when the virtual outline of the cube was visualized on the measuring board. To diminish the jitter, a standard moving average filter of 4 Hz was implemented, which significantly reduced the shaking of the holograms. However, the moving average filter introduced a short time delay, and the noise causing the jitter was included in the position of the holograms. These effects affected the AR visualization error. Improvements to the filter or elimination of the source of the noise could lead to a decrease in the visualization error to within the clinical error margin.

Another visualization improvement can be blending the virtual objects more intuitively in the real environment. In our experiments, the virtual objects were displayed on top of the real object, which can result in occlusion of the real objects. Different visualization methods and enhancements are described in other studies to make the visualization more immersive and to create a better mixed-reality experience,[20,30] which might result in a smaller AR visualization error.

Next to the implementation of AR during surgery, AR can be used in the preoperative phase or during different procedures outside the operation theatre. AR can facilitate the understanding of complex anatomy and can assist with surgical planning during partial nephrectomy.[49] In breast reconstructive surgery,

virtual flap planning or the location of perforating arteries can be projected onto the patient's abdomen prior to surgery.[50] In addition to anatomy visualization and surgical purposes, the implementation of AR in procedures such as (pediatric) resuscitation protocols can increase adherence and reduce errors and deviations.[51]

CONCLUSION

In the current study, the HoloLens was combined with an optical tracking system to improve visualization in IGS and to resolve the switching focus problem. An accuracy study was performed; the results showed that the accuracy was affected by 1.6 mm on average when AR was introduced in an IGS system. There is a large potential for AR combined with accurate tracking systems in a wide diversity of medical disciplines. Especially surgical applications could benefit from the advantages of AR guidance.

REFERENCES

1. Vannier MW, Marsh JL. Three-dimensional imaging, surgical planning, and image-guided therapy. Radiol Clin North Am. 1996;34:545-563.
2. Cleary K, Peters TM. Image-guided interventions: technology review and clinical applications. Annu Rev Biomed Eng. 2010;12:119-142.
3. Grimson WE, Kikinis R, Jolesz FA, Black PM. Image- guided surgery. Sci Am. 1999;280:62-69.
4. Bell RB. Computer planning and intraoperative navigation in cranio-maxillofacial surgery. Oral Maxillofac Surg Clin North Am. 2010;22:135-156.
5. Pratt P, Ives M, Lawton G, et al. Through the HoloLens looking glass: augmented reality for extremity reconstruction surgery using 3D vascular models with perforating vessels. Eur Radiol Exp. 2018;2:2.
6. Guerriero L, Quero G, Diana M, et al., Virtual reality exploration and planning for precision colorectal surgery. Dis Colon Rectum. 2018;61:719-723.
7. Rodby KA, Turin S, Jacobs RJ, et al. Advances in oncologic head and neck reconstruction: systematic review and future considerations of virtual surgical planning and computer aided design/computer aided modeling. J Plast Reconstr Aesthet Surg. 2014;67:1171-1185.
8. Schreurs R, Dubois L, Becking AG, Maal TJJ. Implant-oriented navigation in orbital reconstruction. Part 1: technique and accuracy study. Int J Oral Maxillofac Surg. 2018;47:395-402.
9. Drazin D, Kim TT, Polly DW Jr, Johnson JP. Introduction: intraoperative spinal imaging and navigation. Neurosurg Focus. 2014;36(3). doi:10.3171/2014.1.FOCUS1425
10. Tagaytayan R, Kelemen A, SikLanyi C. Augmented reality in neurosurgery. Arch Med Sci. 2018;14:572-578.
11. Wei B, Sun G, Hu Q, Tang E. The safety and accuracy of surgical navigation technology in the treatment of lesions involving the skull base. J Craniofac Surg. 2017;28:1431-1434.
12. Cimerman M, Kristan A. Preoperative planning in pelvic and acetabular surgery: the value of advanced computerised planning modules. Injury. 2007;38:442-449.
13. Wang JC, Nagy L, Demke JC. Image-guided surgery and craniofacial applications: mastering the unseen. Maxillofac Plast Reconstr Surg. 2015;37:43.
14. Azarmehr I, Stokbro K, Bell RB, Thygesen T. Surgical navigation: a systematic review of indications, treatments, and outcomes in oral and maxillofacial surgery. J Oral Maxillofac Surg. 2017;75:1987-2005.
15. Mezger U, Jendrewski C, Bartels M. Navigation in surgery. Langenbecks Arch Surg. 2013;398:501-514.
16. Luz M, Strauss G, Manzey D. Impact of image-guided sur- gery on surgeons' performance: a literature review. Int J Hum Factors Ergon. 2016;4:229-263.
17. Wang H, Wang F, Leong APY, Xu L, Chen X, Wang Q. Precision insertion of percutaneous sacroiliac screws using a novel augmented reality-based navigation system: a pilot study. Int Orthop. 2016;40:1941-1947.
18. Herrlich M, Tavakol P, Black D, et al. Instrument-mounted displays for reducing cognitive load during surgical navi- gation. Int J Comput Assist Radiol Surg. 2017;12:1599- 1605.
19. Kersten-Oertel M, Gerard IJ, Drouin S, Petrecca K, Hall JA, Collins DL. Towards augmented reality guided crani- otomy planning in tumour resections. In: Zheng G, Liao H, Jannin P, Cattin P and Lee SL, eds. Medical Imaging and Augmented Reality: 7th International Conference, MIAR 2016, Bern, Switzerland, August 24-26, 2016, Proceedings. Cham, Switzerland: Springer; 2016:163-174.
20. Azuma RT. A survey of augmented reality. Presence. 1997;6:335-385.
21. Evans G, Miller J, Pena MI, MacAllister A, Winer EH. Evaluating the Microsoft HoloLens through an augmented reality assembly application. Paper presented at: SPIE Defense + Security; May 5, 2017; Anaheim, CA.
22. Sielhorst T, Feuerstein M, Navab N. Advanced medical displays: a literature review of augmented reality. J Disp Technol. 2008;4:451-467.
23. Qian L, Barthel A, Johnson A, et al. Comparison of optical see-through head-mounted displays for surgical interventions with object-anchored 2D-display. Int J Comput Assist Radiol Surg. 2017;12:901-910.
24. Microsoft. What is mixed reality? https://developer.micro- soft.com/en-us/windows/mixed-reality/mixed_reality. Published March 21, 2018. Accessed August 28, 2018.
25. Pelargos PE, Nagasawa DT, Lagman C, et al. Utilizing virtual and augmented reality for educational and clini- cal enhancements in neurosurgery. J Clin Neurosci. 2017;35:1-4.
26. Hanna MG, Worrell S, Ishtiaque A, Fine J, Pantonowitz L. SIIM 2017 Scientific Session Posters & Demonstrations. Pathology specimen radiograph co-registration using the HoloLens improves physician assistant workflow. https:// cdn.ymaws.com/siim.org/resource/resmgr/siim2017/ abstracts/posters-Hanna.pdf. Accessed August 28, 2018.

27. Morley C, Choudhry O, Kelly S, Phillips J, Ahmed F. SIIM 2017 Scientific Session Posters & Demonstrations. Mixed reality visualization of medical imaging data. https://cdn. ymaws.com/siim.org/resource/ resmgr/siim2017/abstracts/ posters-Morley.pdf. Accessed August 28, 2018.
28. Syed AZ, Zakaria A, Lozanoff S. Dark room to augmented reality: application of HoloLens technology for oral radio- logical diagnosis. Oral Surg Oral Med Oral Pathol Oral Radiol. 2017;124:e33.
29. PS-Tech. Optical tracker PST base. http://www.ps-tech.com/ optical-trackers/optical-tracker-pst-base. Accessed January 7, 2018.
30. Meola A, Cutolo F, Carbone M, Cagnazzo F, Ferrari M, Ferrari V. Augmented reality in neurosurgery: a systematic review. Neurosurg Rev. 2017;40:537-548.
31. Zhang X, Fan Z, Wang J, Liao H. 3D augmented reality based orthopaedic interventions. In: Zheng G and Li S, eds. Computational Radiology for Orthopaedic Interventions. Cham, Switzerland: Springer; 2016:71-90.
32. Zielke MA, Zakhidov D, Hardee G, et al. Developing virtual patients with VR/AR for a natural user interface in medical teaching. In: 2017 IEEE 5th International Conference on Serious Games and Applications for Health (SeGAH); April 2-4, 2017; Perth, Australia.
33. Handels H, Ehrhardt J, Plötz W, Pöppl SJ. Virtual planning of hip operations and individual adaption of endoprostheses in orthopaedic surgery. Int J Med Inform. 2000;58-59:21-28.
34. Swennen GRJ, Mollemans W, Schutyser F. Three- dimensional treatment planning of orthognathic surgery in the era of virtual imaging. J Oral Maxillofac Surg. 2009;67:2080-2092.
35. López-Mir F, Naranjo V, Fuertes JJ, Alcañiz M, Bueno J, Pareja E. Design and validation of an augmented reality system for laparoscopic surgery in a real environment. Biomed Res Int. 2013;2013:758491.
36. Bernhardt S, Nicolau SA, Soler L, Doignon C. The status of augmented reality in laparoscopic surgery as of 2016. Med Image Anal. 2017;37:66-90.
37. Wiles AD, Thompson DG, Frantz DD. Accuracy assessment and interpretation for optical tracking systems. In: Proceedings of SPIE—The International Society for Optical Engineering; May 5, 2004; San Diego, CA.
38. Labadie RF, Davis BM, Fitzpatrick JM. Image-guided surgery: what is the accuracy? Curr Opin Otolaryngol Head Neck Surg. 2005;13:27-31.
39. Ieguchi M, Hoshi M, Takada J, Hidaka N, Nakamura H. Navigation-assisted surgery for bone and soft tissue tumors with bony extension. Clin Orthop Relat Res. 2012;470:275-283.
40. Zhang S, Gui H, Lin Y, Shen G, Xu B. Navigation-guided correction of midfacial post-traumatic deformities (Shanghai Surgical Innovation 26(1) experience with 40 cases). J Oral Maxillofac Surg. 2012;70:1426-1433.
41. Vigh B, Müller S, Ristow O, et al. The use of a head- mounted display in oral implantology: a feasibility study. Int J Comput Assist Radiol Surg. 2014;9:71-78.
42. Zhang X, Chen G, Liao H. High quality see-through surgical guidance system using enhanced 3D autostereoscopic augmented reality. IEEE Trans Biomed Eng. 2016;64:1815- 1825.
43. Mahmoud N, Grasa ÓG, Nicolau SA, et al. On-patient see- through augmented reality based on visual SLAM. Int J Comput Assist Radiol Surg. 2017;12:1-11.
44. Katić D, Spengler P, Bodenstedt S, et al. A system for context-aware intraoperative augmented reality in dental implant surgery. Int J Comput Assist Radiol Surg. 2015;10:101-108.
45. Chen X, Xu L, Wang Y, Hao Y, Wang L. Image-guided installation of 3D-printed patient-specific implant and its application in pelvic tumor resection and reconstruction surgery. Comput Methods Programs Biomed. 2016;125:66- 78.
46. Cutolo F, Carbone M, Parchi PD, Ferrari V, Lisanti M, Ferrari M. Application of a new wearable augmented real- ity video see-through display to aid percutaneous proce- dures in spine surgery. In: De Paolis L and Mongelli A, eds. Augmented Reality, Virtual Reality, and Computer Graphics. Cham, Switzerland: Springer; 2016:43-54.
47. Tuceryan M, Navab N. Single point active alignment method (SPAAM) for optical see-through HMD calibration for AR. In: Proceedings IEEE and ACM International Symposium on Augmented Reality (ISAR 2000); October 5 and 6, 2000; Munich, Germany.
48. Zhang Z. A flexible new technique for camera calibration. IEEE Trans Pattern Anal Mach Intell. 2000;22:1330-1334.
49. Wake N, Bjurlin MA, Rostami P, Chandarana H, Huang WC. Three-dimensional printing and augmented reality: enhanced precision for robotic assisted partial nephrec- tomy. Urology. 2018;116:227-228.
50. Hummelink S, Verhulst AC, Maal TJJ, Hoogeveen YL, Kool LJS, Ulrich DJO. An innovative method of planning and displaying flap volume in DIEP flap breast reconstructions. J Plast Reconstr Aesthet Surg. 2017;70:871-875.
51. Siebert JN, Ehrler F, Gervaix A, et al. Adherence to AHA guidelines when adapted for augmented reality glasses for assisted pediatric cardiopulmonary resuscitation: a randomized controlled trial. J Med Internet Res. 2017;19:e18

CHAPTER 7

Surgical guides versus augmented reality to transfer a virtual surgical plan for open cranial vault reconstruction: a pilot study

Jene Meulstee
Thijs Bussink
Hans Delye
Tong Xi
Wilfred Borstlap
Thomas Maal

Advances in Oral and Maxillofacial Surgery
Published: August 2022
DOI: 10.1016/j.adoms.2022.100334

ABSTRACT

Virtual surgical planning of an open cranial vault reconstruction enables a faster, safer and better surgical procedure for craniosynostosis patients. However, transfer a virtual surgical plan to the patient remains challenging. Although 3D-printed surgical guides can be used, their production is rather time-consuming and expensive. Since augmented reality (AR), allows the user to directly visualize a virtual planning onto the patient, it can be used as an alternative.

By using AR-glasses (Microsoft HoloLens), a new AR-based workflow was developed and compared with surgical guides to transfer the surgical plans on 3D-prints of 10 patients with different types of craniosynostosis.

An accuracy of 2.1 mm and a mean transfer time of 8.24 minutes were reported with the AR workflow as compared to an accuracy of 0.9 mm and a mean transfer time of 50 seconds for surgical guides.

Surgical guides were the most fitting method to transfer virtual surgical plans. The relatively large outliers in the AR workflow meant that the mean accuracy was just outside the clinically acceptable margin. However, the low cost and simplicity make the AR workflow a promising alternative.

INTRODUCTION

Open cranial vault reconstruction (OCVR) is the most commonly used method for the treatment of craniosynostosis patients older than six months.[1–6] During OCVR, the cranial vault is dissected and optimally reconstructed with increased volume and an improved aesthetical shape. Before the actual operation, virtual surgical planning (VSP) can assist the surgical team by virtually simulating the complete procedure in a three-dimensional (3D) space. With VSP, the projected cranial volume could be calculated, cranial shape aesthetics can be reviewed from different perspectives, and crucial outcome parameters (e.g. orbital distance) can be measured.[7,8] This additional insight, and the option to evaluate different surgical strategies could avoid inadequate osteotomies during the actual surgery.[9–11] However, transferring the VSP to the patient in the operation theatre remains a challenge.

3D printing techniques can be used to generate patient-specific guides to intraoperatively transfer the osteotomy patterns and reconstruction positions. This can reduce operation time as well as perioperative blood loss.[10,12–14] Nevertheless, costs up to 1500 euros, and the manufacturing time of several days are significant drawbacks of using 3D printed surgical guides.[12,15,16]

Augmented reality (AR) is a new and innovative visualisation technique that can be used to enhance the real world with virtual objects. By wearing AR glasses, the user can see a 3D representation of the VSP directly projected on the patient,[17,18] and thereby overcoming the limitations of other transfer techniques. Yet, little is known on accuracy and usability of AR for this purpose.

The goal of this pilot study was to develop an AR application to project the VSP directly to the patient. The usability and accuracy of the AR workflow was compared to the surgical guides by transferring the VSP on 10 3D-printed models of craniosynostosis patients.

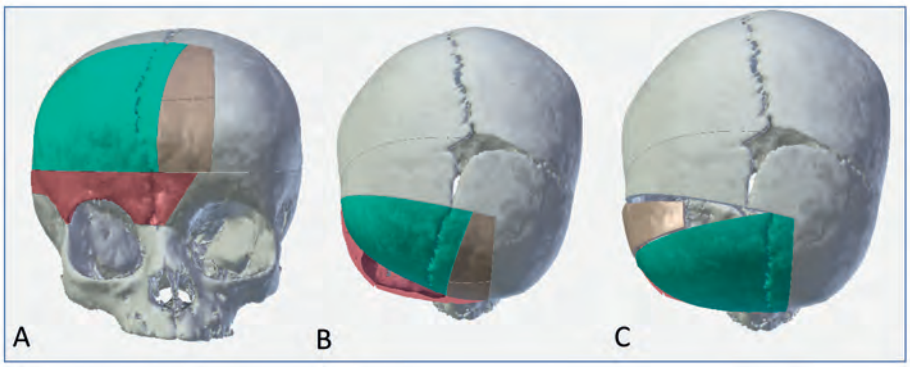

Figure 1: Virtual surgical planning of a plagiocephaly patient, where the fused right coronal suture resulted in a retracted orbit and a flattened forehead. Multiple surgical approaches were simulated during the virtual planning. With a deflection point, a little left from the midline of the nasion, the symmetry of the orbital region could be restored. The forehead was reconstructed on the newly created orbital bar. By simulating the final reconstruction, the osteotomies could be optimized and gaps between the cranial segments minimized. A.) frontal view of the planned osteotomies. B.) top view showing the right orbital advancement (red). C.) top view with a simulation of the forehead reconstruction.

MATERIALS & METHODS

SUBJECTS

This study was approved by the medical ethical review board of the Radboud University Medical Centre, Nijmegen, The Netherlands (no. 2019-6070).

3D models of 10 patients who underwent an OCVR, based on a VSP were retrospectively included (four scaphocephaly, three trigonocephaly and three plagiocephaly cases). An example of a VSP is given in Figure 1. 3D models were created from the patients' computed tomography (CT) scans in 3DMedX (v. 2.1, 3D Lab Radboudumc, Nijmegen, The Netherlands) and 3D printed (Oceanz, Ede, The Netherlands). Additional measuring beacons were appended to every 3D model for performing accuracy tests, as described in the accuracy study section.

Based on the VSP of the patients, surgical guides to transfer the dissection lines were designed in Blender (v. 2.79, the Blender foundation, Amsterdam, the Netherlands) and 3D printed. The guides had a unique fit over the surface of the crania but covered only the part that needed to be dissected. Small recesses were made in the surgical guides at anatomical landmarks. These enabled the user to check if the guides were correctly placed on the 3D models (Figure 2). A pencil was used to mark the dissection pattern on to the 3D shape.

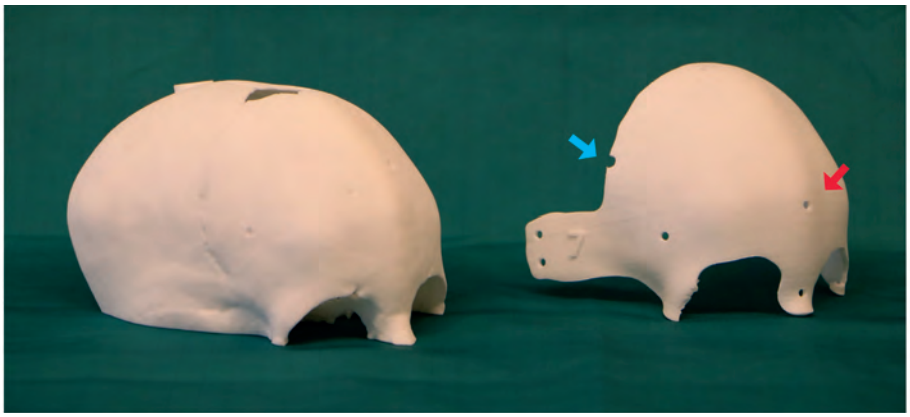

Figure 2: 3D-printed cranial shape of a trigonocephaly patient with surgical guide. The gaps (indicated by red arrow) were used to demarcate the VSP on the patient with a pencil. Small recesses in the guide indicated an anatomical landmark (blue arrow) to check if the surgical guide was correctly positioned.

AUGMENTED REALITY APPLICATION

To show the VSP in AR on the 3D-printed skulls, an application was developed for the HoloLens (first version, Microsoft, Washington, USA). Unity (v5.6.5, Unity Technologies, San Francisco, USA) and the Vuforia AR Unity 3D toolkit (v7.1, PTC Inc., Massachusetts, USA) were used to develop this application. Different phases of the VSP could be visualised on the HoloLens, allowing the user to switch to the original 3D skull model, see the osteotomy lines and see animated instructions how the bone segments should be positioned. To prevent occlusion of the surgical view, solely the intersections points of the osteotomies could be visualized (Figure 3).

PATIENT TRACKING

To directly visualise the VSP on the patient, the position and orientation of the patient were tracked in correlation with the HoloLens. Tracking ensured that the VSP stayed correctly positioned, even when the patient models moved or when the user reviewed the planning from different angles. For this, a 5 x 5 cm stainless steel marker with a laser-engraved quick response (QR) pattern was attached to the calvaria models that could be tracked by the built-in camera of the HoloLens. A stainless-steel pointer, equipped with a second QR marker, was used to indicate five landmarks on the 3D model. With point-based registration, the VSP was instantaneously matched to the cranial shapes. The difference (registration error) was calculated as the root mean square (RMS).

VIRTUAL GUIDANCE

Using a pencil, the user was instructed to mark the (virtual) planning points that were visualised by the HoloLens on the 3D models. A QR marker was attached to the pencil so the HoloLens could also track the pencil's position. This allowed the HoloLens to display a virtual arrow, showing the user how the pencil should be manipulated to target the tip of the pencil to the planning point. The red colour of the virtual arrow turned orange if the offset was below 3 mm and green if it was below 2 mm. In addition, the absolute distance between the pencil tip and reference point was indicated on the user's top-left view (Figure 3).

ACCURACY STUDY

Two observers, who were skilled HoloLens users, performed two experiments twice. In the first experiment, the observers placed the surgical guides on the 10 cranial shapes and demarcated 10 points with a pencil. A digital calliper with 0.01 mm accuracy was used to measure the 2D distance between the marked points and (at least) 5 beacon points. Using these distances and the trilateration principle, the 3D position was reconstructed.[19] The error reported in this study was defined as the Euclidean distance between the marked and planned points. The observers repeated the experiment two weeks later to examine intra-observer variability.

In the second experiment, the same observers used the HoloLens application to transfer the plan. After calibration and registration, 10 holographic points were demarcated with a pencil on the surface of the 3D-printed cranial shapes. Errors were calculated using the beacon points, similar to the approach in the first experiment, and the experiment was likewise repeated two weeks later by the observers.

Student's t-tests with a significance level of alpha = 0.05 were used to compare the sizes of the errors. Backwards linear regression was used to determine the variables that most influenced the outcome. The intraclass correlation coefficient (ICC) was calculated to determine the consistency of the measuring technique.

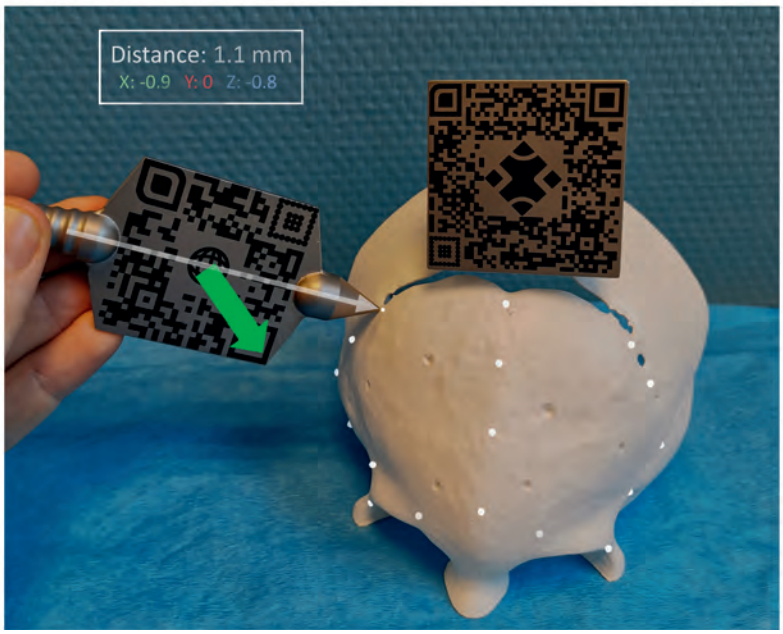

Figure 3: HoloLens application to demarcate the virtual planning points on the 3D-printed cranial shapes. The planning points (white) were virtually visualised on the 3D-prints. The pointer and the pencil (equipped with a QR marker) were tracked. The green arrow in the middle of the pointer indicated how the pointer should be manipulated to target the (virtual) planned point. The distance to the target was displayed in the top-left corner.

RESULTS

For each cranial shape, moment, modality and observer, 10 Euclidean distances were gathered, resulting in a total of 800 measurements. Five measurements were excluded due to measuring errors. Results are presented in Table 1. The average Euclidean distance using the surgical guide (N = 398) was 0.9 ± 0.6 mm. The distances measured using the HoloLens method (N = 397) were significantly higher at 2.1 ± 1.5 mm. The average time needed to transfer the VSP using the surgical guides was 50 ± 14 seconds, which was significantly lower than the time needed for using the HoloLens; 8 min 24 seconds ± 2 min 54 seconds. This time included the calibration, registration and demarcation time.

For both the surgical guides and HoloLens, no significant intra-observer variability was found. A significant difference between the observers was found for both

the surgical guides and HoloLens method, as indicated in Figure 4. There were no significant time differences between the observers in transferring the VSP with the use of surgical guides. There was, however, a significant time difference between the observers when the HoloLens was used. All the results are presented in Table 1.

None of the variables (transfer time, moment of performing the experiment, type of craniosynostosis, registration error and observer) were found to be predictors of the surgical guide outcomes. For the HoloLens outcomes, the observer ($\beta = 0.42$, $p < 0.05$) and the RMS ($\beta = 0.979$, $p < 0.05$) were found to be predicting variables with an overall model fit of $R^2 = 0.26$.

An ICC of 0.989 was found when the two delineations were measured twice, with no significant difference.

Table 1: Results of the error using the surgical guides and HoloLens transfer method

Modality	Subgroup	Variable	Mean ± SD	P value
Surgical Guide	Moment	1	0.9 ± 0.5 mm	0.913
		2	0.9 ± 0.6 mm	
	Observer 1	Moment 1	0.9 ± 0.5 mm	0.377
		Moment 2	1.0 ± 0.6 mm	
	Observer 2	Moment 1	0.8 ± 0.6 mm	0.400
		Moment 2	0.8 ± 0.5 mm	
	Observer	1	0.9 ± 0.6 mm	*0.010
		2	0.8 ± 0.5 mm	
	Time	Observer 1	50 ± 14 s	0.772
		Observer 2	51 ± 14 s	
HoloLens	Moment	1	2.1 ± 1.5 mm	0.707
		2	2.0 ± 1.4 mm	
	Observer 1	Moment 1	1.8 ± 1.3 mm	0.769
		Moment 2	1.9 ± 1.0 mm	
	Observer 2	Moment 1	2.4 ± 1.7 mm	0.496
		Moment 2	2.2 ± 1.6 mm	
	Observer	1	1.9 ± 1.2 mm	*0.002
		2	2.3 ± 1.7 mm	
	Time	Observer 1	615 ± 134 s	*0.000
		Observer 2	392 ± 132 s	
	Registration error (RMS)	Observer 1	0.8 ± 0.1 mm	0.588
		Observer 2	0.9 ± 0.3 mm	

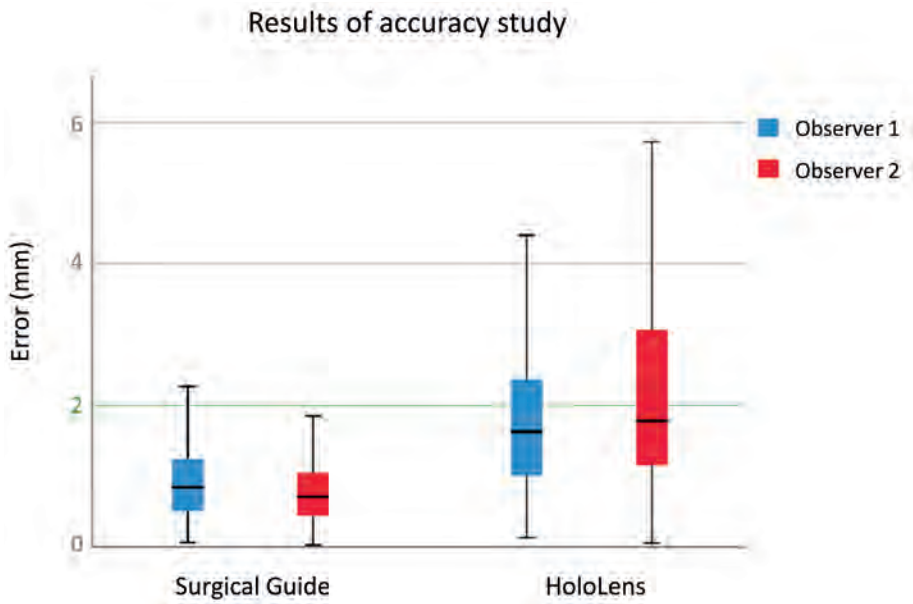

Figure 4: Boxplots of results for both observers.

DISCUSSION

From our experience, and confirmed in previous studies, VSP planning is an advantageous tool to assist the surgical team during the preparation of OCVR surgery.[7,9,20–22] An adequate preoperative plan, created together with the surgical team, in combination with a fast and easy method to execute the planning will make the surgery itself more fluent, predictable and can result in enhanced surgical outcomes.[10,12,15,23]

Two methods to transfer a VSP to a patient have been studied, including an innovative method with AR. 3D prints were used to simulate the clinical situation and made it possible to evaluate both transfer methods.

As was expected, the surgical guides showed excellent results and presented an average error of 0.9 ± 0.6 mm. Although a small difference of 0.1 mm was measured between the observers, we concluded that this error was random because the linear regression did not show any significant correlation.

The time differences of the methods could be explained because the surgical guides could be placed within seconds on the subjects' crania due to their unique fit, while the HoloLens workflow required a few minutes for calibration and registration. In addition, demarcating the planning points through the gaps in the guides was faster than moving a pencil freely in three dimensions in the HoloLens workflow.

We determined that an error margin of 2 mm is acceptable when a patient's plan is transferred, since the handling of the craniotome will always induce a small error and the actual thickness of the osteotomies is difficult to predict. With an average error of 1.9 mm and 2.3 mm for observers 1 and 2, respectively, the HoloLens transfer method was almost accurate enough to meet the clinical threshold of 2 mm. The outliers with relatively large errors had the greatest effects on the results. Figure 4 shows that the median error of the HoloLens method for both the observers was smaller than the mean error (1.6 and 1.8 versus 1.9 and 2.3, respectively). This means, that if outliers and large inaccurate measurements can be eliminated, the average error and the standard deviation of the HoloLens transfer method will fundamentally improve. Errors larger than 3 mm were particularly seen in the results of observer 2. Taking into consideration that observer 1 systematically used more time to transfer the VSP on the cranial shapes (10.25 minutes versus 6.5 minutes), a logical explanation is that observer 1 was more meticulous than observer 2, which resulted in fewer planning points with larger errors. Nevertheless, outliers should be prevented because they can have a tremendous impact on the surgical outcome. The linear regression confirmed that the observer is the largest variable. Therefore, we advise the HoloLens user to be precise and take their time to transfer VSP on the patient. In future studies, more observers should be included to investigate inter-observer variability.

With the AR method developed in this study, no external tracking systems was needed because only the integrated camera of the HoloLens was used, making for a compact and low-cost surgical guidance system. Other studies that used image tracking for the HoloLens involved relatively large markers that limited the manoeuvrability of the surgeon or covered a substantial part of the surgical working area.[24,25] After testing several markers and sizes (unpublished data), we recommend using a 5 x 5 cm marker with many feature points because this is the optimal compromise between marker size and accuracy at a working distance of

0.5–1 meter. The QR pattern was laser-engraved on medical grade stainless steel to make the markers sterilisable and reusable for future surgical implementation.[26] Even under varying surgical lightning, the markers were recognised by the HoloLens.

To prevent any visualisation errors, the observers were instructed to meticulously adjust the position of the HoloLens on their head while looking at the pointer. Only when the holographic pointer had an exact overlap with the real pointer, the HoloLens was considered correctly positioned. This essential but time-consuming and cumbersome step was repeated every time the HoloLens was put on. Future updates of AR glasses with eye calibration, would make this step obsolete.

The binocular display of the HoloLens is one of its key features and provides excellent depth perception that facilitates the inspection of complex 3D anatomical structures.[27] Because projecting large holograms within the surgeon's working view (± 50 cm) can result in discomfort, the virtual planning points were kept small and visualised just above the real models. Furthermore, the coloured indication arrow and the distance to target indication (Figure 3) were placed just outside the focus view of the surgeon in our HoloLens application. This allowed the user to maintain the natural link between the virtual elements and real world and led to increased comfort, sharper visualization and reduced double images. This turned out to be a valuable addition to the experiments, as had already been suggested by Gao et al. who used this in a similar HoloLens application for mandibular surgery.[25]

For craniosynostosis surgery, Han et al. implemented AR to transfer a VSP and described excellent post-op results.[24] Instead of a head-mounted display, they used a video capture of the surgical site and augmented this with the virtual plan. Since (transparent) stereoscopic glasses enable a true 3D perception and makes additional screens superfluous, we believe strongly in the potential of AR-glasses over displays.

Usually, a VSP consists of two phases: marking the osteotomy lines and performing the cranial reconstruction. This study focused on the first phase, which allow an easy and straightforward comparison between transfer methods. Yet, we expect the added value of AR during the reconstruction phase will be more evident because this phase is surgically more challenging and AR could assist the surgeon

by visualising the correct position and orientation of the bone segments, directly in 3D and in the surgical field.

Using the HoloLens for surgical guidance has already been described for various other clinical applications.[17,28–30] Although they affirm the huge potential of AR, these studies also recommend that more research is required. With this pilot study, we aimed to comply to this demand by investigating the accuracy and other aspects as a first step toward the actual implementation of AR for OCVR.

CONCLUSION

Using surgical guides is the fastest and most accurate method to transfer a virtual surgical plan for open cranial vault reconstruction. The AR approach that was developed resulted in almost acceptable accuracy results; however, special attention and caution are required to prevent outliers. Nevertheless, the low cost and simplicity of the AR workflow makes it a promising alternative to surgical guides.

REFERENCES

1. Delye HHK, Arts S, Borstlap WA, et al. Endoscopically assisted craniosynostosis surgery (EACS): The craniofacial team Nijmegen experience. *J Cranio-Maxillofacial Surg*. 2016;44(8):1029-1036. doi:10.1016/j.jcms.2016.05.014
2. Keshavarzi S, Hayden MG, Ben-Haim S, Meltzer HS, Cohen SR, Levy ML. Variations of endoscopic and open repair of metopic craniosynostosis. *J Craniofac Surg*. 2009;20(5):1439-1444. doi:10.1097/SCS.0b013e3181af1555
3. Doumit GD, Papay FA, Moores N, Zins JE. Management of Sagittal Synostosis. *J Craniofac Surg*. 2014;25(4):1260-1265. doi:10.1097/SCS.0b013e3182a24635
4. Lee BS, Hwang LS, Doumit GD, et al. Management options of non-syndromic sagittal craniosynostosis. *J Clin Neurosci*. 2017;39:28-34. doi:10.1016/j.jocn.2017.02.042
5. Braun TL, Eisemann BS, Olorunnipa O, Buchanan EP, Monson LA. Safety outcomes in endoscopic versus open repair of metopic craniosynostosis. *J Craniofac Surg*. 2018;29(4):856-860. doi:10.1097/SCS.0000000000004299
6. Meulstee JW, de Jong GA, Borstlap WA, Koerts G, Maal TJJ, Delye H. The normal evolution of the cranium in three dimensions. *Int J Oral Maxillofac Surg*. 2020;49(6):739-749. doi:10.1016/j.ijom.2019.10.012
7. Mardini S, Alsubaie S, Cayci C, Chim H, Wetjen N. Three-dimensional preoperative virtual planning and template use for surgical correction of craniosynostosis. *J Plast Reconstr Aesthetic Surg*. 2014;67(3):336-343. doi:10.1016/j.bjps.2013.11.004
8. Chim H, Wetjen N, Mardini S. Virtual surgical planning in craniofacial surgery. *Semin Plast Surg*. 2014;28(3):150-158. doi:10.1055/s-0034-1384811
9. Steinbacher DM. Three-Dimensional Analysis and Surgical Planning in Craniomaxillofacial Surgery. *J Oral Maxillofac Surg*. 2015;73(12):S40-S56. doi:10.1016/j.joms.2015.04.038
10. Shah A, Patel A, Steinbacher DM. Simulated frontoorbital advancement and intraoperative templates enhance reproducibility in craniosynostosis. *Plast Reconstr Surg*. 2012;129(6):1011e-1012e. doi:10.1097/PRS.0b013e31824effa7
11. Lu SM, Pessino K, Gray RL, Rodgers SD, Schneider SJ, Bastidas N. Virtual Planning for Exchange Cranioplasty in Cranial Vault Remodeling. *J Craniofac Surg*. 2021;32(1):320-321. doi:10.1097/SCS.0000000000007148
12. Burge J, Saber NR, Looi T, et al. Application of CAD/CAM Prefabricated Age-Matched Templates in Cranio-Orbital Remodeling in Craniosynostosis. *J Craniofac Surg*. 2011;22(5):1810-1813. doi:10.1097/SCS.0b013e31822e8045
13. Ni J, Yang B, Li B. Reconstructive Operation of Nonsyndromic Multiple-Suture Craniosynostosis Based on Precise Virtual Plan and Prefabricated Template. *J Craniofac Surg*. 2017;28(6):1541-1542. doi:10.1097/SCS.0000000000003784
14. Queiros C, Joly A, Paré A, et al. Use of cutting guides during craniosynostosis sequelae surgery: A comparative study between computer-assisted planning and post-operative results. *J Cranio-Maxillofacial Surg*. 2017;45(7):1062-1068. doi:10.1016/j.jcms.2017.03.011
15. Kobets AJ, Ammar A, Nakhla J, et al. Virtual modeling, stereolithography, and intraoperative CT guidance for the optimization of sagittal synostosis reconstruction: a technical note. *Child's Nerv Syst*. 2018;34(5):965-970. doi:10.1007/s00381-018-3746-5
16. Soleman J, Thieringer F, Beinemann J, Kunz C, Guzman R. Computer-assisted virtual planning and surgical template fabrication for frontoorbital advancement. *Neurosurg Focus*. 2015;38(5):E5. doi:10.3171/2015.3.FOCUS14852
17. van Doormaal TPC, van Doormaal JAM, Mensink T. Clinical Accuracy of Holographic Navigation Using Point-Based Registration on Augmented-Reality Glasses. *Oper Neurosurg*. 2019;17(6):588-593. doi:10.1093/ons/opz094
18. Meulstee JWJW, Nijsink J, Schreurs R, et al. Toward Holographic-Guided Surgery. *Surg Innov*. 2019;26(1):86-94. doi:10.1177/1553350618799552
19. Norrdine A. An Algebraic Solution to the Multilateration Problem An Algebraic Solution to the Multilateration Problem. In: *International Conference on Indoor Positioning and Indoor Navigation*. ; 2012:1-4. doi:10.13140/RG.2.1.1681.3602

20. Macmillan A, Lopez J, Mundinger GS, Major M, Medina MA, Dorafshar AH. Virtual surgical planning for correction of delayed presentation scaphocephaly using a modified melbourne technique. In: *Journal of Craniofacial Surgery*. Vol 29. ; 2018:914-919. doi:10.1097/SCS.0000000000004290
21. Seruya M, Borsuk DE, Khalifian S, Carson BS, Dalesio NM, Dorafshar AH. Computer-aided design and manufacturing in craniosynostosis surgery. In: *Journal of Craniofacial Surgery*. Vol 24. ; 2013:1100-1105. doi:10.1097/SCS.0b013e31828b7021
22. García-Mato D, Ochandiano S, García-sevilla M, et al. Craniosynostosis surgery: workflow based on virtual surgical planning, intraoperative navigation and 3D printed patient-specific guides and templates. *Sci Rep*. 2019;9(1):17691. doi:10.1038/s41598-019-54148-4
23. Lopresti M, Daniels B, Buchanan EP, Monson L, Lam S. Virtual surgical planning and 3D printing in repeat calvarial vault reconstruction for craniosynostosis: Technical note. *J Neurosurg Pediatr*. 2017;19(4):490-494. doi:10.3171/2016.10.PEDS16301
24. Han W, Yang X, Wu S, et al. A new method for cranial vault reconstruction: Augmented reality in synostotic plagiocephaly surgery. *J Cranio-Maxillofacial Surg*. 2019;47(8):1280-1284. doi:10.1016/j.jcms.2019.04.008
25. Gao Y, Lin L, Chai G, Xie L. A feasibility study of a new method to enhance the augmented reality navigation effect in mandibular angle split osteotomy. *J Cranio-Maxillofacial Surg*. 2019;47(8):1242-1248. doi:10.1016/j.jcms.2019.04.005
26. Wesselius TS, Meulstee JW, Luijten G, Xi T, Maal TJJ, Ulrich DJO. Holographic Augmented Reality for DIEP Flap Harvest. *Plast Reconstr Surg*. 2021;147(1):25e-29e. doi:10.1097/PRS.0000000000007457
27. Wellens LM, Meulstee J, van de Ven CP, et al. Comparison of 3-Dimensional and Augmented Reality Kidney Models With Conventional Imaging Data in the Preoperative Assessment of Children With Wilms Tumors. *JAMA Netw open*. 2019;2(4):e192633. doi:10.1001/jamanetworkopen.2019.2633
28. Pratt P, Ives M, Lawton G, et al. Through the HoloLens™ looking glass: augmented reality for extremity reconstruction surgery using 3D vascular models with perforating vessels. *Eur Radiol Exp*. 2018;2(1):2. doi:10.1186/s41747-017-0033-2
29. Moreta-Martinez R, García-Mato D, García-Sevilla M, Pérez-Mañanes R, Calvo-Haro J, Pascau J. Augmented reality in computer-assisted interventions based on patient-specific 3D printed reference. *Healthc Technol Lett*. 2018;5(5):162-166. doi:10.1049/htl.2018.5072
30. Müller F, Roner S, Liebmann F, Spirig JM, Fürnstahl P, Farshad M. Augmented reality navigation for spinal pedicle screw instrumentation using intraoperative 3D imaging. Spine J. 2019;000:1-8. doi:10.1016/j.spinee.2019.10.012

CHAPTER 8

Holographic augmented reality for DIEP flap harvest

Tycho Wesselius
Jene Meulstee
Gijs Luijten
Tong Xi
Thomas Maal
Dietmar Ulrich

Tycho Wesselius and
Jene Meulstee
contributed equally
to this work

Plastic and Reconstructive Surgery
Published: January 2021
DOI: 10.1097/PRS.0000000000007457

ABSTRACT

During a deep inferior epigastric perforator (DIEP) flap harvest, the identification and localization of the epigastric arteries and its perforators are crucial. Holographic augmented reality is an innovative technique that can be used to visualize this patient-specific anatomy extracted from a computed tomographic scan directly on the patient. This study describes an innovative workflow to achieve this.

A software application for the Microsoft HoloLens was developed to visualize the anatomy as a hologram. By using abdominal nevi as natural landmarks, the anatomy hologram is registered to the patient. To ensure that the anatomy hologram remains correctly positioned when the patient or the user moves, real-time patient tracking is obtained with a quick response marker attached to the patient.

Holographic augmented reality can be used to visualize the epigastric arteries and its perforators in preparation for a deep inferior epigastric perforator flap harvest.

Potentially, this workflow can be used to visualize the vessels intraoperatively. Furthermore, this workflow is intuitive to use and could be applied for other flaps or other types of surgery

INTRODUCTION

In deep inferior epigastric perforator (DIEP) flap surgery, it is essential to identify the location, size, and relations of the epigastric arteries and its perforators in the patient. Acquiring a computed tomography angiogram or a magnetic resonance angiogram of a patient's abdomen can enhance the preoperative understanding of the surgical site, and reduces surgery time and possibly complications.[1–3] Because the surgeon cannot see these images simultaneously with the operating field, the images have to be memorized during surgery, which limits the full potential of the imaging. Alternatively, Doppler ultrasound can be used to identify the location of the relevant vessels. However, this approach can be lengthy and inaccurate, and does not show the intra-muscular arterial course and the relationship between the perforators.[4–6] An innovative two-dimensional projector to visualize the anatomy on the patient was recently developed,[7–9] but it does not allow the visualization of the anatomy in three dimensions (3D), and the device needs to be operated with at least one hand.

We present a novel workflow to visualize the relevant 3D abdominal anatomy for a DIEP flap harvest with the Microsoft HoloLens (Microsoft Corp., Redmond, Wash.) augmented reality glasses,[10–12] which provide a hands-free 3D visualization and are intuitive to use.

PATIENTS AND METHODS

WORKFLOW

The workflow to achieve a holographic augmented reality visualization consists of four steps: (1) image acquisition and segmentation of the relevant anatomical structures, (2) importing the relevant anatomy to an in-house–developed HoloLens application, (3) real-time tracking of the patient, (4) registration and visualization of the holographic anatomy in the patient. *A video which demonstrates the implementation of our HoloLens workflow to mark the perforators on the abdomen of the patient can be found online on www.PRSJournal.com*

Figure 1: Computed tomographic angiograph slice with a perforator (white arrow) and a radiopaque skin marker (gray arrow).

IMAGE ACQUISITION AND SEGMENTATION

Abdominal nevi are natural skin landmarks that can be used to accurately indicate the same location on the patient's body at different moments in time. Therefore, at least five abdominal nevi are selected to be adhered with 2.3-mm radiopaque skin markers (Suremark; The Suremark Company, Lowell, Mass.). When insufficient nevi are present, other skin marks such as small hemangiomas or scars can be used instead. If these are absent too, markings could be made with henna ink or gentian ink.[13,14] A two-dimensional photograph of the abdomen with the marked nevi is captured, as these nevi will need to be relocated on the patient later (step 4, registration). Subsequently, an abdominal computed tomographic angiograph [Canon (Canon, Inc., Tokyo, Japan) 320-slice computed tomography scanner; slice thickness, 0.5 mm; contrast, Iomeron (Bracco, Tokyo, Japan) 300 mg/ml; flow, 5 ml/second; delay of bolus tracking, 8 seconds] is acquired (Figure 1). After threshold-based segmentation of the computed tomographic angiograph in Maxilim (v2.2.2.1; Medicim NV, Mechelen, Belgium), 3D models of the radiopaque skin markers, the skin, inferior epigastric arteries with its perforators, and the rectus

abdominis muscles are created. Patients are not exposed to additional radiation, because a computed tomographic angiograph is part of the standard protocol for DIEP flap breast reconstruction patients in our clinic.

IMPORT THE ANATOMY MODEL TO THE HOLOLENS APPLICATION

The HoloLens (version 1) is a wireless, head-mounted display that can generate augmented reality by showing holograms in the space around the user. Whereas the holograms stay on the same location in the room, the user can move around to appreciate these from different perspectives. By using the Unity framework (v5.6.7; Unity Technologies, San Francisco, Calif.), an application for the HoloLens was developed to visualize the 3D models as holograms in the patient. The previously segmented 3D models are wirelessly transferred to the HoloLens using the in-house–developed application (Figure 2).

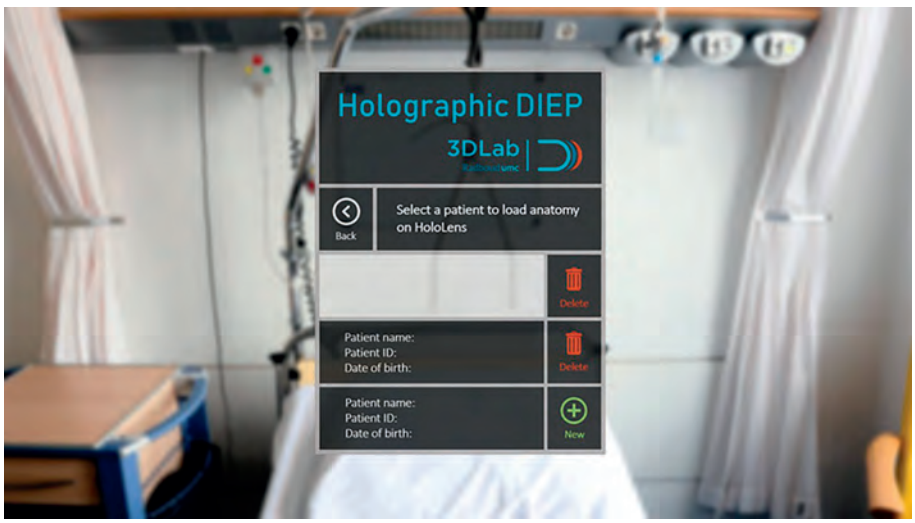

Figure 2: HoloLens augmented reality application loading screen seen from the user perspective.

PATIENT TRACKING

A 5 × 5-cm quick response marker is attached to the skin above the navel of the patient. The HoloLens recognizes and tracks the location and orientation of this quick response marker with the built-in red, green, and blue camera and the Vuforia augmented reality toolkit (v7.1; PTC Inc., Boston, Mass.) (Figure 3). Tracking the quick response marker ensures that the holographic anatomy remains correctly positioned in the next step of the workflow.

REGISTRATION AND VISUALIZATION

To display the holograms in the correct anatomical orientation when looking through the HoloLens, an accurate registration of the holograms with the abdomen of the patient is required. A 3D–printed, sterilizable, stainless steel pointer with a laser engraved second quick response marker was designed in-house. With this pointer, the user indicates the five abdominal nevi on the patient that had radiopaque skin markers on them during the acquisition of the computed tomographic angiograph (Figure 3). The HoloLens registers the 3D locations of the nevi by tracking the second quick response marker on the pointer. By using a Procrustes algorithm, the HoloLens calculates how the imported 3D models from the computed tomographic angiograph should fit over the patient in the room (Figure 4). With voice commands or a holographic menu, the user can switch between the visualization of different anatomical structures. Because the patient's position is tracked by the HoloLens using the quick response marker above the navel, it is possible to inspect the anatomy hologram from different positions, even when the patient or the HoloLens user is moving. Now, the user can use the hologram to mark the perforator locations in preparation for a DIEP flap harvest or use the HoloLens to visualize the course of the epigastric arteries during surgery. In the operating room, dissection can begin while the hologram remains in place, because it is registered to a sterilized quick response code outside the surgical area and does not need the nevi anymore.

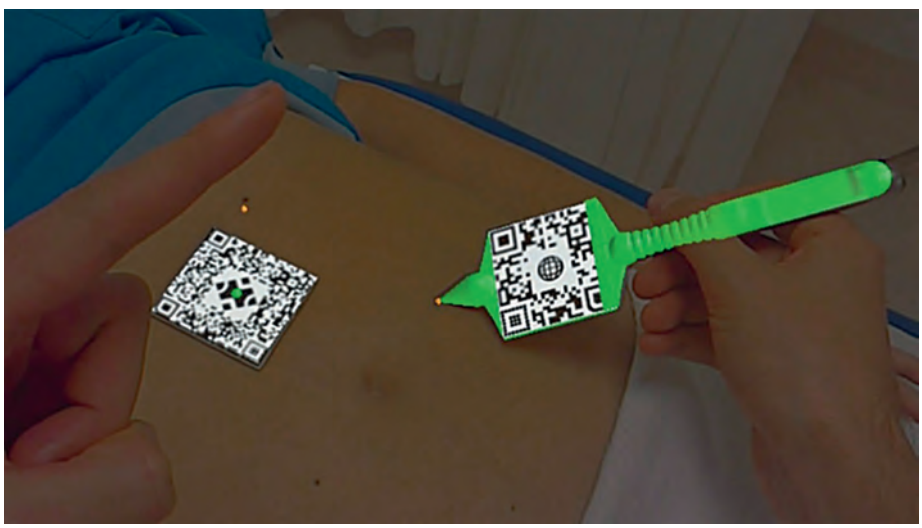

Figure 3: To make the HoloLens register the anatomy hologram to the quick response code above the navel, abdominal nevi are indicated with a stainless-steel pointer that is recognized by the HoloLens.

DISCUSSION

We developed a workflow to visualize relevant anatomy segmented from a computed tomographic angiograph for a DIEP flap harvest directly in the abdomen of the patient with HoloLens augmented reality glasses. Real-time tracking ensures that the anatomy stays correctly fused with the patient, regardless of position changes of the patient or the HoloLens user. The 3D holographic visualization provides an intuitive and strong perception of complex anatomy, in this case, the location of perforators and their relation with epigastric arteries in the rectus abdominis muscle. The workflow is the most advanced described to date, because of the combination of real-time patient tracking and a novel registration method that uses abdominal nevi as natural landmarks. The workflow can be used preoperatively to mark anatomical structures such as vessels on the patient, or intraoperatively to navigate. A limitation of the workflow is that the depth of the hologram is sometimes difficult to estimate, because a real world hand or tool does not interact with the hologram. However, we try to solve this by using a tool that is also displayed as a hologram and therefore can interact with the anatomy hologram. This workflow could be used for other flaps, other types of surgery, or in combination with other innovative technologies.[15–17]

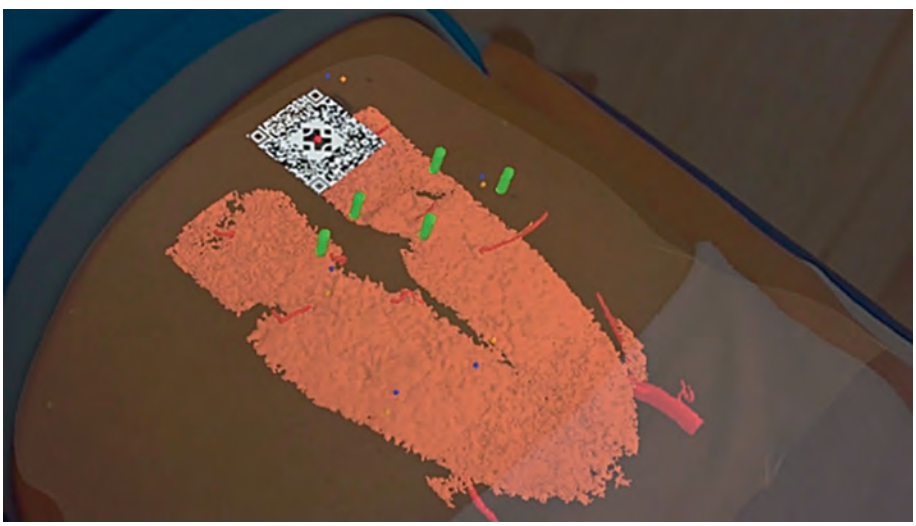

Figure 4: While the HoloLens tracks the patient position by the quick response marker above the navel, the anatomy hologram is visualized. The green cylinders indicate perforator locations on the skin. The user can switch between visualizations of different anatomical structures.

ACKNOWLEDGMENT

The authors would like to thank Dylan Duits for providing professional input during development of the in-house–developed HoloLens application

REFERENCES

1. Wade RG, Watford J, Wormald JCR, Bramhall RJ, Figus A. Perforator mapping reduces the operative time of DIEP flap breast reconstruction: A systematic review and meta-analysis of preoperative ultrasound, computed tomography and magnetic resonance angiography. J Plast Reconstr Aesthet Surg. 2018;71:468–477.
2. Chae MP, Ganhewa D, Hunter-Smith DJ, Rozen WM. Direct augmented reality computed tomographic angiography technique (ARC): An innovation in preoperative imaging. Eur J Plast Surg. 2018;41:415–420.
3. Lam DL, Mitsumori LM, Neligan PC, Warren BH, Shuman WP, Dubinsky TJ. Pre-operative CT angiography and three-dimensional image post processing for deep inferior epigastric perforator flap breast reconstructive surgery. Br J Radiol. 2012;85:e1293–e1297.
4. Shaw RJ, Batstone MD, Blackburn TK, Brown JS. Preoperative Doppler assessment of perforator anatomy in the anterolateral thigh flap. Br J Oral Maxillofac Surg. 2010;48:419–422.
5. Stekelenburg CM, Sonneveld PM, Bouman MB, et al. The hand held Doppler device for the detection of perforators in reconstructive surgery: What you hear is not always what you get. Burns 2014;40:1702–1706.
6. Blondeel PN, Beyens G, Verhaeghe R, et al. Doppler flow- metry in the planning of perforator flaps. Br J Plast Surg. 1998;51:202–209.
7. Hummelink S, Hameeteman M, Hoogeveen Y, Slump CH, Ulrich DJ, Schultze Kool LJ. Preliminary results using a newly developed projection method to visualize vascular anatomy prior to DIEP flap breast reconstruction. J Plast Reconstr Aesthet Surg. 2015;68:390–394.
8. Hummelink S, Verhulst AC, Maal TJJ, Hoogeveen YL, Schultze Kool LJ, Ulrich DJO. An innovative method of planning and displaying flap volume in DIEP flap breast reconstructions. J Plast Reconstr Aesthet Surg. 2017;70:871–875.
9. Hummelink S, Hoogeveen YL, Schultze Kool LJ, Ulrich DJO. A new and innovative method of preoperatively planning and projecting vascular anatomy in DIEP flap breast reconstruction: A randomized controlled trial. Plast Reconstr Surg. 2019;143:1151e–1158e.
10. Bosc R, Fitoussi A, Pigneur F, Tacher V, Hersant B, Meningaud JP. Identification of perforating vessels by augmented reality: Application for the deep inferior epigastric perforator flap (in French). Ann Chir Plast Esthet. 2017;62: 336–339.
11. Frantz T, Jansen B, Duerinck J, Vandemeulebroucke J. Augmenting Microsoft's HoloLens with vuforia tracking for neuronavigation. Healthc Technol Lett. 2018;5:221–225.
12. Sielhorst T, Feuerstein M, Navab N. Advanced medical displays: A literature review of augmented reality. J Disp Technol. 2008;4:451–467.
13. Rathod S, Munshi A, Agarwal J. Skin markings methods and guidelines: A reality in image guidance radiotherapy era. South Asian J Cancer 2012;1:27–29
14. Probst H, Dodwell D, Gray JC, Holmes M. An evaluation of the accuracy of semi-permanent skin marks for breast cancer irradiation. Radiography 2006;12:186–188.
15. Kanevsky J, Safran T, Zammit D, Lin SJ, Gilardino M. Making augmented and virtual reality work for the plastic surgeon. Ann Plast Surg. 2019;82:363–368.
16. Kim YJ, Kelley BP, Nasser JS, Chung KC. Implementing precision medicine and artificial intelligence in plastic surgery: Concepts and future prospects. Plast Reconstr Surg Glob Open 2019;7:e2113.
17. Shortliffe EH. Artificial intelligence in medicine: Weighing the accomplishments, hype, and promise. Yearb Med Inform. 2019;28:257–262

CHAPTER 9

Augmented reality guided condylectomy

Thijs Bussink
Thomas Maal
Jene Meulstee
Tong Xi

British Journal of Oral and Maxillofacial Surgery
Published: February 2022
DOI: 10.1016/j.bjoms.2022.01.008

ABSTRACT

Condylectomy is frequently performed to stop the active growth in cases of unilateral condylar hyperplasia and to enhance the symmetry of an asymmetric mandible. The optimal height and position of the condylar osteotomy line can be planned by using a 3D virtual skull model based on a cone beam computed tomography (CBCT) scan. An accurate transfer of a 3D virtual planned (proportional) condylectomy to the patient is challenging due to the limited surgical access. A new clinical workflow that uses augmented reality to assist a condylectomy is presented step-by-step. This augmented reality based approach has the potential to be implemented in the clinical setting routinely.

INTRODUCTION

Unilateral condylar hyperplasia (UCH) is a rare disorder of progressive nature and is characterized by alterations to facial function and aesthetics.[1,2] UCH is caused by an overactive growth activity in one of the mandibular condyles, but its aetiology is still uncertain and is probably multifactorial.[3] Proportional condylectomy is increasingly being used as an initial treatment in UCH,[4] and is aimed to enhance the symmetry of the mandible and occlusal plane by locating the height of the osteotomy line in such a way that the ramus height of the affected side matches the non-affected side. The key in proportional condylectomy is to be able to place the osteotomy plane at the desired location. The optimal height and position of the condylar osteotomy line can be planned by using a 3D reconstructed virtual skull model based on a cone beam computed tomography (CBCT) scan. Clinically, it remains challenging to transfer a virtually planned condylectomy plane to the patient during surgery. The limited surgical access, the axial location of the condylar head, and the seating of condyle in the fossa often restricts a complete overview of the condylar head and hampers the use of surgical guides. The implementation of augmented reality (AR) can aid surgical interventions by presenting images of 3D virtual surgical planning on the operation field.[5] We present a novel AR-guided workflow for condylectomy.

MATERIAL & METHOD

A 38-year-old female presented at our department with a progressive chin point deviation to the right based on an unilateral condylar hyperplasia. A proportional condylectomy of the left condyle was proposed.

A threshold-based segmentation in IPS CaseDesigner (KLS Martin Group, Tuttlingen Germany) was used to create a 3D model of the mandible from an extended-height CBCT scan (FOV 16 × 22 cm; scanning time 2 × 20 s; voxel size, 0.4 mm; 3D Imaging System, Imaging Sciences International Inc, Hatfield, PA, USA). The osteotomy plane was virtually planned to resolve the discrepancy between the left and right ramal height.

Surgery was performed under general anesthesia with nasotracheal intubation. The left condyle was approached through a post-tragal incision with a limited superior preauricular extension. After gaining access to the condylar head, the surgeon identified the plane of condylectomy visually. Three marking points were place on the lateral condylar surface with a round burr. By wearing Microsoft HoloLens (Microsoft, Washington, USA), the position of three markings was checked using the following steps:

1. A sterile quick response (QR) marker was attached to the lower dentition to allow tracking of the mandibular position through the HoloLens.
2. A stainless-steel pointer, equipped with a second QR marker, was used to check the location of the planned osteotomy line (Figure 1).
3. An inhouse-developed HoloLens application, enabled the surgeon to visualize the planned position of the osteotomy line and the three markings. The HoloLens displayed a virtual arrow at the location of the pointer to direct the surgeon to move the pointer to the planned position (Figure 2).

Next, the actual condylectomy was performed with a round burr based on the markings. The cranial part of the condylar head was removed. Five days following surgery, a postoperative check-up CBCT was acquired. The planned and actual location of the condylectomy planes were compared.

RESULTS AND DISCUSSION

The 3D registration of planned and postoperative mandibular models (Figure 3) showed that on the lateral, anterior and medial side of the condyle, the condylectomy was performed almost exactly as was planned (error ≤ 1 mm). However, the postoperative posterior border of the left condyle was located more caudally compared to the planning. This discrepancy could be a result of the fact that only the lateral position of the osteotomy was verified by the HoloLens.

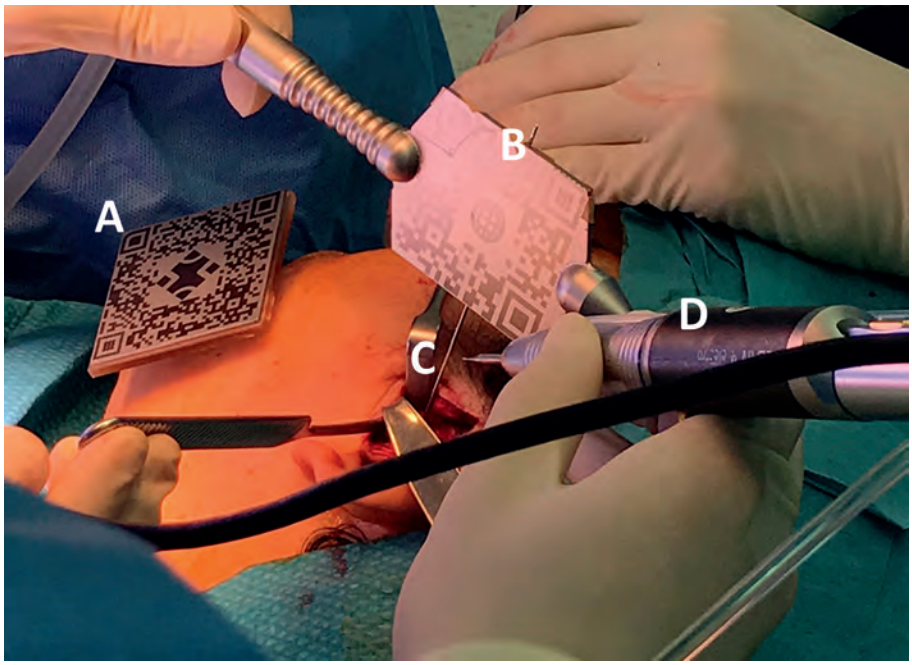

Figure 1: The mandible was tracked by the QR marker fixated on the lower dentition (A). The position of the pointer with laser engraved QR-marker (B) was tracked by the HoloLens and the tip of the Kirschner wire (C) was visualized by the surgeon in the HoloLens. The surgical drill (D) was used to perform the condylectomy.

The accuracy of the presented method should be further investigated in future research. Besides, the software can be improved to make the AR application more intuitive. To eliminate the use of the pointer, the surgical handpiece (and thus the burr) can be equipped with a QR-code so that the position of the burr can be tracked and corrected throughout surgery. The magnitude of the registration error, perception error[6] and surgical error in AR-guided surgery should be investigated thoroughly.

Although conventional surgical navigation systems can be used to guide the user during surgery, the combination of the HoloLens with sterilizable QR markers is an easy and low-cost alternative. This AR solution allows the user to stay focused on the surgical field while attaining feedback from the planning. The surgeon is not forced to switch his/her view to an external monitor as in conventional navigation.

We believe that AR guidance is an adequate method to transfer a virtual planning for various cranio-maxillofacial procedures. Especially during proportional

condylectomy, where surgical guides are impractical, AR guidance is an effective method to assist the surgeon.

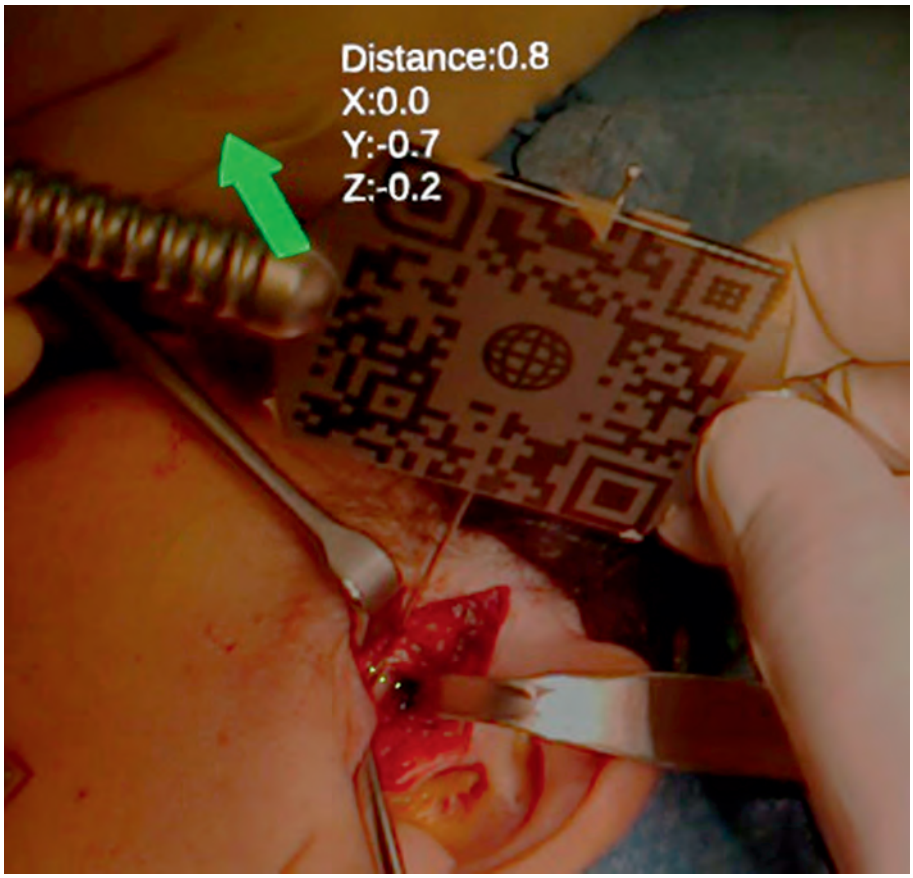

Figure 2: Visualization in the HoloLens: the green arrow indicates how the tip of the pointer should be manipulated to target the planned osteotomy position. The red color of the virtual arrow turned green in case the offset between the planned position of guidance points and the real-time position of the tip of the pointer was below 2 mm. The absolute distance between the pointer and the planned osteotomy point was indicated on the top left.

Figure 3: Lateral view of the preoperative (light gray) and postoperative (dark gray) condyle with the planned (green) and the achieved (blue) osteotomy planes. The three points (red) were projected by the HoloLens and indicated the osteotomy plane. The posterior point was concordant with the planning and the middle point deviated by 1 mm.

ACKNOWLEDGEMENT

We would like to thank Gijs Luijten for designing and developing the QR marker and pointer. We thank Dylan Duits for his help during the development of the HoloLens application.

REFERENCES

1. R.F.S, Rushton MA. Unilateral Hyperplasia of the Mandibular Condyle. Proc R Soc Med. 1946;39(7):431-438. doi:10.1016/0030-4220(48)90183-2
2. Broadway RT, Orth D. Two cases of unilateral hyperplasia of the mandibular condyle. Proc R Soc Med. 1958;51(9):691-693. doi:10.1177/003591575805100901
3. Ghawsi S, Aagaard E, Thygesen TH. High condylectomy for the treatment of mandibular condylar hyperplasia: A systematic review of the literature. Int J Oral Maxillofac Surg. 2016;45(1):60-71. doi:10.1016/j.ijom.2015.09.002
4. Fariña R, Olate S, Raposo A, Araya I, Alister JP, Uribe F. High condylectomy versus proportional condylectomy: Is secondary orthognathic surgery necessary? Int J Oral Maxillofac Surg. 2016;45(1):72-77. doi:10.1016/j.ijom.2015.07.016
5. Kubben P, Sinlae R. Feasibility of using a low-cost head-mounted augmented reality device in the operating room. Surg Neurol Int. 2019;10(1). doi:10.4103/sni.sni_228_18
6. Condino S, Carbone M, Piazza R, Ferrari M, Ferrari V. Perceptual Limits of Optical See-Through Visors for Augmented Reality Guidance of Manual Tasks. IEEE Trans Biomed Eng. 2019;9294(c):1-1. doi:10.1109/TBME.2019.2914517

PART 4

EVALUATION

CHAPTER 10

Longitudinal 3D follow-up and secondary treatment aspects after endoscopic and open scaphocephaly surgery

Guido de Jong
Jene Meulstee
Erik van Lindert
Wilfred Borstlap
Thomas Maal
Hans Delye

Guido de Jong and
Jene Meulstee contributed
equally to this work

Plastic and Reconstructive Surgery
Submitted

ABSTRACT

This retrospective cohort study evaluated the longitudinal three-dimensional (3D) cranial shape developments and the secondary treatment aspects after endoscopically assisted craniosynostosis surgery (EACS) with helmet therapy and open cranial vault reconstruction (OCVR) for scaphocephaly.

Longitudinally collected 3D photos from scaphocephaly patients and healthy infants were evaluated. 3D cranial shape measurements and growth maps were compared between the groups over time. Secondary treatment aspects were compared for the treatment groups.

Both surgical techniques showed their strongest changes directly after surgery with mean parietal 3D growths up to 10 mm. At age 24 months, comparison of head shapes showed mean 3D differences less than ± 2mm with OCVR resulting in a lower vertex and longer cranial length when compared to EACS. At 48 months of age, no measurements were significantly different between treatment groups. Only the total head volume was somewhat larger in the male EACS group at age 48 months ($p=0.046$).

Blood loss in EACS (mean 18 ml, range 0-160 ml) was lower than in OCVR (mean 100 ml, range 15-300 ml, $p<0.001$). Median length of stay after surgery was shorter for EACS (2 days, range 1-5) compared to OCVR (5 days, range 3-8, $p<0.001$).

We conclude that EACS for scaphocephaly shows equal craniometric results at age 48 months and has a better surgery profile compared to OCVR. Early diagnostics and referral for suspected scaphocephaly to allow EACS is therefore recommended.

INTRODUCTION

Scaphocephaly is the result of premature fusion of the sagittal suture and is characterized by an elongated head, a wide and prominent forehead, and a narrow occiput.[1] Scaphocephaly is the most common type of craniosynostosis and occurs in 1.5-4 of 10.000 live births worldwide.[2–5]

Treatment of scaphocephaly aims to correct cranial deformities, prevent increased intracranial pressure, and reduce the risk of developmental delay.[6] Among the wide variety of treatment options, open cranial vault reconstruction (OCVR) is the most common treatment option while minimal invasive methods, such as spring mediated cranioplasty and endoscopically assisted craniosynostosis surgery (EACS) in combination with helmet therapy increase in popularity.[6–9] It is expected that these techniques could result in different cranial shape developments after surgery.

Studies show that the endoscopic technique reduced complication and mortality rates, decreased blood loss, shortened hospital stay, and lowered healthcare costs.[3,7,10–12]

Although the aesthetic and morphological outcome of treatment options is often based on subjective measures,[13,14] 3D stereophotogrammetry in combination with advanced evaluation methods allow objective long-term follow-up of the patients' cranial morphology.

The aim of this study was to evaluate the cranial shape development of scaphocephaly patients with objective 3D analysis methods. In addition, the secondary surgical aspects were evaluated.

MATERIAL AND METHODS

PATIENTS

Ethical approval from the regional institutional review board was obtained (no.2020-6128). Unisutural non-syndromic scaphocephaly patients aging up to 56 months who underwent either EACS or OCVR between 2005 and 2019 at our

institute were included. Patients older than 14 months at the time of surgery are rare in our institution and were excluded.

TREATMENT

For children under the age of 6 months, EACS is performed in our center.[8] During EACS, the fused sagittal suture is removed trough two small skin incisions with the aid of the endoscope, and biparietal stave osteotomies are performed (Figure 1). Helmet therapy starts two weeks after EACS for all patients and continues for a period of approximately 10 months. During this period, every 3 months a 3D photo is made to evaluate head growth and adjust/change/stop the helmet therapy if needed.

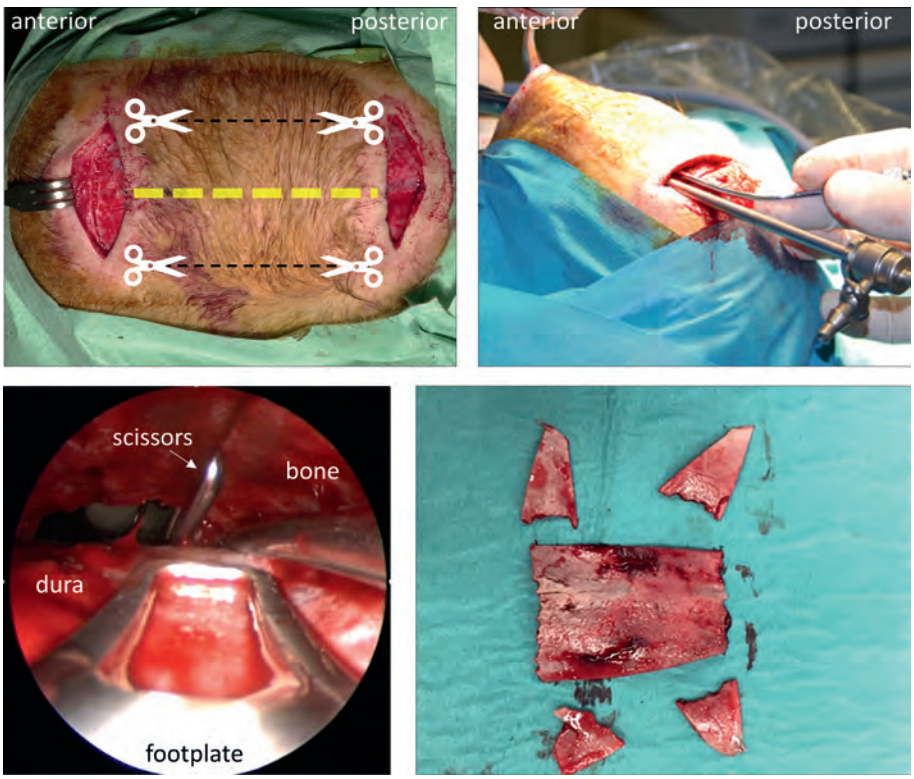

Figure 1: Notable steps in EACS from our institution. Top-left: skin-incisions with schematic overview of affected suture (yellow) and cutting-lines (black). Top-right: external view of minimally invasive removal of affected suture and additional osteotomies. Bottom-left: endoscopic view of minimally invasive removal of affected suture and additional osteotomies. Bottom-right: resected fused sagittal suture and biparietal side-cuts.

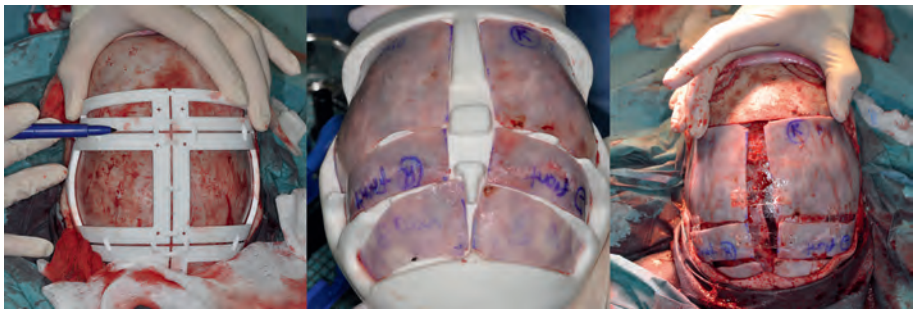

Figure 2: Notable steps in OCVR from our institution. Prior to surgery, the reconstruction is virtually planned and executed by our team to determine the optimal positions of the skull segments and osteotomies. Patient specific surgical guides are used to transfer the planning to the patient. Left: drawing osteotomy-lines on the exposed skull using the guides. Middle: positioning of skull segments in a specific mold prior to fixation. Right: repositioning of expanded skull segment, fixed in place using resorbable plates.

For children older than 6 months at referral, OCVR is performed in our institution. Since 2013, a virtual surgical planning is created for each patient to determine the best surgical strategy. Based on this planning, specific drawing templates are used to demarcate the osteotomy lines and assembly templates are being used for a swift reconstruction of the skull cap (Figure 2). Resorbable plates (SonicWeld, KLS Martin, Tuttlingen, Germany) are used for fixation of the cranial segments.

3D PHOTOS

3D Photos of patients were acquired using the 3DMD Cranial System (3dMDCranial, 3dMD, Atlanta, USA). The 3D photos of patients who underwent treatment were distributed in the nearest age group (3, 6, 9, 12, 15, 18, 24, 36 and 48 months) and distributed in the pre-surgery and post-surgery groups.

3D PHOTO PROCESSING

The same data acquisition, processing and alignment protocols were followed for the 3D photos as described in earlier work.[15–17] All 3D photos underwent quality control and were excluded in case of insufficient quality and were aligned using the Computed Cranial Focal Point (CCFP) method to allow objective evaluation.[16,18]

The scaphocephaly CCFP-offset values were determined using 20 pre-surgery computed tomography scans (CT-scans) of scaphocephaly patients.[16] Reference values were similarly acquired using CT-scans of infants aged 0-48 months.[15] Pre-surgical 3D photos were positioned using the scaphocephaly-specific CCFP-offset. Both the post-surgical OCVR 3D photos and the reference group 3D photos were

positioned using the reference age-specific CCFP-offset values as the head shape of the post-surgery OCVR group was being modelled towards normal shaped heads. The post-surgery EACS 3D photos used scaphocephaly CCFP-offset values interpolated towards the reference value from 6 - 18 months of age. After 18 months, the reference CCFP-offset values were used for the EACS 3D photos.

3D PHOTO MEASUREMENTS

For all 3D photos, the cranial length was measured from the most anterior point to the most posterior point of the cranium and the cranial width was determined by a line perpendicular to the cephalic length.[15] Dividing cranial width by cranial length resulted in the cephalic index (CI). Circumference was measured on the cranial shapes at the crossing points of the cranial width and length. The volume above the sella turcica – nasion plane was calculated. Results were split on gender, type of surgery, and pre or post-surgery status.

GROWTH MAPS

Color-coded growth and shape comparison maps were created to visualize the shape changes of the head and were used to compare the groups. To counter any non-craniosynostosis related asymmetries of the head, the 3D photos were mirrored and averaged over the midsagittal axis prior to analysis. These growth maps visualize the difference between the mean head shapes in two sequential age groups or between two treatment groups. Patients were grouped based on gender, age and treatment. Finally, to investigate the long-term outcome, the results of both surgical strategies were compared at 24 months of age.

SECONDARY TREATMENT ASPECTS

Secondary treatment aspects included: age at surgery, gender, blood loss, surgery time, total anesthesia time, blood-transfusions (peri and post-surgery), hospital stay duration, and intensive care unit (ICU) stay duration. Helmet therapy duration was also obtained for EACS.

STATISTICAL ANALYSIS

For all 3D photo measurements, the mean and standard error of mean (SEM) were computed per dataset per group and a mixed model analysis was performed. Two-tailed t-tests for 3D measurements between age groups per intervention and gender were conducted.

Means and standard deviations were given for normally distributed data. Medians and the range were given for non-normally distributed data. If an outcome value was normally distributed in one sub-group but wasn't in the counterpart group, both values will be reported with medians and ranges for consistency. Level of statistical significance was set at $p<0.05$. For statistical analyses, IBM SPSS Statistics version 25 (IBM Germany GmbH, Ehningen, Germany) was used.

RESULTS

3D PHOTO ACQUISITION

Altogether, 384 3D photos from 106 EACS patients, and 108 3D photos from 34 OCVR patients were used. The EACS and OCVR groups contained 84 and 29 males respectively. A total of 130 reference 3D photos with 64 males (49%) up to the age of 24-months were obtained from an earlier study.[15] The 3D photo distribution is shown in Table 1.

SECONDARY TREATMENT ASPECTS

The secondary treatment aspects of 114 EACS patients (92 males) and 36 OCVR patients (29 males) were collected and presented in Table 2. The male-female ratio was 4 to 1 in both treatment groups. EACS patients had less blood loss, shorter surgery, shorter anesthesia time and a shorter length of stay. Only one EACS case was treated in the ICU for 3 days. In the OCVR group, 25 cases were admitted to the ICU for 1 day each. The remodeling helmet was worn 9.6 months on average (standard deviation=2.4, range =3.9-16.1) after EACS.

Fewer blood transfusions were given during surgery in EACS and the amount of blood given was significantly lower in the EACS group. Remarkably, in both OCVR and EACS groups, the post-surgical transfusion rate was the same (n=7, 19% and n=19, 17% respectively).

Table 1: The number of 3D photos per age-group over pre and post-surgery for EACS and OCVR groups. All groups were divided in male (M) and female (F). mo. = months of age

		Pre-surgery				Post-surgery					
		EACS		OCVR		EACS		OCVR		References	
Group	Age (mo.)	M	F	M	F	M	F	M	F	M	F
1	3	52	13	4	1	4	2			14	12
2	6	18	3	8		33	3	1	1	10	12
3	9			8		47	11	4		13	14
4	12			8	2	47	13	7		10	9
5	15					26	6	9	1	4	7
6	18					12	3	10	3	10	8
7	24					37	8	17	2	3	4
8	36					8	2	4	2		
9	48					29	7	15	1		

Table 2: An overview of the secondary surgical aspects between the EACS and OCVR groups and their respective differences as indicated by the p-values.

	Group		
Parameter	EACS	OCVR	p-value
Male (n, %)	92 (81%)	29 (81%)	0.985
Female (n,%)	22 (19%)	7 (19%)	
Age (months, median, range)	3.9 (2.4-6.6)	9.2(4-14)	<0.001
Blood loss (ml, median, range)	18 (0-160)	100 (15-300)	<0.001
Blood transfusion peri and post-operative (n,%)	21 (19%)	29 (81%)	<0.001
Total amount transfused (ml, median, range)	90 (65-190)	130 (30-250)	<0.001
Length of stay post-surgery (days, median, range)	2 (1-5)	5 (3-8)	<0.001
Length of stay total (days, median, range)	3 (2-7)	5 (4-9)	<0.001

3D MEASUREMENTS

The pre-surgery and post-surgery measurements are shown in Tables 3-6. The graphs of CI, total volume, and circumference are shown in Figure 3. The majority of the pre-surgery values were significantly different from the reference groups in both genders.

Both treatment groups showed an increase of the CI from pre to post-surgery, yet CI was higher in the reference groups. The EACS patients showed an increase in the first months after surgery for both genders, followed by a decline around 9-12

months. OCVR patients have a constant post-surgery CI over time (around 69-71). The CIs of EACS patients showed a decline to approximately that of the OCVR CI values over time, which finally resulted in no significant differences between these groups.

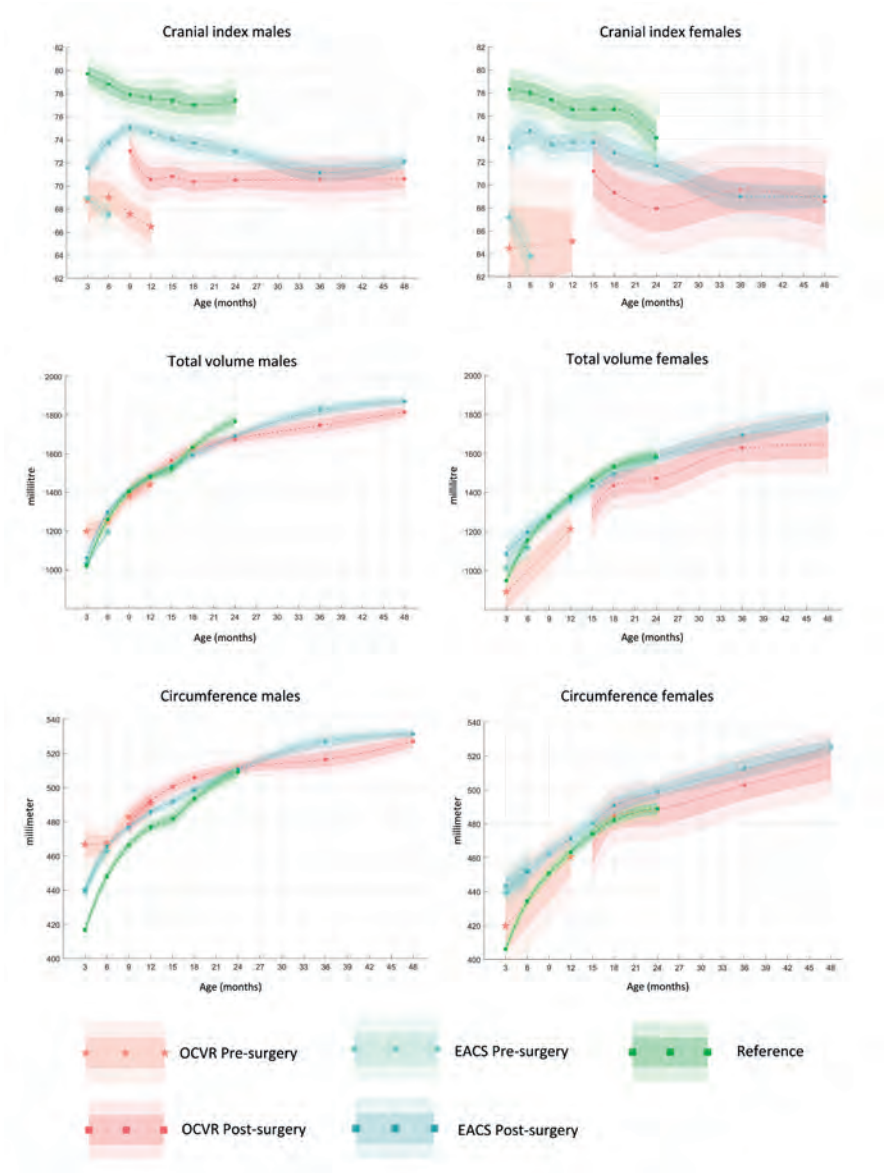

Figure 3: Graphs of the mean and standard error of mean of the cephalic index, total cranial volume and circumference after EACS and OCVR for scaphocephaly at given ages in months.

Cranial width varied but had no clear pattern regarding the significant differences between the surgery groups themselves, and between the surgery groups and references. However, cranial width is significant smaller for EACS and OCVR patients before surgery compared to the references but this difference resolves after surgery for both groups. The cranial length in both groups remained longer compared to the references.

The circumference of both treatment groups were significantly larger than the references in the earlier post-surgery age groups. The volume differences between the treatment groups and the references were minimal.

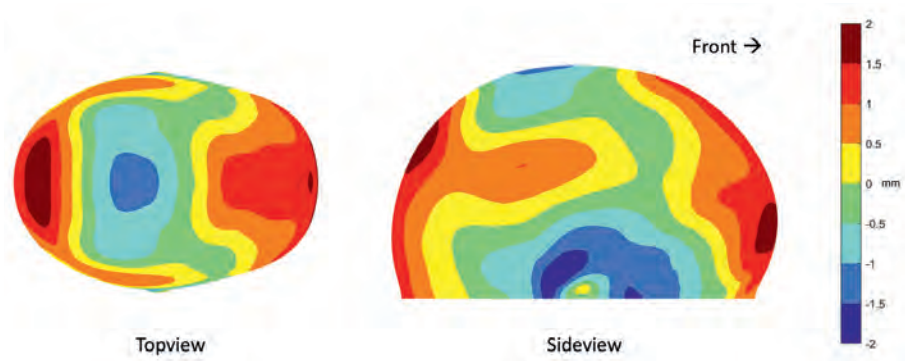

Figure 4: Growth maps indicating the mean head shape differences (in mm) between EACS and OCVR at 24 months of age (post-surgery). The EACS head shape is baseline hence a positive value indicates that the OCVR head shape has localized additional volume over that of EACS and vice versa. Note the color scaling (0.5 mm/ unique color). The length of the EACS head shape is shorter while the vertex is higher and the bitemporal distance larger.

Table 3: The pre-surgery shape measurements of the male scaphocephaly patients. CI =cranial Index, vol. = volume, SEM = standard error of mean, mo. = months, mm = millimetres, ml = millilitre

		Age	Cranial Width (mm)		Cranial Length (mm)		CI		Circumference (mm)		Total Vol. (ml)	
Group	**n**	(mo.)	**Mean**	**SEM**	**Mean**	**SEM**	**Mean**	**SEM**	**Mean**	**SEM**	**Mean**	**SEM**
EACS 1	52	3	111*†	1	161*	1	68.9†	0.5	440*†	*2	1030*	13
EACS 2	18	6	115†	1	170†	1	67.6†	0.8	463†	3	1195†	20
OCVR 1	4	3	117*	3	171*†	3	68.7†	1.9	467*†	7	1199*†	45
OCVR 2	8	6	118†	2	171†	2	69.0†	1.3	467†	5	1249	31
OCVR 3	8	9	120†	2	178†	2	67.6†	1.1	483†	4	1381	28
OCVR 4	8	12	121†	2	182†	2	66.5†	1.3	491†	5	1441	32

* = significant difference between surgery groups, † = significant difference with healthy references

Table 4: The post-surgery shape measurements of the male scaphocephaly patients. CI =cranial Index, vol. = volume, SEM = standard error of mean, mo. = months, mm = millimetres, ml = millilitre

		Age	Cranial Width (mm)		Cranial Length (mm)		CI		Circumference (mm)		Total Vol. (ml)	
Group	n	(mo.)	Mean	SEM	Mean	SEM	Mean	SEM	Mean	SEM	Mean	SEM
EACS 1	4	3	114	1	160†	2	71.6†	0.9	439†	4	1060	29
EACS 2	33	6	123	1	167*†	1	73.8†	0.5	466†	2	1297	16
EACS 3	47	9	128	1	171†	1	75.0†	0.5	477†	2	1408	15
EACS 4	47	12	130	1	174*†	1	74.6*†	0.5	486†	2	1482	15
EACS 5	26	15	131	1	177*†	1	74.0*†	0.5	492*	2	1534	17
EACS 6	12	18	132†	1	180*	1	73.7*†	0.7	499	3	1594	20
EACS 7	37	24	134†	1	185	1	73.0*†	0.5	511	2	1692†	16
EACS 8	8	36	136	1	192	1	71.2	0.8	527*	3	1825	24
EACS 9	29	48	139	1	193	1	72.1	0.5	531	2	1872*	16
OCVR 2	1	6	125	3	176*†	4	70.8†	2.1	483†	9	1376†	67
OCVR 3	4	9	126	2	173†	2	73.0†	1.2	478†	5	1388	37
OCVR 4	7	12	127†	1	179*†	2	70.6*†	1.0	492†	4	1480	31
OCVR 5	9	15	130	1	183*†	2	70.8*†	0.9	501*†	3	1563	27
OCVR 6	10	18	131†	1	185*†	2	70.4*†	0.9	506†	3	1624	27
OCVR 7	17	24	132†	1	187†	1	70.5*†	0.7	512	3	1677†	23
OCVR 8	4	36	134	2	189	2	70.6	1.1	517*	4	1747	34
OCVR 9	15	48	137	1	193	1	70.6	0.8	527	3	1815*	25

* = significant difference between surgery groups, † = significant difference with healthy references

Table 5: The pre-surgery shape measurements of the female scaphocephaly patients. CI =cranial Index, vol. = volume, SEM = standard error of mean, mo. = months, mm = millimetres, ml = millilitre

		Age	Cranial Width (mm)		Cranial Length (mm)		CI		Circumference (mm)		Total Vol. (ml)	
Group	**n**	(mo.)	**Mean**	**SEM**	**Mean**	**SEM**	**Mean**	**SEM**	**Mean**	**SEM**	**Mean**	**SEM**
EACS 1	13	3	109	2	162†	2	67.2†	1.1	439†	5	1011†	27
EACS 2	3	6	107†	3	168†	4	63.8†	2.1	452†	9	1117	53
OCVR 1	1	3	101	6	156	6	64.5	3.7	420	16	893	92
OCVR 4	2	12	112†	4	172	5	65.1†	2.6	461	11	1214†	65

* = significant difference between surgery groups, † = significant difference with healthy references

Table 6: The post-surgery shape measurements of the female scaphocephaly patients. CI =cranial Index, vol. = volume, SEM = standard error of mean, mo. = months, mm = millimetres, ml = millilitre

		Age	Cranial Width (mm)		Cranial Length (mm)		CI		Circumference (mm)		Total Vol. (ml)	
Group	**n**	(mo.)	**Mean**	**SEM**	**Mean**	**SEM**	**Mean**	**SEM**	**Mean**	**SEM**	**Mean**	**SEM**
EACS 1	2	3	117†	2	161†	3	73.3†	1.2	443†	6	1086†	42
EACS 2	3	6	121	2	163†	3	74.7	1.1	451†	5	1196	40
EACS 3	11	9	123	1	168†	2	73.5†	0.9	463†	4	1283	29
EACS 4	13	12	125	1	170†	2	73.7†	0.8	472†	4	1361	29
EACS 5	6	15	128*	1	174†	2	73.7	0.9	480	4	1431	33
EACS 6	3	18	129	2	178†	2	72.8†	1.1	491	5	1494	38
EACS 7	8	24	131*	1	183†	2	71.7	0.9	499†	4	1583	31
EACS 8	2	36	130	2	189	3	69.0	1.2	513	6	1694	42
EACS 9	7	48	133	1	193	2	69.0	0.9	525	4	1783	32
OCVR 5	1	15	121*†	3	170	5	71.2	2.2	466	10	1308†	76
OCVR 6	3	18	124†	3	179†	4	69.3†	1.9	485	8	1437	64
OCVR 7	2	24	123*†	3	181	4	67.9†	2.0	488	9	1473	69
OCVR 8	2	36	129	3	185	4	69.5	2.0	503	9	1628	69
OCVR 9	1	48	131	3	191	5	68.6	2.2	516	10	1648	77

* = significant difference between surgery groups, † = significant difference with healthy references

GROWTH MAPS

The most important growth map is the comparison at 24 months between treated EACS and OCVR patients (Figure 4). The maximum differences are within the -2 mm and +2 mm range. Typically, OCVR treated patients have a more elongated head with a growth focus around the frontal and occipital areas, a somewhat narrow lower temporal region, and a slightly wider lower parietal region. Furthermore, the vertex of OCVR patients is slightly lower. Two examples of children aging 24 months, treated using EACS or OCVR are shown in Figure 5.

The most important findings of the growth maps are reported below and visualized in Figure 4, 6 and 7.

The growth maps of EACS patients from pre to post-surgery for age groups 1 (3 months) and 2 (6 months) both show a strong parietal growth of up to 10 mm (Figure 6). The frontal and occipital growth for the first age group were around 0 and 4 mm respectively. For the second age group, frontal and occipital growth was less compared to the earlier surgery group.

In OCVR, parietal changes up to 10 mm can be seen regardless of the age at surgery (Figure 6). Yet, OCVR also showed differences between pre, and post-surgery depending on the age during surgery. In contrast to EACS, occipital growth up to 7 mm is present between 6 - 9 months; frontal changes remain limited in all age (OCVR) groups. Occipital growth is more present in OCVR for later surgery ages as compared to the earlier surgery ages.

The post-surgery follow-up for EACS patients are shown in Figure 7. From 6 - 9 months of age, a prominent upper parietal growth of 5 mm is noted, with lower parietal growth around 3 mm. Frontal areas grow up to 4 mm. The frontotemporal region only shows 1-2 mm of growth. From 9 - 12 months, only 0-1 mm frontotemporal growth, up to 3 mm occipital growth and a midline growth up to approximately 2.5 mm was noted. Nearly identical growth is present between 9 - 18 months. However, growth at 18 months is more prominent around the occipital and frontal area (up to 5 mm). Between 18 - 24 months, only frontoparietal growth and some lower occipital growth up to 2.5 mm is present. Between 24 - 48 months, some frontotemporal growth (up to 3 mm) is dominant.

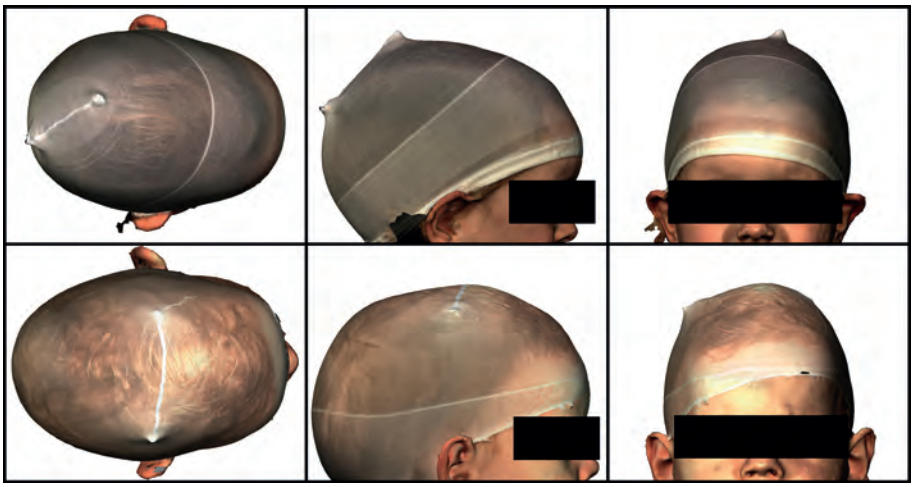

Figure 5: Top row: a 3D photo of a 24 month old child treated with EACS. Bottom row: a 3D photo of a 24 month old child treated with OCVR. From left to right: top view, side view (right), front view.

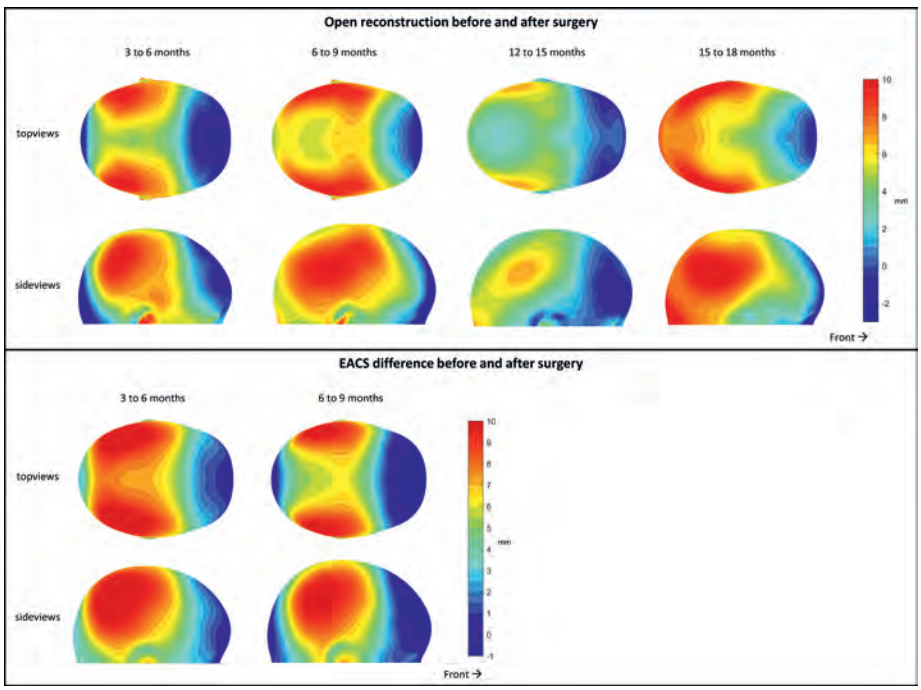

Figure 6: Top: Growth maps indicating the mean head shape differences (in mm) from pre to post-OCVR surgery for 3 - 6 months until 15 - 18 months of age. Bottom: Growth maps indicating the mean head shape differences (in mm) from pre to post-EACS surgery for 3 - 6 months and 6 - 9 months of age. Note the color scaling (0.5 mm/ unique color).

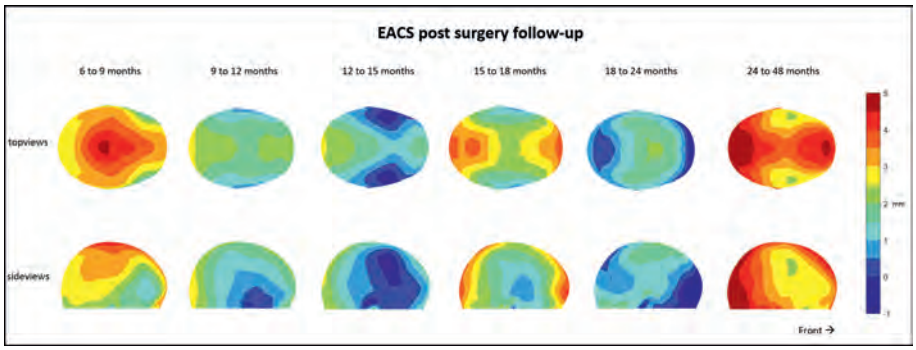

Figure 7: Growth maps indicating the mean head shape differences (in mm) post-EACS surgery for 3 - 6 months until 24 - 48 months of age. Note the color scaling (0.5 mm/ unique color).

DISCUSSION

SECONDARY TREATMENT ASPECTS

In general, EACS performed equal or better than the OCVR in all of the secondary treatment aspects. Only one EACS case was admitted to the ICU due to a non-craniosynostosis-related issue. This suggests that there were no EACS induced ICU admittances in contrast to 25 cases for OCVR.

Curiously, the OCVR blood loss levels in this study seem lower than reported in other studies.[19–22] We think that this could be attributed to the use of virtual surgical planning techniques in our institute, reducing the overall surgical time and blood loss.

Our findings are in line with, and add up to, the growing bulk of reports showing the superior safety profile of minimal invasive techniques such as EACS over open remodeling techniques.[3,11,19–31]

3D MEASUREMENTS

Cranial width shows a strong post-surgical increase in especially EACS. This results in a CI incline in the first months after EACS for both genders, followed by a decline at around 9-12 months. OCVR patients have a constant post-surgery CI over time (around 69-71). The trend of CI over time is in line with other longitudinal studies.[21,23,32] The decline of CI around 9-12 months in the EACS group co-occurs (in most cases) with the stopping of the helmet molding therapy. Therefore, one

could argue that this reflects a 'relapse' caused by ending of the helmet molding effect. However, a similar decline in the reference group can be noted at age 9-12 months. This suggests that this decline does not reflect a 'relapse', but rather a natural growth pattern, as seen in the reference group.

Overall, CI in the EACS group remains higher than in the OCVR, and is significantly different for earlier age groups. For later age groups, the effect diminishes in both genders, with a CI approximating 70.

Pre-surgery studies report CI values in the range of 67-70 which is in line with our findings.[21,26] Most of the post-surgery CI values for scaphocephaly correction remain around the 75-85 range which are higher than ours.[7,12,21,23,26,33–35] This may be due to a demographic difference in the patient population or to the measuring method.[10,36]

The longitudinal circumference changes did not differ between OCVR and EACS and were in line with literature.[7,23] When compared to the normal reference group, we found that in the early age groups circumference data is larger in scaphocephaly patients, but at 24 months, the circumference has obtained normal proportions again, for both treatment groups.

Volume measurements differ per study due to the lack of consensus on volume measuring methods in craniosynostosis.[37] Yet, taking measuring differences into account, we found similar volumes changes for OCVR as reported by others.[35,38] The volume data of EACS patients are very similar to those of our reference group[15] and the OCVR group. Therefore, our data shows that both techniques result in equal and normal intracranial volumes.

GROWTH MAPS

The growth maps of both EACS and OCVR groups (Figure 6 and 7), show an impressive increase in cranial growth. A clear increase of lateral expansion and vertex height can be noticed resulting in a proper lateral profile for both treatment options. In Figure 4, the cranial length of the OCVR is greater compared to the EACS group. This can be explained by the fact that OCVR patients are treated at a later age and thus have longer and larger compensatory growth in the anterior-posterior direction. The vertex height of the EACS group is higher than that of the

OCVR group and showed a natural and appealing spherical shape of the cranium. This contrasts with Le et al. who reported that EACS results in a lower vertex height compared to OCVR.[7] This is an interesting finding, and although we did not measure head height, this could be a valuable additional 3D measurement,[7,10,13,39,40] when comparing different surgical strategies (conventional or minimal invasive), such as spring-mediated cranioplasties.[35,41,42]

During the first months after EACS, the major effect of the growth appears to expand and enlarge the head (Figure 6 and Figure 7). After these first 3-6 months, this expanding effect, mainly present in the cranial width, reaches its limits. However, the helmet therapy is continued on average until around 10 months after surgery. Based on the results, it is unsure whether the helmet therapy still benefits the outcome after this 3-6 month period. As stated before, when looking at the growth maps of 9-12 months and 12-15 months, growth seems to be anterior-posterior oriented, resulting in a decline of CI around 9-12 months. This could be due to the stopping of the helmet therapy at that time, but a similar anterior-posterior growth orientation is seen in growth maps of normal references at the same age.[15] This suggests that perhaps this growth pattern resembles a natural pre-defined pattern and, instead of having a relapse, patients may rather shift towards a normal cranial growth pattern after EACS and helmet therapy. It would be interesting to see whether other groups could confirm these findings, as this might suggest that early re-opening of a fused suture could invoke restoration of the normal growth potential of the head.

On the other hand, helmet therapy seems to increase CI, regardless of being implemented before or without surgery, although the latter raises concerns regarding intracranial pressure.[34,43–45]

LIMITATIONS

Although this study used an extensive dataset, it was not always possible to collect 3D photos on the exact time points due to logistic, technological or patient-specific reasons and this resulted in non-continuous follow-up. Furthermore, the limited amount of 3D photos and unequal gender distribution was the reason why genders were combined in the 3D growth maps. Due to our institution's preference to perform EACS if possible, data for OCVR cases was limited and it was therefore difficult to create meaningful longitudinal growth maps for OCVR.

The designs of the remolding helmets and the patient tailored surgical plans have a very important effect on the final cranial shape. Yet, since it is almost impossible to take these factors into consideration and differentiate further, we decided to group the patients and evaluate the combined outcomes of the patients in the two treatment groups.

Since other institutions might use different surgical and/or treatment techniques, a potential caveat is that the results of this study are only pertinent for our centre. Yet, based on the long-term evaluation and the secondary treatment aspects that were used in this study, our institution's preference for EACS was confirmed.

CONCLUSION

Based on our data and the treatments options used in our center, we conclude that EACS before the age of 6 months is a valid treatment option for the correction of scaphocephaly, as it attains the same surgical results as OCVR up to the age of 48 months. We consider this the preferred treatment option for scaphocephaly due to better secondary treatment aspects. Early diagnostics and referral for suspected craniosynostosis to make EACS a viable option is therefore recommended.

ACKNOWLEDGEMENTS

Several of the authors of this publication are members of the European Reference Network CRANIO- Project ID: "NO 739543"

REFERENCES

1. Heuzé Y, Boyadjiev SA, Marsh JL, et al. New insights into the relationship between suture closure and craniofacial dysmorphology in sagittal nonsyndromic craniosynostosis. *J Anat*. 2010;217(2):85-96. doi:10.1111/j.1469-7580.2010.01258.x
2. Ciurea A V, Toader C, Mihalache C. Actual concepts in scaphocephaly : (an experience of 98 cases). *J Med Life*. 2011;4(4):424-431.
3. Cartwright CC, Jimenez DF, Barone CM, Baker L. Endoscopic Strip Craniectomy: A Minimally Invasive Treatment for Early Correction of Craniosynostosis. *J Neurosci Nurs*. 2003;35(3):130-138. doi:10.1097/01376517-200306000-00002
4. Cornelissen M, Ottelander B den, Rizopoulos D, et al. Increase of prevalence of craniosynostosis. *J Cranio-Maxillofacial Surg*. 2016;44(9):1273-1279. doi:10.1016/j.jcms.2016.07.007
5. Lee HQ, Hutson JM, Wray AC, et al. Changing epidemiology of nonsyndromic craniosynostosis and revisiting the risk. *J Craniofac Surg*. 2012;23(5):1245-1251. doi:10.1097/SCS.0b013e318252d893
6. Doumit GD, Papay FA, Moores N, Zins JE. Management of sagittal synostosis: a solution to equipoise. *J Craniofac Surg*. 2014;25(4):1260-1265. doi:10.1097/SCS.0b013e3182a24635
7. Le M-B, Patel K, Skolnick G, et al. Assessing long-term outcomes of open and endoscopic sagittal synostosis reconstruction using three-dimensional photography. *J Craniofac Surg*. 2014;25(2):573-576. doi:10.1097/SCS.0000000000000613
8. Delye HHK, Borstlap WA, Van Lindert EJ. Endoscopy-assisted craniosynostosis surgery followed by helmet therapy. *Surg Neurol Int*. 2018;9(1). doi:10.4103/sni.sni_17_18
9. Lee BS, Hwang LS, Doumit GD, et al. Management options of non-syndromic sagittal craniosynostosis. *J Clin Neurosci*. 2017;39:28-34. doi:10.1016/J.JOCN.2017.02.042
10. Dvoracek LA, Skolnick GB, Nguyen DC, et al. Comparison of traditional versus normative cephalic index in patients with sagittal synostosis: Measure of scaphocephaly and postoperative outcome. *Plast Reconstr Surg*. 2015;136(3):541-548. doi:10.1097/PRS.0000000000001505
11. Delye HHK, Arts S, Borstlap WA, et al. Endoscopically assisted craniosynostosis surgery (EACS): The craniofacial team Nijmegen experience. *J Cranio-Maxillofacial Surg*. 2016;44(8):1029-1036. doi:10.1016/j.jcms.2016.05.014
12. Jimenez DF, Barone CM, McGee ME, Cartwright CC, Baker CL. Endoscopy-assisted wide-vertex craniectomy, barrel stave osteotomies, and postoperative helmet molding therapy in the management of sagittal suture craniosynostosis. *J Neurosurg Pediatr*. 2004;100(5):407-417. doi:10.3171/ped.2004.100.5.0407
13. Marcus JR, Stokes TH, Mukundan S, Forrest CR. Quantitative and qualitative assessment of morphology in sagittal synostosis: mid-sagittal vector analysis. *J Craniofac Surg*. 2006;17(4):680-686. doi:10.1097/00001665-200607000-00013
14. Delye H, Clijmans T, Mommaerts MY, Sloten J Vander, Goffin J. Creating a normative database of age-specific 3D geometrical data, bone density, and bone thickness of the developing skull: a pilot study. *J Neurosurg Pediatr*. 2015;16(6):687-702. doi:10.3171/2015.4.PEDS1493
15. Meulstee JW, de Jong GA, Borstlap WA, Koerts G, Maal TJJ, Delye H. The normal evolution of the cranium in three dimensions. *Int J Oral Maxillofac Surg*. Published online November 2019. doi:10.1016/j.ijom.2019.10.012
16. de Jong G, Tolhuisen M, Meulstee J, et al. Radiation-free 3D head shape and volume evaluation after endoscopically assisted strip craniectomy followed by helmet therapy for trigonocephaly. *J Cranio-Maxillofacial Surg*. 2017;45(5):661-671. doi:10.1016/j.jcms.2017.02.007
17. Meulstee JW, Verhamme LM, Borstlap WA, et al. A new method for three-dimensional evaluation of the cranial shape and the automatic identification of craniosynostosis using 3D stereophotogrammetry. *Int J Oral Maxillofac Surg*. 2017;46(7):819-826. doi:10.1016/j.ijom.2017.03.017
18. de Jong GA, Maal TJJ, Delye H. The computed cranial focal point. *J Cranio-Maxillofacial Surg*. 2015;43(9):1737-1742. doi:10.1016/j.jcms.2015.08.023
19. Zakhary GM, Montes DM, Woerner JE, Notarianni C, Ghali GE. Surgical correction of craniosynostosis. A review of 100 cases. *J Cranio-Maxillofacial Surg*. 2014;42(8):1684-1691. doi:10.1016/j.jcms.2014.05.014

20. Toma R, Greensmith AL, Meara JG, et al. Quantitative morphometric outcomes following the Melbourne method of total vault remodeling for scaphocephaly. *J Craniofac Surg*. 2010;21(3):637-643. doi:10.1097/SCS.0b013e3181d841d9
21. Gerety PA, Basta MN, Fischer JP, Taylor JA. Operative management of nonsyndromic sagittal synostosis: A head-to-head meta-analysis of outcomes comparing 3 techniques. *J Craniofac Surg*. 2015;26(4):1251-1257. doi:10.1097/SCS.0000000000001651
22. Goyal A, Lu VM, Yolcu YU, Elminawy M, Daniels DJ. Endoscopic versus open approach in craniosynostosis repair: a systematic review and meta-analysis of perioperative outcomes. *Child's Nerv Syst*. 2018;34(9):1627-1637. doi:10.1007/s00381-018-3852-4
23. Ridgway EB, Berry-Candelario J, Grondin RT, Rogers GF, Proctor MR. The management of sagittal synostosis using endoscopic suturectomy and postoperative helmet therapy. *J Neurosurg Pediatr*. 2011;7(6):620-626. doi:10.3171/2011.3.peds10418
24. Jimenez DF, Barone CM. Endoscopic craniectomy for early surgical correction of sagittal craniosynostosis. *J Neurosurg*. 1998;88(1):77-81. doi:10.3171/jns.1998.88.1.0077
25. Barone CM, Jimenez DF. Endoscopic craniectomy for early correction of craniosynostosis. *Plast Reconstr Surg*. 1999;104(7):1965-1973; discussion 1974-5. doi:10.3171/jns.1998.88.1.0077
26. Shah MNN, Kane AAA, Petersen JDD, Woo ASS, Naidoo SDD, Smyth MDD. Endoscopically assisted versus open repair of sagittal craniosynostosis: The St. Louis Children's Hospital experience - Clinical article. *J Neurosurg Pediatr*. 2011;8(2):165-170. doi:10.3171/2011.5.PEDS1128
27. David LR, Proffer P, Hurst WJ, Glazier S, Argenta LC. Spring-mediated cranial reshaping for craniosynostosis. *J Craniofac Surg*. 2004;15(5):370. doi:10.1097/00001665-200409000-00021
28. Jimenez DF, Barone CM, Cartwright CC, Baker L. Early management of craniosynostosis using endoscopic-assisted strip craniectomies and cranial orthotic molding therapy. *Pediatrics*. 2002;110(1 Pt 1):97-104. doi:10.1542/peds.110.1.97
29. Riordan CPP, Zurakowski D, Meier PMM, et al. Minimally Invasive Endoscopic Surgery for Infantile Craniosynostosis: A Longitudinal Cohort Study. *J Pediatr*. 2020;216:142-149.e2. doi:10.1016/j.jpeds.2019.09.037
30. Yan H, Abel TJ, Alotaibi NM, et al. A systematic review and meta-analysis of endoscopic versus open treatment of craniosynostosis. Part 1: The sagittal suture. *J Neurosurg Pediatr*. 2018;22(4):352-360. doi:10.3171/2018.4.PEDS17729
31. Abbott MM, Rogers GF, Proctor MR, Busa K, Meara JG. Cost of treating sagittal synostosis in the first year of life. *J Craniofac Surg*. 2012;23(1):88-93. doi:10.1097/SCS.0b013e318240f965
32. Agrawal D, Steinbok P, Cochrane DD. Long-term anthropometric outcomes following surgery for isolated sagittal craniosynostosis. *J Neurosurg*. 2006;105(5 Suppl):357-360. doi:10.3171/ped.2006.105.5.357
33. Proctor MR. Endoscopic craniosynostosis repair. *Transl Pediatr*. 2014;3(3):247-258. doi:10.3978/j.issn.2224-4336.2014.07.03
34. Hashmi A, Marupudi NI, Sood S, Rozzelle A. Effect of Preoperative Molding Helmet in Patients with Sagittal Synostosis. *J Craniofac Surg*. 2017;28(4):898-903. doi:10.1097/SCS.0000000000003512
35. Klausing A, Röhrig A, Lüchters G, Vogler H, Martini M. Follow-up study to investigate symmetry and stability of cranioplasty in craniosynostosis – Introduction of new pathology-specific parameters and a comparison to the norm population. *J Cranio-Maxillofacial Surg*. 2019;47(9):1441-1448. doi:10.1016/j.jcms.2019.07.001
36. van Lindert EJ, Siepel FJ, Delye H, et al. Validation of cephalic index measurements in scaphocephaly. *Child's Nerv Syst*. 2013;29(6):1007-1014. doi:10.1007/s00381-013-2059-y
37. Seeberger R, Hoffmann J, Freudlsperger C, et al. Intracranial volume (ICV) in isolated sagittal craniosynostosis measured by 3D photocephalometry: A new perspective on a controversial issue. *J Cranio-Maxillofacial Surg*. 2016;44(5):626-631. doi:10.1016/j.jcms.2016.01.023
38. van Veelen M-LC, Jippes M, Carolina J-CA, et al. Volume measurements on three-dimensional photogrammetry after extended strip versus total cranial remodeling for sagittal synostosis: A comparative cohort study. *J Cranio-Maxillofacial Surg*. 2016;44(10):1713-1718. doi:10.1016/j.jcms.2016.07.029
39. Fearon JA, McLaughlin EB, Kolar JC. Sagittal craniosynostosis: Surgical outcomes and long-term growth. *Plast Reconstr Surg*. 2006;117(2):532-541. doi:10.1097/01.prs.0000200774.31311.09

40. Heutinck P, Knoops P, Rodriguez-Florez N, et al. Statistical shape modelling for the analysis of head shape variations. *Submitt to J cranio-maxillo-facial Surg*. 2021;(xxxx). doi:10.1016/j.jcms.2021.02.020
41. Rtshiladze MA, Roy AA, Goltsman D, Hunt J, Reddy R, Gianoutsos MP. The removal of cranial springs used in the treatment of scaphocephaly: A minimal access approach. *J Cranio-Maxillofacial Surg*. 2019;47(11):1706-1711. doi:10.1016/j.jcms.2019.04.001
42. Lehner M, Ferrari-von Klot F, Zundel S, Wendling-Keim D. Osteoclastic craniectomy for scaphocephaly in infants results in physiological head shapes. *J Cranio-Maxillofacial Surg*. 2019;47(12):1891-1897. doi:10.1016/j.jcms.2019.10.006
43. Proctor MR, Rogers GF. Letter to the Editor: Helmets and synostosis. *J Neurosurg Pediatr*. 2012;9(6):680-681. doi:10.3171/2011.10.PEDS11417
44. Marupudi NI, Sood S, Rozzelle A, Ham SD. Effect of molding helmets on intracranial pressure and head shape in nonsurgically treated sagittal craniosynostosis patients. *J Neurosurg Pediatr*. 2016;18(2):207-212. doi:10.3171/2016.1.peds15569
45. Sood S, Rozzelle A, Shaqiri B, Sood N, Ham SD. Effect of molding helmet on head shape in nonsurgically treated sagittal craniosynostosis. *J Neurosurg Pediatr*. 2011;7(6):627-632. doi:10.3171/2011.4.PEDS116

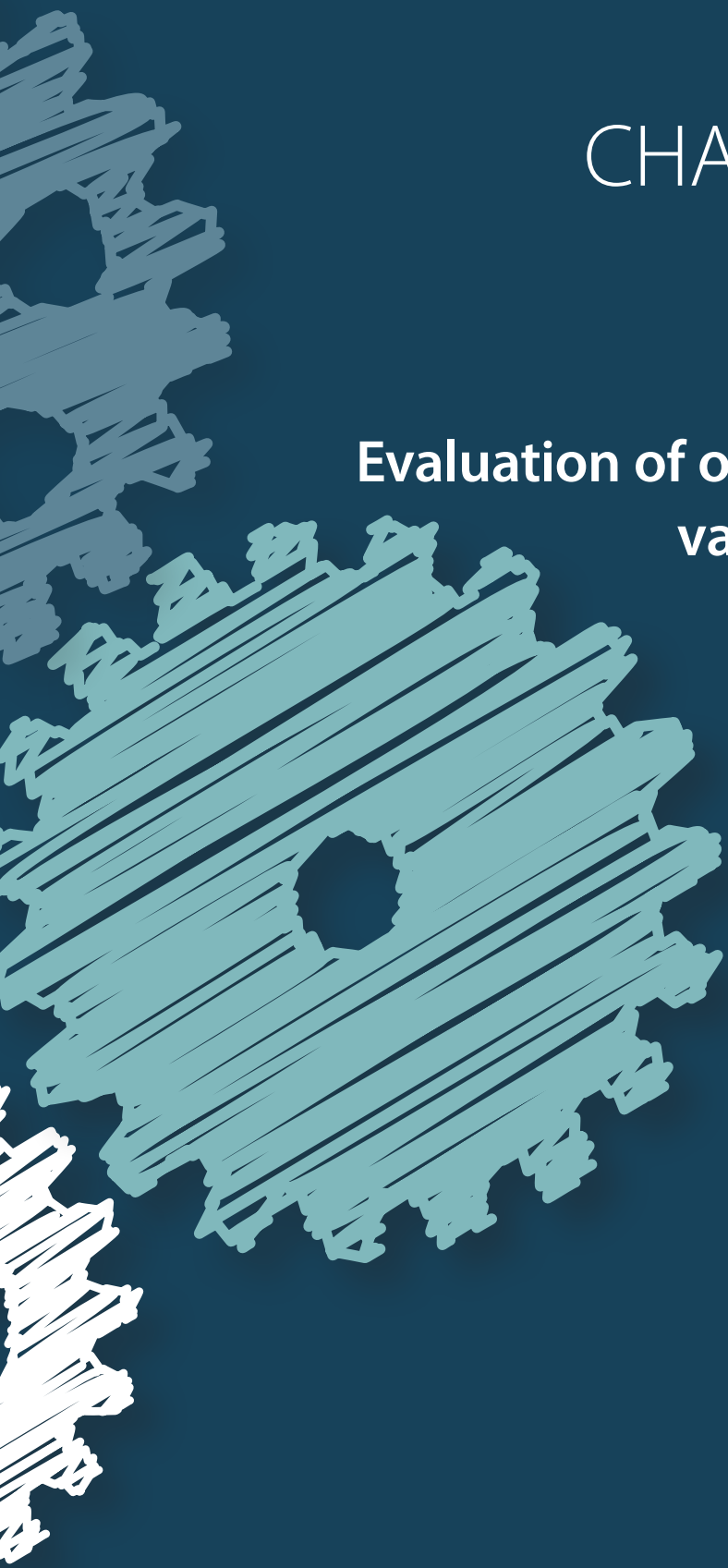

CHAPTER 11

Evaluation of open cranial vault surgery

Jene Meulstee
Arico Verhulst
Marloes Nienhuijs
Hans Delye

INTRODUCTION

Open cranial vault reconstruction (OCVR) is a major surgical procedure with important morbidity that can be performed in many different ways. In **Chapter 4**, we extensively described how a pre-operative (pre-op) three dimensional (3D) virtual surgical planning (VSP) could assists the surgical team during this complex and challenging procedure. In short, VSP provides the possibility to explore OCVR prior to surgery by simulating and visualizing in 3D the effect of different scenarios. The optimal position of the osteotomies can be planned and unnecessary or inadequate osteotomies can be avoided. Therefore, VSP makes it possible to find the best surgical strategy for every individual patient. Moreover, a proper pre-op plan with overall consensus of the surgical team will make the surgery itself more fluent and faster.[1–3]

However, the question remains how accurate the VSP can be realized during surgery. Because each VSP is tailored for individual patients, the best evaluation method is to directly compare the surgical outcome with the VSP. Therefore, a post-operative (post-op) computed tomography (CT) scan was acquired for several patients that allowed us to critically review and assess our surgical result and VSP. This has helped us to improve our planning strategy, transfer method and surgical procedure. This report evaluates two illustrative cases, divided over three surgeries, and elucidates what we have learned from these cases.

CASE SERIES

CASE 1 - PART 1

In 2012, a 3 months old boy suffering from scaphocephaly underwent endoscopically assisted craniosynostosis surgery (EACS). Helmet therapy was initiated after surgery and when the boy turned 1, a nice round and wide cranial shape with a CI of 70 was realized. However, 3 years later the boy started to develop headaches. After extensive counselling, an intracranial pressure (ICP) monitoring device revealed elevated pressure. An OCVR was performed based on a VSP at the age of 4 years. The primary aim was to enlarge cranial volume. Because the relatively old age of this patient could possible limit the osteosynthesis, the secondary aim was to prevent large gaps between the reconstructed bone segments (Figure 2).

CASE 1 - PART 2

Unfortunately, 2 years later the headache complaints of this boy started again and elevated ICP was measured. Based on a new CT-scan, cranial volume and circumference showed a +1 standard deviation from normal. Yet, when the CT-scan was compared to the CT-scan from 2 years earlier, the cranial growth in this interval seemed to be limited. In order to provide sufficient volume and reduce ICP, a second OCVR was performed where was aimed to enlarge the cranial volume with at least 15%.

CASE 2

The second case was a 7 months old boy that suffered from trigonocephaly. Because the patient was older than 6 months, EACS was not an option and an OCVR was indicated. The pre-op CT scan showed a moderate-severe trigonocephaly with a prominent metopic ridge. Therefore, an open reconstruction with a fronto-orbital advancement was planned and performed at the age of 12 months.

METHODS

3D reconstructions were created using Maxilim (V2.3.0, Medicim NV, Mechelen, Belgium) based on a CT-scan (slice thickness 0.5 mm, slice increment 0.5 mm, Aquilion ONE, Toshiba, Tochigi, Japan). In a virtual environment, the VSP was designed and various scenarios were tested (Blender3D, v. 2.79, the Blender foundation, Amsterdam, the Netherlands). Figures 2, 3 and 7 show the VSP of case 1 - part 1, case 1 - part 2 and case 2 respectively.

In case 1 - part 1, the VSP was converted to multiple measurements that indicate the distance from a clear anatomical landmark to an essential point in the planning (e.g. the corners of an osteotomy line) (Figure 1). During surgery, these measurements and a ruler were used to demarcate the 3D planning on the patient.

For case 1 - part 2 and case 2, surgical guides for the demarcation and reconstruction were created in 3D Studio Max (Autodesk, San Rafael, CA, USA) and 3D printed using selective laser-sintering (KLS Martin group, Tuttlingen, Germany).

All post-op scans were voxel based aligned on the skull base and the final alignment was manually checked and corrected if necessary. The post-op scan of case1 - part 1 was acquired two months after surgery, the scan of case 1 - part 2 several days after surgery and the scan of case 2 was acquired two months after surgery.

RESULTS AND DISCUSSION

CASE 1 - PART 1

During surgery, the various measurements were measured out with a ruler on the patient's cranium. The post-op CT-scan showed a significant volume increase. A zigzag over the midline created five grooves that fitted together and equally divided the newly formed gaps between the bone segments. The size, position and length of the grooves followed the planning. This proved that we were able to accurately demarcate the VSP on the patient's skull and performed the osteotomies. However, a discrepancy of the caudal osteotomy at the base of the reconstruction can be noticed (Figure 2). This indicates that the demarcation of the horizontal osteotomy line was less accurate.

Because the lateral length between the grooves (the length of the gaps) was measured on the VSP, it was possible to mimic this during surgery. This helped to realize the aimed lateral extension. This was confirmed by the post-op scan that showed that the lateral diameter of the reconstruction matched the VSP.

Although the post-op CT-scan indicates that the osteotomies were performed according to the planning, the reposition of the bone segments showed a discrepancy. The angle between the left and right part is flatter compared to the planning which resulted in a slightly wider, but lower reconstruction. The vertex height is 7 mm lower compared to the planning. This illustrates the difficulty of reproducing the exact angulation of bone segments in surgery.

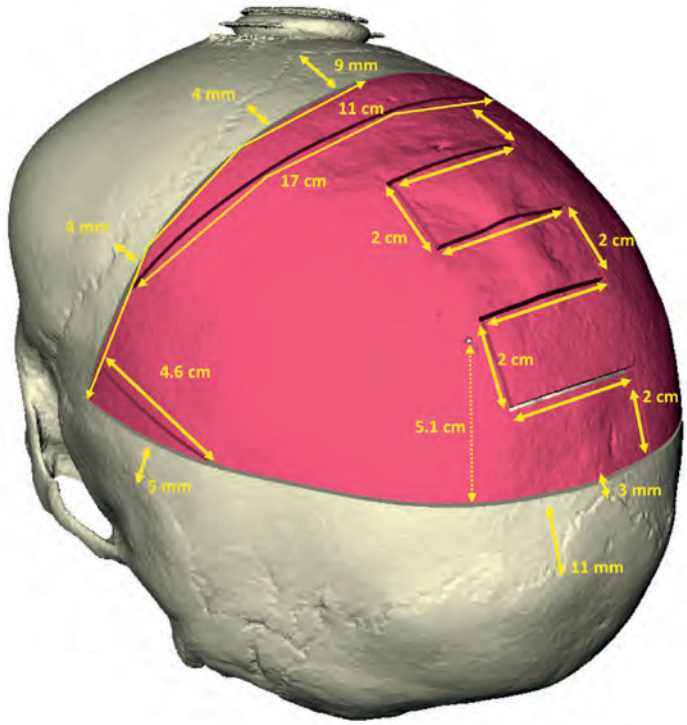

Figure 1: Case 1 - part 1: the original cranial shape (white) and the planned osteotomy lines to create three segments (red). The 3D-VSP was expressed in various measurements. Using anatomical landmarks and a ruler, these measurements were used during surgery to demarcate the planned osteotomy lines on the patient.

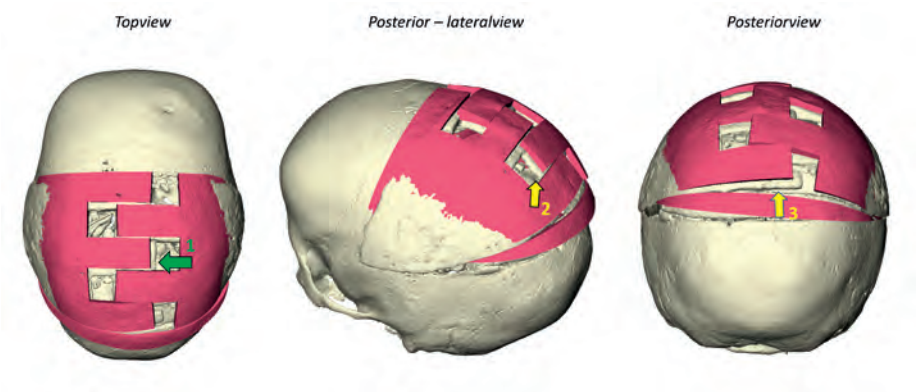

Figure 2: Case 1 - part 1: post-op result (white) compared to VSP (red). Grooves were created and reconstructed according to the planning (green arrow 1). The lateral view showed that we realized a 7 mm lower vertex hight than was planned (yellow arrow 2). The orientation between the two red parts did not match the planning (yellow arrow 3).

CASE 1 - PART 2

During the second OCVR, surgical guides for the demarcation and the reconstruction were manufactured and used. The demarcation template had a unique fit on the cranial shape. Several gaps were created to indicate clear anatomical landmarks (green arrow in Figure 4) to check if the demarcation template was perfectly positioned. Using this template, the demarcating phase was performed within a minute. This is significantly faster than using rulers and landmarks to transfer a planning, which takes around 10 to 15 minutes. Another advantage is when blood or cooling water from the craniotome erases the planning, the surgical guides could easily be used again to redo the demarcation.

The reconstruction templates allow the surgeon to mostly reconstruct the shape outside the patient which stimulates manoeuvrability and a fast placement of the fixation plates.

The guides dictate how the bone segments should be positioned and how much space between the segments was required. The curvature of the guides enabled the surgical team to fixate the bone segments in the correct orientation relative to each other.

On the anterior and caudal side of the reconstruction guide, a lid was created that showed the correct position and orientation when the reconstructed part was placed back into the patient. This lid had an overlay on the cranial base to prevent a tilt. Although this lid was very helpful, we recommend to make this lid even longer to create more overlap with the cranial base.

After the correct position was ensured, the reconstructed shape was fixated to the cranial base. Finally, bone strips were created around the anterior and caudal borders to prevent steps between the skull base and the reconstructed parts. Furthermore, the bone strips created some additional volume.

Considering the post-op evaluation, it could be concluded that the position and orientation matched very accurately on the planning. Although the right side is 2 mm lower (yellow arrow Figure 3), the left side matched perfectly. This is in contrast with the first OCVR where the incorrect rotation of the segments appeared to have to most prominent deviation from the planning.

Because the primary goal was to create more cranial volume, it was satisfying that the post-op volume calculated was almost identical to the planned volume increase (234 ml versus 218 ml correspondingly). The extra volume could be explained by the bone strips around the reconstructed area.

The thickest bicortical bone segments were split to harvest more bone to stimulate the osteosynthesis (Figure 6). The smaller monocortical bone fragments were placed into the gaps between the larger segments following the contour of the reconstruction.

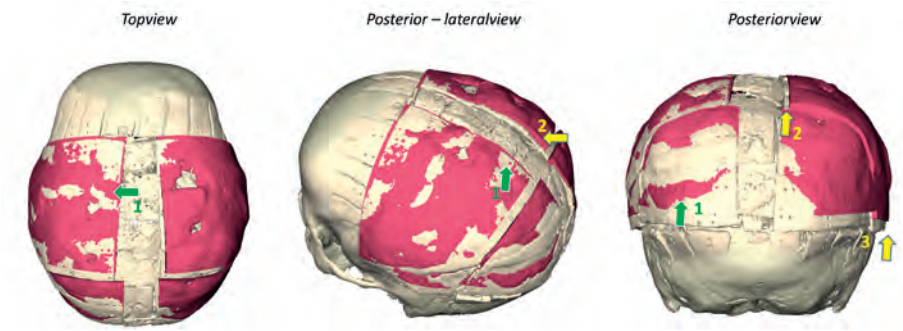

Figure 3: Case 1 - part 2: post-op result (white) compared to the VSP (red) of second OCVR. The result matched closely with the VSP. Green arrow 1 indicates the perfect match of the left parietal part. The right parietal parts were 3 mm more proximal positioned (yellow arrow 2 and 3).

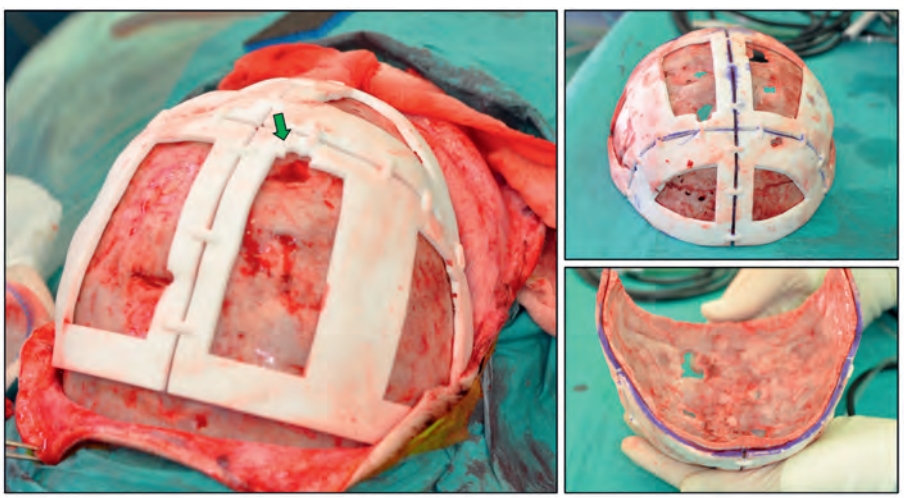

Figure 4: Case 1 - part 2: surgical guides used for demarcation of the planning. The contour of the guides fitted seamlessly on the cranial shape. Gaps were used to indicate distinctive anatomical landmarks to check the positioning (green arrow).

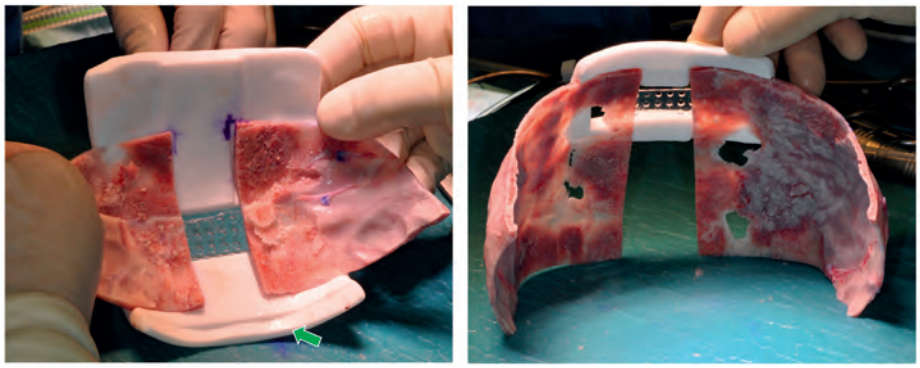

Figure 5: Case 1 - part 2: surgical guides used for the reconstruction. Spacers and overlap indicate how the bone segments should be positioned in the correct orientation. While segments are placed in the guides, fixation material could be placed. The new cranial shape can be reconstructed aside from the patient which allows surgeons to work fast and accurate. The extra lid (green arrow) could be placed on the cranial base of the patient to assure the reconstruction could be placed back into the patient correctly.

Figure 6: Case 1 - part 2: the thicker bone segments were split to create more bone. These bone fragments were used to fill the gaps between the larger bone segments.

Table 1: Case 1 - part 2: the pre-op CT-scan, the VSP and the post-op CT-scan were used to calculate the actual, the planned and the realized intracranial volume.

	Total Volume	Posterior Volume (surgical site)	Increase
Pre-op CT-scan	1465 ml	1078 ml	
Virtual Surgical Planning	1683 ml	1296 ml	218 ml (15% of total volume)
Post-op CT-scan	1699 ml	1312 ml	234 ml (16% of total volume)

CASE 2

Similar as in the previous case, the demarcation and reconstruction guides facilitated a fast and fluent surgical procedure during the trigonocephaly reconstruction. Several months after surgery, the patients showed a nice round and wide forehead and the prominent metopic ridge was replaced by a smooth

and flat surface. This was concluded clinically and determined on the 3D photo analysis. However, when the post-op CT-scan was compared to the planning, several points of improvements could be noted.

The most noticeable deviation was the shape of the orbital bar, which showed a much smaller angle on the post-op scan than in the planning (see α, Figure 7). This could be observed because the nasion lies anterior of the planning while the lateral cantii were more posterior located. Due to this, the planned anterior displacement of 13 mm was not met and only 8 mm was realized (Figure 8).

There are two reasons for this. The first one is that during surgery, the pieces did not fit perfectly in the reconstruction guide. Because we created a lid on top of the guide, it was difficult to seamlessly fit the bone segments into the guide and small inaccuracies caused by the osteotomy created interference. This could be illustrated in Figure 9. Therefore, we recommend to create a guide that only covers the outside contour (and not the top) of the orbital bar. The second reason is that we did not cut, but bended the lateral parts of the orbital bar. This was done to stimulate osteosynthesis but this also made it more difficult to reproduce the steep angle of the planning (Figure 9).

If we look at the frontal parts of the forehead, we can also see a discrepancy between outcome and planning. This is a logical consequence because we positioned the frontal parts directly on the orbital bar. Both in the planning as in the scan, the frontal parts are following the contour of the bar perfectly. This is another argument that the reconstruction of the orbital bar should be (more) precise. Another recommendation is to create one guide for the reconstruction of the orbital bar and the forehead. In this case, we used three different guides for all the parts but this was cumbersome to use during surgery and a single guide will probably make the reconstruction more accurate.

Even though we were aware that we did not apprehend the planned lateral widening during surgery, the post-op scan showed a poorer result than we expected. It should be noted however, that we planned 3 mm overcompensation. Nevertheless, the main lesson is that we should try to follow the planning more strictly during surgery.

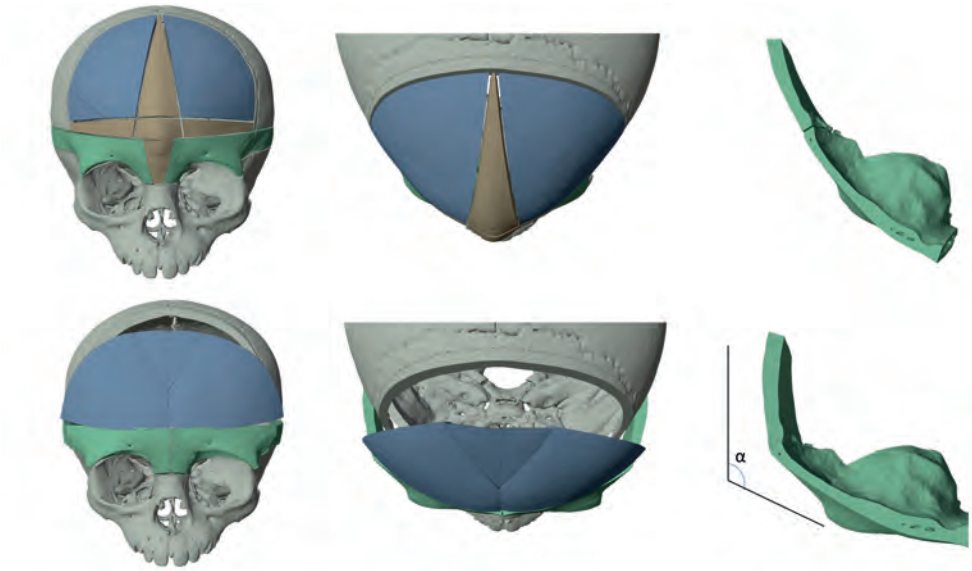

Figure 7: Case 2: planned osteotomy lines (upper) and planning (lower) of case 2. Note the steep angle (alpha) of the planning.

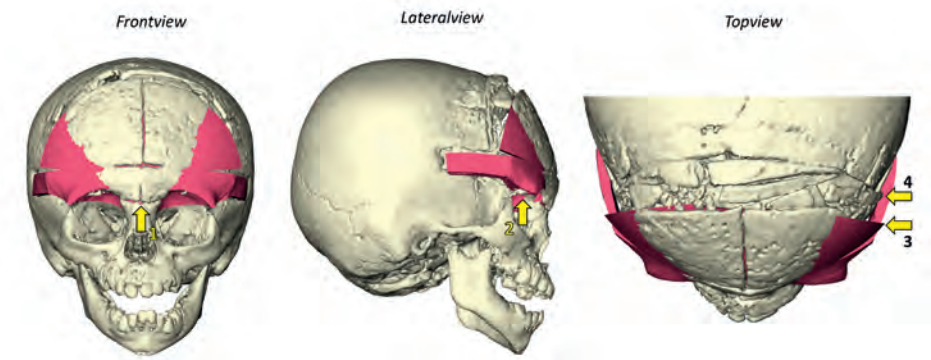

Figure 8: Case 2: post-op cranial reconstruction (white) matched on the VSP (red). The orbital bar was smaller reconstructed than was planned. In the post-op scan we found an anterior advancement of 8 mm (measured at the lateral orbital cantus, yellow arrow 2) whereas 13 mm was aimed for.

CONCLUSION

Comparing post-op CT-scans to the VSP enabled an objective evaluation. This helped us improve and understand the planning, transfer and surgery of open cranial vault reconstructions. This completed the cycle between diagnosis – planning – surgery and evaluation.

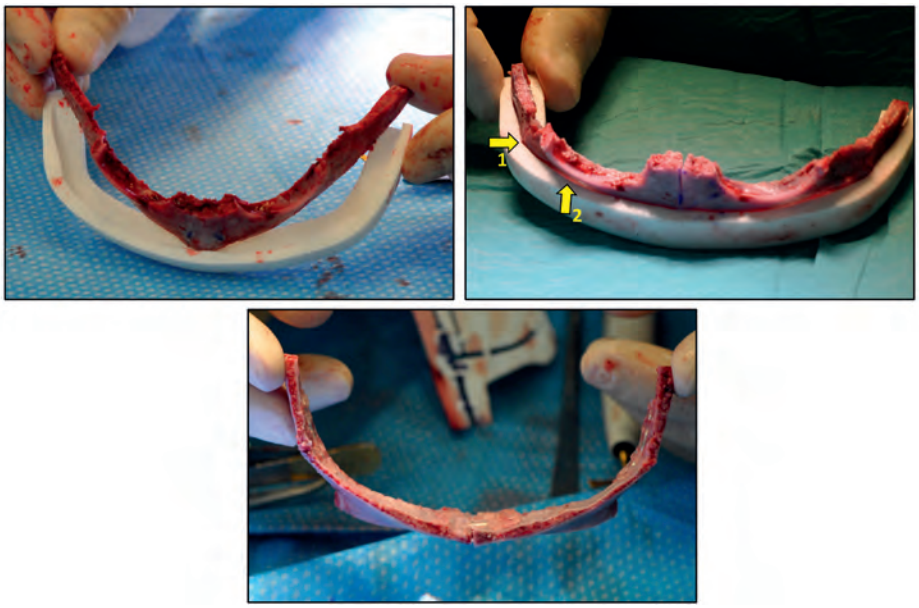

Figure 9: Case 2: orbital reconstruction. Top left: original and surgical guide. Top right: bar reconstructed in template. Because the bar was bended at point 1 and not completely cut, a small discrepancy could be noticed (yellow arrow 2) that resulted in a steeper reconstruction of the orbital bar (down under).

The post-op analysis of the first reconstruction revealed that it is possible to perform the osteotomies according the VSP without demarcation or reconstruction guides, but finding the exact orientation of the bone segments remains challenging. This was the most prominent aberration in this case.

In the second surgery of the first case (case 1 - part 2), the surgical guides helped to make the surgical procedure faster and more fluent. Moreover, the post-op CT-scan was largely in accordance with the VSP. The positions and orientations of almost all bone segments matched the VSP and the aimed volume increase was amply achieved and therefore, the surgical goal was realized.

The second case helped us realize that larger and simpler guides should be used during fronto-orbital advancement. In addition, we should be more strictly during surgery to achieve the planned orbital angle.

REFERENCES

1. Khechoyan DY, Saber NR, Burge J, et al. Surgical outcomes in craniosynostosis reconstruction: The use of prefabricated templates in cranial vault remodelling. J Plast Reconstr Aesthetic Surg. 2014;67(1):9-16. doi:10.1016/J.BJPS.2013.09.009
2. Shah A, Patel A, Steinbacher DM. Simulated frontoorbital advancement and intraoperative templates enhance reproducibility in craniosynostosis. Plast Reconstr Surg. 2012;129(6):1011e-1012e. doi:10.1097/PRS.0b013e31824effa7
3. Mardini S, Alsubaie S, Cayci C, Chim H, Wetjen N. Three-dimensional preoperative virtual planning and template use for surgical correction of craniosynostosis. J Plast Reconstr Aesthetic Surg. 2014;67(3):336-343. doi:10.1016/j.bjps.2013.11.004

CHAPTER 12

General discussion and future perspectives

Together, the four parts of this thesis form the gear train that represents a clinical process. Although the care and treatment of craniosynostosis patients is the main focus of this thesis, other clinical implementations for plastic, orthognathic and renal surgery are presented.

Each of the parts; diagnosis (1), planning (2), surgery (3), and evaluation (4), are considered as a single gear. Yet, for an optimally functioning process, not only should the gears themselves work properly but each gear's interactions with the other gears should also be seamless. This creates coherence and brings the complete clinical process to a higher level. This also means that an improvement to a single gear can help the entire system to work more efficiently. In the final chapter of this thesis, the individual parts as well as the gear train as a whole are evaluated. In addition, this chapter shows how future updates and developments can stimulate the gears to turn faster and improve the entire clinical workflow.

PART 1 - DIAGNOSIS

The treatment of craniosynostosis is characterized by many follow-up moments where the cranial shape is assessed and the patient's development is monitored closely. Earlier research, presented by the 3D Lab Nijmegen and other centers, confirms the potential of 3D stereophotogrammetry for such assessments, given its fast acquisition time, high accuracy, reproducibility and lack of ionizing radiation. In Part 1 of this thesis, the applicability of 3D stereophotogrammetry for clinical practice in craniofacial surgery was investigated. The powerful combination of 3D stereophotogrammetry and several 3D analysis methods has allowed us to make the evaluation of cranial shape and growth more objective and accurate. 3D stereophotogrammetry has meanwhile become a cornerstone of clinical consultation and is now fully nested in our clinical workflow. Semi-transparent 3D overlays and 3D color-coded distance maps have proved to be excellent tools during clinical consultation and provide the patients, their parents and the CFA team with relevant information (Figure 1). In summary, the answer to the research question *Can the diagnosis and follow-up of craniosynostosis be improved by the implementation of 3D stereophotogrammetry?* is a clear *yes*.

SOFTWARE USABILITY

Future developments could extend the impact of this workflow. One suggestion is that we should aim to make (new) research data more easily accessible in clinic. For example, the cranial development of a large group of patients and controls that was studied in **Chapter 2** and **Chapter 10** resulted in many graphs and 3D growth maps, but similar capabilities have not yet been implemented in the software that we use during clinical consultation. Further automation of our software should make it possible to instantly compare a 3D photo of an individual patient to the average growth maps or compare a skull circumference to the reference values in our dataset. This would make clinical consultation even more insightful and make the evaluation of individual patients more straightforward.

Currently, the clinical workflow for the evaluation of cranial shapes still contains many manual and user-dependent steps, such as the placement of landmarks needed for pre-alignment. Although we aimed to automate this step in previous work, we were not successful with our attempts. Gladfully, other methods based on texture, 3D geometry or deep learning demonstrate the possibilities of automatic landmark placement on 3D photos.[1,2] This will further automate and simplify the workflow which makes it more operable for other specialists (e.g. physicians). This improvement will allow other Dutch and international centers to use our software easily. Another very important advantage is that when the same methods are used, surgery-related outcome measurements become more easily exchangeable and comparable. This will lead to an objective comparison of treatment results and will help achieve the best possible treatment method for individual patients.

NEW METHODS FOR AUTOMATIC IDENTIFICATION AND EVALUATION

To make detection and evaluation of cranial deformities clearer, a new method was developed to easily describe the 3D shape of the skull (**Chapter 3**). With principal component analysis (PCA), this method can automatically isolate the most important shape variations in a large set of 3D photos. PCA uses only a few outcome measurements to describe the complete 3D morphology of the cranial shape, so this method has the potential to improve the currently used clinical diagnostic methods for cranial abnormalities. The PCA model, created from and based on normal cranial shapes, was able to identify all 40 craniosynostosis patients. At that moment, the dataset that was used for training and testing was small, the age range between patients and references was between 3 and 6 months, and

all shapes were scaled to the same size to correct for growth. In addition, we did not differentiate between males and females. Since we discovered in **Chapter 2** that both age and sex influence the cranial shape, it would be very interesting if we could train the PCA model with this larger and more stringently-selected dataset (see also Appendix **Chapter 2**). Training the PCA model with more cranial variations (by including abnormal cranial shapes) may also improve the model's robustness.

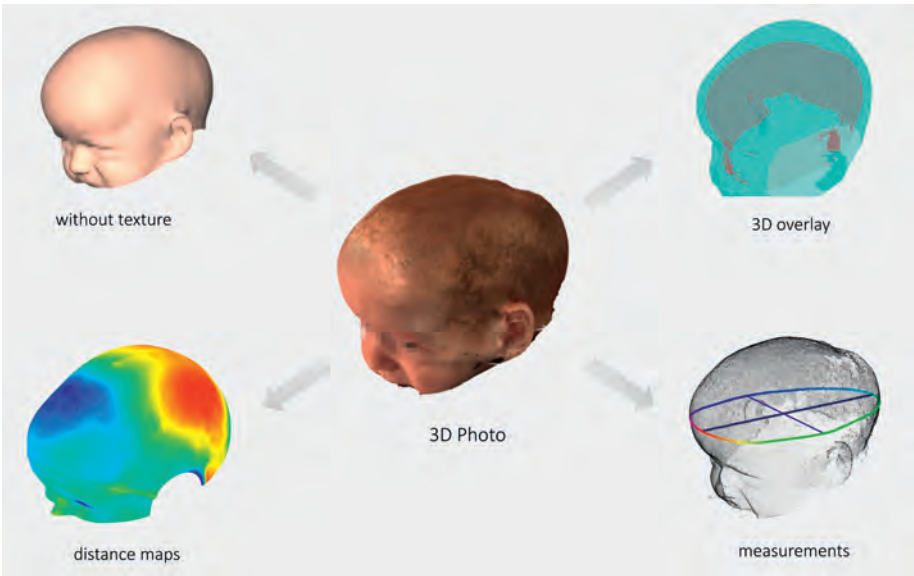

Figure 1: Various visualization and analysis options which are used by the treatment team and shown to patients during clinical consultation and follow-up to objectively evaluate cranial shape changes.

In a recent study by our group, a machine learning technique, 'deep learning', was used to classify a set of 3D photos as normal, scaphocephaly, trigonocephaly, or plagiocephaly. Out of 196 photos, 195 subjects (99.5%) were correctly classified and only one plagiocephaly patient was misclassified as normal.[3] This proves the enormous potential of deep learning methods for the classification of craniosynostosis.[4,5] Unfortunately, a consequence of deep learning is that the features that are used to classify a patient are unknown. This is satisfactory for classification but is not ideal during follow-up. Features that describe a deformation (such as the principal components discussed in **Chapter 3**) could also be used to quantify the severity of the deformation and could therefore be used during follow-up by checking whether or not a certain deformation improves. Alternatively,

attention maps or class-activation maps derived from deep-learning models could also give a degree or a quantification. Therefore, the ideal future method consists of a deep learning method with comprehensive features. This provides a robust method that can be used for both classification and quantification of cranial deformations.

Figure 2: Additional gears will enable the complete gear system, that represents the clinical workflow, to work more efficient.

NEW DEVELOPMENTS IN ACQUIRING 3D PHOTOS

Above all, making 3D photogrammetry more accessible at home or at other clinical sites will be a massive improvement. All our studies benefited from an excellent but rather expensive 3DMD cranial photo system, as well as from proper-trained photographers and technical medicine students who are always willing to make 3D photos. Unfortunately, these advantages are not always and everywhere available. New developments, such as the fully automated smartphone-based 3D capturing system that uses a skin cap with markers, could solve this problem.[6,7] Other methods that use 2D photos from different angles and a machine-learning approach are also promising.[8] If a 3D photo can be cheap and easily acquired in sufficient quality for our classification and analysis tools, we could diagnose patients earlier and make follow-up more convenient.

PART 2 – PLANNING

VIRTUAL SURGICAL PLANNING IMPROVEMENTS

In **Chapter 4**, we considered seven benefits of using a virtual surgical planning (VSP) for open cranial vault reconstruction (OCVR) of craniosynostosis patients. Some benefits are confirmed in the literature, which states that it leads to a simpler, safer and more efficient workflow.[9–11] However, VSP is not (yet) standard care in most centers. An important reason for this is that experienced surgeons are able to achieve satisfactory results without VSP and, therefore, the additional pre-surgical time and investment in 3D planning technology do not outweigh the benefits. Regrettably, it is impossible to properly assess the success of the realized clinical outcome if there is no preoperative plan available for comparison. This makes claims about aesthetical outcomes rather subjective, and also makes it difficult for our group to present convincing evidence. We can, however, share our experience that comparing the post-op CT scan to the VSP has helped our team significantly to improve both the planning and the surgery itself (**Chapter 11**). This illustrates the coherence between planning and evaluation.

However, an important drawback of the current planning process is that it is done in a rather conventional way: Only a single surgical approach can be simulated at one time, and there is no possibility to dynamically adjust a (virtual) osteotomy after the (virtual) reconstruction has been made. This makes virtual planning time consuming and somewhat cumbersome. If future updates allow dynamically adjustable osteotomies, different surgical strategies could be evaluated and tested faster. This makes real-time backward planning possible (benefit 4 in **Chapter 4)** and will result in faster virtual planning and more creativity during the planning process. Another limitation of the current workflow is that the calculation of the (intended) intracranial volume, when the bone segments are virtually positioned to their new position, is very complex and time-consuming. The planning's workflow would be significantly improved if this calculation could be automated and implemented in such a way that the intended volume could be showed in real-time during the planning process for every scenario or modification.

In summary, the actual impact of virtual surgical planning is very difficult to quantify, but, as described in **Chapter 4,** our experience was very positive. Although additional pre-surgical time and 3D expertise is required for planning and preparation, for OCVR as for renal tumor resections (described in **Chapter 5**)

the use of VSP is now part of the standard clinical workflow. This proves the usability of VSP during the planning of complex surgery.

The above-mentioned possibilities are a clear answer to the central research question of Part 2: *What are the (dis)advantages of 3D planning during the preparation of craniosynostosis surgery?*

PLANNING IN A REAL 3D SPACE

Since 3D virtual planning is used in many surgical disciplines, it seems somehow contradictory that, for many cases, 2D visualizations screens are used to create a 3D planning strategy. Therefore, a future shift toward (real) 3D visualized virtual planning can be expected. Real 3D visualization could be created by a stereoscopic view, such as the semi-transparent video see-through displays in the Microsoft HoloLens. This facilitates a realistic perspective when the user explores virtual content such as an anatomical model. Studies focusing on education and training also support the hypothesis that stereoscopic augmented reality (AR) improves anatomy learning.[12,13] In a randomized controlled trial, the Leiden University Medical Center found that medical students who used AR improved their anatomical knowledge, enjoyed the learning, found it easy and intuitive to use, and would recommend it to their fellow students.[14] Furthermore, they found that students with lower visual-spatial abilities achieved higher test results when learning anatomy in stereoscopic AR. On the contrary, Bölek et al. found in their meta-analysis that insufficient evidence is yet available to confirm the added value of AR for education. They state that more high quality study designs are required to investigate the actual added value for education[15] (as is true for almost all types of AR research at this moment).

Next to viewing anatomy, stereoscopic AR has advantages when used during the virtual planning of interventions. Visualization options and animations in an AR space make it possible to explore a surgical planning in a dynamic and intuitively manner. In this way, AR could also be an ideal platform for a realistic visualization of different surgical strategies and their predicted outcomes.[16] AR visualization could also improve the 'communication' between different users who are working together to create, adjust or discuss a VSP. Once easy and simple tools are created, users will be able to fine-tune a virtual plan, make small adjustments, and provide adequate feedback to the technical physician who created the planning. This will improve upon the current workflow, where various 2D screenshots from different angles are used to mimic the 3D planning. Furthermore, it is likely that when virtual

planning shifts from a 2D to an 3D-AR environment, the gap between planning and surgery will shrink, which will stimulate the willingness and urgency of using AR during an intervention (Part 3). In order to make the diagnostic and planning AR workflow applicable, the AR visualization method must be enhanced with application specific software tools.

Clinical applications include, but are not limited to the following examples:

CRANIOSYNOSTOSIS SURGERY

Creating a virtual craniosynostosis planning requires complex software for manipulating and dissecting the viscero- and the neurocranium. In the current workflow, all team members are looking at a 2D screen and diligent provide instructions to the technical physician who modifies the 3D model. This is time-consuming, inefficient and it hampers creativity. Using the AR module, every member of the team can visualize, operate and modify the 3D cranial planning, can cut the 3D model, enlarge specific parts and simulate different scenarios in 3D. In this way, the AR visualization stimulates creativity and enables all experts in the team to provide input. Also, rotating a curved bone segment influences the cranial contour from the side, top and frontal view. Stereoscopic 3D visualizing allows the user to inspect this adjustment instantly from all sides.

Figure 3: Craniosynostosis planning in the AR-space. Using AR glasses the user can see the (new) 3D position of the bone segments and the animated view shows how the segments should be moved (Topdoks, NPO Zapp, November 2019)

CARDIOTHORACIC SURGERY

During transcatheter aortic valve implantation (TAVI) procedures, a replacement aortic valve is placed over the native valve via a catheter in the femoral artery. To maximise safety, precise TAVI preplanning is required, which consists of selecting the best fitting valve as well as determining what route to the heart is the least tortuous, has the least calcifications and has the widest diameter. These characteristics are sometimes hard to interpret in 2D. 3D AR visualization can overcome these limitations and improve the pre-operative planning and preparation of these procedures. Special software tools were developed by our AR team to measure the angulation, length, trajectories and diameter of arteries in 3D. Compared to conventional TAVI planning on 2D slices, the intuitiveness and 3D visualization capabilities of AR provided important benefits when preparing for this procedure.[17] At this moment, the creation of the TAVI AR model requires a preparation time of six hours. Future research should aim to reduce this time to a maximum of 30 minutes to ensure implementation of this application in the standard clinical workflow.

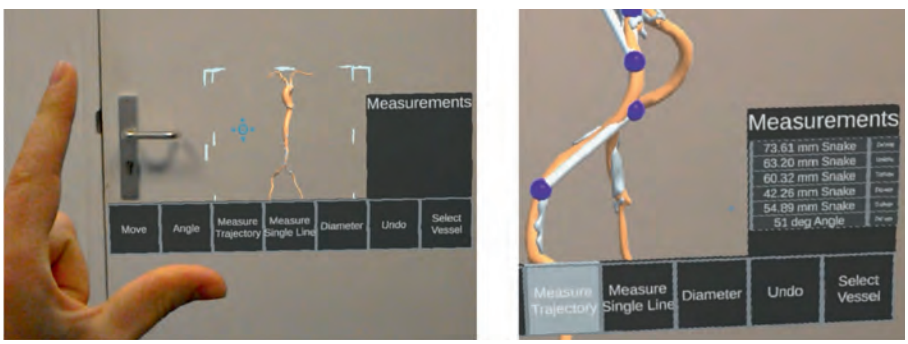

Figure 4: AR planning of transcatheter aortic valve implantation (TAVI). Diameter variations along the aorta can be visualized and measured.

KIDNEY SURGERY

In addition to the discussion in **Chapter 5**, regarding the added value of AR visualization for the preparation of renal tumor removal, recent (unpublished) research at the Princess Máxima Center (PMC) proved that using 3D models and AR visualization improved the multidisciplinary collaboration of care professionals.[18] Since this study, the use of AR models has become standard care for every patient in the PMC with renal tumors. In this procedure, different anatomical structures are segmented from an MRI scan, and a specially developed MRI sequence

visualizes blood vessels.[18] These data are then processed by the Radboudumc 3D Lab to create interactive models on the HoloLens, where the surgeon is able to create the optimal surgical strategy by inspecting the relation of the tumor to the surrounding anatomy. If future developments of the AR models can predict which efferent renal arteries supply which part of the kidney, it might even be possible to simulate a saver partial resection of the kidney. This, in combination with dynamic resection planes that can be manipulated in the AR environment, will improve the treatment of children with renal tumors. In addition, research is also focusing on making the kidney and renal models deformable. This is an important capability for the next step: using the AR kidney models in surgery.

Figure 5: The preparation of renal tumor surgery with augmented reality ('Helden van het Maxima', NPO September 2019)

EVALUATION OF PEDIATRIC BURN INJURIES

12

Pediatric burn injuries are devastating and adequate treatment is essential to realize the most optimal outcome possible for these children. Medical specialists which are confronted with these young patients should be proper trained for different scenarios. With an interactive AR application, medical specialists can be trained in a realistic environment. In this application, burn injuries at different stages can be (virtually) evaluated and treated. A collection of 2D and 3D photos of real burn injuries can be combined with an interactive 3D model of infants. This interactive

AR model can provide realistic and objective training for medical professionals. Users can evaluate the burn injury simultaneously, delineate the area of the burn, determine the extent of injury and try different treatment options. In September 2020, the first pediatric burn training with AR was given at our University hospital.

AUGMENTED REALITY VERSUS VIRTUAL REALITY

In all previous sections, AR is considered to be the most fitting technique for our purposes. However, virtual reality (VR) also meets the demands of stereoscopic view, since it too can simulate different surgical scenarios and generate intuitive user interactions. Virtual reality is widely implemented in the training and gaming industry. It has a spectacular stereoscopic 3D visualization capacity and a large field of view (FOV) that might make VR an even better solution for the exploration of 3D content. Nevertheless, we believe that AR is the best candidate in our future pursuit to create the ultimate diagnostic, planning and communication tool because it has several advantages. With AR, only the subject needs to be rendered, and not the complete surrounding. This means that less powerful hardware is required for AR. Due to this, the designs of AR headsets are wireless and more ergonomic (presumably, even in future devices). This stimulates free movement of users and improves multiuser communication. In addition, because the user's view is always free, communication with other users is still possible in a joined session. Therefore, AR has many advantages for collaborative and embodied communication.[14,16]

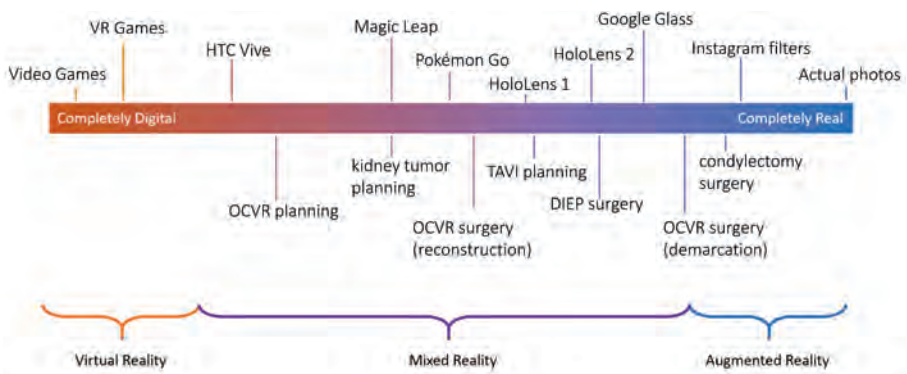

Figure 6: Spectrum of the virtual and the real world. On top, the location of VR and AR devices on this spectrum are shown. Below, the positions of several clinical applications are indicated.

Figure 6 illustrates the spectrum between a 'Virtual' and a 'Real' environment and shows that choosing the optimal technique is not a black-and-white choice but

a combination involving both environments. For example, future developments of AR are focusing to shift more to the 'virtual side' of this spectrum by improving the FOV etc. At the same time, VR applications are aiming to slide to the 'real side' by adding realistic user input (such as haptic feedback gloves) in their enclosed environment. The Magic Leap AR device is an interesting example. The stereoscopic optical see-trough displays of the Magic Leap have a large FOV (40° x 30° versus 30° x 17.5° of the HoloLens), a higher resolution (1280 x 960 versus 1268 x 720 of the HoloLens) and eye tracking capabilities that make virtual content more realistic. Remarkably, Magic Leap also uses dark see-through glasses (probably to increase the contrast between the real world and virtual content), which has the undesirable consequence of making the blending of the virtual and the real world poorer. Therefore Magic Leap glasses are more useful for applications on the virtual side, than is the HoloLens.

Future AR devices will have different positions in this spectrum. Locating the "sweet spot" depends on application-specific demands, but we firmly believe that the most optimal location is at the right side of the spectrum. Subsequently, this will also facilitate a smooth transition to the transfer phase (from Part 2 to Part 3).

PART 3 – SURGERY

IMPROVE THE SURGICAL WORKFLOW

Improvements, more research and greater acceptance will ensure that in the future the implementation of AR during surgery is guaranteed. As stated earlier, the success of surgical implementation also depends on the implementation of AR in other parts of the clinical process. In general, there are four important reasons why, and how AR will change the surgical workflow.

Reason 1 - 3D visualization

When AR becomes the standard for surgical planning (Part 2), surgeons will be more willing to use AR during surgery. At this moment, AR visualization is facing a chicken or egg causality dilemma: a planning is converted to 2D because there are no 3D displays that can be used during surgery but at the same time, the urge to use 3D displays is low because every 3D planning is degraded to simple 2D measures. Fortunately, it is obvious what need to be done to solve this dilemma:

first, we (the 3D Lab) should stop providing 2D measures to the clinicians. We should stop providing the clinicians with length measures that explain how a bone fragment should be moved. We should stop expressing the roll, pitch, yaw, and anterior displacement in numbers to describe how a maxilla should be repositioned. We should stop creating reference points on an orbital floor implant to deduce its position. Instead, we should start using AR glasses as soon as possible. The potential of 3D visualization methods in the operation theatre by means of 3D computer screens, 3D holographic projectors and various kinds of stereoscopic AR glasses is described in many studies.[16,19–23] The main concern of earlier studies are the high costs, the cumbersomeness of using new tools during surgery, and the lack of comparative studies. Yet, the latest AR glasses (e.g. the HoloLens 2), are easy to use, cheap and widely available, and could therefore make 3D visualization accessible in every OR. In addition, future research should also focus on the usability of AR glasses during surgery and eliminating factors that are cumbersome.

Reason 2 - From diagnostic to instructive

Because medical images can be viewed quickly and easily at different locations with AR glasses, it can be expected that medical imaging, initially acquired for diagnostic purposes, will also be consulted during interventions. For example, CT-angio scans used in free flap surgery assess the number and accessibility of perforators (blood vessels). Yet, the same scans could be used (after automatic segmentation and reconstruction) to visualize the course and position of these perforators in 3D at the correct anatomical position in the patient.

This was illustrated in **Chapter 8**, where pre-surgical information was used during a breast reconstruction with a microsurgical DIEP flap. A diagnostic CT-angio scan was segmented and transformed to a 3D visualization in the HoloLens. In combination with real-time tracking and a novel registration method using the patient's abdominal skin marks, the surgeon was able to see the complex anatomy directly on and in the patient. In follow-up research (not yet published), this innovative workflow was tested in ten patients in a pre-surgical preparation setting, and demonstrated that the HoloLens can indicate perforator locations within a clinical margin of 10 mm. This is promising for clinical implementation because this workflow does not demand millimeter accuracy. The usability, intuitiveness and the set-up are the most important factors that will decide when AR will be

integrated in the clinical workflow.[20] When new developments and research can realize this, the DIEP application experience will be of great value and can be used for other free flaps and used in many clinics.[24] This example shows how AR can facilitate a shift from diagnostic imaging to image-guided surgery.

Reason 3 - Replacing surgical guides

A third reason why the implementation of AR during surgery is expedient is because it can provide guidance during surgical procedures that cannot be provided by other methods. For example, during key-hole surgery or during a proportional high condylectomy, the small surgical field makes the use of surgical guides impossible. For these applications, AR guidance is an effective method to assist the surgeon. In addition, AR guidance allows the user to stay focused on the surgical field while attaining feedback from the plan and the surgeon is not forced to switch his or her view to an external monitor where conventional navigation data are normally displayed. During the AR-guided condylectomy in **Chapter 8**, a pointer was used to indicate the planned positions. The next step should be to equip the surgical handpiece directly with AR guidance. In that way, the pointer is no longer required, which makes the process even more intuitive and frees up some space in this small surgical field. In addition, AR will facilitate the guidance of the direction during the drilling.

Figure 7: A hologram shows the surgeon the location and the course of arteries in the abdomen and their relation with other organs, such as the muscle and skin.

Even when surgical guides could be used, the relatively high costs, the additional manufacturing time, and the inflexibility are serious limitations. For a surgical craniosynostosis procedure, the production of an osteotomy and a reconstruction guide requires eight days and costs around 1,400 euros (**Chapter 4** and **Chapter 7**). While time and cost are likely to be reduced in future with newer 3D printing techniques, these limitations are completely absent when using AR guidance. Even though **Chapter 7** concluded that surgical guides are more accurate at this point, we believe that AR will have a major impact on clinical practice because it can be made easily and widely accessible, reduce costs and eliminate the manufacturing time of surgical guides.

There are two important phases when the planning is transferred in OCVR: marking the osteotomy lines, and performing the cranial reconstruction. **Chapter 7** focused only on the first phase, because this allowed a scientifically fair and straightforward comparison between the AR method and the surgical guides. However, in retrospect, it would have been far more interesting to evaluate the reconstruction phase, because this is surgically more challenging. In addition, when bone segments are not cut precisely, these segments might not fit into the guides. Considering this, the real added value of AR could be to provide assistance to the surgeon how to reconstruct the bone segments. Following this, a hybrid solution that uses surgical guides for delineation and AR for reconstruction might be a future direction that should be investigated. The simple, smartphone-assisted AR application that was used by Alshomer et al. confirms that this is probably the most logical first step toward clinical implementation.[25]

There is another important benefit of using AR instead of surgical guides: in future applications, the AR-tracking system could anticipate potential user errors in case the surgeon has to deviate from the original surgical planning. For example, if (for any reason) the surgeon deviates from the planning in his first cut in the fibula, the segments might not fit together (even if the rest of the cuts are made accurately). An AR guidance system could compensate for this error. Because the saw is tracked by the AR system and the planning is only 'virtual', the AR guidance system could automatically evaluate every action of the surgeon and adjust the subsequent osteotomies of the planning. In this way, a more dynamic guidance system will be available.[26] Figure 8 shows an impression of a first prototype of such a dynamic guidance system.

Although conventional surgical navigation systems can be used to replace surgical guides, the high costs (around 50,000 euros) of these systems makes AR glasses a low-cost alternative. In addition, this AR solution allows the user to stay focused on the surgical field while attaining feedback from the planning; the surgeon is not forced to switch his or her view to an external monitor where conventional navigation data are normally displayed. Therefore, AR guidance is an adequate method to transfer a virtual planning for various cranio-maxillofacial and other procedures.[27,28]

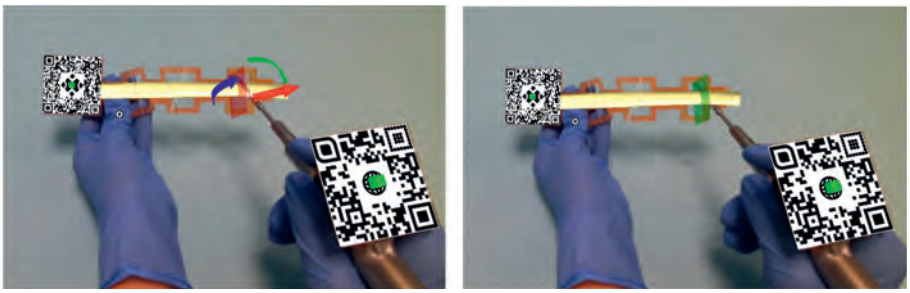

Figure 8: AR visualization of a fibula segment-osteotomy. The user is guided by the holographic arrows to manipulate the saw in the correct position and orientation (left). When saw is held correctly, the osteotomy plane becomes green. In future updates, the actual trajectory of the saw could be used to adjust the subsequent osteotomies.

Reason 4 - Enable complex planning

A fourth reason why AR will revolutionize the current surgical routine is that it will simplify the execution of complex surgical planning. Providing adequate feedback about a plan is very important in almost every surgical procedure. For example, during cranial reconstructions or when placing an orbital implant, the presence in the operation theater of the technical physician who made the planning is advisable because he or she can help clarify the plan during surgery. Although this illustrates the importance of technical physicians, this could mean that making a complex surgical plan may not be desirable if there is no intra-operative feedback available. In such a situation, AR guidance could help, since AR can intuitively visualize how an object, implant or instrument should be manipulated or positioned, step-by-step (Figure 3). When the execution of a VSP becomes easier, more advanced virtual surgery plans can, and will be created.

Currently, many different image-guided surgery systems are being developed to guide surgeons during complex tasks. For example, dental implants can

be positioned with the X-Guide system (Nobel Biocare, Zürich, Switzerland), orthopedic screws can be placed using other systems,[29,30] and yet another 3D guidance systems has been developed to accurately positioning orbital floor implants.[31] All these methods require specialized tools or a tracking system that is developed for a single purpose. AR could display the virtual content in the real environment, which makes application much simpler and could therefore be used for various purposes. This will facilitate mass adoption of image-guided surgical applications and indeed make AR guided surgery a disruptive technology.

TECHNICAL IMPROVEMENTS

Before AR can become fully implemented into the surgical workflow, there are some technical aspects that needs to be improved. Since registration and tracking fulfill a fundamental role in AR-guided surgery, various future optimizations are desired for both aspects.

Figure 9: several factors that will enhance the diagnose-planning-surgery-evaluation cycle.

POINT-BASED REGISTRATION

In **Chapter 8**, point-based registration (PBR) in combination with skin marks proved to be a very practical and successful method for our DIEP application. A limitation of PBR is the potential Fiducial Localization Error (FLE), caused by the user who

indicates the landmarks.[32,33] Yet, because AR can visualize a potential mismatch of each landmark directly on the patient, the registration landmarks could be adjusted to improve the overall registration. This is a substantial reason why PBR could work better in AR than in an image guided surgery (IGS) systems. In future research, the automatic detection of landmarks will be used to improve the PBR. Pepe et al. presented a markerless PBR method that automatically detects landmarks in the face and uses these for registration on the HoloLens.[34] Especially for the detection of skin markers during DIEP flap preparation, an automatic detection algorithm for abdominal nevi would improve the workflow of **Chapter 8**.

SURFACE-BASED REGISTRATION

Similar to PBR, surface-based registration (SBR) uses a surface to align the virtual data on a patient and is often used in neurosurgery.[35] SBR requires a surface with sufficient curvature, such as the face. With a (mobile) 3D surface scanner, the surface of a patient in the operation room can be scanned and the virtual content can be matched. Especially for craniosynostosis surgery, SBR could really improve the accuracy and minimize the complexity of current registration methods. Because the bony cranium has an evident and unique curvature, matching the image data will be relatively easy and accurate. When SBR is implemented, the current limitation of PBR (e.g., too few clear landmarks) should be surmounted. Various tests with (semi-) mobile 3D scanners were performed in our group and showed that the quality was sufficient (Figure 10). However, a long scanning and processing time (around 15 minutes) makes this workflow not suitable for intra-operative use at this moment. Nevertheless, SBM is a realistic and promising future option once it can satisfy some requirements. These include a fast set up time (less than five minutes), a fast scanning time (less than one minute) and a fast processing time (less than a few minutes). Fortunately, the newest generation 3D scanners, such as the Artec Eva (Artec3D, Luxembourg, Luxembourg) and the Einscan Pro HD (SHINING 3D, Hangzhou, China) and several other scanners already fulfils these requirements.[36] Therefore, future research should focus on the implementation of 3D scanning during surgery in a manner that does not hamper the surgical routine too much.

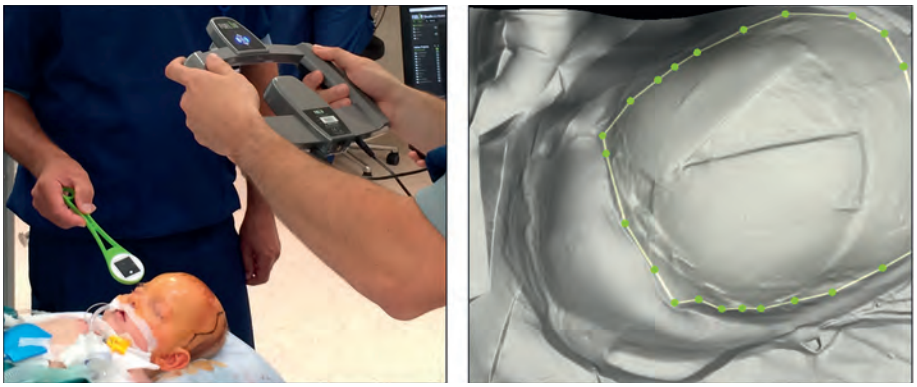

Figure 10: 3D surface scanning in the operation theatre. Left: the hand-held 3D scanner was used to capture the 3D geometry of a patient's head shape. Right: the hand-held 3D camera was used during surgery to capture the position and orientation of the reconstructed bone segments.

SPLINT-BASED REGISTRATION

New 3D scanning techniques could also be used to perform the registration step in advance of the actual surgery. In **Chapter 9**, an intra-oral scan was acquired of a patient's dentition. Next, a dental splint was modeled and printed with a tight and unique fit on the (digital) dentition and was equipped with a QR marker. During the surgical procedure, the splint with QR marker was placed on the dentition of the patient. This made a registration process obsolete and the HoloLens was able to directly visualize the virtual content on the correct position. This contributed to a fast and accurate workflow. Based on the results and experience of **Chapter 9**, a dental splint is an excellent registration method that could be used for AR guidance in the head and neck area. It requires more complex preparation steps, but improves usability during the intervention. Schreurs et al. performed an extensive cadaveric study to investigate the registration accuracy of various methods and found that splint-based registration is as accurate as bone anchored fiducials (with optical tracking).[37] Although more research is required, especially in terms of usability, other studies using this registration method for other IGS implementations confirm the potential of this method. This method could be applied in head and neck oncology, orthognathic surgery, trauma surgery or implant surgery,[38–40] or, with some additional landmarks, even for neurosurgical procedures.[41]

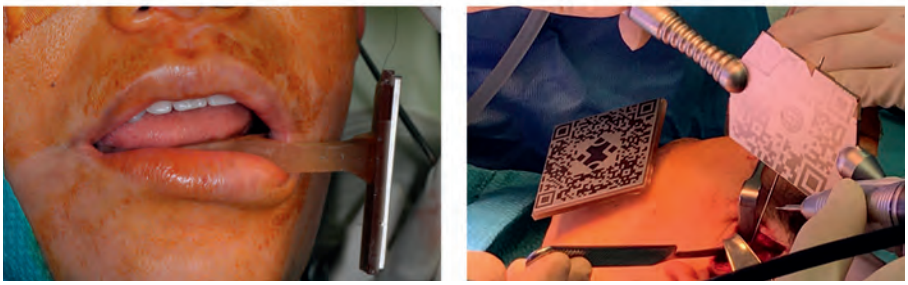

Figure 11: A virtual impression of the patient's dentition was captured with an intra-oral scanner. In combination with 3D printing, a splint with an unique fit on the lower dentition was created and used to hold a QR marker (left). The QR could be tracked by the HoloLens during a high condylectomy (right).

ARTIFICIAL INTELLIGENCE-BASED REGISTRATION

Future procedures could use a combination of Artificial Intelligence (AI) and computer vision techniques to improve and automate the registration. This could eliminate user error since indicating markers, making a 3D scan or fabricate a splint will no longer be required. Various toolkits, including the Vuforia toolkit that was used in this thesis for marker tracking, are currently being explored as possible AI-based registration methods.[42,43] These methods use a Deep Neural Network (DNN) and artificially created 2D images as an input. These images are automatically converted from the 3D virtual data (e.g., a cranial shape). By artificially adjusting various parameters such as scale, lightning, color, viewing angle, and noise (to simulate blood stains or reflections), a dataset of millions of different 2D images can be generated.[43] Next, a DNN could be trained with this dataset, and when a new 2D image, captured in the operation theatre, is given to the DNN system, the best fitting registration parameters could be estimated. This AI system correlates the 3D planning data directly to a set of 2D images of the surgical site by, for example, using the built-in HoloLens camera. This method is very promising because it does not require user input, is relatively fast, requires only a 2D camera feed, and can be performed multiple times if necessary. Initial research in collaboration with the *Elisabeth-TweeSteden* hospital is currently being performed by our group. However, future studies are required to evaluate the usability and accuracy of this method for different clinical applications.

This method could be used for registration, but if it can be optimized and made to work really fast, it could be used for tracking, as well. This method could possibly be applied to register targets that are prone to deformation, such as moving organs, patients with swelling, and soft tissue.

Figure 12: Example of AI object tracking. A deep neural network is used to match the virtual model of a motorcycle (white lines), including the tags, on a real physical object of a motorcycle (https://www.ptc.com/en/products/vuforia).

TRACKING

After registration, tracking ensures a real-time location update of the patient and instruments. The HoloLens uses a build-in method for tracking and stable placements of holograms. This 'spatial mapping' relies on flat and non-moving objects for optimal performance. However, in the operation theatre, the movements of the surgical team and instruments around the patient result in a constantly altering space, which hampers a proper working of this spatial mapping and introduces drift in the holograms.[44] In **Chapter 6,** an external tracking system was added to the HoloLens, which significantly improved its accuracy. However, a downside is that an external tracking system was required to track at least three objects (the HoloLens, the patient and an instrument), and all objects needed to be in the line of sight of the external camera. Later, due to software updates and more research, we discovered that QR marker tracking is able to produce similar accuracy results within the working distance of a surgeon. In addition, there is a lower risk that objects are out of sight because QR tracking uses the built-in (color) camera of the HoloLens and is therefore more practical. For these reasons, QR-marker tracking will be part of further research.

Since the best fitting tracking method depends on the clinical application, it is likely that future solutions for AR guidance will switch to other tracking methods. For tracking objects inside the patient (such as organs inside the patient's

body during open surgery), electromagnetic tracking (EM) have proved to be the best tracking option.[45] An ideal tracking system should be highly accurate, avoid radiation exposure, be cost- and time-effective, and be simple in use and maintenance.[46] Regrettably, the tracking methods that are actually at the surgeon's disposal depend on hospital policy, industry tenders and service contracts. In addition, the high costs (up to 100,000 euros for a single tracking module), limits general implementation and could also be the reason why IGS is not standard care for many clinical applications. Since every technique has the same goal (providing real time transformation updates), a basic software module to which various tracking systems could be connected would be a revelation. This will allow users to choose the best fitting tracking method for every clinical application.

A universal module would also stimulate the use of new tracking methods. This will be more obvious when we compare the 'Surgical Tracking' market with the 'Gaming Tracking' market. An interesting example is the HTC Lighthouse tracking system, developed to track the headset and controllers of a gamer in VR. This system needs two or more small 'lighthouses,' which send-out sweeps of light. Various tiny sensors on the controllers detect these light sweeps, and the delay between sending and receiving is used to calculate the distance to the lighthouses and their orientation. This system outperforms conventional surgical tracking systems with a submillimeter precision, a 60 Hz refresh rate and a field of view of 4.5 x 4.5 m.[47] Furthermore, this system has been critically tested by a large number of gamers, who use it to throw knifes at zombies (instead of using knifes to dissect patients). And above all, the cost of this system is approximately 470 euros.

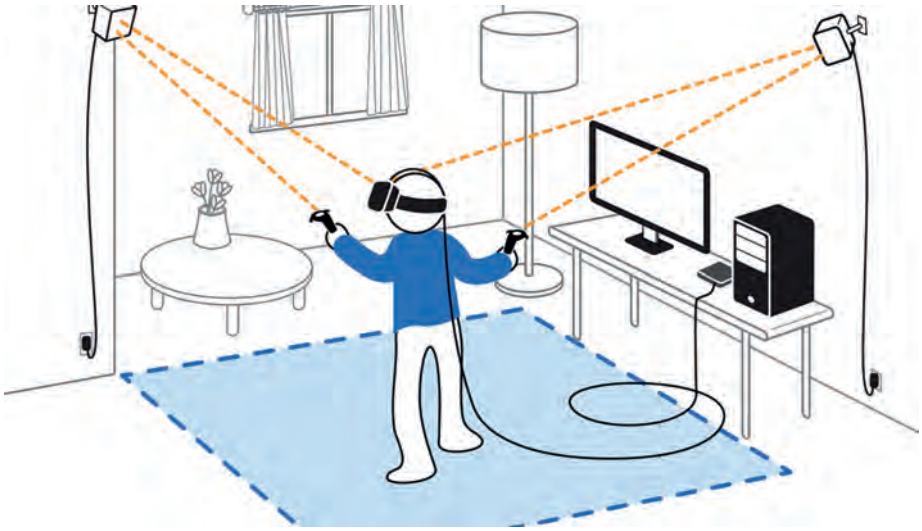

Figure 13: Schematic overview of the HTC Lighthouse tracking system, used to track the position of the user and his instruments (https://hackaday.io/project/160182-hivetracker).

ROBOTIC ASSISTED SURGERY

Another method that can assist surgeons to operate more efficiently, accurately and precisely is the surgical robot.[48] In the scope of this thesis, robotic assisted surgery could be used to transfer or execute a VSP and strengthen the relationship between planning and surgery. Research indicates that, in specific cases, robotic assisted surgery results in less blood loss, fewer complications, shorter hospitalizations and better cosmetic results.[49,50] Considering OCVR, robotic assistance could improve the following steps during surgery.

First, a robotic arm equipped with a pencil could draw the planned osteotomy lines on the patient's cranium. Because the robot can use the 3D planned osteotomy lines directly as input, surgical guides or AR visualization becomes redundant. A prototype for this application was developed by our group[51] (figure 14). This implementation is a logical first step because it is minimally invasive and low-risk.

Second, replacing the pencil with a piezo-surgical instrument enables the robot to perform the osteotomies directly. From the planning CT scan, the robot knows the exact bone thickness at every position and will take this into account when the bone is cut or milled. Although this step is highly invasive and errors could lead to severe harm to the patient, correct use will result in straight and accurate osteotomy lines and will effectuate an optimal reconstruction.

Third, a robot could 'assist' the surgeon by holding the (perfectly) cut bone segments steady on their new position. Because the robot imposes the exact orientation and location of the segments, the surgeon can directly place the fixation material. A similar idea was presented by Lee et al., who used a robot to hold a maxilla in place during a LeFort 1 osteotomy.[52] Because the reconstruction part is surgically the most challenging step during OCVR, the added value of robot assistance is probably most evident in this step.

Figure 14: Robotic assisted demarcation of virtually planned osteotomy lines on a craniosynostosis patient. Experimental set up in collaboration with Twente University.

WORKFLOW GUIDANCE

In addition to guidance during surgery, AR could also assist during other (complex) clinical workflows, such as the resuscitation of newborns. In this acute situation, medical professionals work together in a team and follow a protocolized workflow. At the Radboudumc neonatology department, an advanced AR-based decision support algorithm has been designed in collaboration with the 3D Lab. A HoloLens application helps the team leader structure all the workflow steps. Data from medical equipment, including saturation, temperature and heartrate, are real-time streamed to the HoloLens (Figure 15). Certain steps in the standard workflow such as, 'check if temperature is between 35-37 degrees', could be skipped if the HoloLens algorithm detects that the temperature is in the acceptable range.[53] The vital parameters of the newborn and the step by step instructions are visualized in the work field of the supervisor, who can review all parameters at one glace without losing the patient out of sight or losing contact with the other team members.

A major advantage of AR-assisted workflows is that it enables the user to execute a more complex protocol. Since there is a limit to how much information a user can process during an intervention (information overload), including more steps, or adding more checks, could lead to misuse of the protocol, especially for less experienced or less trained users. For this reason, the standardized protocol that is used world-wide, is a tradeoff between complexity and practicality. However, with the AR-based clinician support system, executing a workflow can be made much simpler, and as a consequence the protocol itself can be made more complex while at the same time better suit the clinical situation.

Because the HoloLens is able to record the complete procedure, new insights regarding resuscitation can be collected. All of the time frames in which decisions are made or instructions are provided can be stored, along with all the vital signs. Combining all this data results in an exceptional dataset. With artificial intelligence and further research, this dataset can be explored to optimize and fine-tune various protocols. In the future, the use of this AR-assisted workflow guidance can be used for other applications, such as resuscitation of adults, performing an ABC procedure of trauma patients, or as support for paramedics at remote locations.

Figure 15: The vital signs of a newborn, requiring resuscitation, are displayed above the patient. Step-by-step instructions help the team leader guide the intervention (Tsang et al.[53])

PART 4 - EVALUATION

In the previous parts, potential future clinical implementations were presented and discussed. However, the care and cure of craniosynostosis patients was the main focus of this thesis, and in Part 4, we pursued a long-term follow-up of a large number of patients. This gave us the opportunity to objectively reflect our own work and completed the cycle of diagnosis – planning – surgery and evaluation.

In **Chapter 10** we showed that the evaluation of surgical methods helps us determine the best possible care for individual patients. We concluded that EACS in combination with helmet therapy is an adequate method to treat scaphocephalic patients. In future research, the treatment of other craniosynostosis forms, such as trigonocephaly and plagiocephaly, will also be investigated. Since plagiocephaly can lead to severe asymmetrical facial abnormalities, a beautiful aesthetic result is even more paramount. This is one of the reasons that plagiocephaly treatment should be similarly evaluated in order to determine objectively the best possible treatment for this condition.

In **Chapter 10**, the clinical outcomes of the EACS with helmet therapy were presented and compared to the normal reference values *and* the OCVR treatment was compared to the normal reference values. It should be noted, however, that it was not strictly possible to make a direct comparison between both treatments because the inclusion criteria (such as age at the time of surgery) were very dissimilar. The average results of EACS are more accurate than the average results of OCVR. This is because the same strategy was used for all EACS patients, while different surgical strategies were used for the OCVR patients since a tailored surgical plan was created for every individual patient. Nevertheless, the 3D distance maps demonstrate that EACS and helmet treatment leads to very satisfactory results. Moreover, when the surgical outcome parameters are taken into account, it is evident that EACS is a very adequate and appropriate treatment for scaphocephaly patients.

Another limitation of the study is that while the design, fabrication and adjustment of the redression helmets have an important influence on the EACS treatment, we did not take all helmet-related parameters into consideration. Although the direct and live evaluation of 3D photos during clinical consultation gives us the possibility

to adequately and accurately evaluate the cranial change between the present and earlier moments, this change does not say anything about the corrective shape of the redression helmet. For example, if we detect an undesirable change of shape, we cannot determine whether this is caused by a wrong helmet design, or something else. If we could include the design of the helmet in this process, we would be able to monitor treatment and check whether the helmet has sufficient redressing potential left. Therefore, the exchange of 3D information between the CFA-team and the helmet orthoptists could lead to interesting insights and could improve collaboration between patients and care providers.

The redression helmet of the future might be a smart helmet. Nesting various sensors into the helmet could improve the therapy and lower the burden. For example, heat sensors in the helmet could inform parents when head temperature becomes too high, which might be useful during fever or in extreme summer temperatures. Pressure sensors could tell parents when it is time to visit the helmet orthotist and also help the orthotists to diagnose where the helmet needs further adjustments. In additions, this smart helmet could accurately monitor how much the helmet is actually worn by the patient during treatment and therefore generate important data for future research.

In **Chapter 11**, we demonstrated how a 3D technique could be used for the post-operative evaluation of individual cases of open reconstructive surgery and how it helped our team to improve and understand the planning, transfer and surgery of open cranial vault reconstructions. In combination, **Chapters 10** and **11** provided the answer to the final research questions: *Could 3D techniques be used to evaluate surgery and treatment outcomes? Could this be implemented and does this benefit the treatment of (new) patients?* And with this, the cycle between diagnosis – planning – surgery and evaluation is completed.

FINAL WORDS

Throughout the various parts and chapters, this thesis evaluated and improved the clinical care and cure of craniosynostosis patients by using 3D technology. The four parts of this thesis form the gear train that represents a clinical process. The presented innovations did not only advance the operation of the individual gear

wheels, but they also helped the entire system to work more efficiently and more coherently. This has brought the whole clinical process to a higher level.

This thesis allows validated and accepted technology (e.g., 3D stereophotogrammetry and 3D printing) to be efficiently integrated into the current clinical process. The potential implementation of new (unmatured) technology (e.g., virtual surgical planning and AR) was explored, as well.

Since we were intimately involved during the consultation, planning and surgery of patients, we were able to identify the clinical shortcomings and demands. This enabled us to target our innovations and, as a result, many of the technological solutions presented in this thesis have found their way into clinical practice. On the other hand, this project has shown that it can be very beneficial to investigate how technological innovations can be used to solve clinical problems for other disciplines. **Chapters 5**, **8** and **9** are examples of this. This creates a cross-over that allows technology or research to be carried out faster.

Finally, the most important factor that helped the gear train to work seamlessly was the close collaboration between the physicians, the technical physicians and the 3D Lab. This open-minded, critical and accessible working environment was fundamental to accomplish the goals of this project.

REFERENCES

1. Fadaifard H, Wolberg G, Haralick R. Multiscale 3D feature extraction and matching with an application to 3D face recognition. *Graph Models*. 2013;75(4):157-176. doi:10.1016/j.gmod.2013.01.002
2. Zhang Z, Dai Y, Sun J. Deep learning based point cloud registration: an overview. *Virtual Real Intell Hardw*. 2020;2(3):222-246. doi:10.1016/j.vrih.2020.05.002
3. de Jong G, Bijlsma E, Meulstee J, et al. Combining deep learning with 3D stereophotogrammetry for craniosynostosis diagnosis. *Sci Rep*. Published online 2020.
4. Bhalodia R, Dvoracek LA, Ayyash AM, Kavan L, Whitaker R, Goldstein JA. Quantifying the Severity of Metopic Craniosynostosis: A Pilot Study Application of Machine Learning in Craniofacial Surgery. *J Craniofac Surg*. Published online 2020. doi:10.1097/SCS.0000000000006215
5. Zhou X, You L, Zhang G, Zhao W, Greives M, David L. *Clinics in Surgery Automated Sagittal Craniosynostosis Classification from CT Images Using Transfer Learning OPEN ACCESS*. Vol 2020.; 2020. Accessed August 30, 2020. http://clinicsinsurgery.com/
6. Barbero-García I, Lerma JL, Mora-Navarro G. Fully automatic smartphone-based photogrammetric 3D modelling of infant's heads for cranial deformation analysis. *ISPRS J Photogramm Remote Sens*. 2020;166(April):268-277. doi:10.1016/j.isprsjprs.2020.06.013
7. Barbero-García I, Lerma JL, Miranda P, Marqués-Mateu Á. Smartphone-based photogrammetric 3D modelling assessment by comparison with radiological medical imaging for cranial deformation analysis. *Meas J Int Meas Confed*. 2019;131:372-379. doi:10.1016/j.measurement.2018.08.059
8. Callejas Pastor CA, Jung I-Y, Seo S, Kwon S Bin, Ku Y, Choi J. Two-Dimensional Image-Based Screening Tool for Infants with Positional Cranial Deformities: A Machine Learning Approach. *Diagnostics*. 2020;10(7):495. doi:10.3390/diagnostics10070495
9. Macmillan A, Lopez J, Mundinger GS, Major M, Medina MA, Dorafshar AH. Virtual surgical planning for correction of delayed presentation scaphocephaly using a modified melbourne technique. In: *Journal of Craniofacial Surgery*. Vol 29. ; 2018:914-919. doi:10.1097/SCS.0000000000004290
10. Lopresti M, Daniels B, Buchanan EP, Monson L, Lam S. Virtual surgical planning and 3D printing in repeat calvarial vault reconstruction for craniosynostosis: Technical note. *J Neurosurg Pediatr*. 2017;19(4):490-494. doi:10.3171/2016.10.PEDS16301
11. Seruya M, Borsuk DE, Khalifian S, Carson BS, Dalesio NM, Dorafshar AH. Computer-aided design and manufacturing in craniosynostosis surgery. In: *Journal of Craniofacial Surgery*. Vol 24. ; 2013:1100-1105. doi:10.1097/SCS.0b013e31828b7021
12. Kamphuis C, Barsom E, Schijven M, Christoph N. Augmented reality in medical education? *Perspect Med Educ*. 2014;3(4):300-311. doi:10.1007/s40037-013-0107-7
13. Pulijala Y, Ma M, Pears M, Peebles D, Ayoub A. Effectiveness of Immersive Virtual Reality in Surgical Training—A Randomized Control Trial. *J Oral Maxillofac Surg*. 2018;76(5):1065-1072. doi:10.1016/j.joms.2017.10.002
14. Bogomolova K, van der Ham IJM, Dankbaar MEW, et al. The Effect of Stereoscopic Augmented Reality Visualization on Learning Anatomy and the Modifying Effect of Visual-Spatial Abilities: A Double-Center Randomized Controlled Trial. *Anat Sci Educ*. Published online 2019. doi:10.1002/ase.1941
15. Bölek KA, De Jong G, Henssen D. The effectiveness of the use of augmented reality in anatomy education: a systematic review and meta-analysis. *Sci Rep*. 2021;11(1):15292. doi:10.1038/s41598-021-94721-4
16. Kim YOY, Kim H, Kim YOY. Virtual Reality and Augmented Reality in Plastic Surgery: A Review. *Arch Plast Surg*. 2017;44(3):179-187. doi:10.5999/aps.2017.44.3.179
17. Smees C, Meulstee J, Groot Jebbink E, Nijveldt R. *Development of an Augmented Reality Application to Support Preplanning of TAVI Procedures*.; 2019.
18. Fitski, Matthijs; Meulstee, Jene; Littooij, Annemieke; Van de Ven, Cornelis; Van der Steeg, Alida; Wijnen M. MRI Based 3-Dimensional Visualization Workflow for the Preoperative Planning of Nephron-Sparing Surgery in Wilms'Tumor Patients. *Surg Innov*. Published online 2020.
19. Van Gestel F, Frantz T, Vannerom C, et al. The effect of augmented reality on the accuracy and learning curve of external ventricular drain placement. *Neurosurg Focus*. 2021;51(2):E8. doi:10.3171/2021.5.FOCUS21215

20. Dennler C, Bauer DE, Scheibler A-G, et al. Augmented reality in the operating room: a clinical feasibility study. *BMC Musculoskelet Disord*. 2021;22(1):451. doi:10.1186/s12891-021-04339-w
21. Vávra P, Roman J, Zonča P, et al. Recent Development of Augmented Reality in Surgery: A Review. *J Healthc Eng*. 2017;2017:1-9. doi:10.1155/2017/4574172
22. Birkfellner W, Figl M, Huber K, et al. A head-mounted operating binocular for augmented reality visualization in medicine - design and initial evaluation. *IEEE Trans Med Imaging*. 2002;21(8):991-997. doi:10.1109/TMI.2002.803099
23. Gavaghan KA, Peterhans M, Oliveira-Santos T, Weber S. A Portable Image Overlay Projection Device for Computer-Aided Open Liver Surgery. *IEEE Trans Biomed Eng*. 2011;58(6):1855-1864. doi:10.1109/TBME.2011.2126572
24. Hummelink S, Verhulst AC, Maal TJJJ, Hoogeveen YL, Schultze Kool LJ, Ulrich DJOO. An innovative method of planning and displaying flap volume in DIEP flap breast reconstructions. *J Plast Reconstr Aesthetic Surg*. 2017;70(7):871-875. doi:10.1016/j.bjps.2017.04.008
25. Alshomer F, Alazzam A, Alturki A, Almeshal O, Alhusainan H. Smartphone-assisted Augmented Reality in Craniofacial Surgery. *Plast Reconstr Surg - Glob Open*. 2021;9(8):e3743. doi:10.1097/GOX.0000000000003743
26. Snoeijink T. Augmented Reality guided osteotomies of the fibular bone in mandibular reconstructions. Published online 2020.
27. Ayoub A, Pulijala Y. The application of virtual reality and augmented reality in Oral & Maxillofacial Surgery. *BMC Oral Health*. 2019;19(1):1-8. doi:10.1186/s12903-019-0937-8
28. Yoon JW, Chen RE, Kim EJ, et al. *Augmented Reality for the Surgeon: Systematic Review*. Vol 14. John Wiley and Sons Ltd; 2018:e1914. doi:10.1002/rcs.1914
29. Müller F, Roner S, Liebmann F, Spirig JM, Fürnstahl P, Farshad M. Augmented reality navigation for spinal pedicle screw instrumentation using intraoperative 3D imaging. *Spine J*. 2019;000:1-8. doi:10.1016/j.spinee.2019.10.012
30. Gibby JT, Swenson SA, Cvetko S, Rao R, Javan R. Head-mounted display augmented reality to guide pedicle screw placement utilizing computed tomography. *Int J Comput Assist Radiol Surg*. 2019;14(3):525-535. doi:10.1007/s11548-018-1814-7
31. Schreurs R, Dubois L, Becking AGG, Maal TJJJ. Implant-oriented navigation in orbital reconstruction. Part 1: technique and accuracy study. *Int J Oral Maxillofac Surg*. 47(3):395-402. doi:10.1016/j.ijom.2017.09.009
32. Widmann G, Stoffner R, Bale R. Errors and error management in image-guided craniomaxillofacial surgery. *Oral Surgery, Oral Med Oral Pathol Oral Radiol Endodontology*. 2009;107(5):701-715. doi:10.1016/j.tripleo.2009.02.011
33. Labadie RF, Davis BM, Fitzpatrick JM. Image-guided surgery: what is the accuracy? *Curr Opin Otolaryngol Head Neck Surg*. 2005;13(1):27-31. doi:10.1097/00020840-200502000-00008
34. Pepe A, Trotta GF, Mohr-Ziak P, et al. A Marker-Less Registration Approach for Mixed Reality–Aided Maxillofacial Surgery: a Pilot Evaluation. *J Digit Imaging*. Published online 2019:1008-1018. doi:10.1007/s10278-019-00272-6
35. Ballesteros-Zebadúa P, García-Garduño OA, Galván de la Cruz OO, Arellano-Reynoso A, Lárraga-Gutiérrez JM, Celis MA. Assessment of an image-guided neurosurgery system using a head phantom. *Br J Neurosurg*. 2016;30(6):606-610. doi:10.3109/02688697.2016.1173188
36. Fan Y, Jiang D, Wang M, Song Z. A new markerless patient-to-image registration method using a portable 3D scanner. *Med Phys*. 2014;41(10):101910. doi:10.1118/1.4895847
37. Schreurs R, Baan F, Klop C, et al. Virtual splint registration for electromagnetic and optical navigation in orbital and craniofacial surgery. *Sci Rep*. 2021;11(1):10406. doi:10.1038/s41598-021-89897-8
38. Zhu M, Liu F, Chai G, et al. A novel augmented reality system for displaying inferior alveolar nerve bundles in maxillofacial surgery. *Sci Rep*. 2017;7:42365. doi:10.1038/srep42365
39. Zhu M, Chai G, Lin L, et al. Effectiveness of a Novel Augmented Reality-Based Navigation System in Treatment of Orbital Hypertelorism. *Ann Plast Surg*. 2015;00(00):1-7. doi:10.1097/SAP.0000000000000644
40. Joda T, Gallucci GO, Wismeijer D, Zitzmann NU. Augmented and virtual reality in dental medicine: A systematic review. *Comput Biol Med*. 2019;108(January):93-100. doi:10.1016/j.compbiomed.2019.03.012
41. Luebbers HT, Messmer P, Obwegeser JA, et al. Comparison of different registration methods for surgical navigation in cranio-maxillofacial surgery. *J Cranio-Maxillofacial Surg*. 2008;36(2):109-116. doi:10.1016/j.jcms.2007.09.002

42. Vuforia Developer Portal |. Accessed August 3, 2020. https://developer.vuforia.com/
43. Akgul O, Penekli HI, Genc Y. Applying Deep Learning in Augmented Reality Tracking. In: *Proceedings - 12th International Conference on Signal Image Technology and Internet-Based Systems, SITIS 2016*. Institute of Electrical and Electronics Engineers Inc.; 2017:47-54. doi:10.1109/SITIS.2016.17
44. Frantz T, Jansen B, Duerinck J, Vandemeulebroucke J. Augmenting microsoft's HoloLens with vuforia tracking for neuronavigation. *Healthc Technol Lett*. 2018;5(5):221-225. doi:10.1049/htl.2018.5079
45. Bernhardt S, Nicolau SA, Soler L, Doignon C. The status of augmented reality in laparoscopic surgery as of 2016. *Med Image Anal*. 2017;37:66-90. doi:10.1016/j.media.2017.01.007
46. Liebmann F, Roner S, von Atzigen M, et al. Pedicle screw navigation using surface digitization on the Microsoft HoloLens. *Int J Comput Assist Radiol Surg*. 2019;14(7):1157-1165. doi:10.1007/s11548-019-01973-7
47. Borges M, Symington A, Coltin B, Smith T, Ventura R. HTC Vive: Analysis and Accuracy Improvement. In: *IEEE International Conference on Intelligent Robots and Systems*. Institute of Electrical and Electronics Engineers Inc.; 2018:2610-2615. doi:10.1109/IROS.2018.8593707
48. Poon H, Li C, Gao W, Ren H, Lim CM. Evolution of robotic systems for transoral head and neck surgery. *Oral Oncol*. 2018;87:82-88. doi:10.1016/j.oraloncology.2018.10.020
49. Bergé SJ. Be prepared for the next decade. In: *Face to Face*. ; 2020:10-17. https://issuu.com/iaoms/docs/f2f_march_2020
50. Liu HH, Li LJ, Shi B, Xu CW, Luo E. Robotic surgical systems in maxillofacial surgery: A review. *Int J Oral Sci*. Published online 2017. doi:10.1038/ijos.2017.24
51. Pilon AJM, Koot EL, Woude R Van Der, et al. Robot-guided translation of a preoperative 3D planning during open- vault reconstruction of craniosynostosis. Published online 2019.
52. Han JJ, Woo S-Y, Yi W-J, Hwang SJ. A Robot Arm and Image-Guided Navigation Assisted Surgical System for Maxillary Repositioning in Orthognathic Surgery: A Phantom Skull-Based Trial. *Appl Sci*. 2020;10(4):1549. doi:10.3390/app10041549
53. Tsang KD, Ottow MK, van Heijst AFJ, Antonius TAJ. Electronic Decision Support in the Delivery Room Using Augmented Reality to Improve Newborn Life Support Guideline Adherence. *Simul Healthc J Soc Simul Healthc*. 2022;Publish Ah. doi:10.1097/SIH.0000000000000631

CHAPTER 13

Summaries

Summary

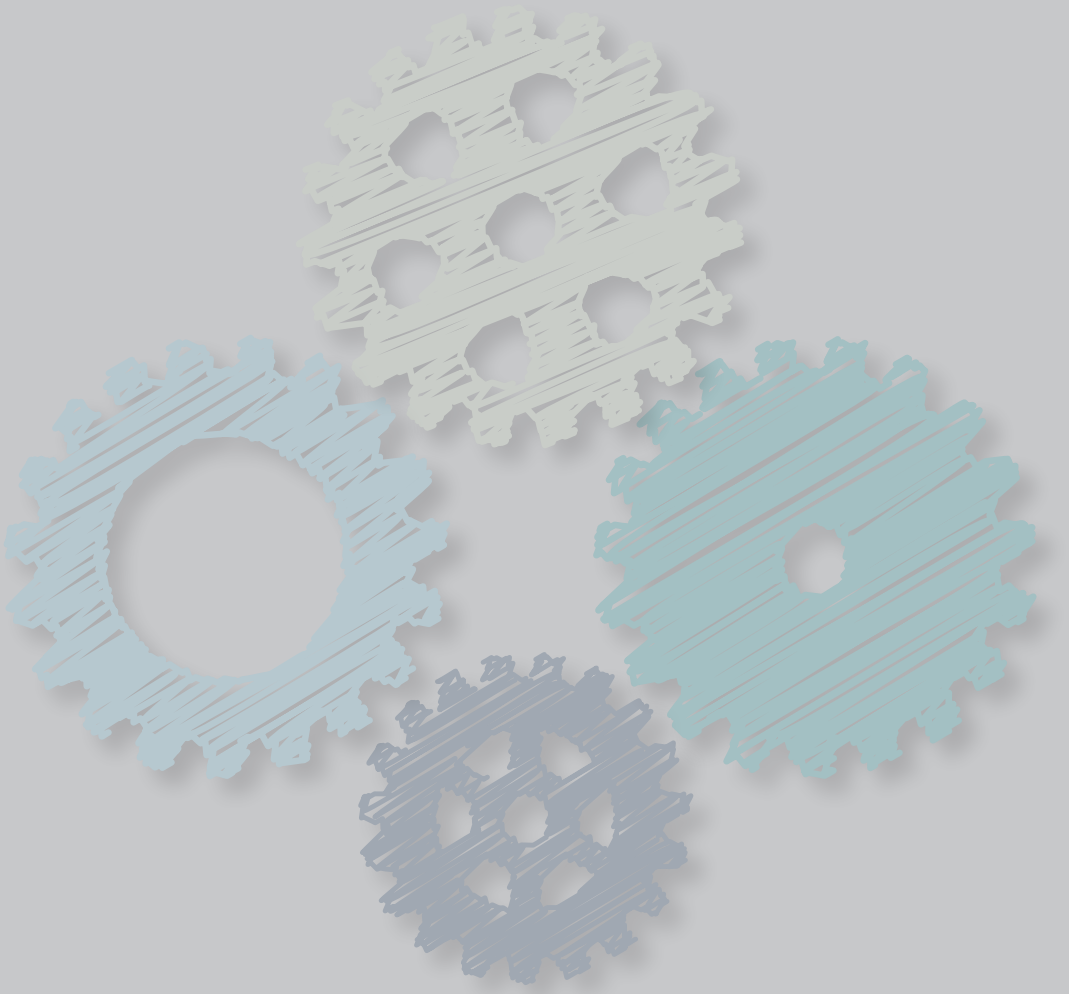

PART 1

This thesis explores how the clinical care of craniosynostosis patients can be improved through the deployment of three dimensional (3D) technology. The first part describes how 3D stereophotogrammetry can be implemented in clinical practice, to become a cornerstone in the treatment of craniosynostosis patients. Due to its low acquisition time, high accuracy, reproducibility and lack of ionizing radiation, 3D stereophotogrammetry is the ideal technique to diagnose, monitor and evaluate cranial abnormalities. In **Chapter 2**, 3D stereophotogrammetry was used to establish a reference control group to gain insight into the normal development of the cranial shape of the (Dutch) population and investigated the normal variation within this population. Since early detection is key in endoscopically assisted craniosynostosis surgery (EACS), normative reference data are essential to adequately detect potential abnormalities. The advanced 3D evaluation methods demonstrated interesting results. For example, this study found that in the first year of life, the focus of growth is in the anterior region of the head, while the focus of growth shifts to the posterior region at a later age. These findings are crucial because they make the diagnosis and follow-up of patients more adequate and reliable. In addition, because the same alignment and analysis methods were used for different image modalities (CT soft-tissue, CT hard-tissue and 3D stereophotogrammetry), multimodality evaluation is possible.

Chapter 3 presents a method based on principal component analysis (PCA) for cranial shape evaluation. This PCA model is able to automatically isolate the most important shape variations in a large set of 3D photos. As PCA uses only a few outcome measurements to describe the complete 3D morphology of the cranial shape, this method has the potential to improve the currently used clinical diagnostic methods for cranial abnormalities. The presented model was trained with cranial shapes of healthy new-borns and was able to successfully identify scaphocephaly or trigonocephaly in 40 patients.

The result of the first part is that the powerful combination (3D photos with 3D analysis methods) allows us to make the evaluation of the cranial shape more objective and accurate; it is now fully nested in the clinical workflow and has advanced the clinical consultations. Furthermore, this combination made it possible to create datasets of normal references and patients. In addition, semi-

transparent 3D overlays and 3D distance maps proved to be excellent tools during clinical consultation and provide the patients and the treatment team with relevant information.

PART 2

The second part of this thesis focuses on 3D virtual surgical planning (VSP). In **Chapter 4,** we share our experience of using VSP for the preparation of open cranial vault surgery. Seven important benefits of VSP are considered from which we could conclude that VSP helps our team to improve the surgical strategy; it aids the surgical procedure and leads to a simpler, safer and more efficient workflow. Despite the benefits, virtual planning is carried out in a rather conventional way, which makes it time-consuming and somewhat cumbersome. If future updates allow a more dynamic workflow, the testing of various surgical strategies can be faster, which will lead to a more efficient planning process.

Furthermore, novel visualization technologies can help to improve the preparation and planning of surgeries. In **Chapter 5**, a novel workflow is presented, where augmented reality (AR) is used to study complex anatomy to prepare for paediatric kidney surgery. An expert panel of paediatric surgeons tested whether AR visualizations improved understanding during the preparation of surgery. The added value of AR proved to be significant, and similar to the use of custom generated 3D prints. AR visualization for preparation has become standard for the preparation of kidney tumour patients in the Princess Máxima Center.

PART 3

The third part focuses on new methods to transfer a VSP to the operation room. By using AR, a virtual overlay can be created within the surgeon's view. In this way, a predefined virtual surgical plan, or a segmented anatomical structure, can be observed directly at the corresponding position on a patient.

In **Chapter 6**, a new concept is described where an optical tracking system is combined with an AR head-mounted display, the Microsoft HoloLens. This

implementation reveals that it is possible to project the virtual planning directly in the work field of the surgeon. The most important advantage is that it solves the switching focus problem, allowing the surgeon to look continuously at the surgical site instead of switching to a monitor when consulting the virtual planning. If a HMD with a stereoscopic view is used to achieve AR, relevant virtual information can be visualized in 3D at their anatomical position, resulting in a more intuitive visualization.

In **Chapter 7**, an AR application was developed to transfer a VSP for open cranial vault surgery. Since AR can display the planning directly on the patient, it can be an alternative for surgical guides, which are time-consuming to produce and rather expensive. In this study, we found that considerably longer time was required to transfer a planning when the AR workflow was used. Therefore, we concluded that surgical guides are presently the most fitting method to transfer a VSP. In addition, the relatively large outliers in the AR workflow meant that the mean accuracy was just outside the clinically acceptable margin. However, the low cost and simplicity make the AR workflow still a promising alternative to surgical guides.

In **Chapter 8**, an AR-guided workflow is presented to transfer pre-surgical information to patients during a breast reconstruction with a deep inferior epigastric artery perforator (DIEP) flap. The 3D visualization in the HoloLens provides an intuitive and strong perception of the complex anatomy, segmented from a CTA scan. This enables the user to view the relation of the perforator with the rectus abdominis muscle. Real-time tracking and a novel registration method using the patient's abdominal birthmarks ensures that the anatomy stayed correctly fused with the patient, regardless of position changes of the patient or the surgeon. Since the AR-DIEP application will be used for global orientation, the workflow does not demand millimeter accuracy. The usability, intuitiveness and set-up are the most important factors that will decide if AR will be integrated in clinical workflow in the future. Therefore, if new developments and research can realize this, the DIEP application will be of great value and can be used for other (free) flaps.

Chapter 9 shows that AR guidance was an effective method to assist the surgeon during a condylectomy. Since the small surgical opening makes the use of surgical guides impractical, AR is probably the best method to indicate to the surgeon

where to create the osteotomy. In addition, this AR solution allows the user to stay focused on the surgical field while attaining feedback from the planning. In this first step, a pointer was used to indicate the planned position.

PART 4

In **Chapter 10,** the clinical outcomes of the EACS with helmet therapy are presented and compared to the normal reference values. Furthermore, the clinical outcomes of the open cranial vault treatment are also compared to the normal reference values. The 3D distance maps demonstrate that EACS and helmet treatment leads to very satisfying results. Moreover, when the surgical outcome parameters are taken into account, it is evident that EACS is an adequate and appropriate treatment for scaphocephaly patients.

In **Chapter 11**, post-operative CT scans of patients, treated by open reconstructive surgery, were evaluated. Comparing the post-operative CT to the VSP enabled an objective evaluation which helped us improve and understand the planning, and transfer of this planning. Through the cases, we have learned how important an accurate transfer can be and demonstrated the benefits of surgical guides. This gave us the opportunity to reflect on our own work and complete the cycle of diagnosis, planning, surgery and evaluation.

Samenvatting (Dutch)

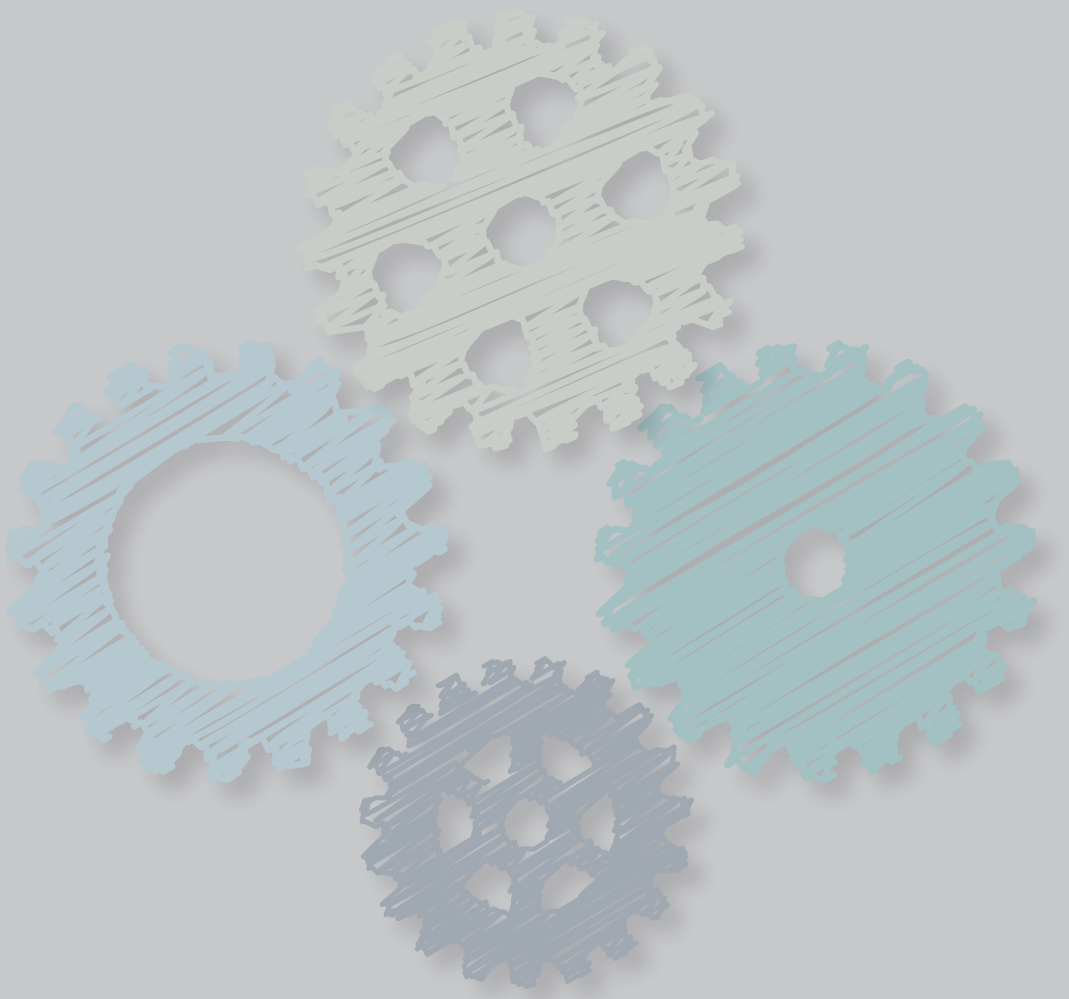

DEEL 1

Dit proefschrift verkent hoe de klinische zorg voor craniosynostose patiënten kan worden verbeterd door de inzet van drie dimensionale (3D) technologie. Het eerste deel beschrijft hoe 3D-stereofotogrammetrie in de kliniek kan worden geïmplementeerd en een essentieel onderdeel kan zijn tijdens de behandeling van craniosynostose patiënten. Door de korte acquisitietijd, hoge nauwkeurigheid, reproduceerbaarheid en het ontbreken van ioniserende straling, is 3D stereofotogrammetrie de ideale techniek om schedelafwijkingen te diagnosticeren, monitoren en evalueren. In **Hoofdstuk 2** zijn 3D foto's van een controlegroep gemaakt en gebruikt om inzicht te krijgen in de normale ontwikkeling van de schedelvorm van een Nederlandse populatie. De referentiewaarden die hieruit zijn opgesteld kunnen gebruikt worden om de schedelvorm van craniosynostose patiënten vroeg en adequaat te evalueren. De gebruikte 3D-evaluatiemethoden lieten interessante resultaten zien, zo ligt bijvoorbeeld de groeifocus in het eerste levensjaar in het voorste deel van het hoofd, terwijl later juist het achterste deel meer groeit. Deze bevindingen worden gebruikt om de diagnose en follow-up van patiënten op verschillende leeftijden adequater en betrouwbaarder te maken. Dit is belangrijk tijdens de follow up van patiënten die endoscopisch geassisteerde craniosynostose chirurgie (EACS) hebben ondergaan en daarna een bepaalde tijd een redressiehelm moeten dragen. Doordat dezelfde registratie- en analysemethoden zijn gebruikt voor verschillende beeldmodaliteiten zoals CT-weke delen en CT-benige delen, was het mogelijk resultaten onderling te vergelijken.

Hoofdstuk 3 beschrijft een nieuwe methode voor de evaluatie van de schedelvorm, gebaseerd op principale componentenanalyse (PCA). Dit PCA-model is in staat om automatisch de belangrijkste vormvariaties te isoleren in een grote set van 3D-foto's. Omdat PCA slechts enkele uitkomstmetingen gebruikt om de volledige 3D-morfologie van de schedel te beschrijven, heeft deze methode de potentie om de huidige klinische evaluatiemethoden voor schedelafwijkingen te verbeteren. Het PCA-model werd getraind met 3D-foto's van gezonde pasgeborenen en was in staat om bij 40 patiënten met succes scaphocephaly of trigonocephaly te identificeren.

Het resultaat van het eerste deel is dat de krachtige combinatie (3D-foto's met 3D-analysemethoden) ons in staat stelt om de evaluatie van de schedelvorm objectiever en nauwkeuriger te maken; het is nu volledig geïmplementeerd in de klinische workflow en heeft de spreekuren verbeterd. Bovendien kon met deze combinatie een grote set met normale referentie data gecreëerd worden. Het gebruik van transparante 3D-overlays en 'distance maps', waarmee in kleur de veranderingen gevisualiseerd kunnen worden, blijken uitstekende hulpmiddelen en voorzien de patiënten en behandelaars van relevante informatie.

DEEL 2

Het tweede deel van dit proefschrift beschrijft het gebruik van een 3D virtuele operatieplanning (VSP). Voor veel chirurgische ingrepen, ook binnen de mond-, kaak- en aangezichtschirurgie is het gebruik van een VSP al de standaard. **Hoofdstuk 4** beschrijft onze ervaring met het gebruik van een VSP voor open schedelreconstructies bij craniosynostose patiënten. Op basis van zeven belangrijke voordelen kan geconcludeerd worden dat een VSP de operatiestrategie verbetert en dat dit leidt tot een eenvoudigere, veiligere en efficiëntere workflow. Ondanks deze voordelen wordt de virtuele planning op een vrij conventionele manier uitgevoerd en is daardoor tijdrovend en enigszins omslachtig. Als toekomstige updates een meer dynamische workflow mogelijk maken, kan het testen van verschillende chirurgische strategieën sneller gaan, wat zal leiden tot een efficiënter planningsproces.

Echter kan ook de inzet van nieuwe visualisatie methoden de voorbereiding en planning van operaties verbeteren. In **Hoofdstuk 5** wordt een nieuwe workflow gepresenteerd, waarbij augmented reality (AR) wordt gebruikt om complexe anatomie te bestuderen ter voorbereiding van nier-tumor resecties bij kinderen. Verschillende kinderchirurgen testten of AR-visualisaties hielpen tijdens de voorbereiding van deze complexe chirurgische ingrepen. Hieruit bleek dat AR, net als 3D prints, een toegevoegde waarde hebben wanneer deze worden ingezet. AR wordt nu standaard gebruikt ter voorbereiding op nier-tumor operaties in het Prinses Máxima Centrum.

DEEL 3

In het derde deel zijn nieuwe methoden onderzocht om een VSP te kunnen gebruiken in de operatiekamer. Middels AR kunnen virtuele objecten direct in het werkveld van de chirurg gevisualiseerd worden en hiermee kan een VSP, of een bepaalde anatomische structuur, direct op de correcte positie op of in een patiënt worden waargenomen.

In **Hoofdstuk 6** is een nieuw concept ontwikkeld waarbij een optisch navigatiesysteem gekoppeld is aan een AR bril, de Microsoft HoloLens. Deze combinatie maakt het mogelijk om de virtuele planning direct in het werkveld van de chirurg te projecteren. Het belangrijkste voordeel is dat de chirurg continu gefocust kan blijven op het chirurgisch werkveld en niet op een externe monitor hoeft te kijken waarop de planning, vaak vanuit een ander perspectief, doorgaans wordt weergegeven. Daarnaast gebruikt een AR-bril een stereoscopisch beeld waardoor de beelden *echt* in 3D, en zeer intuïtief gevisualiseerd kunnen worden op de juiste positie in de ruimte.

In **Hoofdstuk 7** zijn twee methoden onderzocht om een VSP van een schedelreconstructie over te brengen op de patiënt. Hiervoor is een AR-toepassing ontwikkeld waarbij de planning direct op de patiënt kan worden weergegeven. Dit kan een alternatief zijn voor chirurgische mallen, die tijdrovend en duur zijn om te produceren. Uit dit onderzoek bleek echter dat aanzienlijk meer tijd nodig was wanneer de AR-workflow werd gebruikt en daarom hebben we geconcludeerd dat chirurgische mallen momenteel nog de meest geschikte methode zijn om een VSP over te brengen. Bovendien zorgden de relatief grote uitschieters in de AR-workflow ervoor dat de gemiddelde nauwkeurigheid net buiten de klinisch aanvaardbare marge lag. De lage kosten en eenvoud maken de AR-workflow echter wel een veelbelovend alternatief.

In **Hoofdstuk 8** wordt een AR-geleide workflow gepresenteerd om preoperatieve informatie te projecteren op patiënten tijdens een borstreconstructie middels een 'deep inferior epigastric artery perforator' (DIEP) lap. De 3D-visualisatie in de HoloLens zorgt voor een juiste perceptie van de complexe anatomie, die gesegmenteerd is uit een scan. De gebruiker kan hierdoor heel intuïtief de relatie van de perforator met de spier bekijken. Een nieuwe registratiemethode waarbij moedervlekken op de buik van de patiënt worden gebruikt zorgt voor

een correcte positie van de anatomie, ongeacht positieveranderingen van patiënt of chirurg. Aangezien deze AR-DIEP applicatie zal worden gebruikt voor globale oriëntatie, vereist de workflow geen millimeternauwkeurigheid. De bruikbaarheid, intuïtiviteit en opzet zijn de belangrijkste factoren die zullen beslissen of AR in de toekomst zal worden geïntegreerd in de klinische workflow. Ondanks dat meer onderzoek nodig is, kan de AR-DIEP applicatie van grote waarde zijn en kan ook ingezet worden voor andere (vrije) lappen.

Hoofdstuk 9 laat zien dat AR begeleiding een effectieve methode is om de chirurg te assisteren tijdens een condylectomie. Omdat een kleine chirurgische toegangsweg het gebruik van chirurgische mallen onmogelijk maakt, is AR waarschijnlijk de beste methode om de chirurg te wijzen waar de osteotomie moet komen. Deze AR-oplossing stelt de gebruiker in staat om gefocust te blijven op het chirurgische veld en tegelijkertijd feedback te krijgen van de planning. In deze eerste stap werd door middel van een pointer de geplande positie aangegeven.

DEEL 4

In **Hoofdstuk 10** worden de klinische uitkomsten van EACS in combinatie met helmtherapie gepresenteerd en vergeleken met normale referentiewaarden en de klinische uitkomsten van open schedelreconstructies. De 3D-distance maps laten zien dat EACS in combinatie met helmtherapie tot zeer fraaie resultaten leiden. Wanneer bovendien de chirurgische uitkomstmaten worden meegenomen, is het duidelijk dat EACS een adequate en geschikte behandeling is voor scaphocephaly patiënten.

In **Hoofdstuk 11** is van een aantal patiënten het eindresultaat van een open reconstructie vergeleken met het VSP dat van tevoren werd opgesteld. Door gebruik te maken van de postoperatieve CT scan werd een objectieve 3D evaluatie mogelijk. Dit heeft ons geholpen de planning, overdracht en operatie van open schedelreconstructies beter te doorgronden en te verbeteren. Zo is geleerd hoe belangrijk een nauwkeurige overdracht is en worden de voordelen van chirurgische mallen gedemonstreerd. Hiermee is het eigen werk geëvalueerd en de cyclus van diagnose, planning, operatie en evaluatie volbracht.

CHAPTER 14

Appendix

Curriculum Vitae

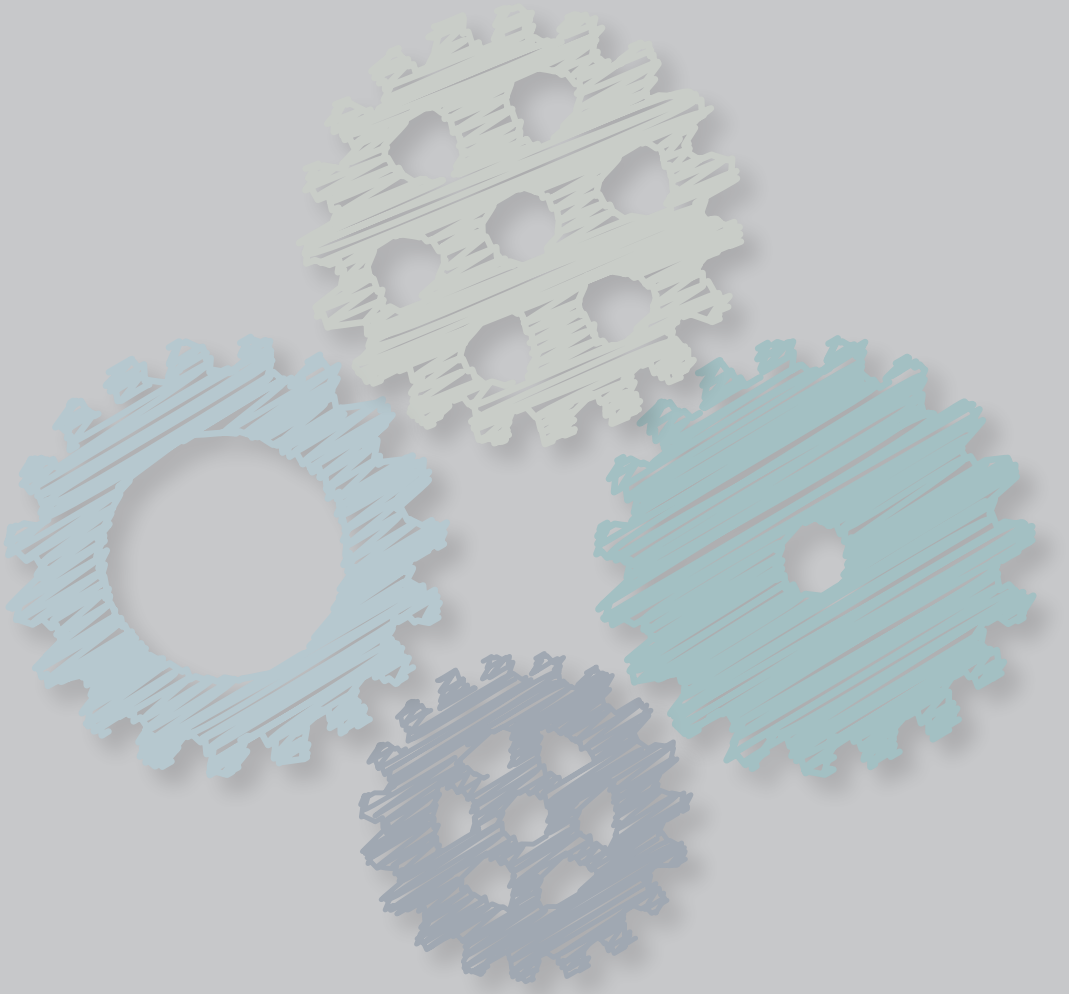

Jene was born on the 28th of March, 1986 in Arnhem, the Netherlands. After graduation from high school (VWO, Rhedens Rozendaal) in 2005, he started his study technical Medicine at the University of Twente. He received his bachelor degree in 2010 and completed his study with a master into Robotics and Imaging in October 2013. During his study period, Jene has participated in the student board of study association S.V. Paradoks in 2009 where he was responsible for the external relations. Jene was member Philosophic fraternity Panta Rhei where he also joined the board in 2010. After internships at the Antoni van Leeuwenhoek hospital (NKI-AVL) in Amsterdam and in the St. Elizabeth Hospital in Willemstad, Curacao, Jene did his graduation internship at the oral and maxillofacial department in the Radboudumc where he first came in contact with the craniofacial (research) team and the 3D Lab.

After his graduation, Jene worked in a collaboration project between the Radboudumc and the University Medical Center Groningen (UMCG) in 2014. The goal of this project was to implement new methods for orthognathic surgery by using advanced 3D planning software. After this, Jene continued his graduation project in the form of a Ph.D. in the 3D Lab. In 2016, Jene was the Chairman of the Conference Committee 2016 at NVvTG (Dutch Society of Technical Medicine) where he and his team organized an international conference.

In October 2020, Jene started as senior product developer at Augmedit, a start-up focussing on Augmented Reality technology for surgical interventions.

Portfolio

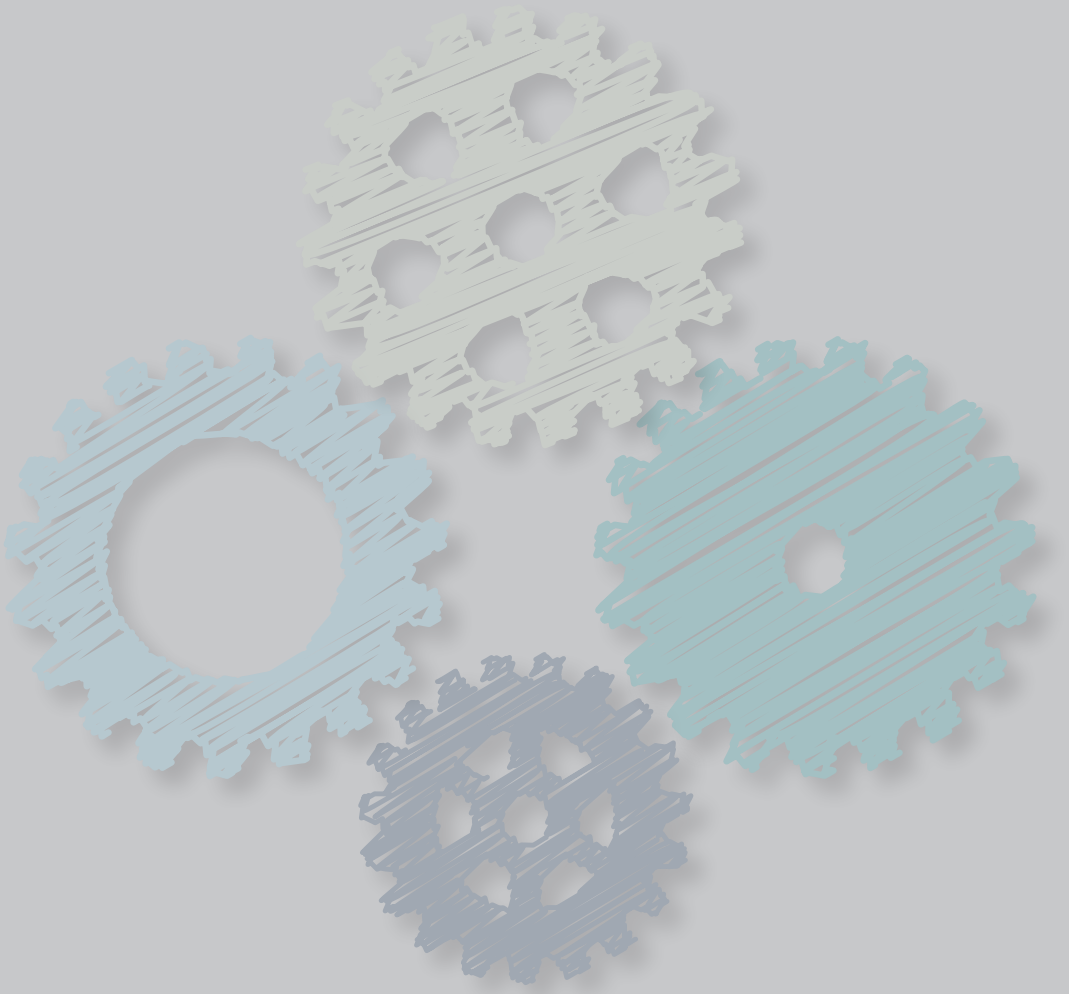

PUBLICATIONS AND SUBMISSIONS (THIS THESIS)

1. The normal evolution of the cranium in three dimensions **[Chapter 2]**
   Meulstee JW, de Jong GA, Borstlap WA, Koerts G, Maal TJJ, Delye H.
   Int J Oral Maxillofac Surg. 2020 Jun;49(6):739-749. doi: 10.1016/j.ijom.2019.10.012. Epub 2019 Nov.
2. A new method for three-dimensional evaluation of the cranial shape and the automatic identification of craniosynostosis using 3D stereophotogrammetry **[Chapter 3]**
   Meulstee JW, Verhamme L, Borstlap WA, Van der Heijden F, De Jong GA, Xi T, Bergé SJ, Delye H, Maal TJJ.
   Int J Oral Maxillofac Surg. 2017 Jul;46(7):819-826. doi: 10.1016/j.ijom.2017.03.017. Epub 2017 Apr.
3. Comparison of 3-Dimensional and augmented reality kidney models with conventional imaging data in the preoperative assessment of children with Wilms tumors **[Chapter 5]**
   Wellens LM, Meulstee JW, van de Ven CP, Terwisscha van Scheltinga CEJ, Littooij AS, van den Heuvel-Eibrink MM, Fiocco M, Rios AC, Maal T, Wijnen MHWA.
   JAMA Netw Open. 2019 Apr 5;2(4):e192633. doi: 10.1001/jamanetworkopen.2019.2633.
4. Toward Holographic-guided surgery **[Chapter 6]**
   Meulstee JW, Nijsink J, Schreurs R, Verhamme LM, Xi T, Delye HHK, Borstlap WA, Maal TJJ.
   Surg Innov. 2019 Feb;26(1):86-94. doi: 10.1177/1553350618799552. Epub 2018 Sep.
5. Surgical guides versus augmented reality to transfer a virtual surgical plan for open cranial vault reconstruction: a pilot-study **[Chapter 7]**
   Meulstee JW, Bussink T, Delye H, Xi T, Borstlap WA, Maal TJJ
   Advances in Oral and Maxillofac. Surgery. 2022 Aug 6. doi: 10.1016/j.adoms.2022.100334
6. Holographic augmented reality for DIEP flap harvest **[Chapter 8]**
   Wesselius TS, Meulstee JW, Luijten G, Xi T, Maal TJJ, Ulrich DJO.
   Plast Reconstr Surg. 2021 Jan 1;147(1):25e-29e. doi: 10.1097/PRS.0000000000007457.
7. Augmented reality guided condylectomy **[Chapter 9]**
   Bussink T, Maal TJJ, Meulstee JW, Xi T
   Br J Oral and Maxillofac Surg. 2022.02. doi: 10.1016/j.bjoms.2022.01.008
8. Longitudinal 3D follow-up and surgical safety outcomes after endoscopic and open scaphocephaly surgery **[Chapter 10]**
   De Jong G, Meulstee JW, Van Lindert E, Borstlap W, Maal TJJ, Delye H
   Submitted to Plast Reconstr Surg.

PUBLICATIONS AND SUBMISSIONS (OTHER)

9. Brain tumor evaluation and accuracy in spatial understanding: 3D visualisation compared to MRI ***(submitted)***
Fick T, Meulstee JW, Köllen M, Van Doormaal J.A.M, Van Doormaal T.P.C, Hoving E.W.
Submitted to YAMA oncology

10. Augmented reality guided osteotomies of the fibular bone in mandibular reconstructions ***(submitted)***
Snoeijink T, Weijs W, Meulstee JW, Dik E
submitted to International Journal of oral & maxillofacial surgery

11. Fully automatic brain tumor segmentation for 3D evaluation in augmented reality
Fick T, Van Doormaal J, Tosic L, Van Zoest R, Meulstee JW, Hoving E, Van Doormaal T
Neurosurgery focus 2021 Aug; 51(2). doi: 10.3171/2021.5.FOCUS21200

12. MRI-Based 3-Dimensional visualization workflow for the preoperative planning of nephron-sparing surgery in Wilms' tumor surgery: a pilot study
Fitski M, Meulstee JW, Littooij A, Van der Ven CP, Van der Steeg, AFW, Wijnen MHWA
Journal of Healthcare Engineering, 2020, doi: 10.1155/2020/8899049

13. Combining deep learning with 3D stereophotogrammetry for craniosynostosis diagnosis.
de Jong G, Bijlsma E, Meulstee JW, Wennen M, van Lindert E, Maal T, Aquarius R, Delye H.
Sci Rep. 2020 Sep 18;10(1):15346. doi: 10.1038/s41598-020-72143-y.

14. Nasolabial shape and aesthetics in unilateral cleft lip and palate: an analysis of nasolabial shape using a mean 3D facial template.
Kuijpers MAR, Maal TJJ, Meulstee JW, Carels CEL, Bronkhorst EM, Bergé SJ, Fudalej PS.
Int J Oral Maxillofac Surg. 2021 Feb;50(2):267-272. doi: 10.1016/j.ijom.2020.06.003

15. Three-dimensional facial volume analysis using algorithm-based personalized aesthetic templates.
Tuin AJ, Meulstee JW, Loonen TGJ, Kraeima J, Spijkervet FKL, Vissink A, Jansma J, Schepers RH.
Int J Oral Maxillofac Surg. 2020 Oct;49(10):1379-1384. doi: 10.1016/j.ijom.2020.01.013

16. Three-dimensional facial development of children with unilateral cleft lip and palate during the first year of life in comparison with normative average faces.
Brons S, Meulstee JW, Loonen TGJ, Nada RM, Kuijpers MAR, Bronkhorst EM, Bergé SJ, Maal TJJ, Kuijpers-Jagtman AM.
PeerJ. 2019 Jul 30;7:e7302. doi: 10.7717/peerj.7302

17. Uniform 3D meshes to establish normative facial averages of healthy infants during the first year of life.
Brons S, Meulstee JW, Nada RM, Kuijpers MAR, Bronkhorst EM, Bergé SJ, Maal TJ, Kuijpers-Jagtman AM.
PLoS One. 2019 May 20;14(5):e0217267. doi: 10.1371/journal.pone.0217267

18. Bone-borne surgically assisted rapid maxillary expansion: A retrospective three-dimensional evaluation of the asymmetry in expansion.
Huizinga MP, Meulstee JW, Dijkstra PU, Schepers RH, Jansma J.
J Craniomaxillofac Surg. 2018 Aug;46(8):1329-1335. doi: 10.1016/j.jcms.2018.05.021

19. Radiation-free 3D head shape and volume evaluation after endoscopically assisted strip craniectomy followed by helmet therapy for trigonocephaly.
de Jong G, Tolhuisen M, Meulstee JW, van der Heijden F, van Lindert E, Borstlap W, Maal T, Delye H.
J Craniomaxillofac Surg. 2017 May;45(5):661-671. doi: 10.1016/j.jcms.2017.02.007

20. The effect of aging on the three-dimensional aspect of the hand: A pilot study.
Hoevenaren IA, Wesselius TS, Meulstee JW, Vreeken RD, Maal TJ, Ulrich DJ.
J Plast Reconstr Aesthet Surg. 2017 Apr;70(4):495-500. doi: 10.1016/j.bjps.2016.12.003

21. Endoscopically assisted craniosynostosis surgery (EACS): The craniofacial team Nijmegen experience.
Delye HH, Arts S, Borstlap WA, Blok LM, Driessen JJ, Meulstee JW, Maal TJJ, van Lindert EJ.
J Craniomaxillofac Surg. 2016 Aug;44(8):1029-36. doi: 10.1016/j.jcms.2016.05.014

22. Development of a three-dimensional hand model using three-dimensional stereophotogrammetry: assessment of image reproducibility.
Hoevenaren IA, Meulstee JW, Krikken E, Bergé SJ, Ulrich DJ, Maal TJ.
PLoS One. 2015 Sep 14;10(9):e0136710. doi: 10.1371/journal.pone.0136710.

23. A new 3D approach to evaluate facial profile changes following BSSO.
Meulstee JW, Liebregts J, Xi T, Vos F, de Koning M, Bergé S, Maal T.
J Craniomaxillofac Surg. 2015 Dec;43(10):1994-9. doi: 10.1016/j.jcms.2015.08.007

24. Evaluation of the anterior mandibular donor site one year after secondary reconstruction of an alveolar cleft: 3-dimensional analysis using cone-beam computed tomography.
van Bilsen MW, Schreurs R, Meulstee JW, Kuijpers MA, Meijer GJ, Borstlap WA, Bergé SJ, Maal TJ.
Br J Oral Maxillofac Surg. 2015 Oct;53(8):719-24. doi: 10.1016/j.bjoms.2015.04.023

PRESENTATIONS AND LECTURES

- July 2021: European Association for Cranio-Maxillo-Facial Surgery (EACMFS), Paris, France (digital)
  Title: Augmented Reality
- June 2019: European Cleft Palate Craniofacial Association (ECPCA), Utrecht, the Netherlands
  Title: Future perspectives and 3D imaging (Key note co-presentation)
- June 2019: European Cleft Palate Craniofacial Association (ECPCA), Utrecht, the Netherlands
  Title: The normal evolution of the cranium in 3D
- April 2019: Dutch patient association Craniofacial deformities LAPOSA, Kaatsheuvel, the Netherlands
  Title: Virtuele planningstechnieken bij craniosynostose en Goldenhar
- February 2019: Innovation Meet-up, Arnhem, The Netherlands
  Title: 3D innovations for clinical practise
- September 2018: European Association Cranio and Maxillo-Facial Surgery (EACMFS), Munchen, Germany
  Title: The normal evolution of the cranium in 3D
- May 2018: International Paediatric Simulation Society (IPSS), Amsterdam, The Netherlands
  Title: Augmented reality as a tool to prepare for surgery (key note)
- May 2018: European Society for Paediatric Neurosurgery (ESPN), Bonn, Germany
  Title: The 3D evolution of the normal cranial shape
- October 2017, ICCAS conference, Leipzig, Germany
  Title: The Radboudumc 3D Lab: planning and preparation
- October 2017, KIO course, Nijmegen, The Netherlands
  Title: Planning and evaluation in craniosynostosis
- June 2017: Medicine conference UMC Leiden, The Netherlands
  Title: Emerging technologies in medicine

- February 2017, Conference Technical Medicine, Amersfoort, The Netherlands
  Title: Augmented Reality
- January 2017, S.O.R.G. Research Meeting, Haarlem, The Netherlands
  Title: Virtual planning in craniosynostosis Surgery
- June 2016, VCMS conference, Nijmegen, The Netherlands
  Title: Voorspelbaar plaatsen van tandwortelimplantaten
- November 2015, Opening MITeC operation Room, Nijmegen, The Netherlands
  Title: The operation room of the future (presentation for Queen Máxima of the Netherlands)
- November 2015, NVSCA-najaarsvergadering: Schisis en Craniofaciale afwijkingen, Heereveen, The Netherlands
  Title: A new 3-dimensional method for the evaluation of facial deformities
- April 2015, Conference Center for Medical Imaging North-East Netherlands, Twente, The Netherlands
  Title: Effective Eyes for beautiful hands.
- November 2014, 58e Najaarsvergadering van de Nederlandse Vereniging voor Mondziekten, Kaak- en Aangezichtschirurgie, Bussum, The Netherlands
  Title: De rol van virtuele 3d-planningen in open reconstructieve craniofaciale chirurgie
- November 2014, NVSCA-najaarsvergadering: Schisis en Craniofaciale afwijkingen, Rotterdam, The Netherlands
  Title: De rol van virtuele 3d-planningen in open reconstructieve craniofaciale chirurgie
- September 2013, International Conference on Oral and Maxillofacial Surgery (ICOMS), Barcelona, Spain.
  Title: The use of 3d stereophotogrammetry in the post-operative treatment and evaluation of endoscopic assisted repair of craniosynostosis
- November 2013, Scientific Meeting Dutch Association for Cleft Palate and Craniofacial Anomalies, Gent, Belgium
  Title: The assessment and quantification of the cranial vault in newborns in 3D
- November 2013, 57e Najaarsvergadering van de Nederlandse Vereniging voor Mondziekten, Kaak- en Aangezichtschirurgie. Assen, The Netherlands
  Title: Ontwikkeling van een objectieve meetmethode voor een 3d evaluatie van de schedelvorm.
- November 2012, NVSCA-najaarsvergadering: Schisis en Craniofaciale afwijkingen, Maastricht, the Netherlands.
  Title: Computation of an average cranial shape of new-borns using 3d stereo-photogrammetry

SUPERVISION

- Supervisor of more than 20 students (3 months internship, 2nd year master students Technical Medicine, UTwente)
- Supervisor of 6 graduation internships (1 year internship, 3rd year master students Technical Medicine, UTwente)
- Supervisor of 3 projects groups from the Radboudumc Innovation program
- Supervisor of 2 students from multimedia and content design (HAN Hogeschool Arnhem-Nijmegen)
- Supervisor of student from Game design (Breda university of Applied Science)

COURSES

- SCRUM: certified product owner 2020
- Insight Discovery 2020
- Scientific integrity 2019
- BROK course 2018
- Perfecting your academic writing skills 2017
- Graduate School (RIHS) introductory course 2016
- Scientific Writing for PhD Candidates 2015
- Introduction day Radboudumc 2015
- KIO course Cleft palate 2014

Research and data management

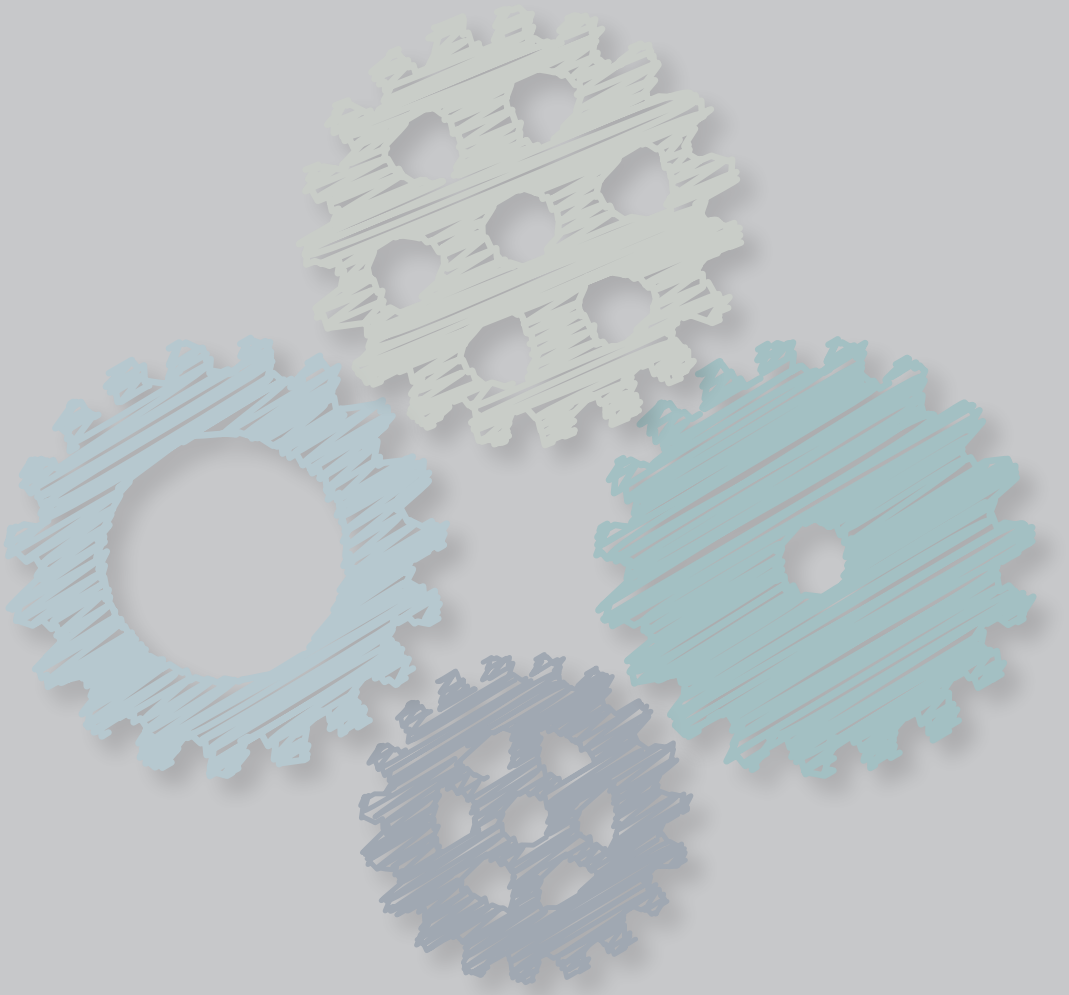

The studies in this thesis which used patients or patient data were conducted in accordance with the principles and ethical standards of the Helsinki declaration. Patient consent was obtained if required. The medical ethics committee on Research Involving Human Subjects region Arnhem-Nijmegen has given approval to conduct the studies described in chapter 2 (file number: 2018-4935), chapter 3 (file number: NL17934.091.07), chapter 7 (file number: 2019-6070), chapter 9 (file number 2019-5986) and chapter 10 (file number: 2020-6128). Official approval from the medical research ethics committees of the University Medical Center Utrecht, the Netherlands was obtained for chapter 5.

The privacy of the participants in this study was warranted by use of encrypted and unique individual subject codes and the FAIR principle was applied. The source data used in chapter 2 ,3, 4, 7, 10 and 11 including modified 3D images, are stored and are **f**indable on the Radboudumc department servers of the mond-, kaak- en aangezichtschirurgie. The location is \\umcsanfsclp01\mka_mka\MKA\Jene Meulstee\PhD. The original source data (scans, 3D photo's etc.) are stored and backed-up on the dedicated patient servers of the 3D lab. For security and protection, **a**ccess to the server locations is provided using role based access control, regulated by the 3D Lab and Radboudumc IT department. To make the data **I**nteroperable, 3D software used for viewing, analysis and planning and custom made software tools which were used in this thesis are listed or stored on the same location to make the data **r**eusable for analysis.

Custom made augmented reality applications were created and used for the research described in chapters 5, 7, 8 and 9. 3D models of patients (holograms), were uploaded and hardcoded integrated in the software application installed on the HoloLens hardware. Patient metadata was removed if possible. For security reasons, research applications were removed from the HoloLens hardware after completion of the research. Applications and projects are stored on the 3D Lab's server locations.

The data will be saved for 15 years after termination of the respective studies. Using the patient data and analysis methods in future research is possible with renewed approval from the medical ethical committee. The datasets analysed during these studies are available from the corresponding author(s) on reasonable request and with approval from the legal and ethics department.

CHAPTER 15

Dankwoord

Het blijft voor mij heel bijzonder dat de vele ideeën, onderzoeken en projecten die ik de afgelopen jaren samen met velen van jullie heb kunnen doen nu gebundeld zijn in dit manuscript. Ik ben erg trots op het eindresultaat. De weg hiernaartoe voelde soms lang, maar vooral inspirerend en leerzaam. Het was mij absoluut nooit gelukt zonder samen te werken en alle hulp die mij geboden is. Hierbij wil ik graag een aantal mensen in het bijzonder bedanken.

Beste **Thomas**, direct na mijn eerste kennismaking met jou en het 3D Lab voelde ik mij op mijn plek. Naast de vele innovaties en projecten die er plaatsvinden, is het vooral de sfeer en gezelligheid die het 3D Lab tot een geweldige plek maken. Naast jouw oprechte interesse in mensen heb je altijd wel een geintje of een grappig verhaal gereed. Dit heb ik vaak ervaren tijdens de vele tripjes en congressen, waarbij vooral het avondprogramma in Brugge en Barcelona mij nog goed bijstaan. Via constructies bij MITeC en in Groningen, is het mede door jouw inzet gelukt om een plek bij het 3D Lab te krijgen. Jouw deur stond altijd open; wat soms vervelend was als ik tijdens mijn stage te laat was en langs jouw kamer moest lopen, maar verder vooral heel fijn om even iets te bespreken. Je hebt mij vaak geholpen om tegenslagen te relativeren en de vele ideeën en suggesties die jij had hebben vaak geleid tot nieuwe inzichten. Het is mooi dat ik de afgelopen jaren zelf heb kunnen zien hoe jouw inzet en visie ervoor hebben gezorgd dat het 3D Lab is uitgegroeid tot een volledige entiteit binnen en buiten het Radboud. Ik heb altijd enorm opgekeken naar jouw kennis en hoe goed jij de visie en het werk van het 3D Lab kon presenteren. Het was fantastisch om mee te maken hoe jij uiteindelijk hoogleraar bent geworden en het was een eer om een onderdeel daarvan zelf te mogen presenteren tijdens jouw oratie. Jij geeft mensen de mogelijkheid en ruimte om te kunnen werken aan een visie, zonder daarbij te veel te sturen of mensen te verplichten het via een vaste route te doen. Deze ruimte heeft mij geholpen een eigen draai te geven aan projecten en mijn interesses uit te kunnen diepen. De vrijheid heeft er aan bijgedragen dat ik een fantastische tijd heb gehad in het 3D Lab.

Beste **Wilfred**, het is alweer lang geleden dat ik jou op de POK bevlogen hoorde vertellen over craniosynostose en de vele onderzoeksideeën die jij daarbij had. In de jaren die volgden hebben wij samen met het team stap voor stap de 3D beeldvorming uitgerold in de kliniek en het een vast onderdeel gemaakt van het spreekuur. Jij benadrukte altijd hoe belangrijk het is om de ouders betrokken te

houden bij de behandelingen zodat de helmpjes goed werden gedragen. Je bent erg toegewijd, je was altijd bereikbaar, zorgde dat je zelf bij alle spreekuren en operaties kon zijn en hebt je verschrikkelijk hard ingezet voor de patiënten en het CFA-team. Je staat bekend om je enorme klinische ervaring maar sprak vaak jouw waardering uit naar de jonge, meer technische mensen van het 3D Lab. Je was altijd geïnteresseerd in nieuwe technieken en innovaties en vond het zichtbaar leuk hierover mee te denken en maakte hier altijd tijd voor vrij. Of dat nou op onze kamer was, of bij jou thuis in de tuin of bij de pool(-tafel).

Ik vond het altijd ontzettend leuk om samen een voordracht te geven, zoals we dat bijvoorbeeld bij MITeC hebben gedaan. Maar ook als ik ergens alleen presenteerde was jij er, je zorgde dat je vooraan zat en hielp mij altijd uitvoerig bij de voorbereiding en wenste mij succes. Ook na ieder CFA spreekuur, planning of een operatie, kwam even een bedankje. Het zijn dat soort dingen geweest die ervoor hebben gezorgd dat ik mij gewaardeerd heb gevoeld. Ik weet dat jij het liefst had gewild dat 'focus is key' wat vaker was toegepast tijdens mijn promotietraject en liever had gezien dat het sneller was gegaan (en ik zelf ook wel). Toch bleef jij altijd geïnteresseerd en stond je achter de projecten die wij deden, was je altijd bereid mee te denken en je mening te geven over de nieuwe technieken. Als jouw kamergenoot zag ik dat echt iedereen even bij jou binnenviel voor een advies of vroeg om even mee te kijken. Dat typeert goed hoe jij bent. Je was altijd bereid om te helpen en bent heel toegankelijk. Wilfred, ik wil jou ontzettend bedanken voor de afgelopen jaren, de kansen die jij voor mij hebt gecreëerd en alle ondersteuning. Ik hoop dat we nog vaak blijven afspreken en samen de nieuwe dingen in ons leven kunnen bespreken bij een borreltje!

Beste **Hans,** je bent absoluut een van de meest toegewijde en slimste dokters die ik ken. Jouw goede band en leuke omgang met de patiënten maakte alle CFA spreekuren inspirerend en leuk om te doen. Wat hebben wij vaak samen naar het scherm zitten turen tijdens het maken van een operatieplanning, die we eindeloos bleven bijschaven tot het optimale behandelplan eruit rolde. Jij was altijd duidelijk wat je wilde en dat kon ik waarderen. Ik ben je erg dankbaar voor alle suggesties en verbeteringen die je voor mij had. Dit heeft mij geholpen tijdens de uitvoering en het schrijven van mijn onderzoeken. Ik dank je bovenal voor het geduld en de steun en die jij mij hebt gegeven.

Beste **Stefaan**, in mijn allereerste stageweek was ik zo onder de indruk van een voordracht die u gaf op een congres in Brugge, dat ik direct zeker wist dat ik wilde blijven bij het 3D Lab en de MKA. De visie die u uitdraagt hoe (3D) technologie de zorg nu en in de toekomst kan verbeteren zijn altijd inspirerend. De creatieve projecten die u organiseerde of bij betrokken was, zoals hei-dagen en retraites maakte de MKA tot een inspirerende werkomgeving. De waardering die u vaak liet blijken tijdens een overdracht, wanneer een complexe operatie was uitgevoerd met 3D technologie, waren altijd een stimulans. Uw directe en goede feedback waren altijd een aanvulling en hebben vaak geholpen om het op een andere manier te kunnen bekijken. De feedback die u gaf op mijn eerste artikel was indrukwekkend en weet ik nog zeer goed. Toch heeft dit heel veel bijgedragen aan het verloop van mijn promotietraject en hier heb ik veel van geleerd. Eén van de vele leuke projecten die ik heb gedaan is het schrijven van de 3D Lab Grant geweest. Waarbij niet alleen het resultaat, maar ook het proces daarnaartoe stimulerend en leerzaam was.

Beste **Guido**, ik heb altijd veel plezier gehad in onze lange en intensieve samenwerking voor de verschillende onderzoeken rondom craniosynostose. Ik heb veel ontzag en respect voor jouw (technische) kennis en kunde en de manier waarop jij kon analyseren en programmeren. Het was altijd mooi om te zien hoe jij vol enthousiasme kon vertellen over ideeën of projecten die je aan het doen was. De inzet van AI op verschillende vakgebieden waren indrukwekkend. Ik weet zeker dat jij jouw expertise verder kan uitbouwen in de komende jaren.

Beste **3D Lab collega's;** Beste **Timen, Robin, Gert, Dylan, Bas, Joost, Anouk** en alle **stagiaires.** Ik wil jullie bedanken voor de geweldige tijd die we samen hebben gehad en de reis die we hebben gemaakt. Vanuit een klein groepje is het uitgegroeid tot een grote professionele club slimme mensen. De vele projecten maakte werken met jullie altijd inspirerend en afwisselend.

Luc, jij hebt mij inhoudelijk altijd kunnen helpen. Jij was altijd in voor leuke projecten en nieuwe dingen, of we nou een paardenrace gingen maken, een robot gingen ophalen in Twente, een navigatiesysteem gingen testen bij jou op zolder of een 3D printer installeren in Bernhoven. Dank voor de leuke tijd.

Rinaldo, ik heb het altijd indrukwekkend gevonden wat jij kan, hoe makkelijk jij een planning of een malletje maakte en wat je hebt betekend voor het 3D Lab. Ik wens je al het geluk in Polen.

Arico en **Frank**, ik bewonder hoe jullie jezelf essentieel hebben gemaakt en nu de drijvende kracht zijn achter heel veel operatieplanningen in allerlei verschillende ziekenhuizen. Respect had ik ook, als ik zag hoe gemakkelijk jullie een dubbele frikandel met mayo op de vrijdag naar binnen werkten. Ik wil jullie bedanken voor de vele leuke momenten. De pubquiz op de boot, de vele biertjes in de Aesculaaf of de karaoke in München; het was altijd lachen met jullie. Wellicht zie ik jullie snel nog eens bij een augmented reality hackathon.

Beste **Han**, uiteindelijk is het ons gelukt om de HoloLens te koppelen aan het navigatiesysteem maar wat zijn we lang bezig geweest om alles werkend en kloppend te krijgen! Ik ben nog steeds ontzettend trots dat daar een mooie publicatie uit is voortgekomen. Zonder jouw keiharde inzet en doorzettingsvermogen was dat nooit gelukt.

Beste **Tycho**, je was al langer een goede vriend dus ik vond het vooral gezellig toen jij je bij het 3D Lab voegde. Maar al snel bleek dat werken met jou ook heel inspirerend is. Je bent kritisch, analytisch en weet informatie op waarde te schatten en je bent daardoor in staat adequate beslissingen te nemen. Het begeleiden van studenten en het opzetten van onderzoek namen we heel serieus en bleek voor ons beiden echt een drijfveer. Ik hoop van harte dat we onze onvoltooide plannen snel verder kunnen uitwerken.

Beste **Ruud,** ik weet nog goed toen jij als groentje bij het 3D Lab kwam afstuderen. Ik was zelf al ruim vier dagen bezig en moest jou vaak nog met van alles helpen. Gelukkig pikte jij alles snel op en was je binnen de kortste keren de meester en de grappenmaker van de afdeling. Ik vind het mooi om te zien hoe jij altijd jezelf gebleven bent. Jij was altijd proactief bezig om anderen te helpen bij onderzoeken en projecten. Je zorgde er dan niet alleen voor dat inhoudelijk het niveau steeg maar ook dat er plezier en gezelligheid was. Ik heb dat vaak meegemaakt met de vele tandtechnischeheelgenees studenten die wij begeleidden en de vele borrelclubjes die daar weer uit volgden. Dagenlang zaten wij tegenover elkaar in het noodgebouw te 'onderzoeken' en aan het eind van de dag ruilden wij onze

dagbaan in voor de tennisbaan, bowlingbaan, of de Wylerbaan. Jouw humor, enthousiasme en vrolijkheid hebben mij veel werkplezier bezorgd. Maar vooral onze vriendschap, en de gesprekken die we hadden in Anneke of de Aesculaaf waarin we het leven en het 3D Lab doorspraken waren fantastisch. Ik kijk er naar uit om in onze nieuwe functies nog vele jaren samen te kunnen werken.

Beste **Tom**, ook werken met jou voelde als vriendschap. Jouw inzet en hulp voor de facial mesh projecten die we samen hebben gedaan hebben geresulteerd in mooie projecten.

Beste **Thijs**, jouw enthousiasme voor zowel augmented reality als de craniosynostosezorg maakte dat wij een gedeelde passie hadden. Ik vind het knap wat jij hebt neergezet en de inzet die jij hebt getoond.

Beste **stafleden**, oud-staf, aios, oud-aios, beste **Casper**, **Willem**, **Eric**, **Tim**, **Thijs**, **Martien**, **Gert**, **Rik**, **Jeroen**, **Stefanie** en **Teuntje**, graag wil ik jullie bedanken voor de fijne samenwerking in de afgelopen jaren. De nauwe samenwerking, het enthousiasme en de open en vriendelijke sfeer binnen de MKA hebben ervoor gezorgd dat voor mij de relevantie van een technisch geneeskundige duidelijk werd. Daarnaast ook dank voor de vele informele en gezellige gesprekken in de koffiekamer, en tijdens de borrels en uitjes.

Beste **Marloes**, jij was een fantastische collega en kamergenoot. Ik heb groot respect voor al die dingen die jij hebt opgepakt toen je het stokje van Wilfred overnam en dat je daarnaast ook nog allerlei 3D Lab projecten en stagiaires hebt geholpen. Jouw leuke persoonlijkheid en oprechte interesse maakt dat ik met heel veel plezier terugkijk op onze samenwerking.

Beste **Tong**, van jou heb ik veel geleerd. Jij hebt mij vaak geholpen bij het reviseren van artikelen en teksten. Vooral de uitleg en achterliggende gedachte die jij daarbij gaf, *waarom* iets beter anders verwoord kan worden waren voor mij vaak eyeopeners. Je bent vriendelijk, snel en benaderbaar. Ik ben ervan overtuigd dat jij in de toekomst jouw onderzoekslijnen verder gaat uitbouwen tot grote projecten.

Beste dames en heren van de poli, secretariaat, administratie, verpleging, omloop en OK-assistenten, ook jullie wil ik bedanken voor de vele leuke en gezellige momenten en de fijne werksfeer rondom de MKA.

Beste **Erik van Lindert**, **Jessica, Leanne**, **Tim Antonius**, **Dietmar** en **Robin Nijveldt** en vele andere professionals van het Radboud. Ik wil jullie ook bedanken voor de vele leuke gesprekken, samenwerkingen en/of projecten die we samen hebben gedaan.

Beste **Joep**, **Rutger**, **Johan** en **Jorien,** jullie wil ik heel erg bedanken voor de leuke samenwerking die wij hebben gehad. De warmte en vriendelijkheid die in Groningen heerst zijn onmiskenbaar. De passie die jullie hebben voor de kliniek en het onderzoek was mooi om te zien. Ik heb een super tijd gehad in Groningen en dat is vooral aan jullie te danken.

Beste **Marc, Lianne** en **Matthijs**, ook jullie dank voor de leuke samenwerking en mooie projecten die wij samen hebben mogen doen met het Prinses Máxima Centrum.

Beste **Ferdi**; dank voor alle hulp die jij hebt geboden tijdens mijn afstuderen, wat de basis heeft gevormd van dit manuscript. Ook wil ik graag alle andere professionals van de UTwente bedanken voor de goede samenwerking en begeleiding van alle stagiaires.

Beste patiëntjes, ouders van patiënten, kindjes en ouders die hebben meegewerkt aan het controle onderzoek, dank voor de bereidheid, interesse en medewerking. Het was niet altijd makkelijk wanneer de panty over het hoofd getrokken moest worden en wij jullie instrueerde om achterover hangend te balanceren op de stoel. Met Bumba op de achtergrond, foto na foto maken en hopen dat er een geschikte tussen zat. Zonder jullie geduld en inzet was dit proefschrift nooit tot stand gekomen.

Lieve **Ouders**, als jullie mij niet eindeloos achter de broek hadden aangezeten op de middelbare school was ik nooit aan studeren toegekomen. Tijdens mijn studie, toen de vele afleidingen ook voor wat vertraging zorgde, hebben jullie mij altijd gesteund en merkte ik dat ik vaak bij jullie kwam om advies. De oprechte

verwondering en trots die jullie hadden toen ik mijn P, en later bachelor en master diploma behaalde maakte mij erg gelukkig. Ik vond het fantastisch dat jullie 's avonds laat gelijk naar Nijmegen zijn gereden om mij te feliciteren toen bleek dat mijn manuscript was goedgekeurd. Jullie blijdschap en enthousiasme raakte mij diep. Ik kijk er naar uit om het feest met jullie te vieren. **Renske**, ik vind het een eer en heel mooi dat jij mij gaat begeleiden en helpen bij de verdediging van mijn proefschrift.

Lieve **Sanne**, de mooie momenten die wij het afgelopen jaar samen hebben meegemaakt, met in het bijzonder de geboorte van ons vrolijke mannetje Moos, heeft mij alleen maar meer doen beseffen dat ik zo ontzettend gelukkig ben met jou en de dingen om ons heen.

Ik bewonder aan jou dat jij altijd doorzet, ook als het je even tegenzit. Jouw gedrevenheid en passie voor je werk en alles wat je doet kan mij ontzettend stimuleren. Het gemak waarmee jij van alles organiseert, bedenkt en initieert vind ik knap. Jouw drive om iedereen te helpen en gelukkig te maken heeft op mij altijd een goed effect. Ook tijdens mijn promotietraject hielp jij mij om te relativeren, kansen te zien en uitdagingen te zoeken als die soms even weg leken.

Als ik één ding zeker weet, is dat jij net zo blij bent als ik dat dit boek nu af is. Ik ben je dankbaar voor je geduld en ik kijk er naar uit om het feest vooral met jou te vieren. Ik verheug mij op de vakantie en de tijd die we met z'n drietjes gaan doorbrengen!

VIEW IN 3D